

**STUDIES ON HYDROGEN INTERACTION
WITH VANADIUM AND VANADIUM-
ALUMINUM ALLOYS**

BY

SANJAY KUMAR

Enrolment Number: CHEM01200904010

BHABHA ATOMIC RESEARCH CENTRE

A thesis submitted to the
Board of Studies in Chemical Science Discipline

In partial fulfillment of requirements
For the Degree of

DOCTOR OF PHILOSOPHY

of

HOMI BHABHA NATIONAL INSTITUTE



October, 2012

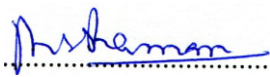
HOMI BHABHA NATIONAL INSTITUTE

Recommendation of the Viva Voce Board

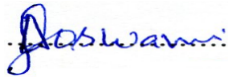
As member of the Viva Voce Board, we certify that we have read the dissertation prepared by **Shri Sanjay Kumar** entitled “**Studies on hydrogen interaction with vanadium and vanadium-aluminum alloys**” and recommend that it may be accepted as fulfilling the dissertation requirement for the degree of Doctor of Philosophy.

Dr. D. Das (Chairman)  Date: 16.03.2013

Dr. N. Krishnamurthy (Research Guide)  Date : 16.03.2013

Dr. M Sundararaman (External Examiner)  Date: 16.03.2013

Dr. Shyamala R Bhardwaj (Member)  Date: 16.03.2013

Dr. A. Goswami (Member)  Date: 16.03.2013

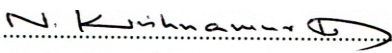
Dr. S.C. Parida (Member)  Date: 16.03.2013

Final approval and acceptance of this dissertation is contingent upon the candidate's submission of the final copies of the dissertation to HBNI.

I hereby certify that I have read this dissertation prepared under my direction and recommend that it may be accepted as fulfilling the dissertation requirement.

Date: 16th March 2013

Place: BARC, Mumbai


Prof. (Dr.) N. Krishnamurthy
(Guide)

STATEMENT BY AUTHOR

This dissertation has been submitted in partial fulfillment of requirements for an advanced degree at Homi Bhabha National Institute (HBNI) and it is deposited in the library to be made available to borrowers under rules of the HBNI. Brief quotations from this dissertation are allowable without special permission, provided that accurate acknowledgement of source is made. Requests for permission for extended quotation or reproduction of this manuscript in whole or in part may be granted by the competent authority of HBNI when in his or her judgment the proposed use of the material is in the interests of scholarship. In all other instances, however, permission must be obtained from the author.



(Sanjay Kumar)

DECLARATION

I, hereby declare that the investigation presented in the thesis has been carried out by me.
The work is original and has not been submitted earlier as a whole or in part for a degree /
diploma at this or any other Institution / University.



(Sanjay Kumar)

*Dedicated to my
Lovely parents*

Acknowledgements

*At the juncture of this milestone achievement, I would like to express my sincere gratitude to number of people to whom I am really indebted to for their help, support and motivation in all my endeavors. At the outset I wish to record my heartfelt gratitude and indebtedness to my child hood science teacher **Shri Ramnandan Singh** (BSC Babu) whose magical and inspiring teaching at the school level deeply motivated me to choose research in materials science as my scientific career.*

*I would like to express my deep and sincere gratitude to my research guide, Professor and outstanding scientist **Dr. Nagaiyar Krishnamurthy** for his invaluable guidance, constant encouragement, unstinted inspiration, keen interest and good wishes. His wide knowledge and his logical way of thinking on critical scientific problems have been of great value for me. I am also grateful to him for being patient while critically reviewing this thesis. This thesis would not have been possible without the guidance, help, support, critical analysis and valuable suggestions from **Dr. G.P. Tiwari, Dr. R.N. Singh** and **Dr. Alok Awasthi** who have been truly invaluable to me both on an academic and a personal level, for which I am extremely grateful. I am also thankful to them for sharing their excellent knowledge and scientific understanding with me. Their enthusiasm, deep engagement in research and critical analysis strategy of experimental data has made a deep impression on me.*

*I wish to express my sincere thanks to my colleague **Shri T.S.R.Ch. Murthy** for his diversified help, fruitful scientific discussions and moral support*

offered to me from time to time throughout the course of the Ph.D research work. My special thanks goes to my colleagues and my dear friends **Shri D. K. Sahoo**, **Shri J.K. Soneber** and **Shri R.D. Bedse** for their moral support, diversified help, and several funs which will always be remembered. They have been very patient while listening to me whenever I was excited about a new scientific idea.

I would like to thank **Dr. Abhishek Mukherjee** for helping out with X-ray powder diffraction analysis and for numerous enlightening and exciting discussions about almost everything ranging from natural science to politics. Also special thanks to **Dr. Ashok Arya** for general support and many stimulating and fruitful discussions connected to Fermi energy concepts and their applications. I would like to thank my fellow Ph.D. student **Mrs. Manju Taxak** and M.Tech project trainee, **Shri Amit Tirpude** from IIT Bombay for their co-operation and help during the experiments and data analysis.

It gives me immense pleasure to thank the members of the doctoral committee **Prof. D. Das** (Chairman), **Prof. A. Goswami** (Member), **Prof. Shymala R. Bhardwaj** (Member) and **Dr. S.C. Parida** for their critical review and suggestions during the progress review and pre-synopsis viva-voce. It is my great privilege to acknowledge the trust and support extended by **Prof. A.K. Suri**, Director, Materials Group since my joining this department. I also gratefully acknowledge the help rendered by all the members of Materials Processing Division, Materials Science Division and Fusion Reactor Materials Section for their co-operation and help during my Ph.D work.

Today I really miss my elder brother **Er. Vijay Kumar Singh** (IAS) who taught me how to walk high even in the most arduous times. I am sure his

*eternal soul will be very happy seeing me achieve this success. Finally, I owe my heartfelt gratitude and indebtedness to my **parents** and **sisters** who have always encouraged me to follow my heart and inspired my inquisitive mind throughout my childhood and career. It is their inspiration, encouragement, blessings and support that helped me to achieve what I am today.*

*I am forever grateful to my lovely wife, **Dr. Anamika** for being supportive, enduring and forgiving during the last three years, and to my lovely son **Master Shreyansh (Inu)**, for helping me to remember that there are more important things to do in life than the work. My deepest gratitude also goes to my brother in-law **Shri Samarjeet Kumar** and sister in-law **Mrs. Kriti Singh** for being supportive and for showing interest in proofreading of almost all my published manuscripts.*

*Lastly, I am thankful to all the unknown **reviewers** of my published scientific articles/papers whose comments always upgraded my scientific thought and opened a new way of thinking.*

(Sanjay Kumar)

Preface

Completing the Ph.D degree has been one of the most cherished dreams of my life right from the early days of my graduation. The outcome of the dreams comes in the form of the present Ph.D thesis. This thesis is submitted in partial fulfillment of the requirements for the Ph.D degree at the Homi Bhabha National Institute, Mumbai, India. The thesis presents the results obtained during my work at the Fusion Reactor Materials Section, Materials Group, BARC during the period of September, 2009 to June, 2012. The work has been performed under the supervision of **Prof. (Dr.) Nagaiyar Krishnamurthy**, Outstanding Scientist and Head - Fusion Reactor Materials Section. The motivation for the work presented in this thesis is the fact that our society in the future will inevitably face some serious challenges due to limited supply of fossil fuels and global warming issues. A possible solution to these problems is a gradual transition from the hydrocarbon based society to the hydrogen society i.e. a society in which hydrogen is the primary energy carrier. Hydrogen can be produced by electrolysis using electricity from renewable energy sources and, ultimately, energy conversion can be performed with water being the only by-product thereby eliminating CO₂ emissions. The vision for the transport sector is that all cars utilize fuel cells instead of a traditional combustion engine and that they are powered by hydrogen. However, one of the great show stoppers is the shortcomings of current hydrogen storage technologies, especially concerning hydrogen capacity and operating temperature. One of the areas within the hydrogen storage technologies showing great potential is solid state hydrogen storage in metals and complex hydrides. The storage of hydrogen in the form of metal hydride appears promising because of high volumetric hydrogen absorption capacity along with excellent absorption-desorption kinetics. Superior structural integrity over a large number of absorption- desorption cycles makes it more cost-effective. Immobilized form, low volume of storage system and low equilibrium hydrogen plateau pressure enhance its practical applicability in a safe mode for

storage, transportation and commercial applications. Refractory metals with body centered cubic (bcc) structure are known to be good permeation to hydrogen due to its open structure. Vanadium in metallic form has inherently showed superior hydrogen storage capacity in comparison to other hydride forming metals like titanium, uranium and zirconium because of its bcc crystal structure. Hydrogen storage capacity of vanadium exceeds the corresponding values of the AB_5 hydrogen storage alloy system and it is comparable to AB_2 hydrogen storage alloy systems at ambient temperature and pressure. Vanadium based alloys are known to be good permeation to hydrogen and it could be developed as a hydrogen permeable membrane to be used for the tritium segregation in connection with the world fusion reactor program. Vanadium-titanium-chromium (V-Ti-Cr) alloy with substantially varying composition of Ti and Cr is a potential candidate material for hydrogen storage due to its high volumetric hydrogen absorption capacity, good cyclic properties and absorption-desorption kinetics compared to other hydrogen storage materials. Vacuum arc-melting of the constituent metal in its high pure form is the most conventional route for the synthesis of the alloys and intermetallics. Vanadium-titanium-chromium alloy has also been produced by this process for various structural applications. Key issues in this synthesis process are the production cost because it uses expensive high pure metals, and inhomogeneity because of insufficient mixing due to density and melting point differences of the constituent elements. Vanadium and its alloys are generally produced via aluminothermy processes in which appropriate mixture of metal oxides has been reduced by aluminum. The process is highly cost-effective. However, the product retains a few atomic percentages of aluminum even after electron beam refining. Effects of aluminum on hydrogen absorption parameters of V-H system will be useful to implement the aluminothermy to produce vanadium and its alloys for various applications where hydrogen solubility and absorption kinetics are the key concern. The present thesis deals with the hydrogen interaction properties of vanadium metal and

vanadium aluminum alloys. High priority has been given to presentation of the results obtained during my Ph.D period. This has resulted in a number of peer-reviewed international publications. **Paper 1** is directly related to materials synthesis and it served as the foundation of this thesis. **Paper 2 and 3** are related to solid solubility and hydride phase stability. **Paper 4, 5 and 6** explained the effects of aluminum on kinetics and thermodynamics of vanadium-hydrogen system. Furthermore, some of the concepts introduced in **paper 7** have been extended to also apply to the kinetics of solid state hydrogen storage materials. **Paper 8** is the effects of aluminum on the thermodynamics properties of V-H system. Vanadium is also known to be exerts a positive effects on the hydrogen absorption kinetics of the hydrogen storage alloys. This has been explained in **paper 9** with reference to LaNi_5 . **Paper 10 and 11** are review papers concluding the investigation carried out worldwide on vanadium based hydrogen storage materials. In addition, results have been presented on a number of **national and international meetings and symposia in the form of posters, proceedings papers**. Peer-reviewed high impact factor International Publications from the Ph.D work has been listed below:

Publications in International Journals from the Ph.D work [11]

Paper [1]

Sanjay Kumar and N Krishnamurthy

Synthesis of V-Ti-Cr alloys by aluminothermy co-reduction of its oxide

International Journal of Processing and Application of Ceramics 2011;5(4):181-6.

Paper [2]

Sanjay Kumar, M Taxak, N Krishnamurthy, A K Suri and GP Tiwari

Terminal solid solubility of hydrogen in V-Al solid solution

International Journal of Refractory Metals and Hard Materials 2012; 31: 76-81

Paper [3]

Sanjay Kumar, M. Taxak, N Krishnamurthy

Hydrogen absorption kinetics of V₄Cr₄Ti alloy prepared by aluminothermy process

International Journal of Hydrogen Energy 2012; 37(4): 3283-91.

Paper [4]

Sanjay Kumar and N Krishnamurthy

Variation of activation energy of hydrogen absorption of vanadium as a function of Al

International Journal of Hydrogen Energy, 2012; 37(18) 13,429-36.

Paper [5]

Sanjay Kumar and N Krishnamurthy

Effects of aluminum on solubility and β phase stability of vanadium-hydrogen system

International Journal of Refractory Metals and Hard Materials 2012; 35: 191–5.

Paper [6]

Sanjay Kumar, M Taxak and N Krishnamurthy

Hydrogen absorption kinetics of V-Al alloy

Journal of Thermal Analysis and Calorimetry 2012; DOI: 10.1007/s10973-012-2558-1.

Paper [7]

Sanjay Kumar M Taxak and N Krishnamurthy

Synthesis and hydrogen absorption in V-Ti-Cr alloy

Journal of Thermal Analysis and Calorimetry 2012; DOI 10.1007/s10973-012-2643-5.

Paper [8]

Sanjay Kumar and N Krishnamurthy

Effects of Aluminum on standard enthalpy and entropy of vanadium-hydrogen solid solution

Int J Hydrogen Energy 2013, HE-D-13-00850, under review.

Paper [9]

Sanjay Kumar, A Tirpude, M Taxak and N Krishnamurthy

Hydrogen absorption kinetics in ball milled V+ 80wt% LaNi₅ composite

Journal of Alloys and Compounds 2012, doi: 10.1016/j.jallcom.2013.03.001.

Paper [10]

Sanjay Kumar and N. Krishnamurthy

Development of vanadium based hydrogen storage materials: a review

Progress in Materials Science 2012; to be submitted.

Paper [11]

Sanjay Kumar, M Taxak and N Krishnamurthy

Solid state hydrogen storage methods: theories and applications

Indian Thermal Society of India, ITAS 2012, Invited paper to be submitted

International/National Symposium Proceedings [08]

- [1] Sanjay Kumar, M Taxak and N Krishnamurthy. Hydrogen absorption kinetics in V-Al alloys. Proceeding of the 18th International Symposium on Thermal Analysis, Editors: R Agrawal, L Varshney, YK Bhardwaj, RA Jat, S K Rakshit, K L Ramkumar 2012; 333-5.
- [2] Sanjay Kumar, M Taxak and N Krishnamurthy. Synthesis and Hydrogen absorption Kinetics of V₄Cr₄Ti alloys. Proceeding of the 18th International Symposium on Thermal Analysis, Editors R. Agrawal, L Varshney, YK Bhardwaj, RA Jat, SK Rakshit, KL Ramkumar 2012; 315-7.
- [3] Sanjay Kumar, M Taxak and N. Krishnamurthy. Solid solubility of hydrogen in V-Ti-Cr-Al alloys synthesized by aluminothermy. 49th NMD and 65th ATM 13-16 Nov 2011 Hyderabad India Editors Dr. Amol A Gokhale and Dr. Shrikant V Joshi; p 63
- [4] Sanjay Kumar, M Taxak and N Krishnamurthy. Interaction of hydrogen with pure vanadium. 49th NMD and 65th ATM 13-16 Nov 2011 Hyderabad India Editors Dr. Amol A Gokhale and Dr. Shrikant V Joshi. p 89
- [5] M Taxak, Sanjay Kumar, N Krishnamurthy, A K Suri and G P Tiwari. Effect of aluminum on the equilibrium solubility of hydrogen in vanadium. Proceedings of 3rd International Symposium on Materials Chemistry (2010) Mumbai India Editor Dr. R K Vatsa; p 113.
- [6] Sanjay Kumar, A Awasthi, R.N. Singh and N Krishnamurthy. Solid Solubility in Vanadium-Aluminum alloys. HEM 2009, Mumbai, India, Editor Dr. R.N Singh; p 46
- [7] N. Krishnamurthy, Sanjay Kumar, A. Awasthi. Preparation of binary alloys of refractory metals by co-reduction: Group V Metals alloy. Vol.1 RM30/1-RM30/10, 17th Plansee Seminar Proceeding, Plansee Group, Austria 2009; 1-10.
- [8] Sanjay Kumar, M Taxak and N Krishnamurthy. Hydrogen absorption kinetics in ball milled V+80wt.% LaNi₅ composite, International Symposium on Metal-Hydrogen Systems-Fundamentals and Applications- 21-26 October, 2012 Kyoto, Japan.

Contents

Topics	Page no
Synopsis	xv-xxiii
List of Figures.....	xxiv-xxvii
List of Tables	xxviii
Acronyms.....	xxix
1. Introduction.....	1-19
1.1 Hydrogen storage methods: a review.....	3
1.2 Vanadium: a wonderful metal.....	6
1.3 Theory of metal-hydrogen interaction.....	9
1.4 Metal-hydrogen reactions: mechanism and kinetics.....	11
1.5 Thermodynamics of metal-hydrogen system.....	15
1.6 Aim and objectives of present Ph.D project	17
2. Review of literature.....	20-49
2.1 Introduction.....	22
2.2 Hydrogen absorption-desorption in vanadium metal.....	23
2.3 Vanadium hydride phase stability.....	28
2.3.1 VH_2 (γ) phase stability.....	28
2.3.2 V_2H and $V(H)$ (β and α) phase stability.....	29
2.4 Storage capacity of vanadium base alloys.....	30
2.4.1 Binary alloys.....	30
2.4.2 Ternary alloys and laves phases.....	32
2.5 Kinetics and thermodynamics.....	38
2.6 Electronic consideration of hydride stability and absorption capacity.....	42
2.7 Hydrogen diffusion and permeation.....	45
2.8 Summary and conclusions.....	49
3. Materials and methods.....	50-78
3.1 Introduction.....	52
3.2 Materials Synthesis.....	52
3.2.1 Vacuum Arc melting.....	52
3.2.2 Aluminothermy followed by electron beam melting.....	53
3.3 Apparatus used in the present study.....	55
3.3.1 Sieverts apparatus.....	55
3.3.2 Modified Sieverts apparatus.....	58
3.4 Methods used for solubility and kinetics studies.....	59
3.4.1 Activation of the sample	59
3.4.2 Hydrogen solubility calculation using pressure drop methods.....	60
3.4.3 Hydrogen solubility calculation by gravimetric method.....	61
3.4.4 Enthalpy calculation using solubility data	62
3.4.5 Kinetics equation.....	62

3.4.6 Activation energy.....	64
3.5 Analytical techniques.....	65
3.5.1 Scanning electron microscopy (SEM).....	65
3.5.2 Energy-dispersive X-ray spectroscopy (EDS/EDS).....	67
3.5.3 X-Ray diffraction (XRD).....	68
3.5.4 Inert gas fusion technique (N,O,H).....	70
3.5.5 X-Ray florescence (XRF)	73
3.5.6 Differential thermal analysis (DTA).....	74
3.5.7 Inductively coupled plasma atomic emission spectroscopy.....	76
3.6 Summary and Conclusions.....	78
4. Results and discussion.....	79-151
4.1 Materials preparation	81-93
4.1.1 Introduction	81
4.1.2 Thermodynamics of aluminothermy process.....	81
4.1.3 Vanadium metal and vanadium-aluminum alloys.....	83
4.1.4 Characterization of vanadium-aluminum alloys.....	86
4.1.5 V-Ti-Cr alloys by aluminothermy process	89
4.1.6 Mechanism of refining process	92
4.2 Vanadium-hydrogen solid solution	94-111
4.2.1 Introduction.....	94
4.2.2 Solution behaviour of hydrogen.....	94
4.2.3 Hydrogen solubility.....	98
4.2.4 Theories on hydrogen solubility.....	103
4.3 Phase stability.....	112-120
4.3.1 Introduction	112
4.3.2 VH_2 (γ) phase.....	112
4.3.3 α and β phase.....	114
4.3.4 Pressure composition isotherm of V-Ti-Cr alloy.....	119
4.4 Thermodynamics and Kinetics.....	121-151
4.4.1 Introduction.....	121
4.4.2 Enthalpy, Entropy and Gibbs free energy of V-H solution....	121
4.4.3 Hydrogen absorption kinetics of V-Al & V-Cr-Ti alloys.....	127
4.4.4 Effects of vanadium on the H absorption kinetics of $LaNi_5$..	147
5. Summary and conclusions.....	152-156
5.1 Summary and conclusion	154
5.2 Future scope of the work.....	155
6. Bibliography	157-166

Synopsis

Preamble

Apart from the numerous applications of vanadium and its alloys as structural materials in advanced energy and many engineering systems, vanadium and its alloys are also attractive functional materials for hydrogen storage as well as hydrogen permeation. Aluminothermic reduction followed by vacuum refining including electron beam melting is a standard process to produce vanadium and its alloys. However, aluminum enters as impurities in as reduced metal and may persist or even deliberately retained through usual refining processes. In this context it is relevant to study the effect of aluminum on the key parameters of vanadium-hydrogen interaction pertinent to hydrogen storage and hydrogen permeation [1-2]. This is the subject matter of the present Ph.D project.

Introduction

In the search of alternative energy sources, hydrogen emerges as a promising, renewable and eco-friendly option for transportation and energy storage and many other everyday applications [3]. Production, purification, storage and transportation of hydrogen play an important role in the development of hydrogen-based ecofriendly economy. The issues related to the application of hydrogen as a portable fuel for a variety of commercial applications hinges on the development of a suitable, safe, portable and user-friendly hydrogen storage system [4]. Hydrogen could be stored by various methods, such as compressed gas at high pressure, low temperature (20K) cryogenic liquid hydrogen and solid hydrogen in the form of metal or alloy (intermetallic) hydride. Each mode of storage system has its own issues. For example safety is the major concern related to the storage and transportation of hydrogen in the form of compressed gas. Storage in the form of liquid hydrogen is impractical for the commercial and domestic application as it requires expensive and unwieldy cryogenic vessel. Hydrogen storage in the form of a metal or an intermetallic hydride and other chemical compound requires suitable material which could absorb massive amount of hydrogen and also release it on demand. The storage of hydrogen in the form of metal hydride appears promising because of high volumetric hydrogen absorption capacity and excellent absorption-desorption kinetics. Superior structural integrity over a large number of absorption-desorption cycle makes it

more cost-effective. Immobilized form, low volume of storage system and low equilibrium hydrogen pressure enhance its practical applicability as a safe mode for storage, transportation and uses [5-6].

The world fusion reactor program currently proceeding is based on magnetic confinement of deuterium–tritium (D-T) plasma. Tritium along with helium will be generated by neutrons from plasma causing nuclear transmutations of lithium in the ceramic breeder (Li_2TiO_3) and the lead-lithium coolant [7-8]. The tritium thus produced will be flushed out and segregated from the helium using suitable tritium permeable material. The selection of the suitable tritium permeable materials to be used for the segregation of tritium efficiently from the helium is a subject matter of investigation. Tritium being the isotope of hydrogen, behaves similar to hydrogen and hence, investigation of hydrogen interaction study of the potential permeable material will be useful for the tritium as well.

Vanadium in metallic form inherently shows superior hydrogen storage capacity in comparison to other hydride forming metals like titanium, uranium and zirconium because of its bcc crystal structure. Hydrogen storage capacity of vanadium exceeds the corresponding values for the AB_5 hydrogen storage alloy system and it is very much comparable with AB_2 hydrogen storage alloy systems at ambient temperature and pressure [9-10]. Vanadium has been known as a good permeator to hydrogen also and it can be developed as a hydrogen permeable membrane to be used for the hydrogen segregation. The issues related to the metallic vanadium as a hydrogen storage material are the absorption-desorption mechanism and activation [11]. The mechanism of hydrogen absorption in vanadium, initiated with the formation of vanadium-hydrogen solid solution phase, $\text{V}(\alpha)$, which on further hydrogenation precipitated as β hydride phase (V_2H). Furthermore the γ phase (VH_2) is formed when it is fully hydrogenated. The β phase is stable upto 600K. Therefore, the hydrogen desorption reaction from the β phase never occurs at ambient temperature. The γ phase is not so stable, as its hydrogen absorption and desorption reaction can take place at moderate temperature and pressure. On hydrogen desorption, γ phase is converted into β phase. Thus, only half amount of hydrogen absorbed in metallic vanadium could be used in the subsequent hydrogen absorption-desorption process. This amount is, however, not enough for practical applications and recognition of metallic vanadium as hydrogen storage material. Besides, hydrogen absorption-desorption mechanism of γ (VH_2) phase is superior over the other hydrogen storage materials [12-15]. Therefore, it would be desirable to increase the usable hydrogen capacity of vanadium by controlling the stability of the β phase.

Vanadium and its alloys can be produced via aluminothermic reduction of appropriate mixture of oxides. However, the product can retain several atom percentage of aluminum even after purification by evaporating aluminum using electron beam melting. Vanadium-aluminum alloys can also be made by design. Therefore it is relevant to investigate the effect of aluminum on the vanadium-hydrogen system so that aluminothermy could be employed to produce vanadium and its alloys for the various hydrogen storage and hydrogen permeation applications.

Materials and methods

The vanadium metal and the alloys used in the present investigation were synthesized directly by aluminothermic process. For the comparative study, the alloys were simultaneously prepared using pure components by vacuum arc melting. In the aluminothermy process, starting oxides of respective metals were mixed with the aluminum and additive like KClO_3 (for heat boosting) and CaO (for slag fluidizing) were added, whenever it was necessary. The mixture was loaded in refractory lined steel reactor and the reaction was initiated by igniting a trigger mixture of KClO_3 and Al . The reactions were highly exothermic and heat of reaction was sufficient to completely melt the slag and reduced metal and cause their separation into two layers. The reactions involved in the thermit process are given below



The metals/alloys separate from the slag due to the density differences and solidify as easily separated ingot. The alloys thus obtained were refined by electron beam melting. These refined metal and alloys bottoms were sliced using electric discharge machine (EDM). Sliced pieces were hot rolled to desired sample thickness and then annealed.

A Sieverts apparatus fabricated in house was extensively used for the study of hydrogen solubility, kinetics and hydride phase stability. A thermobalance attached to the Sieverts apparatus has been used to study the isobaric hydrogen absorption kinetics. In all the hydrogen charging experiments the samples were first activated by heating to 1100K-1200K under high vacuum condition (10^{-7} torr) before exposure to hydrogen. Throughout the investigation, Scanning Electron Microscope-Energy Disperse analysis (SEM-EDS), Electron Probe Beam Analysis (EPMA) and

Inert-gas fusion techniques were extensively used to ensure the homogeneity of the alloys. The phase identifications were done using X-ray diffraction (XRD) analysis. Thermogravimetric and Differential Thermal Analysis (TG-DTA) were used in the hydride decomposition and phase stability studies.

Results and discussion

Equilibrium hydrogen solubility

The effects of aluminum on the equilibrium solubility of hydrogen have been studied in the temperature ranges of 250-900K and pressure ranges of 50 torr to 1000 torr. In the low temperature range the equilibrium phases were α (V(H)) and β (V₂H). Higher temperature range only solid solution, V(H), α phase has been observed. The observation was in accordance with the vanadium-hydrogen phase diagram. Hydrogen solubility decreases with temperature in low temperature range. Marginal increase in hydrogen concentration with temperature has been recorded at high temperature range. In both temperature ranges a common observation was the substantial decrease in equilibrium hydrogen solubility with aluminum content of the alloy

Enthalpy and entropy of hydrogen desorption

Enthalpy and entropy of solution of hydrogen related to Sieverts constant K_s as follows

$$\ln K_s = \frac{\Delta H^\circ}{RT} - \frac{\Delta S^\circ}{R} \quad (4)$$

Where K_s is a Sieverts constant, ΔH° and ΔS° are the standard enthalpy and entropy of vanadium hydrogen solid solution respectively. The Sieverts constant at a particular pressure and temperature has been obtained by using Sieverts Law:

$$H/M = K_s \sqrt{p} \quad (5)$$

Where H/M is the atomic ratio of hydrogen to metal and p is pressure in Pascal. The condition for the above equation is that, the dissolved hydrogen should be within the solubility limit. Applying these equations, standard enthalpy and entropy of solution of hydrogen in vanadium solid solution has been investigated as function of aluminum content. Furthermore enthalpy was separately measured for V & (V, Al) - H solid solution using DTA by dehydrogenation of the V(α) phase. The

results obtained by these two techniques have shown good agreement. The results revealed standard enthalpy increasing and entropy decreasing with aluminum content.

Hydride phase stability

The pressure composition isotherm (PCT) have been investigated for $V + H_2 = VH_2$ equilibrium reaction. It was revealed that the equilibrium pressure for VH_2 (γ) phase is higher for the vanadium-aluminum alloys as compared to pure vanadium. The hydrogen desorption from β phase of vanadium has been investigated using TG-DTA. Hydride of pure vanadium (β phase) sample has been decomposed by heating it at the rate of $2K\ min^{-1}$ in a Setaram make thermogravimetric analyzer unit (TG-DTA). A two step weight loss was observed. Corresponding endothermic peaks found to be present at the same temperature on the DTA pattern. The combined curve of TG-DTA clearly indicates that the gas desorption phenomena occurred in two steps. The first desorption step started at $\sim 487K$ while the other desorption step was at $\sim 596K$ temperature. Futhermore, XRD analysis revealed that low temperature peak P_1 appears due to the transformation of the β phase to the α phase containing hydrogen, high temperature peak P_2 will be originate due to transformation of this bcc (α) phase to the hydrogen-free bcc vanadium. The effects of aluminum on the decomposition behavior of β hydride were studied by DTA. Low temperature hydride phase $\beta [(V,Al)_2H]$ of vanadium aluminum alloys were decomposed at the identical conditions as discussed. The two endothermic peaks were observed during the decomposition of first two aluminum containing β phase (V_2H) samples: vanadium 0.78% aluminum and vanadium 1.02 wt % aluminum. The low temperature peak was reduced substantially for the sample that contains 1.53 wt % aluminum. In the DTA analysis, it was also observed that the shape and the position of the two endothermic peaks change significantly with aluminum content. For example, low temperature peak became broader with aluminum content and then substantially reduced for the vanadium aluminum alloys with aluminum concentration higher than 1.5 percent. The DTA analysis indicates that the high temperature peak, which was at 596K for $V(\alpha)$ phase of pure vanadium shifted to 585, 574 and 561 K for α phase of $V_{0.78}Al$, $V_{1.01}Al$ and $V_{1.53}Al$, respectively. The results indicates the modification in the stability of $V(\alpha)$ as well as β phase due to aluminum.

Apparent activation energy

Activation energy is another important parameter to characterize hydrogen storage as well as hydrogen permeable materials. The kinetics and mechanism of a reaction usually studied by fitting the time dependent reacted fraction $\alpha(t)$ to various analytical rate expressions, through which intrinsic rate limiting steps are obtained. The intrinsic rate limiting step is the slowest step of the reaction. Solid-gas reaction is usually controlled by the diffusion process and the reaction kinetics rate equation can be expressed as follows:

$$\frac{d\alpha}{dt} = k(T)f(\alpha) \quad (6)$$

Where α is the fraction reacted at time t , $k(T)$ temperature dependent rate constant. Two techniques were employed in the present study to obtain the data for reacted fraction α , namely constant pressure and variable mass techniques using thermobalance attached to the Sieverts apparatus:

$$\alpha = \frac{m_t - m_0}{m_{\infty} - m_0} \quad (7)$$

and constant volume variable pressure in the Sieverts apparatus

$$\alpha = \frac{p_0 - p_t}{p_0 - p_{\infty}} \quad (8)$$

$f(\alpha)$ is the function about the reaction mechanism, integral of $f(\alpha)$ is expressed as $g(\alpha)$:

$$g(\alpha) = \int \frac{d\alpha}{f(\alpha)} = k(T)t + C \quad (9)$$

$f(\alpha)$ or $g(\alpha)$ refers to the reaction mechanism function. Mechanism function included nucleation and growth [$g(\alpha) = (-\ln(1-\alpha))^{2/3}$], one-dimensional diffusion [$g(\alpha) = \alpha^{1/2}$] and three-dimensional diffusion [Ginstling-Brounshtein equation $g(\alpha) = (1-2\alpha/3)-(1-\alpha)^{2/3}$]. The α - t kinetic curve derived using Eq 7 or Eq 8 gives the data for t and α , which were linearly fitted based on Eq (6) or (9). The mechanism of hydrogen absorption in the alloy is decided by the function $f(\alpha)$ or $g(\alpha)$ giving the best linearity. The mechanism of hydrogen absorption and the kinetic parameter 'k(T)' were obtained from the linear regression fitting. Based on the Arrhenius equation, the apparent activation energy of hydrogen absorption in the alloy was calculated. The activation energy has been determined for V4Ti4Cr synthesized by aluminothermy process. The result revealed that activation energy was higher than reported value in which the alloys were prepared through arc melting of pure

components. The activation energy of a series of V-Al alloys has been investigated and revealed that the activation energy linearly increased with aluminum.

Pressure composition isotherm (PCT)

V and V-Al alloys

The pressure-composition-isotherm (PCT) measurements are performed at 350K temperature for vanadium and vanadium-aluminum alloys using Sieverts type apparatus, to evaluate the stability of the γ phase. The value of the pressure at the centre of each plateau is referred to as the plateau pressure. It has been observed that the plateau pressure for the V-Al alloy is substantial higher compare to pure vanadium. Increase in the plateau pressure has been explained on the basis of electronegativity and the atomic radius of the alloying elements.

V4Cr4Ti alloy

The Pressure composition isotherm (PCT) is measured at 400K for V4Cr4Ti alloy prepared by aluminothermy. Relatively [15] small hysteresis with two plateau pressure has been observed. Substantial reduction in the absorption capacity (1.8 weight % hydrogen) has also been observed. The results on hydrogen solubility in vanadium and vanadium- aluminum alloys has been explained including explanations on the basis of variation of Fermi energy level of vanadium vis a vis aluminum addition [1-10].

Conclusions

- ✎ Aluminothermy process is a route to produce vanadium and also vanadium-aluminum alloys. The further refining process could considerably reduce the aluminum content. Vanadium-aluminum solid solution follows the Vegards Law and hardness of the V-Al alloys followed the simple solid solution effect.
- ✎ Titanium could be loaded in vanadium matrix through aluminothermy process which indeed difficult to reduce alone by aluminum due to less exothermicity of the reaction.
- ✎ The increase in lattice parameter upon aluminum addition should increase the hydrogen solubility as per the existing theory. However the solubility of hydrogen in single phase as well as co-existing two phase region is significantly reduced by the presence of aluminum.

- ✎ The enthalpy and entropy of the vanadium hydrogen solution were obtained using Sieverts constant measurements. The enthalpy data obtained were further verified using DTA technique. It was observed that both, enthalpy as well as entropy of the hydrogen solution in vanadium is increased by the presence of aluminum as a consequence desorption from the solid solutions required less temperature.
- ✎ Substantial modification in the β phase decomposition was observed with aluminum content. It was assumed that kinetics could be one of the reasons and hence activation energy was calculated in a series of vanadium-aluminum alloys.
- ✎ The activation energy of hydrogen absorption in V4Cr4Ti was higher than the reported value in which these alloys were prepared through vacuum arc melting of high pure component possibly due to the presence of aluminum in the former. The absorption mechanism changes with temperature. At lower temperature nucleation and growth, one-dimensional diffusion process and three-dimensional diffusion process control the reaction however, at higher temperature three-dimensional diffusion process control the reaction.
- ✎ Activation energy of hydrogen absorption by vanadium linearly varied with aluminum concentration and all the alloys followed a mechanism of three-dimensional diffusion process.
- ✎ PCT curve of V and V-Al alloy has been found similar to a bcc metal. However, the equilibrium plateau pressure was higher for V-Al compared to vanadium.
- ✎ PCT curve of V4Cr4Ti alloys show two plateau pressures this is due to the presence of aluminum and also substantial reduction in hydrogen capacity has been observed compared to reported value.
- ✎ The kinetics and mechanism of hydrogen solubility of LaNi₅ was substantially improved by the presence of vanadium.

References

- [1] Lototsky MV, Yartys VA, Zavaliy IY. Vanadium-based BCC alloys: phase-structural characteristics and hydrogen sorption properties. *J Alloys Compds* 2005; 404-406:421-6.
- [2] Seo CY, Kim JH, Lee PS, Lee JY. Hydrogen storage properties of vanadium based bcc solid solution metal hydride. *J Alloys Compds* 2003; 348: 252-7.
- [3] Marban G, Solis T V. Towards the hydrogen economy. *Int J Hydrogen Energy* 2007; 32: 1625-37.

- [4] Schlapbach L, Zuttel A. Hydrogen-storage materials for mobile applications. *Nature* 2001;414:353-8
- [5] Elena D. An overview of advance materials for hydrogen storage. *J Mat Proc Tech* 2005; 162-163: 169-77.
- [6] Sakintuna B, Lamari-Darkrim F, Hirscher M. Metal hydride materials for solid hydrogen storage: A review. *Int J Hydrogen Energy* 2007; 32:1121-40.
- [7] Sanjay Kumar and Krishnamurthy N. Corrosion of Fe₉Cr₁Mo steel in stagnant liquid lead-lithium eutectic. *Fusion Eng Des* 2012 doi 10.1016/j.fusengdes. 2012.01.014.
- [8] Nishimura C, Komaki M, Amano M. Hydrogen permeation characteristics of vanadium–molybdenum alloys. *Tran Mater Res. Soc. Jpn* 1994; 18B:1273-76.
- [9] Kuriwa, T Tamura, T Amemiya, T. Fuda, A. Kamegawa, H. Takamura, M. Okada, New V-based alloys with high protium absorption and desorption capacity, *J Alloys Compds*, 293–295 (1999) 433-36.
- [10] Seo C Y, Kim J H, Lee P S, Lee J Y, Hydrogen storage properties of vanadium-based bcc solid solution metal hydrides, *J Alloys Compds*, 348 (2003) 252-57.
- [11] Yukawa H, Yamashita D, Ito S, Morinaga M, Yamaguchi S. Compositional dependence of hydriding properties of vanadium alloys at low hydrogen pressures. *J Alloys Compds* 2003; 356-357: 45-9.
- [12] Song XP, Pei P, Zhang PL, Chen GL. The influence of alloy elements on the hydrogen storage properties in vanadium-based solid solution alloys. *J Alloys Compds* 2008; 455:392-7.
- [13] Rex BM and Yoshihara M. The Diffusion of Hydrogen in B.C.C V-Ti Solid Solutions. *J Phy.Chem. Solid* 1987; 48, 7:661-5.
- [14] Ewald V, Edward R K. Thermodynamic properties in the System Vanadium-Hydrogen, Niobium –Hydrogen and Tantalum-Hydrogen. *J Phy Chemistry* 1969; 73(3) :683-92.
- [15] Miao H, Wang WG. Mechanisms of improving the cyclic stability of V-Ti based hydrogen storage electrode alloys. *J Alloys Compds* 2010; 508:592-8.

S. No.	Figure Captions	Page No.
1.1	Simple schematic Lennard-Jones potential energy diagram of chemisorption of hydrogen on metals	10
1.2	Schematic illustration of the different mechanisms involved in the formation of a metal hydride	12
1.3	Two major classes of hydrogenation/dehydrogenation curves.	14
1.4	Pressure-Composition-Isotherms (PCI) for a hypothetical metal hydride	15
1.5	Hydride formation enthalpy, ΔH_f per mole hydrogen as a function of the plateau temperature at 760 Torr	17
1.6	Schematic work plans of the Ph.D program	19
2.1	The monoclinic structure of the V-H β phase	24
2.2	Vanadium-hydrogen phase diagram at one atmosphere of hydrogen pressure	26
2.3	The structure of hyperstoichiometric β , ϵ , δ vanadium hydride as projected on the (100) plane	27
2.4	Variation of plateau pressure corresponding to γ hydride phase of vanadium with alloying elements	28
2.5	Alloying effects on the decomposition of β phase and desorption from the α phase.	30
2.6	Variation of absorption capacity of V-Ti-Cr alloys	37
3.1	Raw materials used for the synthesis of vanadium metals and alloys	54
3.2	Process flow sheet of metal and alloys preparation by open bomb aluminothermy	55
3.3	Sieverts Apparatus: Indigenously designed and developed in the laboratory	56
3.4	Schematic diagram of the Sieverts apparatus design, developed and used in the present study	57
3.5	Modified Sieverts apparatus with thermobalance (a) Indigenously developed in the laboratory (b) Schematic diagram	59
3.6	A typical vanadium based sample (a) before activation (b) after activation	60
3.7	Schematic diagram of a SEM instrument	66
3.8	Schematic diagram showing the principle of energy disperse spectroscopy (EDS) used for the composition analysis	68

3.9	Schematic diagram of a typical XRD used for the phase's analysis in the present investigation	69
3.10	Schematic diagram of inert-gas fusion technique used in the study to determine the non-metallic impurities in the sample	72
3.11	Schematic principle of XRF analysis	74
3.12	Differential thermal analysis unit used to determine the enthalpy of hydrogenation process	76
3.13	Schematic diagram of Inductively coupled plasma atomic emission spectroscopy (ICP-AES)	78
4.1.1	Gibbs free energy diagram all the three reactions	82
4.1.2	Vanadium-aluminum thermite along with completely refined product vanadium	84
4.1.3	X-Ray diffraction analysis of vanadium metals prepared by aluminothermy process and refined by electron beam analysis	85
4.1.4	Optical micrograph and SEM-EDS analysis of the vanadium sample prepared through aluminothermy process metals	86
4.1.5	Vanadium-aluminum phase diagram	87
4.1.6	X-Ray analysis of the V-18 wt% aluminum	88
4.1.7	Variation of lattice constant and Vickers hardness of V–Al alloys as a function of Al content	89
4.1.8	V-Ti-Cr alloy finger prepared by aluminothermy process, refined by electron beam melting followed by homogenization by vacuum arc melting	90
4.1.9	XRD analysis of V ₄ Cr ₄ Ti alloy	91
4.1.10	SEM-EDS analysis of the samples indicating the phase homogeneity and alloy composition	92
4.2.1	Vanadium-hydrogen phases diagram	95
4.2.2	(1) XRD pattern of bcc (α) phase vanadium with different amount of soluble hydrogen (a) vanadium (b) vanadium with 240 ppm hydrogen (c) vanadium with 322 ppm hydrogen (d) vanadium with 405 ppm hydrogen (e) vanadium with 457 ppm hydrogen (2) Variation of lattice parameter with respect to hydrogen concentration	96
4.2.3	Relative change in lattice parameter variation with hydrogen concentration	97
4.2.4	Hydrogen solubility curve at (1) constant pressure (760 Torr) (2) Constant	

1	temperature (350K) for vanadium and vanadium aluminum alloys	99
4.2.5	XRD analysis of (a) V0Al, (b) V5Al, (c) V10Al, (d) V14Al, (e) V0Al+550 ppm H, (f) V5Al+488 ppm H, (g) V10Al+336 ppm H, and (h) V14Al+227 ppm H: PCPDF 28–1058: Mo K_{α}	101
4.2.6	(a) Isobaric (250 Torr) hydrogen solubility as function of aluminum at different temperature (b) Isothermal (973K) hydrogen solubility as function of aluminum at different pressure	102
4.2.7	Electrical resistivity of vanadium and vanadium-aluminum alloys at room temperature	107
4.2.8	Aluminum –hydrogen phase diagram	110
4.3.1	γ phase stability of (a) Vanadium 1.532 wt% aluminum Al (b) Vanadium 0.784 wt% aluminum (c) High pure vanadium	113
4.3.2	X-ray diffraction patterns of as such prepared V_2H	114
4.3.3	(a) TG-DTA study of decomposition pattern of β phase of pure vanadium hydride. (b) X-ray diffraction patterns of decomposition pattern of β phase of pure vanadium hydride	115
4.3.4	DTA study on effects of aluminum on decomposition pattern of $(V,Al)_2H$ (a) V1.532 wt% Al, (b) V1.014 wt% Al, (c) V0.784 wt% Al and (d) pure V	117
4.3.5	PCT curve of the V4Cr4Ti alloy prepared by aluminothermy process at 330K	119
4.4.1	Variation of Sieverts constant with temperature and aluminum concentration	122
4.4.2	$\log(K_s)$ versus $1/T$ plot for entropy and enthalpy calculation	123
4.4.3	Variation of standard enthalpy and entropy with aluminum content	124
4.4.4	Variation of Gibbs free energy of hydrogen solid solution as function of aluminum content	125
4.4.5	Steps involved in hydrogen absorption process	127
4.4.6	Thermogravimetric curve for hydrogen absorption in V-Al alloys	130
4.4.7	α -t kinetics curve for the hydrogen absorption in V-Al alloys	130
4.4.8	Reaction mechanism function curve for hydrogen absorption in V-Al alloys	131
4.4.9	Arrhenius plot for Activation energy calculation	132
4.4.10	Isothermal instantaneous pressure curves of (a) V5wt% Al (b) V10wt% Al (c) V14wt% Al alloys	133

4.4.11	Reacted fraction α -t curves of hydrogen absorption at different temperatures in (a) V5wt%Al (b) V10wt%Al (c) V14wt% Al alloys	134
4.4.12	Mechanism function of hydrogen absorption in (a) V5wt%Al (b) V10wt%Al (c) V14wt%Al alloys	135
4.4.13	(1) Arrhenius plot of hydrogen absorption reaction rate in (a) V-14wt%Al (b) V-10wt%Al (c) V-5wt % Al alloys.(2) Variation of activation energy with aluminum contents	136
4.4.14	XRD analyses of (a) V14wt%Al (b) V10wt%Al and (c) V5wt%Al after hydrogenation	138
4.4.15	Weight gain curve due to hydrogenation of V4Cr4Ti alloy during the continuously heating process. (b) Isothermal weight gain curve during hydrogenation of V4Cr4Ti alloys at different temperatures	140
4.4.16	(a) Reacted fraction curves of hydrogen absorption in V4Cr4Ti alloys at different temperatures b Hydrogen absorption rate curve with respect to time and temperature of V4Cr4Ti alloy at different temperatures	142
4.4.17	Relation of reaction function with time in different hydrogen absorption reaction stages of V4Cr4Ti at 373 K (a)Incubation period; (b) first hydrogen absorption period; (c) second hydrogen absorption period	144
4.4.18	Relation of reaction mechanism function with time in different hydrogen absorption reaction stages of V4Cr4Ti at 413 K (a) First hydrogen absorption (b) Second hydrogen absorption period	145
4.4.19	(a) Relation of common mechanism functions with time for hydrogen absorption in V4Cr4Ti between 373 K and 773 K (b) Arrhenius plot of hydrogen absorption reaction rate in V4Cr4Ti alloy	146
4.4.20	SEM Microstructure of (a) as prepared composite (b) After 20 hydriding-dehydriding cycle.	148
4.4.21	Phase analysis of composite using X-Ray analysis technique	149
4.4.22	Isothermal hydrogen absorption kinetic curve	150
4.4.23	Relative hydrogen absorption equilibrium time	150

S. No.	Table captions	Page No.
1.1	Important properties of metallic vanadium	6
2.1	Kinetics data of different alloys of vanadium	39
2.2	Effect of alloying elements on enthalpy and entropy changes for formation and dissociation of γ -dihydride, hysteresis factor, slope of plateau and hydrogen absorption rate of V-Ti based alloys	40
3.1	Mechanism functions responsible for the hydrogen absorption process	63
4.1.1	Effects of slag flux and fluidizer on the % yield of V-Al thermit	83
4.1.2	Chemical composition of a typical V-Ti-Cr alloy	90
4.2.1	Chemical composition of vanadium metal and vanadium-aluminum alloys	98
4.2.2	Composition of the V-Al alloys the present investigation analyzed by chemical analysis	101
4.4.1	Standard enthalpies and entropies of solution of hydrogen in vanadium aluminum alloys	124
4.4.2	Three dimensional diffusion mechanism involved in the gas solid reaction which is used in the present study to select the suitable mechanism function	128
4.4.3	Chemical composition of the crude thermit	129
4.4.4	Chemical composition of V-Al alloys used in the present investigation	133
4.4.5	Temperature depended kinetics parameters, mechanism equation and apparent activation energies in V-Al alloys	136
4.4.6	Chemical composition of V4Ti4Cr alloy	139
4.4.7	Temperature depended kinetics parameters and mechanism equations of V4Cr4Ti alloy	146

Acronyms

K_s	: Sieverts constant
K	: Kelvin/Kilo
T	: Temperature
n	: Number of mole
H	: Enthalpy
S	: Entropy
G	: Gibbs free energy
t	: Time
ν	: Frequency
α	: Phase (solid solution)/ reacted fraction
β	: Hydride Phase (VH/V ₂ H)
γ	: Hydride phase VH ₂
ω	: Weight
μ	: micron
ϵ	: Nonstoichiometric phase
Ω	: Resistance
Δ	: Change
m	: Mass
E_a	: Activation energy
P_a	: Pascal
<i>a.u.</i>	: arbitrary unit
p	: pressure
χ	: Mole fraction
Ψ	: Wave function
h	: Planks constant
ρ	: density
σ	: Conductivity
V	: Volume
f	: Fugacity

Chapter... 1

Introduction

Contents

1.1 Hydrogen storage methods: a review.....	3
1.2 Vanadium: a wonderful metal.....	6
1.3 Theory of metal-hydrogen interaction.....	9
1.4 Metal-hydrogen reaction: mechanism and kinetics.....	11
1.5 Thermodynamics of metal-hydrogen system.....	15
1.6 Aim and objectives of present Ph.D project.....	17

1.1 Hydrogen storage methods: a review

Energy options for the future are being explored and investigated to control the global warming and reduce the dependence over the limited crude oil and other fossil fuels. Nuclear fission based alternate energy option is promising. However, high capital investment, radioactive waste management and public acceptance are the major factors to its continued application. Tidal, wind, hydro and the solar energy are the other energy options available in the environment. However, most of these options have low energy density. Besides, the large area required for solar energy and the geographical region specific nature of many of these have restricted their applications. Hydrogen is being actively evaluated as an alternative, portable and eco-friendly energy carrier for domestic and commercial/industrial applications [1-4].

The fusion reactor program is based on magnetic confinement of deuterium–tritium (D-T) plasma in a configuration that not only aims at high grade heat extraction from the plasma but also breeding of tritium in the blanket by nuclear transmutations in the ceramic breeder (Li_2TiO_3) and the lead lithium coolant ($\text{Pb}_{83}\text{Li}_{17}$) [5]. The tritium thus produced will be purged out by helium and separated from the helium purge gas using suitable gas permeation and collection system. The selection of the suitable tritium permeable material to be used for the segregation of tritium efficiently and effectively from the helium is a subject matter of the investigation. Tritium being an isotope of hydrogen, behaves essentially similar to hydrogen in this matter and hence study of hydrogen interaction with the potential hydrogen permeable materials will prove useful for the tritium as well.

Hydrogen production, safe storage and transportation are the major issues in the context of the application of hydrogen as portable fuel in various devices. A number of investigations have been carried out on the production of hydrogen. However, on the safe storage and transportation of hydrogen, the investigations are actively continuing. Hydrogen

could be stored and transported by various methods. These can be generalized into three groups, gas liquid and solid forms. Each one of it has its own advantages and limitations as described below.

Gas

Storage of hydrogen as a gas at high pressures in steel container is a mature technology. However, the volumetric energy density of hydrogen is low compared to gasoline. In fact volumetric energy density is seven times lower than gasoline even at 700 bars pressure. Another issues is the relatively large contribution from the container material to the overall weight of the storage system which is reducing the gravimetric energy storage density. Composite materials with higher tensile strength than steel are under development which may offer improved gravimetric hydrogen storage density. These are serious safety issues relating to high pressure hydrogen storage.

Liquid

Another potential hydrogen storage method is in the liquid form using cryogenic vessel. Liquid hydrogen is usually stored at 20 K at ambient pressure in open systems to prevent pressure build-up. The advantage of liquid hydrogen is its high gravimetric energy density, whereas the drawback is a low volumetric energy density. Another drawback is the energy used for liquefying which amounts up to 40% of the energy content of the liquefied hydrogen.

Solid state

Hydrogen storage in solid state materials is diverse. The methods which recently have attracted most attention are storage in metal hydrides and hydrides of intermetallic compounds which is based on the fact that many metallic and intermetallic systems reversibly absorb large quantities of hydrogen. Hydrogen storage in the form of metal and intermetallic hydrides can roughly be grouped into low temperature hydrides which release hydrogen at

one atmosphere and at room temperature but with hydrogen capacity restricted to less than 2.5 weight percent of hydrogen for example $\text{FeTiH}_{1.8}$, LaNi_5H_6 , $\text{V}(\text{TiCr})\text{H}_2$ and high temperature hydrides which require heating to 500K or above for hydrogen desorption but with hydrogen capacities up to 12.6 weight percent hydrogen, for example LiH , B_2H_6 . The volumetric energy density of solid state hydrogen is usually higher than liquid hydrogen as well as compressed hydrogen gas at high pressure.

Currently compressed gas and liquid hydrogen are used in fuel cell powered automobiles. However, issues such as safety and the need for a hydrogen supply infrastructure have to be resolved. Solid-state hydrogen storage systems are expected to be simpler for the engineering design of vehicles and considerably safer than the liquid or gas storage of elemental hydrogen.

The high solubility of hydrogen in vanadium because of its bcc crystal structure and rapid rate of diffusion at elevated temperatures make vanadium a key component in devices for hydrogen storage and permeable applications [6-9]. The terminal solid solubility and absorption capacity of hydrogen in the vanadium based alloys is high particularly when alloyed with Cr and Ti [10-11]. However in the future, some issues are still to be resolved in the development of vanadium based hydrogen storage and permeable membrane [12]. These include, synthesis route, surface properties, chemical treatment during the hydrogen charging; mechanical treatment made on the materials in order to enable the gas adsorption inside the bulk; the amount of reactive surface taken into account in the gas adsorption calculations and the presence of impurities which can contribute to modify the electronic density in Fermi level of the host matrix [13]. Therefore, it is essential to elucidate the gas absorption mechanism in the solid materials.

1.2 Vanadium: a wonderful metal

The metal vanadium has several unique physical, chemical, mechanical and nuclear properties and its alloys are potentially useful in number of high technology applications. The physical and chemical properties of vanadium metal are given in the Table 1.1.

Atomic number	: 23
Atomic weight	: 50.94
Crystal structure	: bcc
Density kg/m ³	: 6100
Melting point °C	: 1910
Boiling point °C	: 3450
Vapor pressure at melting point , Pa	: 2.70
Thermal expansion coefficient at 20°C-100°C per °C	: 8.3 x 10 ⁻⁶
Thermal conductivity at 25°C W/m.K	: 60.00
Electrical resistance at 20°C , μΩ cm	: 0.25
Superconductivity temperature, K	: 5.13
Young's modulus, GPa	: 130
Poisson's ratio	: 0.36
Ultimate tensile strength , MPa	: 190
Yield strength. MPa	: 103
Elongation. %	: 39
Hardness VPN	: 55
Thermal neutron absorption cross-section, m ² /atom	: 4.7x 10 ⁻²⁸
Capture cross section for fast (1MeV) neutrons , m ² /atom	: 3x 10 ⁻³¹

Vanadium is a soft ductile metal with a low density and fairly high melting point. Its thermal conductivity is significantly lower than copper but better than all other refractory metals. The elastic modulus of vanadium is considerably higher than titanium. The metal has good mechanical properties and these properties are remarkably improved by alloying. Vanadium has low absorption cross-section for thermal neutrons and its capture cross-section for fast neutrons is also low. Its superconducting transition temperature is above the liquid helium temperature and some alloys and intermetallic compounds of vanadium exhibit highly enhanced superconducting properties with improved high field capabilities. Vanadium exhibits good corrosion resistance in a variety of chemical media. The metal has good resistance to attack by sea water though not as good as titanium.

Vanadium is resistant to attack by hydrochloric acid, dilute sulphuric acid and by alkali solutions. Oxidizing acids like nitric acid, hydrofluoric acid and concentrated sulphuric acid attack vanadium. The metal however exhibits excellent corrosion resistance towards molten alkali metals like lithium, sodium and the eutectic alloy Pb-17Li. Massive vanadium is relatively inert towards oxygen and nitrogen at room temperature. The metal is quite prone to oxidation and nitridation when hot. It picks up oxygen and nitrogen and these elements severely embrittle the vanadium. Vanadium reacts with chlorine at 180°C and forms volatile chlorides. The reaction with fluorine leads to the formation of a hard surface layer of vanadium fluorides which to some extent prevents further reaction. Bromine and iodine react with vanadium at high temperature and high pressure. There are several important potential uses of pure vanadium metal. Pure vanadium is used to prepare alloys like V-Ti-Cr which are considered as a suitable structure material for the fusion reactor. They are also considered as materials for use as cladding for uranium oxide fuel in liquid metal cooled fast breeder reactor. These uses have been based on vanadium alloy's excellent stability to neutron irradiation, high temperature creep strength, and corrosion resistance in molten metals.

Besides, vanadium is a neutron transparent and also a low activation metals i.e. it does not undergo nuclear transmutation to radioactive isotopes of long half life. Another important application of vanadium is in the area of high field superconductivity in which the intermetallic compound V_3Ga excels. Even though its transition temperature is 15.4 K which is much lower than 18.3 K of Nb_3Sn , the vanadium compound exhibits better superconducting characteristics than Nb_3Sn at fields larger than 11 T. V_3Ga is prepared from the pure elemental compounds by a process generally known as the bronze process in which the conductor is first fabricated in the final form and the superconducting phase is formed by heat treatment.

The Laves phase alloys $V_2(Zr, Hf)$ have also been described as usual superconducting materials. Vanadium is also used as diffusion barrier between copper and tin in commercial multifilamentary Nb_3Sn superconductor. Vanadium is a component in commercial Fe-Co magnetic materials known by trade name Permendur, Supermendur and Vicalloy. In the new class of materials known as the long range ordered alloys, vanadium finds use in such composition as $(Fe, Co, Ni)_3V$. These alloys exhibit high yield strength at high temperatures and among their other uses, application as fusion reactor materials has also been suggested on account of their good resistance to irradiation induced swelling. Vanadium is also useful in the bonding of titanium to steel. Vanadium is a vital component in a number of titanium alloys used in the aerospace industry. Most important among them is the alloy Ti-6Al-4V. In the manufacture of this alloy vanadium is added in the form of V-Al master alloy. Vanadium is also added to aluminum and copper alloys resulting in significant enhancement in their physical and mechanical properties. The most important application of vanadium is as additive to steels and iron. Vanadium added in small quantities (usually a fraction of 1%) produces grain refinement and hardening ability in steels, imparts wear resistance, weldability,

and high temperature strength. It is used mainly in the high strength low carbon alloys (HSLA) steels, tool steels, alloy steel, plain carbon steels, forging steels and cast iron.

It is this application which supported the very existence of vanadium industry. Another application of vanadium mainly as vanadium pentoxides, ammonium metavanadate and vanadium oxytrichloride, is in the commercial industry as oxidation catalyst in a variety of commercially important processes ranging from the manufacture of sulphuric acid to the production of ethylene propylene rubbers such as the EPDM rubber for the automobiles. The metals hydrogen interaction characteristics may earn vanadium a great role in the hydrogen storage/permeable application.

1.3 Theory of metal-hydrogen interaction

Transition metal hydrides have a range of properties and hydrogen interaction behavior. The hydrides formed by the early transition metal hydrides are generally very stable. Titanium hydride, TiH₂ requires heating to above 723 K for decomposition and on moving to right in the periodic table the hydrides become less stable. Around the middle of the transition metals (Mn, Fe) the stability goes through a local minimum. The late transition metals are unstable under ambient conditions [14] for example, CdH₂ decomposes at 93 K. The bonding characteristics of transition metal with hydrogen are excellent as these are purely metallic in character [14]. The formation of transition metal hydride is a very complex process and the overall process could be expressed by the following reaction:



The reaction is exothermic and the it is misleading from the kinetics point of view as the formation of metal hydride does not occur in single step reaction.

The overall reaction between the gas phase hydrogen and a solid metal is schematically illustrated in Fig.1.1 where the one-dimensional Lenard-Jones Potential (LJP) of atomic hydrogen (orange line) and molecular hydrogen is shown (maroon line) [1]. Far

away from the surface, the two lines are separated by molecular hydrogen dissociation energy which is 218 kJ per mole of hydrogen. Hydrogen molecule moving towards the surface will start sensing a Vander Waals attractive force (point 1 in Fig 1.1). However this is weak force (0-20 kJ per mole of hydrogen). Furthermore, as the molecule moves closer to the metal surface the potential energy increases due to repulsion and at some point potential energy of the hydrogen molecule will intersect with the potential energy of the atomic hydrogen. Beyond this point, it is essential that two hydrogen atoms bonded to the metal surface rather than bonded to each other. Hence dissociation will occur. If this intersection is at a potential energy larger than zero relative to gas phase hydrogen (point 2) dissociation is said to be activated and the height of point 2 determines the activation barrier. If the intersection is located at approximately zero potential energy, dissociation is said to be non-activated (point 3). In the former case only a fraction of hydrogen molecules with energy larger than the activation barrier will be able to dissociate.

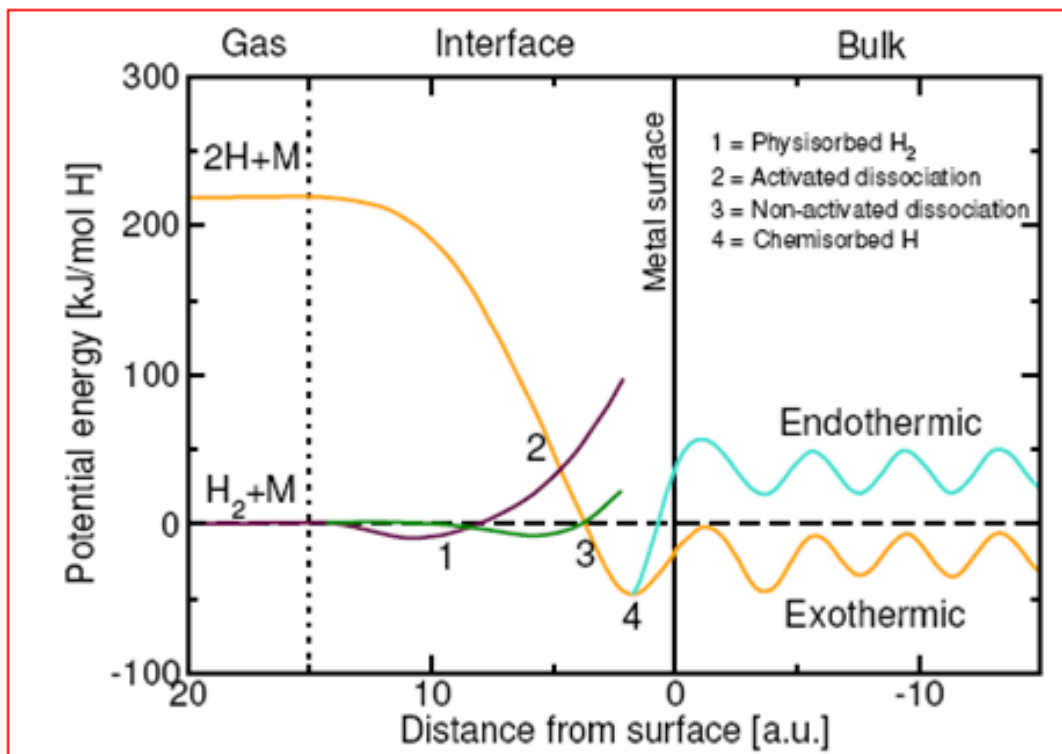


Fig 1.1: Simple schematic Lennard-Jones potential energy diagram of chemisorption of hydrogen on metals [1]

After dissociation of the hydrogen atoms, a potential energy minimum is shown as point 4 which corresponds to the hydrogen atoms being bonded to the metal surface and the process is known as chemisorption. The exothermicity or endothermicity of the chemisorption reaction would be decided by the strength of hydrogen-metal and hydrogen-hydrogen bonding. Beyond the point of chemisorption, the hydrogen atoms can penetrate the first metal atomic layer into the subsurface through an activated process from which it can diffuse into the bulk of the metal and form a metal-hydrogen solid solution. If the potential energy of bulk hydrogen atoms is below zero relative to gas phase hydrogen, hydrogen solid solution is said to be exothermic, likewise if the potential energy of bulk hydrogen atoms is above zero hydrogen solid solution is said to be endothermic.

1.4 Metal-hydrogen reactions: mechanism and kinetics

A schematic visualization of the interaction of hydrogen with a metal is given in Fig 1.2. The figure shows all the individual reaction steps including those in the bulk of the metal. The formation of the metal hydride can be divided into the following elementary reactions [15].

Dissociation/adsorption

The first step is the dissociative adsorption of hydrogen on the metal/intermetallic/hydride surface.

Surface penetration

From the surface the hydrogen atoms penetrate into the sub-surface.

Bulk diffusion

From the sub-surface, the hydrogen atoms can diffuse into the bulk or from the bulk into the matrix.

Hydride formation

Hydrogen atoms in the bulk (corresponding to a solid solution) can precipitate into hydride nuclei which can grow to larger hydride grains by trapping of additional hydrogen atoms. The formation of a hydride phase complicates the picture somewhat since hydrogen diffusion can also take place through the hydride [16]. For dehydrogenation, the process is the reverse i.e. the hydride phase decomposes and hydrogen atoms diffuse to the sub-surface and subsequently to the surface, where the hydrogen atoms recombine and desorb as H_2 .

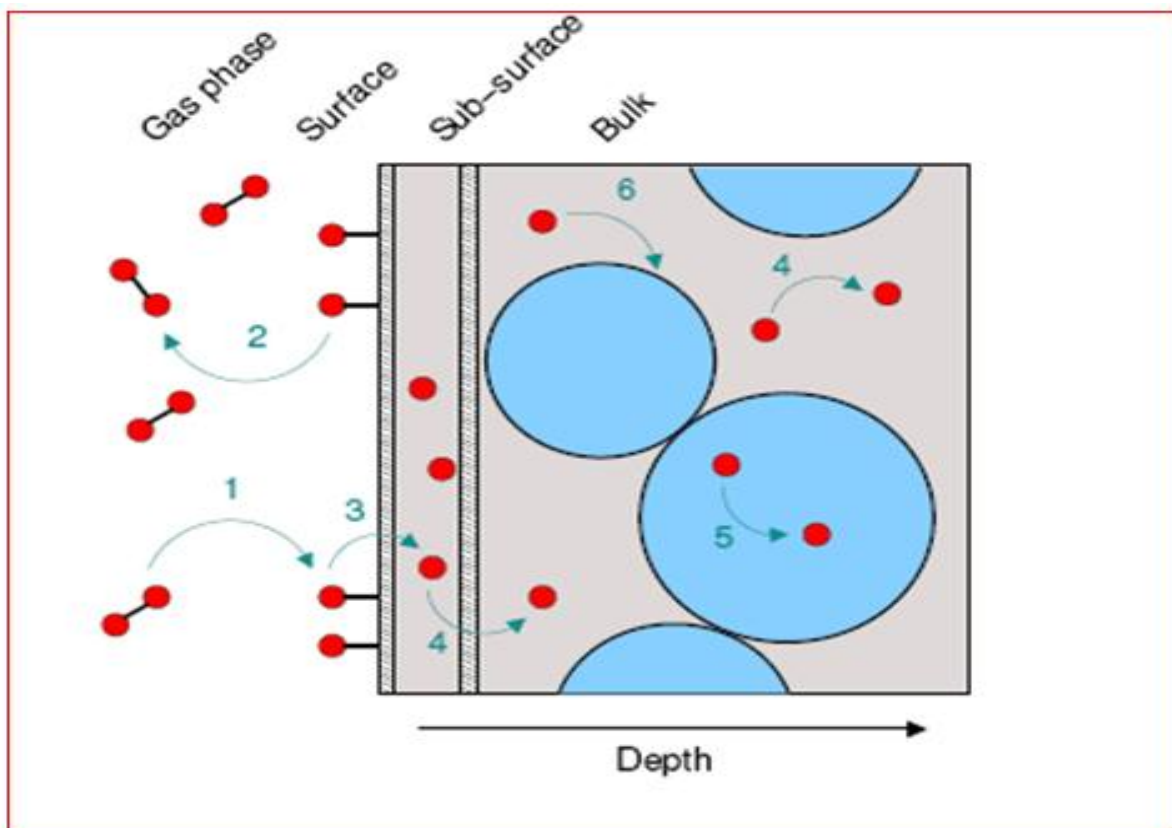
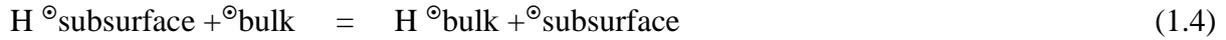
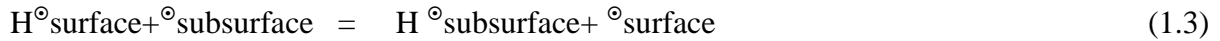


Fig. 1.2: Schematic illustration of the different mechanisms involved in the formation of a metal hydride. Hydrogen atoms are shown in red, the metal host lattice is shown in grey, and the metal hydride is shown in blue 1: surface attraction 2: desorption because of molecular attraction 3: Physisorption and subsurface penetration 4: Bulk diffusion 5: Diffusion through the hydride phase 6: hydride phase attraction [1]

A reaction mechanism can be proposed on the basis of the above reversible elementary steps. The dissociation, surface penetration and diffusion are written out in simplified manner for illustration as follows:



The free site where one hydrogen atom can attach is denoted by ‘ \ominus ’. The overall rate could be decided by each of the elementary reactions. By working out a material balance and suitable choice of geometry along with appropriate initial and boundary conditions, one can solve for the hydrogen concentration both as a function of space as well as time without a priori choice of a rate limiting step. When experimental kinetic data is fitted with a rate equation, hydride nucleation or growth or two/three dimensional diffusion process seems to be popular choices for the rate limiting process. When examining the shape of the experimental hydrogenation or dehydrogenation curves, i.e. macroscopic hydrogen uptakes/releases as a function of time, two major patterns emerge, one with a monotonically decreasing uptake rate and one with a sigmoidal shape. The two classes are shown in Fig 1.3. The former corresponds to curve A and the latter corresponds to curve B. Curve A is usually rationalized in terms of either a surface process such as dissociation or a bulk diffusion as the rate limiting step. Curve B is usually rationalized in terms of a nucleation and growth mechanism limiting the overall kinetics. Nucleation and growth kinetics is usually explained by a Johnson-Mehl-Avrami (JMA) rate equation [16-18]. The JMA equation has the following form:

$$\alpha(t) = 1 - \exp(-(k(T)t)^n) \quad (1.5)$$

The parameters describing nucleation and growth rates are contained within an effective kinetic parameter, $k(T)$. The exponent, n , is often referred to as the Avrami exponent. The temperature dependency of the rate constant $k(T)$ is usually described by an Arrhenius relation.

$$k(T) = A e^{-E_a/RT}, \quad (1.6)$$

Where A is a frequency factor or pre-exponential factor, R is molar gas constant and E_a is the activation energy. The JMA equation explains not only curves with a sigmoidal shape, but also parabolic curves where diffusion may be rate limiting, where n is allowed to have values of 1 or less. This is probably why the JMA model is often applied when dealing with the kinetic of hydrogenation and dehydrogenation of metal hydrides and its use sometimes results in conclusions about a diffusion process being rate limiting because during deviation of the JMA equations diffusion process has been considered. It is also interesting to note that a sigmoidal uptake curve can be result of a hydride with a protective surface oxide layer as observed for vanadium-aluminum alloy.

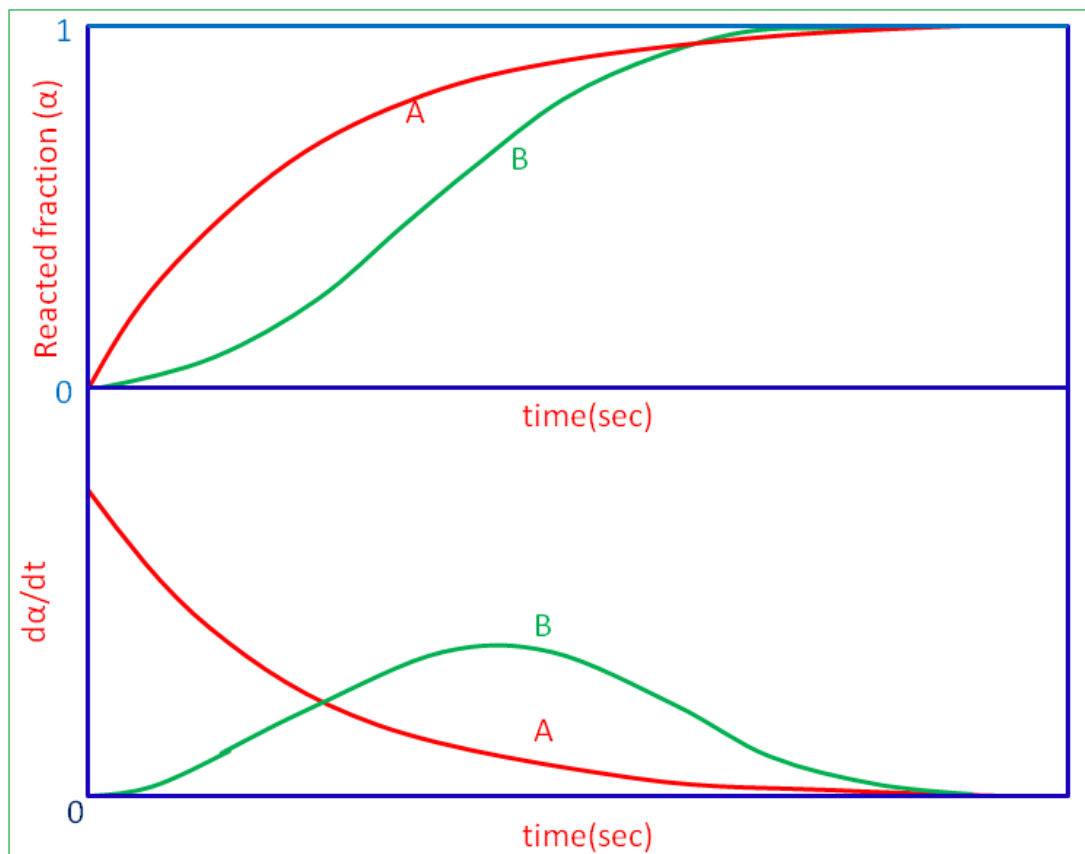


Fig. 1.3: Two major classes of hydrogenation/dehydrogenation curves. The hydrogen uptake is shown in the upper part; the hydrogenation rate is shown in the lower part

During the first hydrogenation, cracks are developed in the oxide layer due to the volume expansion of the hydride formed underneath. Even though the JMA equation

provides a good linear fit, any conclusions about nucleation and growth being rate limiting in such a process should be examined carefully.

1.5 Thermodynamics of metal-hydrogen system

The Pressure Composition Isotherm

Several key properties of a metal hydride summarises by the pressure composition isotherm (PCI). A typical PCI curve is shown in Fig 1.4.

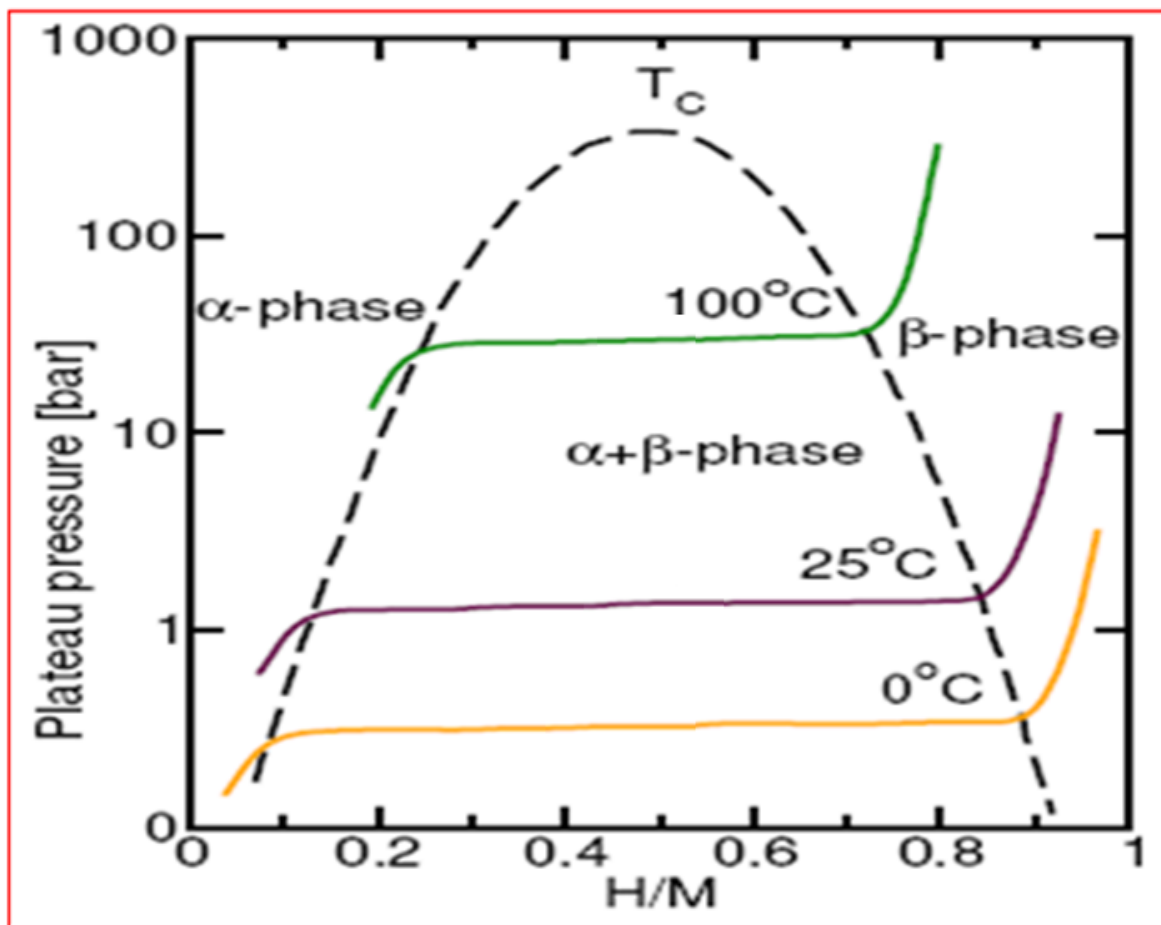


Fig. 1.4: Pressure-Composition-Isotherms (PCI) for a hypothetical metal hydride [1]

At a particular temperature, the amount of absorbed hydrogen (H/M is the hydrogen to metal stoichiometric ratio) slightly increased with pressure. This corresponds to the formation of a solid solution of hydrogen which is denoted as α phase. When the maximum

solubility of hydrogen in the α phase is reached the hydride phase (β phase) will start forming. Increasing the hydrogen pressure further will now result in a substantial increase in the absorbed amount of hydrogen.

The relation between the phase, component and degree of freedom for metal hydrogen system could be represented by usual thermodynamics relation as below:

$$F = C - P + 2 \quad (1.7)$$

Where F is the degree of freedom, P is the number of phases and C is the number of chemical species. Thus, existence of one additional phase leads to the loss of a degree of freedom. The pressure at which this transformation takes place is referred as the plateau pressure and in this region α phase and β phase co-exist. When the stoichiometric hydride has formed completely depleting α phase one additional degree of freedom is regained and the additional absorption of hydrogen will now require a large pressure increase. This corresponds to the solid solution of hydrogen in the β phase. The plateau pressure gives valuable information about reversible storage capacity from the width of the plateau and the position of the plateau at a given temperature may give an idea of the stability of the hydride. Stable hydrides will require higher temperatures than less stable hydrides to reach a certain plateau pressure.

Thermodynamic properties from PCI

Enthalpy and entropy are two basic thermodynamic parameters which can be related to equilibrium solid solubility of hydrogen, in α phase. These two parameters are related to the Sieverts constant K_s as follows [19]

$$\ln K_s = \frac{\Delta H^\circ}{RT} - \frac{\Delta S^\circ}{R} \quad (1.8)$$

Where, K_s is a Sieverts constant, ΔH° and ΔS° are the standard enthalpy and standard entropy of metal- hydrogen solid solution, respectively. The Sieverts constant at a particular pressure and temperature has been obtained by using Sieverts law [20]:

$$H/M = K_s \sqrt{p} \quad (1.9)$$

Where H/M is the hydrogen to materials ratio within the solubility limit.

Using equation 1.8 and equation 1.9 standard enthalpy and standard of gas solid reaction could be investigated. Using standard enthalpy and standard entropy standard Gibes free energy could be calculated using relation as:

$$\Delta G^0 = \Delta H^0 - T\Delta S^0 \quad (1.10)$$

Where, ΔG^0 is Gibbs free energy and other symbols have their usual meanings.

The hydride formation enthalpy of different metal hydrides are presented in Fig. 1.5.

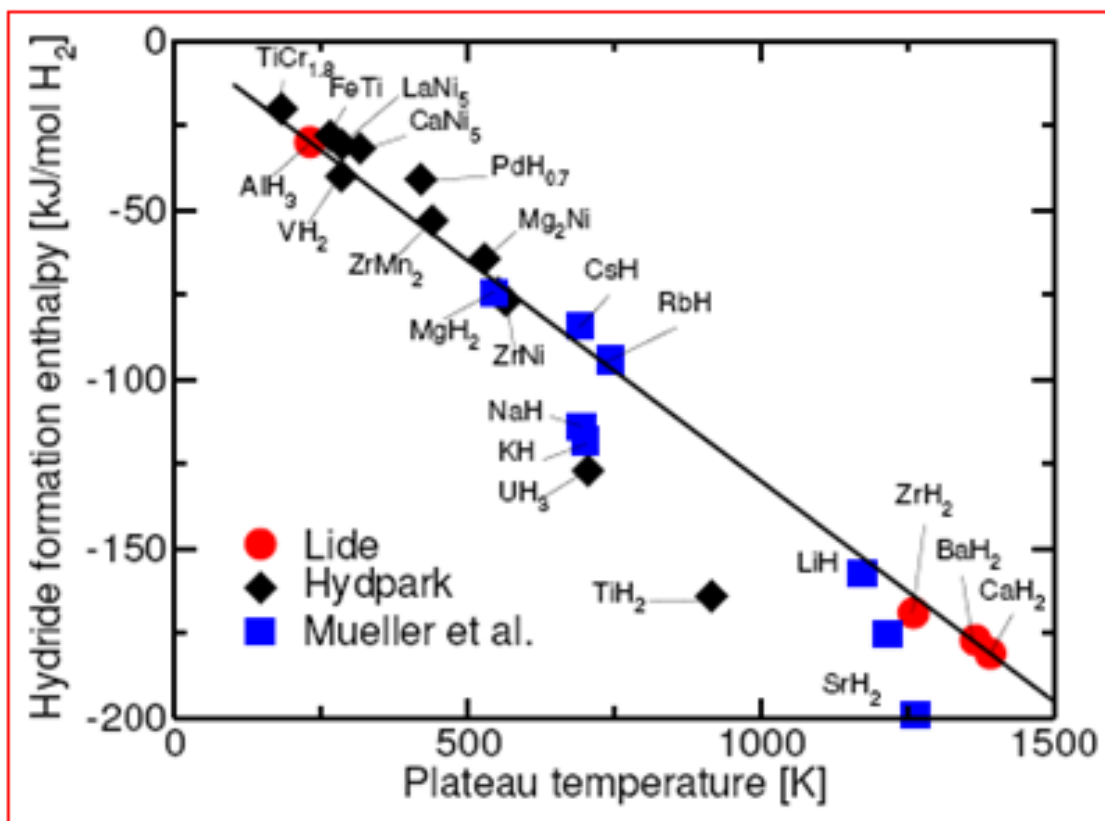


Fig. 1.5: Hydride formation enthalpy, ΔH_f per mole hydrogen as a function of the plateau temperature at 760 Torr [1]

1.6 Aim and objectives of present Ph.D project

The aim of the present study is to examine the hydrogen-vanadium interaction and the effects of alloying element aluminum with vanadium on this interaction. The objectives of the present investigation can be summarized as follows and diagrammatically shown in Fig 1.6.

- ✎ Preparation and characterization of vanadium, vanadium-aluminum and V-Ti-Cr alloys by thermit process, electron beam melting and vacuum arc melting.
- ✎ Study on terminal solid solubility of hydrogen in metallic vanadium as a function of temperature and hydrogen pressure.
- ✎ Effects of aluminum on the terminal solid solubility of hydrogen in vanadium.
- ✎ Determination of standard enthalpy and standard entropy of vanadium-hydrogen solid solution using Sieverts equation and differential thermal analysis.
- ✎ Study on the effects of aluminum on standard enthalpy and entropy of vanadium-aluminum hydrogen solid solution.
- ✎ Study on the hydrogen absorption kinetics and mechanism of vanadium and V-Al alloys
- ✎ Study on hydrogen absorption kinetics and mechanism of V₄Ti₄Cr alloy
- ✎ Pressure composition isotherm (PCT) curve of pure vanadium and V₄Cr₄Ti alloy
- ✎ Thermogravimetric study on the decomposition of vanadium hydride
- ✎ Effects of Aluminum on the decomposition pattern of vanadium hydride.
- ✎ The kinetics and mechanism of hydrogen solubility of V-LaNi₅ composites.

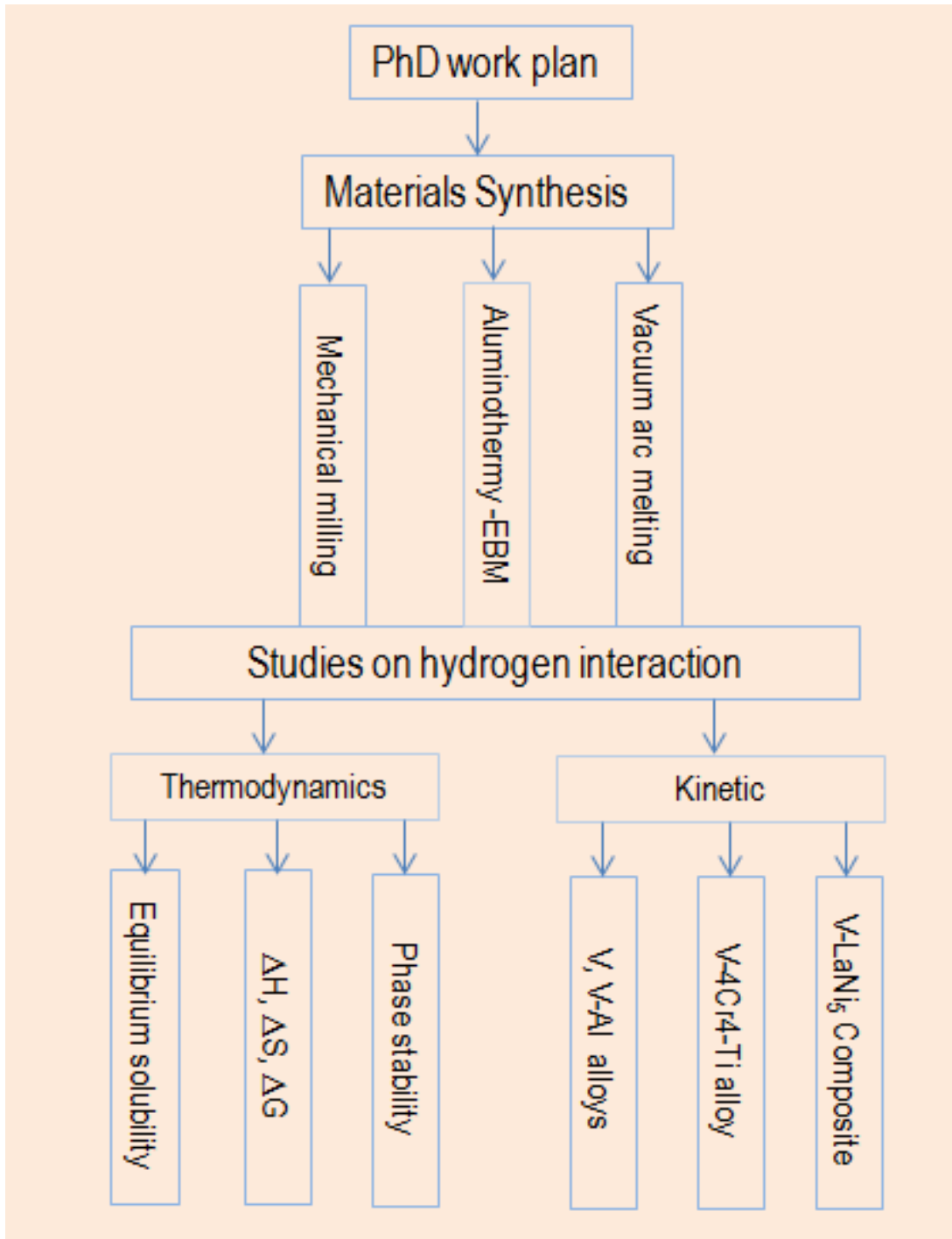


Fig. 1.6: Schematic work plan of the Ph.D program

Chapter... 2

Review of literature

Contents

2.1 Introduction.....	22
2.2 Hydrogen absorption-desorption in vanadium metal.....	23
2.3 Vanadium hydride phases stability.....	28
2.3.1 VH_2 (γ) phase stability.....	28
2.3.2 V_2H and $V(H)$ (β and α) phase stability.....	29
2.4 Storage capacity of vanadium base alloys.....	30
2.4.1 Binary alloys.....	30
2.4.2 Ternary alloys and laves phases.....	32
2.5 Kinetics and thermodynamics.....	38
2.6 Electronic consideration of hydride stability and absorption capacity.....	42
2.7 Hydrogen diffusion and permeation.....	45
2.8 Summary and conclusions.....	49

2.1 Introduction

Achieving sustainable energy supply-clean environment combination is a major challenge at present for the scientists and engineers. Global efforts to decrease the global warming problem by reducing the CO₂ emission and a disaster of Chernobyl revived the search for alternative energy option. In this context, all three isotopes of hydrogen, (H, D, T) are poised to emerge as most important element both in primary electric power generation and as energy carrier in energy transportation [21]. On the one hand controlled and sustainable D-T fusion is the most important technological breakthrough anticipated with energy sector and on the other hand hydrogen is being considered as an ideal high density energy carrier for a multitude of industrial and household applications [2, 22-23]. It is a non polluting medium for the storage and transportation of energy. The portability of hydrogen is based on the sophistication of hydrogen storage methods [24]. Present potential hydrogen storage methods are hydrogen gas at high pressure and cryogenic liquid at low temperature (20 K). Each mode of storage system has its own technology and safety issues. For example, safety is the major concern related to the storage and transportation of hydrogen in the form of compressed gas. Storage in the form of liquid hydrogen is impractical for the commercial and domestic application as it requires expensive and unwieldy cryogenic vessel because hydrogen gas has good energy density by weight but poor energy density by volume. The physically or chemically combined form of storage of hydrogen in suitable materials has potential advantages [7]. In this regard, metals and intermetallic materials are a class of promising and effective media because of high storage capacity at relatively low equilibrium hydrogen pressure and maintaining the volumetric density even better than that of liquid hydrogen [7, 25]. It is interesting to note that hydrogen acts mainly as a metal when it is absorbed in transition metals and consequently the interaction mechanism of hydrogen with metal and intermetallic is quite interesting [18]. A wide range of stoichiometric and non-

stoichiometric compounds form when metals interact with the hydrogen. Hydride of single phase has limited application in hydrogen storage application because of the high thermodynamic stability of these hydrides [20]. Therefore, investigations were carried out for a wide range of alloys with two or more components in order to find out the materials that meet the practical requirements [21].

Generally alloy hydrides show complex thermodynamic behaviours and phase diagrams than the pure metal hydride. However, the absorption capacity is significantly increased and more suitable for commercial hydrogen storage applications [4]. As one kind of metal-based hydrogen storage alloys, vanadium based body centred cubic structure (bcc) solid solution alloys exhibited potentially attractive properties for practical application such as reasonably good hydrogen storage capacity and lower hydrogen absorption-desorption temperature particularly from the γ (VH_2) phase [26-28]. The main issues relating to the vanadium based alloys for commercial applications are poor initial activation and effective hydrogen absorption capacity [11, 29]. However, the absorption-desorption pattern and the effective hydrogen storage capacity could be possibly be improved by alloying with suitable elements [30-39].

2.2 Hydrogen absorption-desorption in vanadium metal

The mechanism of hydrogen absorption in vanadium metal initiated with the formation of vanadium-hydrogen solid solution (α phase) which on further hydrogenation precipitated as β_1 hydride phase (V_2H). Furthermore, first order phase transition from β_1 phase to β_2 phase (VH) progressed on further hydrogenation. Both of these phases (β_1 and β_2) are known as β phase. The structure of VH phase is shown in Fig 2.1. Finally, the γ phase (VH_2) is formed when the metal is fully hydrogenated [31]. For the β phase the first plateau hydrogen pressure for this hydride formation is very low at a moderate temperature [32].

Therefore, the hydrogen desorption reaction from the β phase never occurs at ambient temperature.

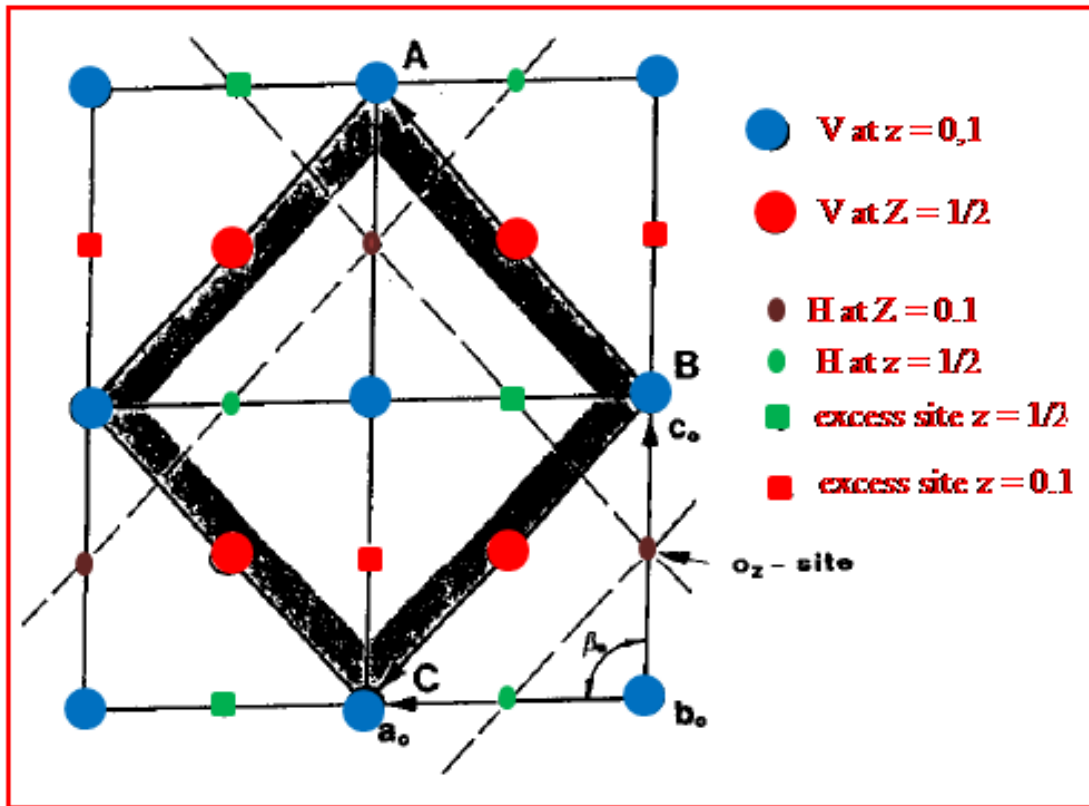


Fig.2.1: The monoclinic structure of the VH β phase. Most of the hydrogen atoms occupy octahedral sites

The γ phase is not so stable and hydrogen absorption and desorption reactions from this phase take place at moderate temperature and pressure as shown in the equation 2.1



Thus, only half the amount of hydrogen absorbed in vanadium metal could be used in the subsequent hydrogen absorption-desorption process. This amount is, however, not enough for practical applications of vanadium metal as hydrogen storage material [33-39]. The alloying elements have a great effect on the phase stability, absorption-desorption kinetics as well as the hydrogen absorption capacity [40-60]. However, there is a limitation of the alloying process for the modification to a desired properties, for example to improve the activation

process of vanadium based alloys the alloying element must have atomic radii at least 5% smaller than those of the vanadium matrix [41]. Another issue related to the good cyclic behavior and could be controlled by alloying with suitable alloying element is the pulverization as a result of hydriding-dehydriding cycles which eventually deteriorate the hydrogen absorption capacity and plateau pressure. Plateau pressure and absorption capacity are basically functions of electron to atom ratio as well as lattice constant. The existence of critical e/a ratio for the maximum absorption capacity is reported by Matumura et al. [41]. The e/a ratio could be controlled by suitable alloying element. The changes in the plateau pressure and absorption capacity are linearly related to lattice parameter of the alloy as well. The alloying elements which contract the host lattice raise the plateau pressure, whereas alloying elements which expand the host lattices decreases the pressure [42]. Aluminum is a very useful alloying component for all the refractory metals. It changes the desorption mechanism and reduces the activation temperature of many two component systems including vanadium [43]. The hydrogen absorption kinetics in vanadium and vanadium based alloys has been reported earlier by many researchers [44-47]. Kinetics of vanadium based hydrogen storage materials are compared with the laws of first order reaction kinetics or with Johnson-Mehl type equation [18-20]. The first order reaction is typical for homogeneous reactions in a single phase where the reaction rate is proportional to the amount of un-reacted reactant, but they are not suited for the description of a heterogeneous gas-solid reaction. The Johnson–Mehl model is not suited for the description of internal kinetics [18]. The absorbed solution of hydrogen in bcc vanadium forms α phase. In general, lattice parameter linearly increases with the hydrogen concentration indicating regular solid solution behavior. The relevant parameters are [26]:

$$[\Delta v/\Omega]_H = 0.196 \pm 0.003, a_0 = 3.02694 \pm 0.00002 \text{ \AA} \quad (2.2)$$

The term $[\Delta v/\Omega]_H$ is the volume requirement of an atom of isotope H divided by the atomic volume Ω of the pure host metal.

Hydrogen in general fits into the tetrahedral sites and is delocalized upon stress. In delocalized states the diffusion of hydrogen became much faster.

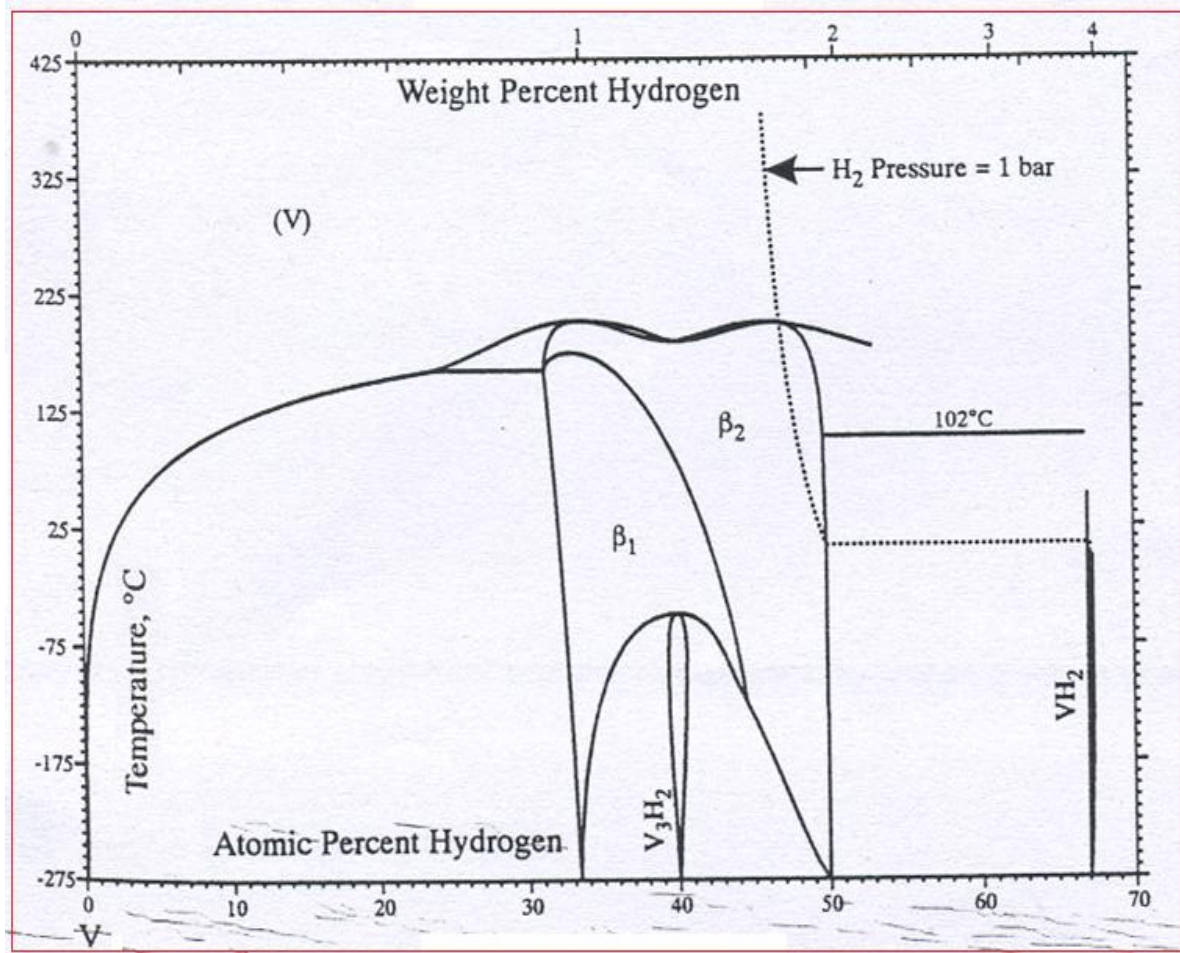


Fig. 2.2: Vanadium-hydrogen phase diagram at one atmosphere of hydrogen pressure [46]

The hydrogen concentration exceeding the terminal solid solubility precipitates as the hydride phase. Initially, the β ($V_{2-x}H_x$) phase forms at low temperature as shown in the vanadium –hydrogen phase diagram, Fig.2.2 which has a composition near to that of V_2H . Interestingly, it was found that the volume increase due to hydrogen absorption is practically pressure independent. Pauling [45] described the β structure as containing linear V-H-V

complexes, with V-H half-bonds with a bond length of about 1.76 Å. The ϵ ($V_{3-x}H_{2+x}$) phase is another high temperature phase formed by the modification of β phase in which hydrogen atoms are distributed in the four octahedral sites $[\frac{3}{4} 0 \frac{1}{4} \frac{1}{4} \frac{1}{2} \frac{1}{4}; \frac{1}{4} 0 \frac{3}{4}; \frac{3}{4} \frac{1}{2} \frac{3}{4}]$ with equal probability.

Another, low temperature phase is δ_H phase which has a composition V_3H_2 . The structure of this phase has been studied by Schober et.al [46]. In this hydride the octahedral interstitials (holes) are occupied. And every third layer of $[0 \bar{1} 1]$ is vacant while the other two layers fully occupied. On further hydrogenation γ phase (VH_2) is formed which has a face centered structure (fcc) [$a_0 = 4.24\text{Å}$]. This hydride is isomorphic with NbH_2 and has a CaF_2 crystal structure. These hydride phase structures are given in the Fig 2.3.

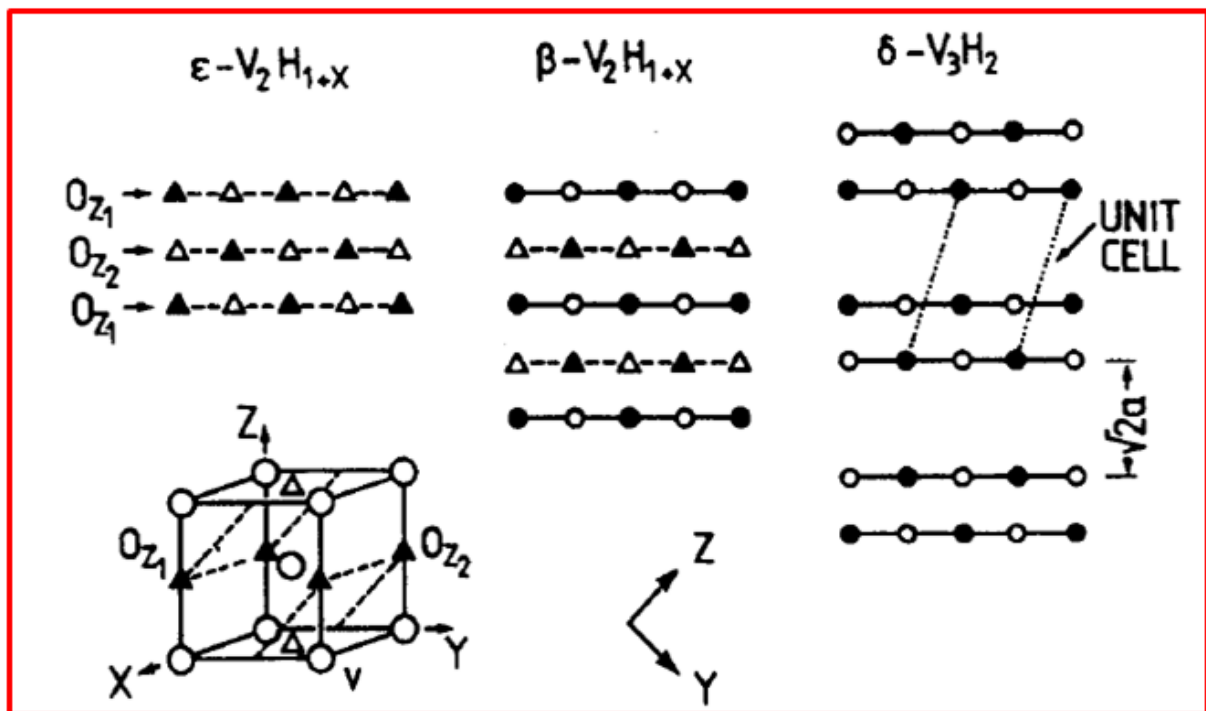


Fig. 2.3: The structure of hyperstoichiometric β , ϵ , δ vanadium hydride as projected on the (100) plane. Full and open triangle indicate partly filled O_z sites at $x=0$ and $\frac{1}{2}$, respectively. Full and open small circle denotes hydrogen atoms on the O_z sites of $x=0$ and $\frac{1}{2}$, respectively

TG-DTA study on fully hydrogenated vanadium [28] revealed the order of dehydrogenation as: $\gamma \rightarrow \beta \rightarrow \alpha \rightarrow \text{bcc V (H free)}$. The decomposition temperatures from these phases are 300 K, 450 K and 750 K respectively for the pure vanadium [28].

2.3 Vanadium hydride phase stability

2.3.1 VH_2 (γ) phase stability

The effect of alloying on the absorption-desorption from the γ hydride phase was studied by Yukawa et.al [42]. The results are summarized in Fig 2.4. As illustrated in the figures the stability of γ phase is strongly dependent on the alloying elements.

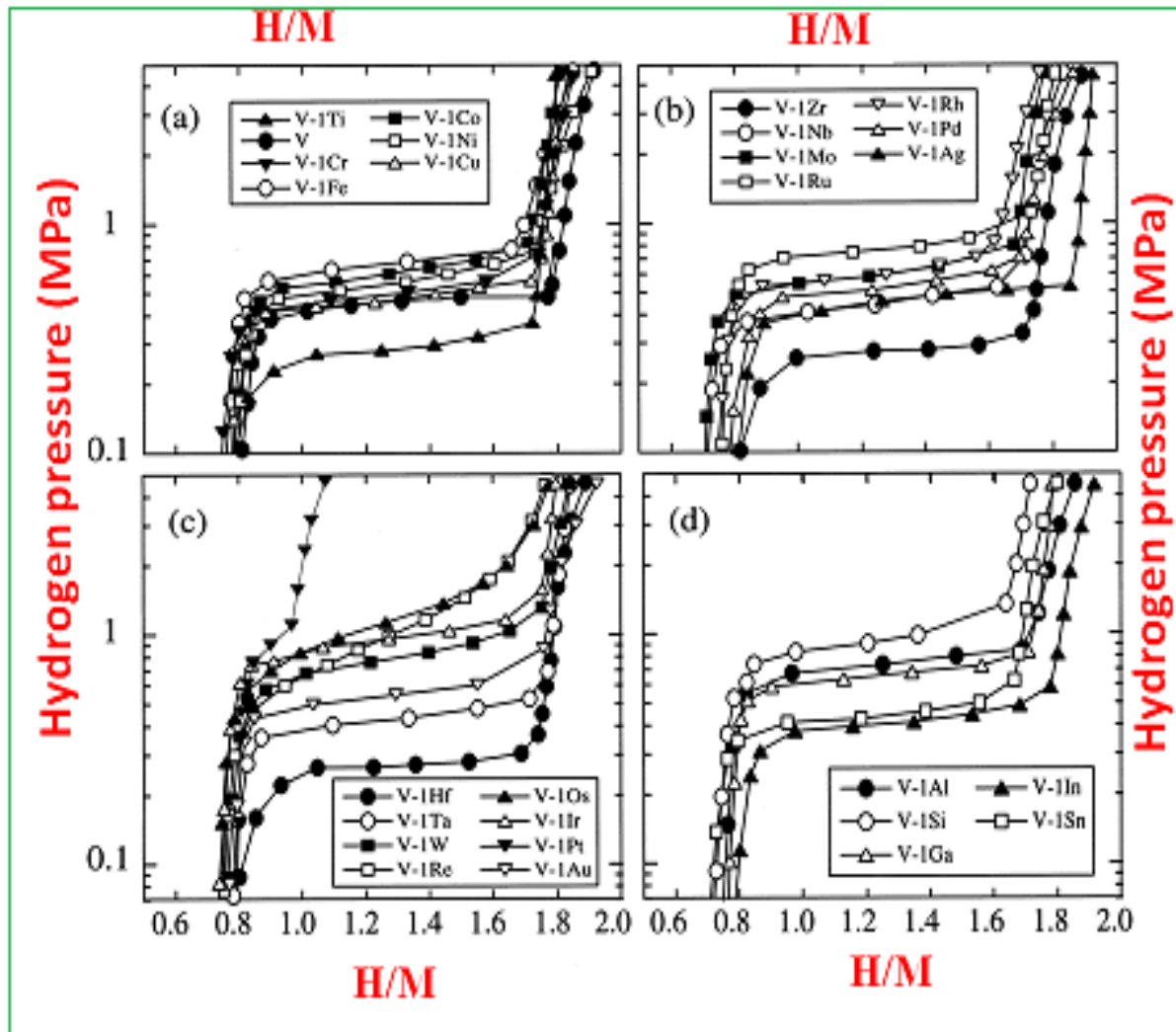


Fig. 2.4: Variation of plateau pressure corresponding to γ hydride phase of vanadium with alloying elements

Addition of alloying elements which contract the host lattice increase the plateau pressure-another criteria for the alloying component selection, while addition of elements which expand the host lattice diminish the plateau pressure (Al is exception) [42]. According to Yukawa et al. [42], plateau pressure may be high in those elements which have small atomic radius or high electronegativity, although it is still difficult to understand the measured change in plateau pressure with alloying elements in term of either atomic radius or electronegativity.

In a least square analysis, the correlation coefficient is about 0.45 between plateau pressure and atomic radius and about 0.66 between plateau pressure and electronegativity. Plateau pressure changes in a regular way following the order of elements in the periodic table. However, the high plateau pressure is observed for group VIII elements (Fe, Ru, Os). The plateau is not observed in V- Pt alloy, and that may be due to the complexity in hydrogenating the alloy. This leads to the lowering of hydrogen absorbed in alloy, H/M, and to the reduction of plateau region in pressure composition isotherm [42].

2.3.2 V₂H and V(H) (β and α) phase stability

The decomposition of β phase changes significantly with alloying addition [31, 42]. A systematic differential thermal calorimetric (DSC) study for various alloying elements is summarized in Fig 2.5. In the figure the peak P₁ is corresponding to V(β) \rightarrow V(α) reaction while peak P₂ is corresponding to V(α) \rightarrow V(hydrogen free) reaction. It is clear from the figure that in case of Mn, Mo and W as alloying element, reaction peak P₁ seems to have disappeared and in case of Mn, Fe, Co, Ni, Rh, Pd, W, and Re, high temperature peak P₂ shifts towards higher temperature side as compared to that of pure vanadium.

The change in shape and position of these peaks with alloying elements may be due to modification of β phase stability by alloying component and the change in kinetics of

hydrogen desorption reaction. Disappearance of P_1 peak in few cases may be due to the stability of β phase even at high temperature.

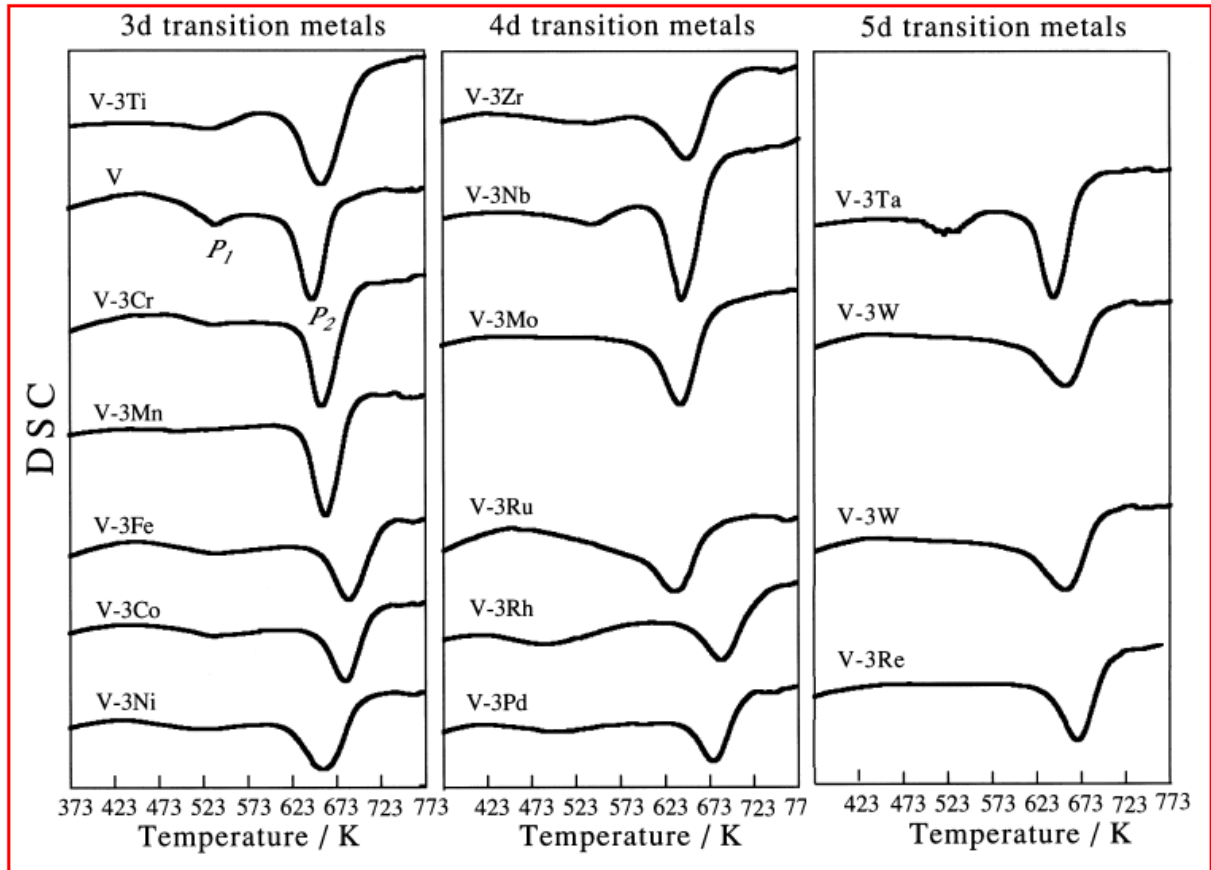


Fig. 2.5: Alloying effects on the decomposition of β phase and desorption from the α phase. Y axis of the Fig. is heat flux in arbitrary units

2.4 Storage capacity of vanadium base alloys

2.4.1 Binary alloys

Metallic vanadium has highest known volumetric hydrogen capacity when it is completely hydrogenated and converted into γ phase (VH_2). As reported earlier [11] hydrogen storage capacity of metallic vanadium is 0.16 g/cm^3 or 2.25 times more than the density of liquid hydrogen ($\sim 0.07 \text{ g/cm}^3$) and relatively high hydrogen weight capacity i.e. 4 wt %. Metals like titanium, zirconium, uranium, nickel and manganese have been found to

absorb relatively large amounts of hydrogen. However, the desorption temperature is higher than that of vanadium. Vanadium showed enhanced absorption capacity upon alloying with these elements [47-52]. These alloying elements also show favorable improvement in the plateau pressure. For example, manganese and nickel is known to improve the first plateau pressure of β phase of vanadium (V_2H) by partial formation of phases like VNi and VMn_2 which improve kinetics and reduces the hydrogen absorption activation energy [29]. Titanium and vanadium forms body centered cubic solid solution in any ratio of the two constituting metals and improved hydrogen absorption properties as investigated by Ono et al. [53]. In fact, V-Ti alloy has body centered structure but the hydride with $H/M = 1$ became body centered tetragonal structure. The hydride with $H/M = 2$ has a face centered cubic structure. This indicates that the structure of the metal sub lattice changed with hydrogenation. However, this has been reported for Ti-V alloy in which vanadium is in large quantity. In the case of Ti-rich alloys, $Ti(V)H$ does not exist but $Ti(V)H_2$ forms with a face centered cubic structure. It has also been reported that vanadium alloys containing Al, Fe, Co, Ni and Cr reveal a large reduction in maximum H/M value [54]. Lynch et al. [55] have discussed decline in hydrogen capacity observed in V-Al and V-Ti based alloys in relation to a critical e/a ratio and have indicated that critical e/a value as 5.1. This e/a ratio rule and relationship between plateau pressure and lattice parameter give useful indications for the estimation of maximum hydrogen absorption capacity and for control of plateau pressure on the addition of alloying elements [12]. Pulverization resistance of V-Ti based alloys was examined by measurement of particle size distribution with up to 300 hydriding cycles. Iron and chromium addition in V-Ti alloys as well as $V_{0.9}Ti_{0.1}$ alloy showed no tendency to become fine powder even after 300 cycles [56-57]. The alloy with Fe addition shows a significant reduction in hydrogen storage capacity with increasing number of cycles whereas Cr addition shows some decrease in effective hydrogen content and also a tendency to increase absorption-desorption

plateau pressure with increasing number of cycles. Certain alloying additions like Cr and Fe help vanadium to retain the body centered cubic crystal structure at room temperatures [40,58]. The V-Cr alloys in fact are body centered cubic solid solutions at high temperatures [12]. Both V and its solid solutions with Cr and Ti can absorb large volume of hydrogen ($H/M=2$) [9,59-64]. It is known that Ti atom has a bigger radius than the Cr atom ($R_{Ti} = 2.00\text{\AA}$, $R_{Cr} = 1.85\text{\AA}$). Hence, alloys with higher Ti have higher lattice constant i.e. larger space for accommodating hydrogen [10]. Hence, in the first cycle, alloys containing more Ti can accommodate more hydrogen. However, the Ti-H bonding is stronger than Cr-H bonding in their hydrogenated state at 298K [10], hence in subsequent cycles, the hydrogen absorption capacity is reduced [10]. On addition of Ti or Cr, vanadium showed the best P-C-T characteristics for V-Ti binary system [40] as compared with V-Cr. However, upon addition of Mo to the vanadium matrix the maximum absorbing capacity decreased [40]. Aluminum too, as solid solution addition is known for its effectiveness of increasing of hydrogen desorption pressure of V-based alloys and substantially reducing the hydrogen absorption capacity [65-69].

2.4.2 Ternary alloys and laves phases

Hydrogen absorption capacity of vanadium could be substantially increased by addition of Ti and Cr together to form the V-Ti-Cr ternary alloy [29, 70]. Retaining the bcc phase of vanadium the hydrogen absorption capacity could be increased up to 35% by volume and 2.88 % by weight. Hydrogen desorption capacity could also be increased upto 1.79 [29]. The kinetics of hydrogen absorption-desorption for bcc V-Ti-Cr alloy became very fast as reported by Libowitz et al. [71]. Replacement of Cr by Fe, Mn, Co and Ni also showed changes in the absorption capacity as well as the absorption-desorption kinetics. For example alloys, $Ti_{0.70} V_{0.30-10} M$ ($M = Fe, Mn, Co, Cr, Ni$) reacted rapidly with hydrogen. High hydrogen absorption capacity of V-Ti-Fe has been reported [48] and being developed to

recover hydrogen gas from a fusion reactor. Expected working temperatures were 573 K for desorption and 253 K for absorption. It was found that a bcc alloy with a composition of $\text{Ti}_{0.435} \text{V}_{0.490} \text{Fe}_{0.075}$ absorbed a large amount of hydrogen [54]. Nomura et al. [54] investigated that the effective capacity for recovery usage of hydrogen is about 2.4 wt% which is almost twice that of conventional intermetallic hydrides such as LaNi_5 . Tsukahara et al. [72] reported on vanadium-based multiphase alloys for electrodes of the Ni-metal hydride battery. $\text{TiV}_3\text{Ni}_{0.56}$ consisted of two phases with different functions. One was Ti-V based solid solution with a bcc structure which absorbed a large amount of hydrogen. The other was a TiNi based compound with a bcc structure which formed three-dimensional network to collect electrons and worked as a catalyst. It has also been reported that another combination of phases in $\text{Ti}_{1-x} \text{V}_x \text{Ni}_{0.56} \text{Hf}$, ($x = 0.046, 0.24$).¹⁷ could also be used. This alloy consisted mainly of a bcc solid solution and also of a C14 Laves phase. Absorption-desorption rate could be improved by inducing the cracks in the alloy. It has been found that cracking was mainly in and around the intermetallic phase, $\text{Ti}_{1-x} \text{V}_x \text{Ni}_{0.56} \text{Hf}$, after five charge-discharge cycles and, as a result, the absorption rate improved because the cracks increased the fresh surface area of alloys. It has been reported [72] that the combined effect of the two phases provided a higher hydrogen absorption capacity than single phase intermetallics. This is one of the important solutions to improve the poor kinetics of bcc hydrogen absorbers. An intermetallic phase which shows fast kinetics assists the hydride formation in the co-existing bcc phase. In the Ti-Cr-V system, the phase diagram indicates the co-existence of bcc solid solution and Laves phases. In addition, V-Ti-Cr alloys showed smaller hysteresis curve than V-Ti-Mn alloys, making them more suitable for application. It was found that the lattice parameter of the bcc phase in the V-Ti-Cr system was in the range of 3.020- 3.040 Å [73]. It is interesting to note that the alloys with these lattice parameters absorbed hydrogen at ambient pressure and temperature after only one activation cycle. The effect of heat treatment

on hydrogen absorption in $\text{VTi}_{30}\text{Cr}_{30}$ which does not form the Laves phase after low temperature heat treatment has been studied earlier [73]. The as-cast alloy had a slant plateau pressure but the alloy treated at 1473 K showed much of a flatter plateau pressure [74-75]. It is interesting to note that the hydrogen capacity of the heat treated alloy reached about 2.2 wt%.

Analysis showed that the heat treated alloys are well homogenized but Ti concentration in the as-cast alloy was observed to vary from place to place. It was observed that when the atomic ratio of Ti/Cr was varied, the equilibrium pressure changed dramatically. A change of 5 at% in composition of the alloy changed the lattice parameter by 0.025 nm and the equilibrium pressure by an order of magnitude. In comparison to the conventional AB_5 and AB_2 intermetallic hydrogen absorbers, the equilibrium pressure of this system is more sensitive to a change in lattice parameter. The slope in plateau comes from the inhomogeneity of the alloy. It means that bcc alloys such as those of the V-Ti-Cr system tend to have a sloping plateau because their equilibrium pressure depends very much on their composition [76]. Therefore, heat treatments to make homogeneous alloys are more important for these bcc alloys than for other intermetallics.

Wang et al [58] thoroughly studied the hydrogen absorption capacity of V-Ti-Cr system. Thermodynamically, the V-Ti-Cr ternary system is a typical bcc solid solution [77-78]. The enthalpies of mixing between constituent elements are respectively, $\Delta H_{\text{Ti-Cr}} = -7.5 \text{ kJ/mol}$, $\Delta H_{\text{Cr-V}} = -2 \text{ kJ/mol}$, $\Delta H_{\text{V-Ti}} = -2 \text{ kJ/mol}$. [79]. So, binary Ti-V and Cr-V are solid solution-forming systems while Ti-Cr forms TiCr_2 Laves phases of the $cF\text{-MgCu}_2$ type (low temperature) and the $hP\text{-MgNi}_2$ type (high temperature) [58]. The Cr-centered icosahedral Ti_6Cr_7 cluster characterizes the local structure of the TiCr_2 Laves phase. According to the topologically efficient cluster-packing structural model [58], the critical ratio R^* of ideally dense-packed icosahedral cluster is 0.902 [80], which is defined as the

ratio of the radius of the center atom r_o to that of the nearest-neighbor shell atom r_l . Here, the Goldschmidt radii of Cr and Ti atoms are respectively 0.128 nm and 0.146 nm, and then the ratio R of the Ti_6Cr_7 cluster is $R = r_o/r_l = 0.128 / [(0.128*6+0.146*6)/12] = 0.934$, where r_l is the average atomic radius of the nearest-neighbor shell atoms Cr_6Ti_6 . The difference represented by $D = (R - R^*)/R^*$ between the actual R and the ideal R^* is 3.5 %, which indicates that the icosahedral cluster Ti_6Cr_7 is quite dense-packed. Thus, the cluster line V- Ti_6Cr_7 has been constructed in the V-Ti-Cr ternary system by linking binary cluster Cr_7Ti_6 with V and presented in Fig 2.6. In the figure, the black circles and neighboring numbers represent the Ti-Cr-V alloy compositions and the H-storage capacities (H/M) of the designed alloys, respectively.

It is noted that the icosahedral cluster line V- Ti_6Cr_7 traverses exactly the composition range with large hydrogen-storage capacities, which verifies the validity of the cluster line approach in the V-Ti-Cr hydrogen-storage alloy system. Furthermore, the best experimental alloy composition $\text{V}_{30}\text{Ti}_{30}\text{Cr}_{40}$ with the largest hydrogen-storage capacity (H/M=1.69) as indicated in Fig 2.6, is approximately expressed with the cluster-plus-glue-atom model of $\text{V}_5(\text{Ti}_6\text{Cr}_7)$ (=V_{27.8}Ti_{33.3}Cr_{38.9}), i.e. one Ti_6Cr_7 cluster glued by five V atoms, where, the number of glue atom V is same to that of glue atom Cu in the MgCu_2 Laves phase [58]. The cluster line approach in the V-Ti-Mn ternary system is similar to that in the V-Ti-Cr system. The enthalpies of mixing between Ti-Mn and Mn-V are respectively $\Delta H_{\text{Ti-Mn}} = -8$ kJ/mol, $\Delta H_{\text{Mn-V}} = -0.8$ kJ/mol. Therefore, Ti and Mn tend to form the TiMn_2 Laves phase while V forms solid solutions both with Ti and Mn. The TiMn_2 Laves phase has an *hP*- MgZn_2 structure and is characterized by Mn-centered dense-packed icosahedral cluster Ti_6Mn_7 ($\Delta = 2.7$ %, $r_{\text{Mn}} = 0.126$ nm). The cluster line V - Ti_6Mn_7 could be constructed in the V-Ti Mn system. Experimental results indicate that the Ti-Mn-V alloy consisting of ternary Laves alloy distributed in bcc-vanadium. The solid solution matrix has a large hydrogen-storage capacity.

This ternary alloy is located near the cluster line V- Ti_6Mn_7 and also close to the $\text{V}_5(\text{Ti}_6\text{Cr}_7)$ composition, indicating that the alloys near the cluster line may have large hydrogen-storage capacities. In case of V-Ti-Fe ternary system, the large enthalpies of mixing between Ti-Fe and Fe-V ($\Delta H_{\text{Ti-Fe}} = -17 \text{ kJ/mol}$, $\Delta H_{\text{Fe-V}} = -8 \text{ kJ/mol}$) favor the formation of intermetallics. Similarly, the Fe-centered dense-packed icosahedra cluster Ti_6Fe_7 ($\Delta = 3.1\%$, $r_{\text{Fe}} = 0.127 \text{ nm}$) exists in the local structure of MgZn₂-type TiFe_2 Laves phase. In V-Ti-Fe ternary system, the V-rich alloy compositions with large hydrogen-storage capacities are also located near the cluster line V- Ti_6Fe_7 . In Ti-Cr-Fe-V and Ti-Cr-Mn-V quaternary systems, Cr - Fe and Cr - Mn can be regarded as a pseudo element M due to their similar atomic radius and similar enthalpies of mixing with Ti or V. Thus, the quaternary Ti-Cr-Fe-V alloy composition $\text{Ti}_{35}\text{Cr}_{25}\text{Fe}_{10}\text{V}_{30}$ with a large H-storage capacity can be expressed as a pseudo ternary composition $\text{Ti}_{35}\text{M}_{35}\text{V}_{30}$, which is located near the icosahedral cluster line V- Ti_6M_7 in the pseudo ternary alloy system and also close to the $\text{V}_5\text{Ti}_6\text{M}_7$ composition [58].

A general characteristic existing in the above Laves phase-related bcc-vanadium solid solution alloy systems A-B-C is that the absolute value of $\Delta H_{\text{A-B}}$ is larger than $\Delta H_{\text{B-C}}$ and $\Delta H_{\text{A-C}}$ and the latter two are close to zero. A-B then forms an AB_2 Laves phase while A-C and B-C tend to form solid solutions. Thus, the dense-packed icosahedral cluster line C- A_6B_7 can be applied into these ternary and pseudo ternary systems and alloy compositions with large H-storage capacities are located near the cluster line.

Kuriwa et al. [81] have reported that the optimum amount of vanadium in the vanadium-based V-Zr-Ti-Ni quaternary alloys is around 75 at.%, with the Laves phase acting as a preferential path for hydrogen transport. V-Ti-Cr alloys with bcc crystal structure are known for its high volumetric hydrogen capacity. Except for Ti, both V and Cr have bcc structures with no allotropic transformations right up to the melting point. Titanium has a high temperature bcc structure beyond 1155K. In the ternary system of V-Ti-Cr, it was shown

by Kuriwa et al. [69] that decreasing Ti and increasing Cr contents can lead to increase of hydrogen desorption pressure of alloys. However, unlimited substitution of Ti by Cr can in fact cause decrease in hydrogen capacity of alloys, the limit of this composition is called as “limitation line”. Therefore, to offset the “limitation line”, it was seen that not only Ti/Cr ratio but also the V content in alloy is an important factor to make alloys with high hydrogen desorption pressure along with high hydrogen capacity. Hence appropriately, compositional optimization of V-Ti-Cr-X alloys (X- alloy additions) influence the effective hydrogen absorption/desorption properties and the hydrogen capacity. Moreover, the melting methods in preparation of V-Ti-Cr alloy [15] and heat treatment conditions [10] also contribute significantly to the overall hydrogen interaction with the alloy.

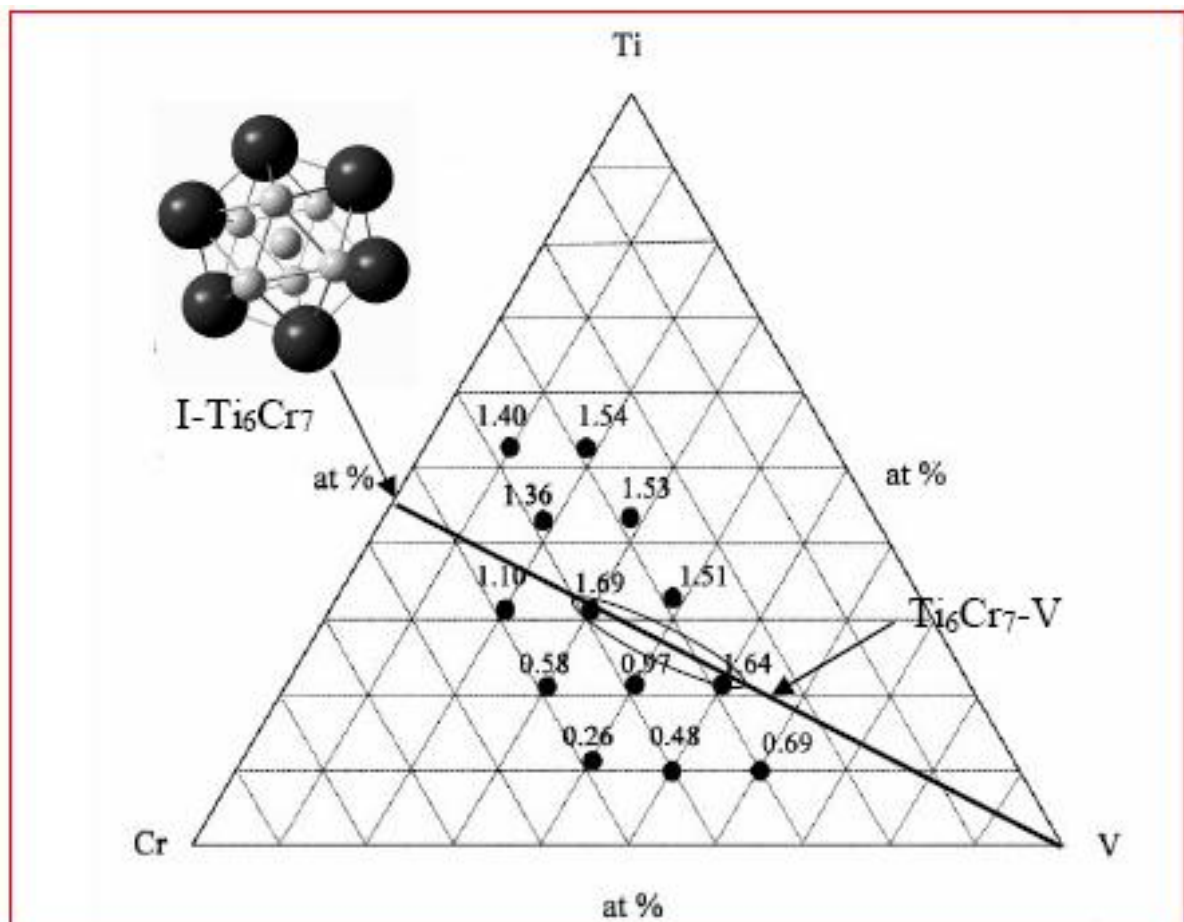


Fig. 2.6: Variation of absorption capacity of V-Ti-Cr alloys

2.5 Kinetics and thermodynamics

Activation energy of hydrogen absorption of vanadium has significantly increases upon addition of oxidation prone elements due to various reasons. Hydrogen absorption-desorption properties of vanadium based intermetallic compounds are summarized in Table 2.1. Hydrogen absorption-desorption kinetics parameter and maximum wt% of hydrogen storage capacity of vanadium based intermetallic compounds increase with Ti content. Similarly rate of hydrogen absorption in V-Ti based alloys increases noticeably with Ti content and decreases on addition of Si and Fe. Hysteresis improvement in V-Ti based alloys cannot be expected on addition of third alloying element and large hysteresis can be attributed to inherent nature of pure vanadium. [12]. Maeland et al. [44], have shown that alloying elements having some restriction for making their use in group V metals to improve their activation; their atomic radii should be at least 5% smaller than those of the host metals. Hysteresis factor $\ln \frac{P_a}{P_d}$ and the slope $\frac{d \ln P}{d(H/M)}$ of plateau pressure are slightly decreased by the addition of Fe, Co, and Ni, although the effects are small. However, Cr addition decreases the slope of plateau pressure but increases the hysteresis slightly as shown in Table 2.1. The change in enthalpy for γ di-hydride formation and decomposition in V-Ti based alloys decreases slightly by alloying with Si, Fe, Co and Ni whereas addition of Cr and Zr does not affect the ΔH value in case of low Ti alloys but Cr addition reduces ΔH value for high Ti alloys. However, entropy change caused by alloying addition in these alloys is relatively small but trend is almost similar as for enthalpy change as shown in Table 2.2 [12]. It is known that Ti is a metal having large affinity for hydrogen, Cr has very low and Nb is an intermediate between these two [19]. The terminal solubility of hydrogen in vanadium increases rapidly with Nb content, as does the terminal solubility of hydrogen in niobium with V content [82].

Table 2.1: Kinetics data of different alloys of vanadium [32-44]

Materials	Temperature (K)	Pressure(bar)	Kinetics (min)	Max wt% of H ₂
5mol% V ₂ O ₅ + MgH ₂	T _{abs} : 523	P _{abs} : 15	T _{abs} : 1.6	3.20
5wt% V + MgH ₂	T _{abs} , T _{des} : 573	P _{abs} , P _{des} : 1-3	t _{abs} : 2, t _{des} : 10	5.00
5at% V + MgH ₂	T _{abs} : 473, T _{des} : 573	P _{abs} : 0.15, P _{des} : 10	t _{abs} : 4.2	5.58
5wt% V + MgH ₂	T _{abs} , T _{des} : 573	P _{abs} , P _{des} : 1-3	t _{abs} : 2, t _{des} : 10	5.00
V 7.45%-Zr 7.4%-Ti 7.4%-Ni	T _{abs} : 298, T _{des} : 313	P _{abs} : 10, P _{des} : 1	No data	2.00
V _{0.375} Ti _{0.25} Cr _{0.30} Mn _{0.075}	T _{abs} , T _{des} : 303	P _{abs} : 50, P _{des} : 0.2	No data	2.20
V-Ti-Cr	T _{abs} , T _{des} : 313	P _{abs} : 100	No data	2.80
V-27 Ti-10 Cr-18 Mn-5Fe	T _{abs} : 333K	P _{abs} : 10 , P _{des} : 1	t _{abs} 8.3	3.01
V _{0.9} TiCr _{1.1}	T _{abs} , T _{des} : 303	P _{abs} : 17, P _{des} : 30	No data	3.50
V ₄₉ Ti _{43.5} Fe _{7.5}	T _{abs} : 253, T _{des} : 573	P _{abs} : 100, P _{des} : 10	t _{abs} : 20	3.90
V-Ti-Cr-Mn	T _{des} : 247-473	P _{abs} : 30, P _{des} : 0.03	No data	3.98
V Ti-10 Cr-18 Mn 32	T _{abs} : 333	P _{abs} : 30, P _{des} : 1	t _{abs} : 8.3	3.36
80 wt% V _{0.9} TiCr _{1.1} + 20 wt% LaNi ₅	T _{abs} , T _{des} : 303	P _{abs} : 17, P _{des} : 0.5	No data	1.50

Increase in $\overline{\Delta H_H^0}$ which reaches at maximum at 75 at% Nb in V may be the cause of an increased solubility of hydrogen in V-Nb alloys. Although the enthalpy for hydrogen solution in Nb is larger than in V, but even though no clear explanation is given for higher value of hydrogen in V-Nb alloys. Entropy changes are not large but they change vary smoothly and continuously with alloy composition [19]. Chromium addition in V strongly reduced the isopiestic solubility of hydrogen. The decrease in solubility may be due to smaller enthalpies of solution and increased entropies which both together result in producing larger Sieverts constant K_s . The change in $\overline{\Delta H_H^0}$ at 30 at% Cr in V was only 6.6 kJ/mol H, but this is good enough for large change in solubility. On the other hand, addition of Ti increases solubility of hydrogen in V-based alloys which again can be considered on the basis of simultaneous effect of above said two factors but in an opposite manner which means increase in enthalpy and decrease in entropy of solution of hydrogen. In 30 at% Ti-V alloy, concentration of hydrogen is 400 times as more as in pure vanadium at the same pressure and room temperature. In addition to increase in isopiestic solubility, Ti addition also enhances the

terminal solid solubility, and no hydride precipitation was observed up to 0.6 H/M in 30 at% Ti alloy even at room temperature. Sieverts law concentration range also increased on addition of Ti in V [19]. Large hydrogen concentration results in deviation from Sieverts law. The positive deviation from Sieverts law may be expected if hydrogen was being trapped and held very tenaciously until the traps were filled whereas negative deviation from Sieverts law may be due to the precipitation of small amount of hydride phase. Upward deviation may be expected due to electrostatic repulsion between hydrogen atoms with increasing H/M ratio.

Table 2.2: Effect of alloying elements on enthalpy and entropy changes for formation and dissociation of γ di-hydride, hysteresis factor, slope of plateau and hydrogen absorption rate of V-Ti based alloys [12-29]

Alloy	ΔH (kJ (mol H ₂) ⁻¹)		ΔS (J (mol H ₂) ⁻¹ K ⁻¹)		$\ln (P_s/P_d)$	$d(\ln P)/d(H/M)$	Time for 80% complete at 273 K (min)
	Abs.	Des.	Abs.	Des.			
Pure V	-	40	-	142	1.6	0.2	40
V _{0.95} Ti _{0.05}	-43	45	-148	140	1.6	0.5	22
V _{0.9} Ti _{0.1}	-48	49	-154	142	1.6	0.8	12
(V _{0.9} Ti _{0.1}) _{0.95} Al _{0.05}	-	40	-	136	-	0.7	15
(V _{0.9} Ti _{0.1}) _{0.99} Si _{0.01}	-	45	-	134	1.8	0.6	21
(V _{0.9} Ti _{0.1}) _{0.95} Cr _{0.05}	-53	49	-177	138	2.0	0.6	12
(V _{0.9} Ti _{0.1}) _{0.95} Fe _{0.05}	-38	40	-138	131	1.5	0.4	33
(V _{0.9} Ti _{0.1}) _{0.98} Zr _{0.02}	-45	49	-142	140	1.9	1.1	10
V _{0.85} Ti _{0.15}	-52	54	-154	146	1.9	1.3	5
(V _{0.85} Ti _{0.15}) _{0.95} Cr _{0.05}	-47	48	-160	143	2.3	0.8	4
(V _{0.85} Ti _{0.15}) _{0.9} Cr _{0.1}	-43	42	-154	135	1.8	1.0	3
(V _{0.85} Ti _{0.15}) _{0.95} Fe _{0.05}	-47	49	-151	143	1.7	1.3	27
(V _{0.85} Ti _{0.15}) _{0.92} Fe _{0.08}	-	46	-	149	1.9	3.1	46
(V _{0.85} Ti _{0.15}) _{0.95} C _{0.05}	-39	41	-136	129	1.7	1.4	3
(V _{0.85} Ti _{0.15}) _{0.95} Ni _{0.05}	-40	41	-139	129	1.7	1.5	5

The interaction coefficients are denoted to quantify the effects of substitutional solutes on the activity coefficient of the interstitial solute (hydrogen). Thus, for a given V-M alloy system, the interaction coefficient (ε_H^M) between hydrogen and metal solute M, in solution is:

$$\varepsilon_H^M \frac{\partial \ln \gamma_H}{\partial X_M} \Big|_{X_M, X_H} \rightarrow 0 \quad (2.3)$$

Where, γ_H is the activity coefficient of hydrogen in the alloy.

X_M and X_H are metal solute concentration and hydrogen concentration, respectively, in atomic fraction γ_H can be substituted by K_s when hydrogen solubility is within the Sieverts law range [19]. In the plots of $\ln K_s$ versus alloy concentration at each temperature, linear behavior is observed up to 10 at% Ti, 20 at % Cr and 25 at % Nb. In these ranges, ε_H^M is constant and was calculated from the slopes of the linear portion. The ε_H^M has large negative value for V-Ti system and it is expected due to increase in hydrogen solubility on Ti addition while it is opposite i.e. large positive value for V-Cr system indicates the strong effect of Cr in reducing the hydrogen solubility in V. However, in case of V-Nb alloys, small negative values reveal the slight increase in hydrogen solubility. In the Sieverts law range, a constant matrix-hydrogen interaction was observed and there is no significant hydrogen–hydrogen interaction in this range. This constant interaction over a wide range of hydrogen concentration may not be expected due to trapping of hydrogen. If localized deep trapping by solute metal atoms was the cause of enhancement of hydrogen solubility in V-Nb and V-Ti systems, then a noticeable dependence of activity coefficient on hydrogen concentration would be there [19].

There would be one value for the hydrogen interaction going into solution in trap sites, and another value for the interaction at higher concentration for the hydrogen dissolved after filling of traps. No such variations are observed in the values of K_s , $\overline{\Delta H_H^0}$ and $\overline{\Delta S_H^0}$ of hydrogen solution with hydrogen concentration even greater than metal solute concentration [83-89]. A significant outcome of hydrogen following Sieverts law over a wide range of H/M ratio is that no thermodynamic correction factors are required in interpreting concentration summary in hydrogen transport phenomenon like thermo transport and diffusion within this range. This is due to constant activity coefficient of hydrogen and it is not dependent on hydrogen concentration. At a given alloy concentration, on moving from Ti to Nb and to Cr,

enthalpy of solution of hydrogen, $\overline{\Delta H_H^0}$, becomes less exothermic and this appears reasonable by considering the relative affinity of hydrogen for Ti, Nb and Cr [19]. The electron to atom ratio increases on moving from Ti to Nb and Nb to Cr. On the basis of Wagner concept [90], as e/a ratio increases, the solubility of hydrogen decreases. Hence, Ti electrons are easily available for bonding to hydrogen atoms as compared to Nb and Cr. This is also confirmed by the highest stoichiometry of stable hydrides of these metals e.g. TiH₂ for Ti, NbH₂ for Nb and no stable hydride for Cr. The concept of site blocking or anti-trapping may be the reasons for decreasing the solubility of hydrogen on the addition of Cr in V-based alloys [91-95]. However, the change in solubility due to Cr concentration does not fit a simplistic near neighbor anti-trapping model. In addition, anti-trapping model would forecast no change in heat of solution on alloying [19].

The entropy of solution decreases with increasing Ti content whereas it increases with increasing Nb and Cr concentration. The small change in entropy is a difference of two larger values, the entropy of solution of hydrogen, $\overline{\Delta S_H^0}$ and the entropy of gas phase, $\frac{1}{2}S_{H_2}^0$. Lattice dynamics, electronic interaction, configurational and lattice dilation effects also contribute to the total value of entropy in solution [19]. Simple trapping of hydrogen in alpha solid solution phase cannot be a single reason to explain the large increase in terminal solid solubility in Nb and Ti based vanadium alloys as compared to pure vanadium. The free energy changes for the hydride phase as a result of alloying must be related to the higher solubility in these alloys [19].

2.6 Electronic consideration of hydride stability and hydrogen absorption capacity

The effect of alloying on the stability of vanadium hydride can be explained on the basis of electronic concepts using DV-X α cluster models, and analysis of electronic structures (41). Energy level structures of VH₂ and V₂H are examined for characterization of chemical

bonding and electronic structures in these hydrides. From the energy level structures, electron density of states is calculated using the overlapping Gaussian functions [41]. The overlap population of electrons and the ionicity of every atom in the cluster are calculated according to the Mulliken population analysis [13]. Bond order ($Q_{vv'}$) is the overlap population of electrons between two atoms v and v' and it is defined as:

$$Q_{vv'} = \sum_l \sum_{ij} C_{il}^v C_{jl}^{v'} \int \psi_i^v \psi_j^{v'} * dV \quad (2.4)$$

Where, ψ_i^v and $\psi_j^{v'}$ are wave function of i and j orbitals of v and v' atoms, respectively.

C_{il}^v and $C_{jl}^{v'}$ are coefficients of magnitude of linear combination of atomic orbitals in the 1st molecular orbital. In case of pure VH_2 and V_2H , Fermi energy level, E_f , lies in the vanadium 3d band, while the vanadium 4s and 4p components are spread over a wide energy range. Hydrogen bonding levels also appear over a wide energy range below E_f . If the overlap population is positive, a bonding-type interaction is operating between the atoms and if it is negative, an anti bonding-type interaction is dominant between atoms [41].

In pure VH_2 , bonding type interactions are operating between the vanadium 3d and hydrogen 1s electrons & between vanadium 4s, 4p and hydrogen 1s electrons in the energy range lower than E_f , thus a strong interaction is observed between vanadium and hydrogen atoms. In case of pure V_2H , electron density profile of 3d band resembles partially that of bcc vanadium, indicating that V-V interaction is important in V_2H . In later part, vanadium 3d-hydrogen 1s interaction is bonding type in the energy ranges upto E_f , while vanadium 4s, 4p-hydrogen 1s interaction is anti bonding type in an energy range of about -5eV to E_f . It is indicating that vanadium 3d-hydrogen 1s interaction is dominant in this hydride [41]. Bond order between atoms in tetrahedron as well as in octahedron change with alloying elements. In pure VH_2 , both V-H & M-H bond order are large and positive while both V-V & M-V bond order are always negative or nearly zero, indicating that there is a strong interaction between hydrogen and V/M atoms. But, in case of V_2H , in contrast to VH_2 , bond orders

between V-V and V-M are always positive and large and this is simply due to shorter V-M bond length in V₂H than in case of VH₂ and this V-M bond length varying considerably with the alloying element, M [41]. Total bond order (T_{BO}) in case of VH₂ and V₂H is given by sum of all M-H bond order in tetrahedron and in octahedron, respectively and calculated by following equations:

$(T_{BO})_{VH_2} = BO (H-M) + 3 * BO (H-V)$ and $(T_{BO})_{V_2H} = 2 * BO (H-M) + 4 * BO (H-V)$, respectively.

Where, BO is the bond order between atoms shown in parenthesis. In case of VH₂, total bond order is nearly constant, i.e. almost independent of the alloying element, M while in case of V₂H, this depends largely on alloying element, M as does H-M bond order. Magnitude of M-V bond order is different for 3d, 4d & 5d transition metals. This is attributed as size difference eg. Zr-V bond order is more negative than V-V bond order because of larger atomic size of Zr than vanadium. The substitution of larger atom for smaller vanadium atom results in lattice expansion and hence, M-V bond length becomes larger than V-V bond length [41]. Ionicity of each atom in the cluster is estimated according to the Mulliken population analysis [44]. Vanadium atoms always possess positive ionicities while hydrogen atoms have always negative. This is because of higher electropositive characteristic of vanadium than hydrogen. Ionicities of alloying elements change considerably with respect to electronegativity of metals (M). These results indicate that charge transfer takes place mainly from vanadium atoms and alloying elements towards the hydrogen-atoms which causes ionic interaction between them [41]. At temperature 313 K, the measured equilibrium hydrogen pressure changes with alloying elements, M as strength of chemical bond changes with M in alloyed VH₂ and this is concerned with the following reaction: $VH + H = VH_2$. Structural stability of pure VH₂ is attributed due to H-V interaction and not because of V-V interaction in it. This is reasonable since crystal structure of VH₂ is completely different from that of

pure bcc vanadium and V-V bond length is much larger in VH_2 than that of bcc vanadium [41]. It is difficult to explain the change in measured hydrogen pressure on the basis of change in covalent bond strength between hydrogen and M atoms because total bond order between hydrogen and metals atoms in tetrahedron scarcely changes with M while an ionic interaction takes place between hydrogen & M atoms due to charge transfer between them, that changes considerably with M [41]. In case of V_2H , both chemical interactions between vanadium and hydrogen atoms & between V-V atoms are present and this structure is the derivative structure of bcc vanadium, however it is expanded and distorted in some way by hydrogenation. On the other hand, in case of VH_2 , chemical interactions between V-H atoms are dominant, but not between V-M atoms. Crystal structure of VH_2 is completely different from the structure of bcc vanadium & it is of CaF_2 type. V-M interactions and its changes with hydrogenation will primarily determine the stability of hydrides in case of V_2H while M-H interaction plays a more important role in the case of VH_2 hydride stability [41].

2.7 Hydrogen diffusion and permeation

Hydrogen transport and diffusion is a function of porosity of the materials [96]. Tanaka and Kimura [79], have found that diffusion of hydrogen in vanadium is reduced by alloying with Ti and Zr. According to Pine et al. [16] and Koiwa et al. [97] addition of alloying elements affect both effective charge number Z^* and diffusion coefficient D. Both effective charge number Z^* and diffusion coefficient D were reduced on the addition of Ti and Cr in vanadium while Mo and Fe have virtually no effect on Z^* and slightly decrease the diffusion coefficient [98]. The decrease in diffusivity and Z^* on the addition of alloying elements has been explained on the basis of trapping effect of substitutional atoms. From the theoretical calculation (98), it was found that a substitutional atom can trap only one hydrogen atom, although justification has not been explained. It was also observed that Z^* decreases with increasing binding energy (B.E.) but appreciable changes are not found after

B.E. ≥ 10 kJ/mol. The decrease in Z^* from 1.94 in pure vanadium to 1.57 in V-4% Ti alloy should be attributed to the change in electronic structure [98]. In the periodic table, on moving from left to right in transition metals series, the number of conduction electrons increases. Hence, addition of Ti to V decreases the number of conduction electrons and the electron drag force resulting in reduction of Z^* of hydrogen. When judged from diffusion data, it was found that B.E. of Ti-H is larger than that of Cr-H in V-based alloys. The smaller reduction in Z^* on the addition of Cr than Ti addition is consistent with trapping effect. On the basis of change in number of conduction electrons, Z^* should substantially increase on the addition of Cr but apparently, this does not happen. This decrease in Z^* is explained on the basis of trapping effect and effect of change in electronic structure for V-Cr alloy was neglected. This indicates the complexity of alloying effect on the electromigration [98].

Ultra-high pure hydrogen can be produced using metallic membranes. V-Ni alloys membranes have larger hydrogen permeability than Pd. In V-Ni-H system, temperature for hydride formation is low and hydrogen embrittlement is improved by increasing Ni content. The apparent hydrogen permeability in alloy membrane can be increased by removing deformation layer formed by mechanical polishing particularly at low temperature. Hydrogen permeability in V-15at% Ni [6] alloy membrane can be increased above 473 K by addition of small amount of deoxidizers such as Ti, Zr, and Y. However, effects of deoxidizer addition were not apparent below 473K. While below this temperature, hydrogen permeability in alloy membranes was strongly affected by surface contamination and Pd-plating conditions. Addition of 0.05 at% Ti in the above said membrane exhibits large hydrogen permeability even at 373 K and at a hydrogen pressure 16 kPa. It is considered that the amount of deoxidizer should not exceed the amount required for decreasing the interstitial impurities in the form of carbide, nitride or oxide. Excess deoxidizer will result in a decrease in hydrogen diffusivity [96]. No significant pressure dependence of hydrogen permeability is observed

above 40 kPa in V-15at% Ni alloy membrane. Hydrogen permeability decreases with decreasing pressure is observed below 40 kPa in these alloys at temperatures 473 K and 573 K [99]. It was noted that there were no cracks in alloy membrane even under an upstream pressure of 219 kPa but cracks were generated at higher pressure of 304 kPa at 473K. The effective diffusion coefficients of hydrogen in V-based alloy membranes are little bit larger than that of Pd, but significantly smaller than that of pure vanadium in temperature range 423-673 K [96]. Hydrogen solubility coefficient of alloy membranes are much smaller than that of vanadium and exhibit a good linearity over the temperature range 423-673 K. Phase transition temperature is depressed by alloying with Ni. The increase in hydrogen solubility caused by Ti addition was not observed above 423 K, but increase in hydrogen diffusivity due to addition of such a deoxidizer was observed. Peterson and Scholader [100] reported that small amount of interstitial oxygen in vanadium resulted in a decrease in hydrogen diffusivity without increasing hydrogen solubility and concluded that solubility and diffusivity results didn't fit a simple trapping model. It was also observed that under polarized light, the needle like hydride phase was optically active in pure vanadium while it was optically inactive in vanadium-oxygen alloys indicated that pure vanadium has its non-cubic structure whereas V-O alloy has a cubic and optically isotropic structure. However, in the oxygen containing specimen, the hydride needles were much smaller and more numerous [101-105]. In such a situation, terminal solid solubility limit may also be influenced by change in crystallography and morphology of the hydride phase. Interstitial oxygen in V-15at% Ni alloy membrane decreases the effective area for hydrogen permeation. Palladium coated V-15at% Ni alloy membrane can be used as a highly efficient hydrogen separation membrane in the temperature range 473-673 K [6, 94]. The two main limitations for the vanadium metal to be recognized as potential material for commercial membranes are its hydrogen embrittlement and surface oxidation [106]. Resistance to hydrogen embrittlement

of vanadium metal can be enhanced by alloying it with materials which are having very low solubility of hydrogen such as Ni and Mo [107] whereas surface oxidation of vanadium can be minimized by a thin coating with Pd. Vanadium based alloys are excellent candidates materials for hydrogen separation membrane because of their high hydrogen permeability and low cost [106]. Effect of impurities on the hydrogen permeation behavior of vanadium is important to understand. Hydrogen permeability of V-Al alloy decreased with Al content [107]. It was found that lattice constant and Vickers hardness of V-Al alloys changes linearly with Al content, following Vegard's law and simple solid solution effect, respectively [106]. Volkl and Alefeld [14] showed that as the distance between interstitial sites increases, the activation energy for hydrogen diffusion increases. Hydrogen permeability of V-Al alloys show linear behavior upto 20 at% Al and further increase in Al content results in rapid drop of permeability while in case of V-Mo alloys, up to 50 at% Mo, linear behavior is observed. It was also noted that when solute content was below 20 at%, the addition of Ni was more effective in decreasing the hydrogen permeability than addition of Al. When Al content was less than 3 at%, little difference is observed in hydrogen diffusion coefficient of V-Al alloys, but further increase of Al content results in considerable decrease of hydrogen diffusion coefficient [107].

Hydrogen diffusion in V-Al alloys obeyed the Arrhenius law: $D = D_0 \exp(-E_D/RT)$ where D is the hydrogen diffusion coefficient, D_0 is the frequency factor and E_D is the activation energy for hydrogen diffusion. Considerable decrease in hydrogen solubility of V-Al alloys was observed when Al content is more than 20 at% whereas hydrogen diffusivity in these alloys kept varied linearly with increase in Al concentration. These results indicate that decrease in hydrogen solubility with Al is the main factor for decreasing the hydrogen permeability in V with addition of Al [107]. Either surface oxidation or blocking effect of Al atoms are two possible reasons for reduction in hydrogen solubility of V with increasing Al

content. As hydrogen solubility of Al is much lower than V and large number of aluminum atoms could be expected to block the sites for hydrogen dissolution in V-based lattice. On the other hand, Al has very high affinity for oxygen and it can assumed that Al_2O_3 film will be preferentially formed on the surface of V-Al alloys with high Al content and this film is the most effective barrier for hydrogen permeation. Hence, effective surface area is reduced with Al for hydrogen permeation, resulting in decrease of hydrogen permeability of V-based alloy with increase of Al content [107]. It has been reported [108-111], that diffusion of hydrogen in vanadium is reduced by alloying with Ti and Zr.

2.8 Summary and Conclusions

Hydrogen absorption capacity of metallic vanadium is excellent because of its bcc crystal structure. Hydrogen absorption capacity of vanadium based alloy is very similar to those of the AB_2 hydrogen storage system at ambient temperature and pressure. All or certain vanadium based alloys inherently show very good hydrogen permeation characteristics excellent hydrogen absorption desorption kinetics and follow simple activation process. Therefore, vanadium based alloys are being actively evaluated as a hydrogen storage medium and as a hydrogen permeable membrane. The prospective of using vanadium and vanadium based alloys as hydrogen storage material and as hydrogen permeable membrane has motivated significant research on the vanadium-hydrogen system.

Chapter... 3

Materials and Methods

Contents

3.1 Introduction.....	52
3.2 Materials Synthesis.....	52
3.2.1 Vacuum Arc melting.....	52
3.2.2 Aluminothermy followed by Electron Beam melting.....	53
3.3 Apparatus used in the present study.....	55
3.3.1 Sievert's apparatus.....	55
3.3.2 Modified Sieverts apparatus.....	58
3.4 Methods used for solubility and kinetics studies.....	59
3.4.1 Activation of the sample	59
3.4.2 Hydrogen solubility calculation using pressure drop methods...	60
3.4.3 Hydrogen solubility calculation by gravimetric method.....	61
3.4.4 Enthalpy calculation using solubility data.....	62
3.4.5 Kinetics equation.....	62
3.4.6 Activation energy.....	64
3.5 Analytical techniques.....	65
3.5.1 Scanning electron microscopy (SEM).....	65
3.5.2 Energy-dispersive X-ray spectroscopy (EDS/EDX).....	67
3.5.3 X-Ray diffraction (XRD).....	68
3.5.4 Inert gas fusion technique (nitrogen, oxygen and hydrogen)....	70
3.5.5 X-Ray fluorescence (XRF).....	73
3.5.6 Differential thermal analysis (DTA).....	74
3.5.7 Inductively coupled plasma atomic emission spectroscopy	76
3.6 Summary and Conclusions.....	78

3.1 Introduction

The detailed description of the materials including, the synthesis routes and sources of raw materials, equipments and techniques used in the particular properties investigation are an essential part of the study. Materials prepared by different synthesis routes may have significantly different behaviors because of compositional variation among other things [15, 43, 45, 50, 71]. For example, alloys of same composition prepared by vacuum arc melting and alloying by mechanically ball milling shows substantially different characteristics. Therefore, complete information about the origin of the materials and the synthesis routes employed to prepare the materials is very important and need to be discussed before any conclusion. Multiple instruments could be used to obtain the same data. The instruments could be conceptually different or difference in the make & model. The data obtained by multiple instruments could result in differences [14, 15, 71, 95, 97, 109, 111]. Hence, details of instruments used in the investigations are important as are the analytical techniques used for characterization. The present chapter provides a complete description of materials, equipments and techniques used in the entire study.

3.2 Materials synthesis

3.2.1 Vacuum arc melting

Vacuum arc melting is most conventional technique to prepare the alloys and intermetallic. In this technique alloying components are blended and melted together in a vacuum arc furnace at temperatures above the slightly above the liquidus of the system. The alloys were homogenized by repeated melting. In the present study high purity (>99.8%), vanadium, V-Al master alloy, titanium (sheet) , chromium (granules) and aluminum (powders)

were used to prepare the V-Al, V-Ti-Cr alloy by vacuum arc melting technique. These metals are thoroughly degreased before charging for arc melting. V-Al master alloy was used to prepare V-Al alloy in desired compositions by diluting master alloy with vanadium. The homogeneity of the alloys prepared was also checked by chemical analysis of the different portion of the sample and the line scanning using energy disperses spectroscopy. All the results have been discussed in results and discussion chapter of the present thesis.

3.2.2 Aluminothermy followed by electron beam melting (EBM)

Most of the vanadium metal and V-Al, V-Ti-Cr alloys used in the present investigation were synthesized by the aluminothermic reduction process [112-116]. Metal oxides (V_2O_5 , Cr_2O_3 and TiO_2) of average particle size 20 μm were used. In a few cases V_2O_5 was synthesized by calcining NH_4VO_3 . The raw materials used in the present investigation are shown in Fig 3.1 All the oxide raw materials were oven dried at 373K under rotary vacuum condition to remove the moisture. The oxides of metals were mixed with the aluminum reductant and the additive $KClO_3$ (for heat boosting) and CaO (for slag fluidizing) were added, as required. The mixture was loaded in refractory lined steel reactor and the reaction was initiated by igniting a trigger mixture of $KClO_3$ and Al. The reactions were highly exothermic and heat of reaction was sufficient to completely melt the slag and reduced metal and keep them molten till their separation into two layers before solidification.

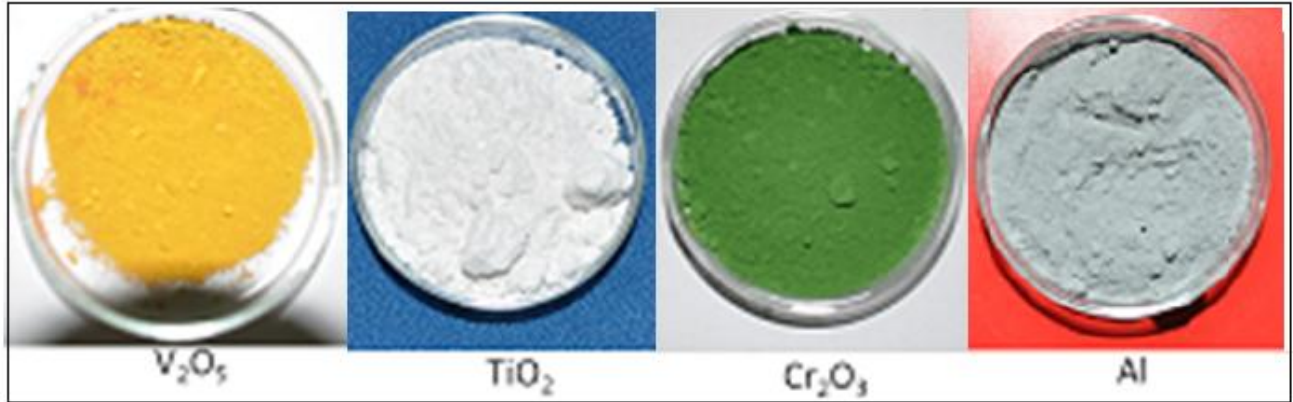


Fig 3.1: Raw materials used for the synthesis of vanadium metals and alloys

The overall reactions involved in the thermit process are given by.



A typical highly exothermic open bomb aluminothermy reaction is shown in Fig 3.2. The metal/alloy separate from the slag due to the density differences and solidify as easily separated ingot. The thermit alloys (V-Al-O/V-Cr-Al-O/V-Ti-Al-O/V-Cr-Ti-Al-O) thus obtained were refined by electron beam melting and homogenized by vacuum arc melting followed by hot rolling to 2 mm thick plate. Hot rolled plates were annealed at 1473 K under a dynamic high vacuum atmosphere ($\sim 10^{-7}$ torr) for 5-6 hours to relieve the residual stresses and to remove the volatile impurities from the surfaces. These plates were sliced using electric discharge machine (EDM). Before hydrogenation, the specimens were metallographically polished up to three delta (3 Δ) finish using emery papers and diamond paste. The mirror finished specimens were preserved in argon gas flushed vacuum desiccators. These specimen were used for all the hydrogen charging experiments

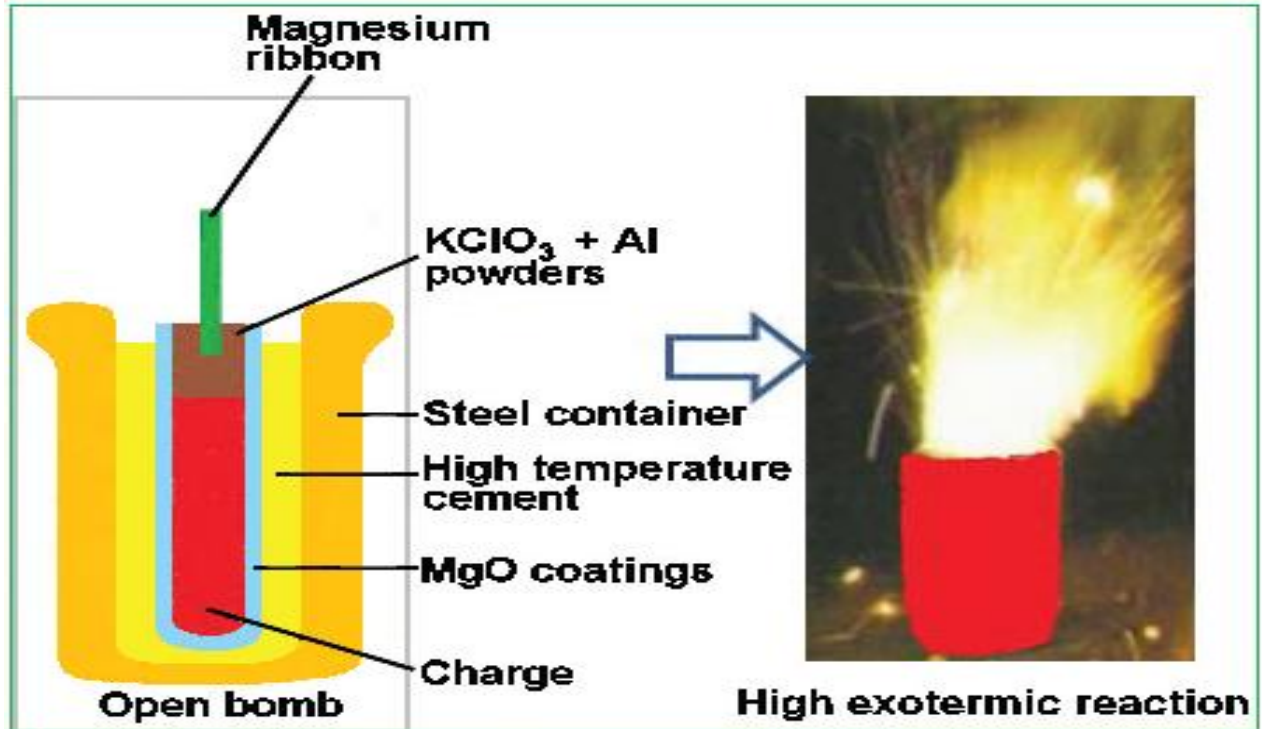


Fig 3.2: Process flow sheet of metal and alloys preparation by open bomb aluminothermy

3.3 Apparatus used in the present study

3.3.1 Sieverts apparatus

Gaseous hydrogen charging technique has been widely used for introducing controlled amount of hydrogen in metals and alloys. In this technique the samples have been heated in hydrogen atmosphere either under constant pressure for different time periods or in a constant volume system. In the former i.e. constant hydrogen partial pressure system, time periods for which the samples is exposed, determines the hydrogen concentration. In constant volume system, the average hydrogen concentration of the sample is estimated from the product of the system volume and the difference between the initial and final partial hydrogen pressure of the system.

In present study constant volume variable pressure techniques were used which is based on the Sieverts principle. An in-house make Sieverts apparatus was extensively used in the present investigation. A photograph of the system is shown in Fig 3.3. A complete schematic of the apparatus is shown in Fig 3.4.

The apparatus consists of mainly four main parts viz the hydrogen source (Hydrogen gas cylinder or PW-SPE-500 CIC make hydrogen generator), reaction chamber, capacitance manometer and vacuum system. Different parts were connected by stainless steel tubes (i.d. 4mm) using compression type fittings. Only needle type valves were used in the system.

While working with hydrogen, the complete gas line manifold has to be absolutely leak proof and leak test should be conducted from time to time. To check the leak tightness of the system, the reaction chamber was maintained at a pressure of 0.1 torr and isolated for 3 continuous days. No change in pressure was observed at the end of this period. The entire system except the reaction chamber is made of 42 mm outer diameter stainless steel tube.

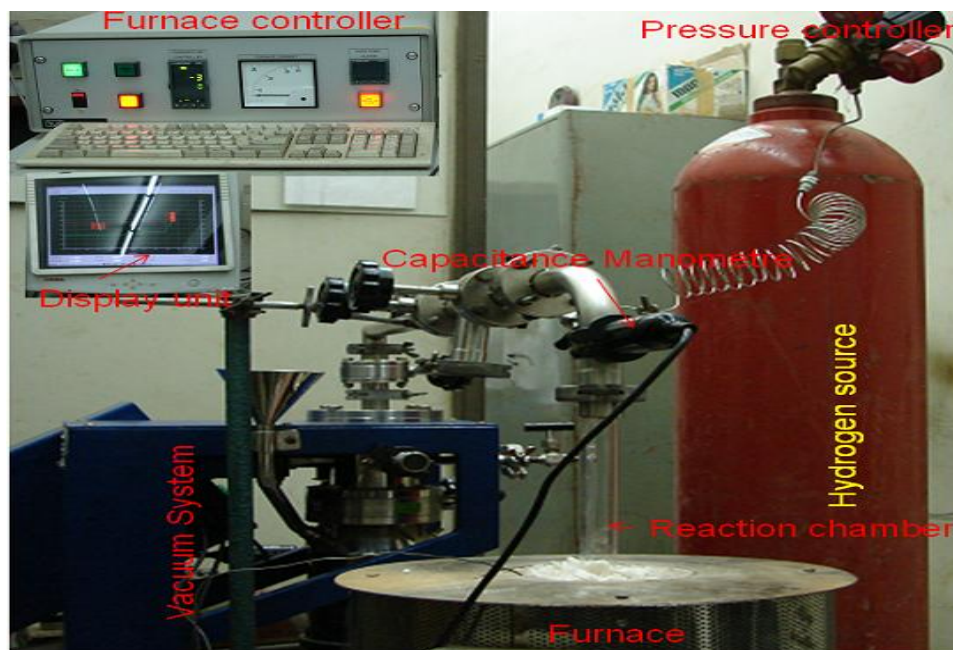


Fig 3.3: Sieverts Apparatus: Indigenously designed and developed in the laboratory

KF couplings with viton gaskets were used for leaktight joints in the system. The reaction chamber is made of one end closed quartz tube of about 400 mm length and 40 mm in diameter. This reaction chamber was connected to the main apparatus using KF coupling. A capacitance manometer is used to measure the hydrogen pressure.

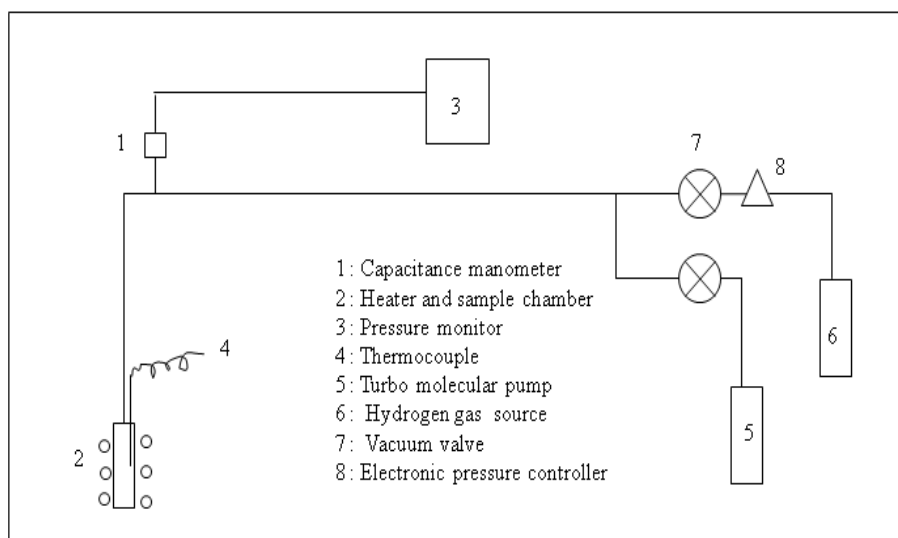


Fig 3.4: Schematic diagramm of the Sieverts apparatus design, developed and used in the present study

In isobaric experiments an electronic pressure controller was used to regulate the hydrogen pressure fluctuation due absorption in the sample. A mass controller flow meter was used to introduce hydrogen gas in a controlled way in the reaction chamber. A resistance heating furnace was used to heat the sample and the reaction chamber. The sample temperature was also measured by using a K type thermocouple adjacent to the sample holder. The system has been calibrated using standard LaNi_5 samples. For the hydrogen charging, the system was evacuated to a dynamic vacuum of the order of 10^{-7} Torr using turbo molecular pump. After this the hydrogen was introduced in a controlled way using the mass flow meter. Depending upon weight of the sample hydrogen was introduced to a predetermined level of pressure; subsequently the

specimen chamber was heated upto a predetermined temperature. Amount of hydrogen picked up by the specimen, was indicated by manometer. The amount of hydrogen picked up by the sample is computed from difference between initial and final pressure readings recorded at the ambient temperature using formulae $[H]_{ppm} = k \Delta p/m$, where; k: apparatus constant (mg/torr), Δp : hydrogen pressure (torr) and m: mass of the specimens (mg). Hydrogen concentration crossed verified by chemical analysis of the sample using inert gas fusion technique as well as by gravimetric methods.

3.3.2 Modified Sieverts apparatus

Hydrogen absorption kinetics is a very important factor for hydrogen storage materials. In the present study a thermobalance attached to Sieverts apparatus has been used to investigate the mechanism of hydrogen absorption-desorption reaction.

The apparatus used in the present investigation is shown in the Fig 3.5. The thermobalance head is of CI electronics make. It consists of a reaction chamber made of quartz, vacuum system and sample holder connected to the thermobalance through a quartz hanger. Reaction chamber could be placed inside the temperature controlled furnace using a manual furnace lifter. Furnace temperature and sample temperature were simultaneously measured by placing two identical K-type thermocouples. The system is having provision to introduce hydrogen gas in a controlled manner.

A CRT display was used to read the instantaneous weight gain and the instantaneous rate of weight gain. An electronic pressure controller was used to maintain the constant pressure. The apparatus has been suitably modified to conduct the isothermal as well as non-isothermal kinetics experiments.

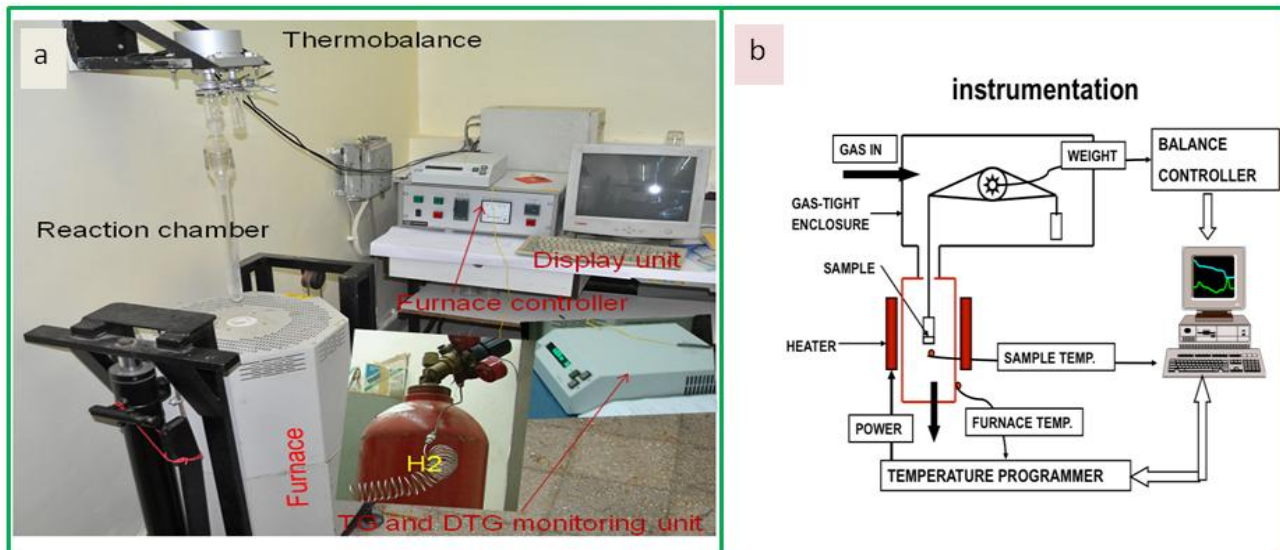


Fig 3.5: Modified Sieverts apparatus with thermobalance (a) Indigenously developed in the laboratory (b) Schematic diagram

3.4 Methods used for solubility and kinetics studies

3.4.1 Activation of the sample

Before the actual hydrogen charging, the sample must be activated. For activation the sample was placed in the reaction chamber and then the chamber was evacuated to 10^{-7} Torr vacuum and temperature was raised to 1200K. The hydrogen gas was then filled in the reaction chamber at 760 Torr and then cooled down to room temperature. The temperature was further raised to 1200K and then reaction chamber was re-evacuated to 10^{-7} Torr to release the entire hydrogen from the sample. The process was repeated several times. This process is commonly employed to activate the sample before hydrogen charging by inducing micro cracks. A typical vanadium based sample before activation and after activation is shown in the Fig 3.6. From the figure it is clear that the substantial modification of the surface happened after activation. Also

multiple micro-cracks were generated by activation process which is indeed required before hydrogen could be charged.

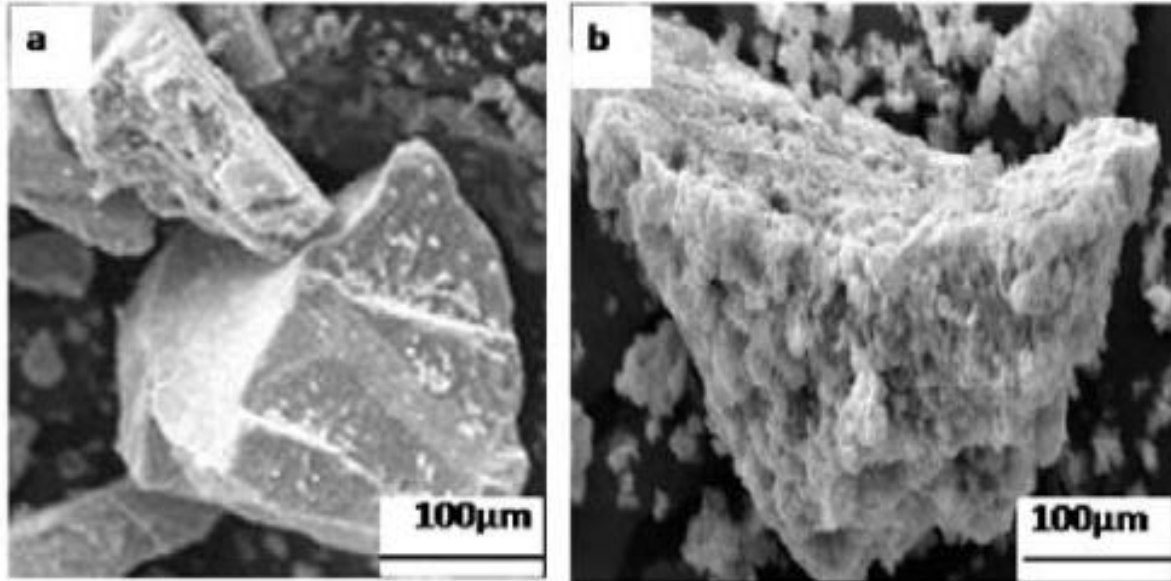


Fig. 3.6: A typical vanadium based sample (a) before activation (b) after activation

3.4.2 Hydrogen solubility calculation using pressure drop methods

Amount of hydrogen dissolved in metals and alloys is estimated by pressure drop value. Let Δp is the difference between the initial and final pressure readings at room temperature; V is the total internal volume of the Sieverts apparatus and 'm' is mass of the sample.

Thus, knowing the mass of the sample and the difference between the initial and final hydrogen partial pressure the mass of hydrogen absorbed by the sample can be estimated with reasonable accuracy as follows:

The number of moles of hydrogen absorbed by the sample is given by:

$$n = \frac{\Delta pV}{RT} \quad (3.4)$$

Using SI unit of pressure change, Δp , volume V universal gas constant R and temperature in Kelvin, no. of moles of hydrogen can be calculated using Eq. 3.4. Thus the mass (in g) of hydrogen atom absorbed by the sample will be $2n$ g

$$(H_{mass})_{gram} = 2 \times \frac{\Delta pV}{RT} \quad (3.5)$$

Hence, the hydrogen concentration in ppm can be approximated as

$$H_{ppm} = \frac{\text{mass of hydrogen in gram}}{\text{initial mass of the sample in gram } (m_s)} \times 10^6 \quad (3.6)$$

$$H_{ppm} = \frac{2 \times \frac{\Delta pV}{RT}}{m_s} \times 10^6 \quad (3.7)$$

For a particular apparatus and laboratory conditions equation 3.7 could be re-written as

$$H_{ppm} = K \frac{\Delta p}{m_s} \quad (3.8)$$

Where K is a constant of the apparatus used in the present study

Thus, knowing the sample mass and difference between the initial and final hydrogen pressure, the average hydrogen concentration in ppm in the sample could be obtained.

3.4.3 Hydrogen solubility calculation by gravimetric technique

Hydrogen concentration has also been determined by the change in weight using highly sensitive microbalance [117-118]. The mass sensitivity of this thermobalance is less than $\pm 0.1 \mu\text{g}$. The calculation used in the method was as follows

$$H_{ppm} = \frac{(\Delta m_{mass\ gain}) \text{ in } mg}{(m_{sample}) \text{ in } mg} \times 10^6 \quad (3.9)$$

Here mass gain as well as the mass of the sample should be in the same unit.

3.4.4 Enthalpy calculation using solubility data

The enthalpy of solution of metal-hydrogen solid solution could be determined using Clausius-Claperon equation as follows [119]

$$\frac{d \ln x}{dT} = \frac{\Delta H}{RT^2} \quad (3.10)$$

where x is the mole fraction of dissolved hydrogen in metal

On integrating above eq. from x_1 to x_2 on left hand side and from T_1 to T_2 on right hand side,

$$\int_{x_1}^{x_2} d \ln x = \int_{T_1}^{T_2} \frac{\Delta H}{RT^2} dT \quad (3.11)$$

$$[\ln x]_{x_1}^{x_2} = \frac{\Delta H}{R} \left[-\frac{1}{T} \right]_{T_1}^{T_2} \quad (3.12)$$

$$\ln(x_2 - x_1) = \frac{\Delta H}{R} \left[\frac{1}{T_1} - \frac{1}{T_2} \right] \quad (3.13)$$

Where ΔH is enthalpy of solution.

The standard enthalpy and entropy of vanadium- hydrogen solid solution could also be calculated using hydrogen solubility data as : $\ln K_s = -\frac{\Delta H_H^\circ}{RT} + \frac{\Delta S_H^\circ}{R}$, Where K_s is a Sieverts constant, ΔH° and ΔS° are the standard enthalpy and entropy of vanadium hydrogen solid solution respectively. The K_s values were calculated using Sievert's law as: $\frac{H}{M} = K_s \sqrt{P}$; Where P is pressure in Pascal. From these data Gibbs free energy could be calculated using equation $\Delta G^\circ = \Delta H^\circ - T\Delta S^\circ$; where symbols have their usual meanings.

3.4.5 Kinetic equation

The mechanism of a reaction is usually checked by fitting the time dependent reacted fraction $\alpha(t)$ to various analytical rate expressions, through which intrinsic rate limiting steps are

obtained. The intrinsic rate limiting step is the slowest step of the reaction. Solid-gas reaction is usually controlled by the diffusion process and the reaction kinetics rate equation can be expressed as follows:

$$\frac{d\alpha}{dt} = k(T)f(\alpha) \quad (3.14)$$

Where, α is the fraction reacted at time t , $k(T)$ temperature dependent rate constant. Two techniques were employed in the present study to obtain the data for reacted fraction α , namely constant pressure and variable mass techniques using thermobalance attached to the Sieverts apparatus:

$$\alpha = \frac{m_t - m_0}{m_{eq} - m_0} \quad (3.15)$$

and constant volume variable pressure in the Sieverts apparatus

$$\alpha = \frac{p_0 - p_t}{p_0 - p_{eq}} \quad (3.16)$$

$f(\alpha)$ is the function about the reaction mechanism, integral of $f(\alpha)$ is expressed as $g(\alpha)$ [95-99]:

$$g(\alpha) = \int \frac{d\alpha}{f(\alpha)} = k(T)t + C \quad (3.17)$$

$f(\alpha)$ or $g(\alpha)$ refers to the reaction mechanism function. The mechanism function that could be controlling the gas –solid reaction could be summarized as in Table 3.1. The α - t kinetic curve derived using Eq 3.13 or Eq 3.14 gives the data for t and α , which were linearly fitted based on Eq (3.12) or (3.15). The mechanism of hydrogen absorption in the alloy is decided by the function $f(\alpha)$ or $g(\alpha)$ giving the best linear fit. The mechanism of hydrogen absorption and the

kinetic parameter ‘k(T)’ were obtained from the linear regression fitting. Based on the Arrhenius equation, the apparent activation energy of hydrogen absorption in the alloy was calculated.

Table 3.1: Mechanism functions responsible for the hydrogen absorption process

Name of function	Type of mechanism		Form of function	
			F(a)	G(a)
Avrami–Erofeev equation	Random nucleation	$n = 1$	$1 - a$	$-\ln(1 - a)$
		$n = 2$	$2(1 - a)[- \ln(1 - a)]^{1/2}$	$[- \ln(1 - a)]^{1/2}$
		$n = 3$	$3(1 - a)[- \ln(1 - a)]^{2/3}$	$[- \ln(1 - a)]^{1/3}$
Parabola law	1-D diffusion, decelerator $a-t$ curve		$1/2a$	a^2
Valensi equation	2-D diffusion, decelerator $a-t$ curve		$[- \ln(1 - a)]^{-1}$	$a + (1 - a)\ln(1 - a)$
Jander equation	3-D diffusion, decelerator $a-t$ curve		$1.5(1 - a)^{2/3}[1 - (1 - a)^{1/3}]^{-1}$	$[1 - (1 - a)^{1/3}]^2$
Anti-Jander equation	3-D diffusion		$1.5(1 + a)^{2/3}[(1 + a)^{1/3} - 1]^{-1}$	$[(1 + a)^{1/3} - 1]^2$
Ginstling–Brounstein equation	3-D diffusion, spherical symmetry		$1.5[(1 - a)^{-1/3} - 1]^{-1}$	$[1 - 2a/3] - (1 - a)^{2/3}$
Zhuralev–Lesokin–Tempelman equation	3-D diffusion		$1.5(1 - a)^{4/3}[(1 - a)^{-1/3} - 1]^{-1}$	$[(1 - a)^{-1/3} - 1]^2$
Chemical reaction equation	Phase boundary reaction	Cylindrical symmetry	$2(1 - a)^{1/2}$	$1 - (1 - a)^{1/2}$
		Spherical symmetry	$3(1 - a)^{2/3}$	$1 - (1 - a)^{1/3}$
		Reaction order	$n = 2$	$(1 - a)^2$

3.4.6 Activation energy

The rate constant k(T) and the activation energy (E) are related by Arrhenius equation, expressed as:

$$k(T) = Ae^{\frac{-E}{RT}} \quad (3.19)$$

Here A is pre-exponential or frequency factor, R is molar gas constant, T is temperature in absolute scale and E is activation energy in J/mol. The above expression may also be written as:

$$\ln k(T) = \ln A - \frac{E}{RT} \quad (3.20)$$

The constant $k(T)$ was calculated from the slope of isothermal hydrogen absorption kinetics curve ($g(\alpha)$ versus time). Slope of $\ln k(T)$ versus $\frac{1}{T}$ gives the value of $\frac{-E}{R}$ which eventually converted into the activation energy E .

3.5 Analytical techniques

3.5.1 Scanning electron microscope (SEM)

Scanning electronic microscope technique is useful to identify the phases present and the morphology of the samples. In present study AIS-2100 CERON make SEM unit was used throughout the investigation. A schematic diagram is shown in Fig 3.7. In a typical SEM, an electron beam is thermionically emitted from an electron gun fitted with a tungsten filament cathode. Tungsten is normally used in thermionic electron guns because it has the highest melting point and lowest vapor pressure of all metals, thereby allowing it to be heated for electron emission, and because of its low cost. Other types of electron emitters include lanthanum hexaboride (LaB_6) cathodes, which can be used in a standard tungsten filament SEM if the vacuum system is upgraded and field emission guns (FEG), which may be of the cold-cathode type using tungsten single crystal emitters or the thermally assisted Schottky type, using emitters of zirconium oxide. The electron beam, which typically has an energy ranging from 0.5 keV to 40 keV, is focused by one or two condenser lenses to a spot about 0.4 nm to 5 nm in diameter. The beam passes through pairs of scanning coils or pairs of deflector plates in the electron column, typically in the final lens, which deflect the beam in the x and y axes so that it scans in a raster fashion over a rectangular area of the sample surface. When the primary electron beam interacts with the sample, the electrons lose energy by repeated random scattering and absorption within a teardrop-shaped volume of the specimen known as the interaction volume,

which extends from less than 100 nm to around 5 μm into the surface. The size of the interaction volume depends on the electron's landing energy, the atomic number of the specimen and the specimen's density. The energy exchange between the electron beam and the sample results in the reflection of high-energy electrons by elastic scattering, emission of secondary electrons by inelastic scattering and the emission of electromagnetic radiation, each of which can be detected by specialized detectors. The beam current absorbed by the specimen can also be detected and used to create images of the distribution of specimen current. Electronic amplifiers of various types are used to amplify the signals, which are displayed as variations in brightness on a cathode ray tube. The faster scanning of the CRT display is synchronized with that of the beam on the specimen in the microscope, and the resulting image is therefore a distribution map of the intensity of the signal being emitted from the scanned area of the specimen..

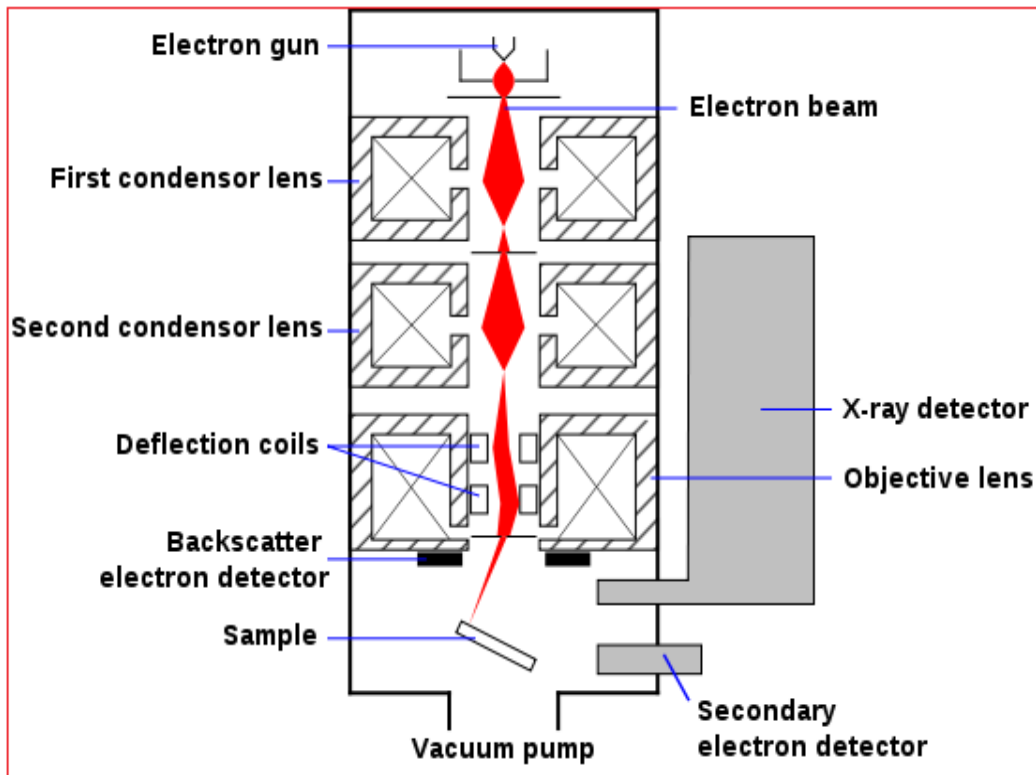


Fig. 3.7: Schematic diagram of a SEM instrument [112]

The image may be captured by photography from a high-resolution cathode ray tube, but in modern machines is digitally captured and displayed on a computer monitor and saved to a computers hard disk

3.5.2 Energy-dispersive X-ray spectroscopy (EDS/EDX)

EDS or EDX is an analytical technique used for the elemental analysis or chemical characterization of a sample. It is one of the variants of X-ray fluorescence spectroscopy which relies on the investigation of a sample through interactions between electromagnetic radiation and matter, analyzing X-rays emitted by the matter in response to being hit with charged particles. Its characterization capabilities are due in large part to the fundamental principle that each element has a unique atomic structure emitting X-rays that are characteristic of an element's atomic structure to be identified uniquely from one another. To stimulate the emission of characteristic X-rays from a specimen, a high-energy beam of charged particles such as electrons or protons (see PIXE), or a beam of X-rays, is focused into the sample being studied (Fig 3.8). At rest, an atom within the sample contains ground state (or unexcited) electrons in discrete energy levels or electron shells bound to the nucleus. The incident beam may excite an electron in an inner shell, ejecting it from the shell while creating an electron hole where the electron was present. An electron from an outer, higher-energy shell then fills the hole, and the difference in energy between the higher-energy shell and the lower energy shell may be released in the form of an X-ray. The number and energy of the X-rays emitted from a specimen can be measured by an energy-dispersive spectrometer.

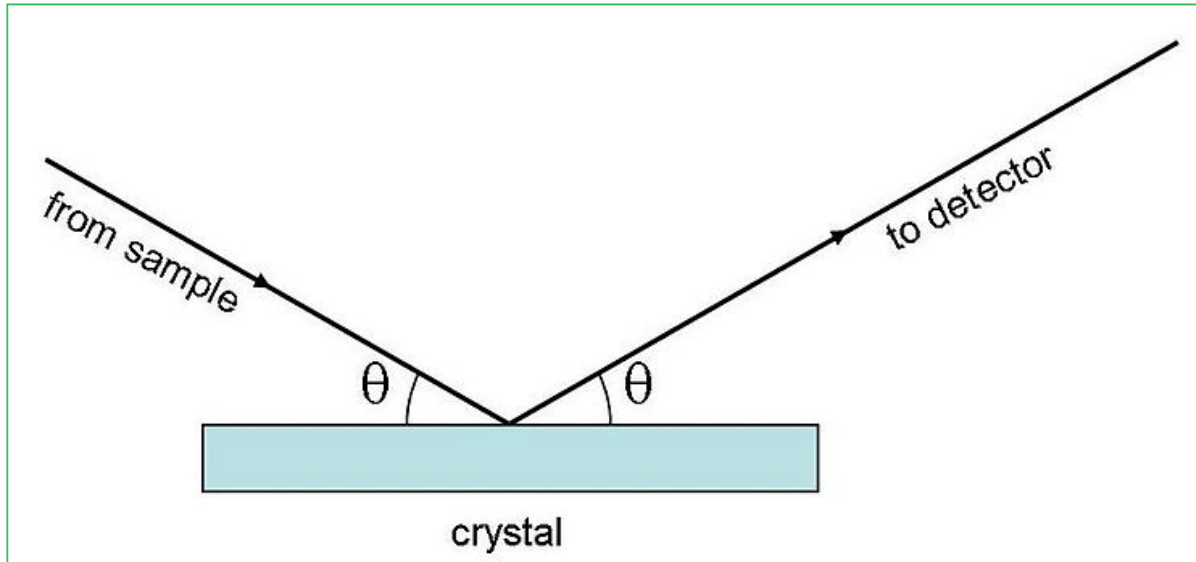


Fig.3.8: Schematic diagram showing the principle of energy disperse spectroscopy (EDS) used for the composition analysis [112]

As the energy of the X-rays are characteristic of the difference in energy between the two shells, and of the atomic structure of the element from which they were emitted, this allows the elemental composition of the specimen to be measured. In the present study AIS-2100 CERON make EDS unit was used.

3.5.3 X-Ray diffraction (XRD)

In the present study M/s Philips make PW 1830 X-ray diffraction unit was used throughout the experiment. X-ray diffractometer consists of three basic elements (Fig 3.9) an X-ray tube, a sample holder, and an X-ray detector. X-rays are generated in a cathode ray tube by heating a filament to produce electrons, accelerating the electrons toward a target by applying a voltage, and bombarding the target material with electrons. When electrons have sufficient

energy to dislodge inner shell electrons of the target material, characteristic X-ray spectra are produced.

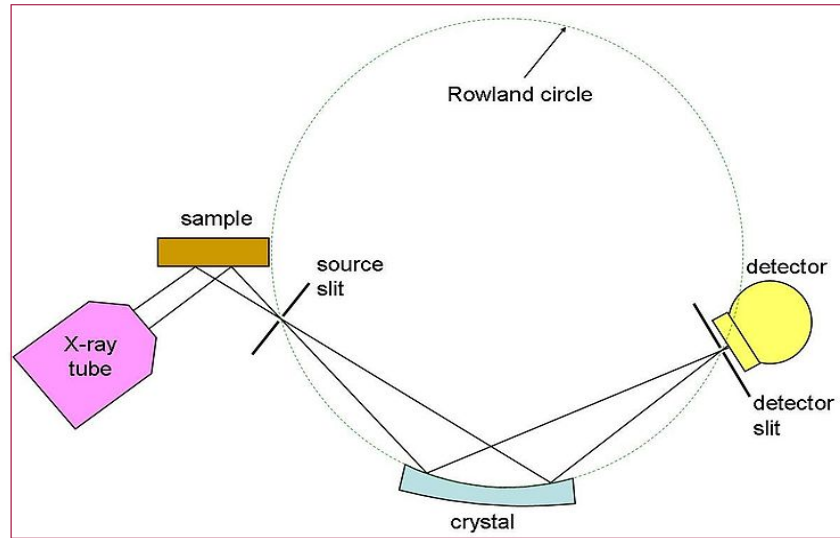


Fig. 3.9: Schematic diagram of a typical XRD used for the phase's analysis in the present investigation [112]

These spectra consist of several components, the most common being K_{α} and K_{β} . K_{α} consists, in part, of $K_{\alpha 1}$ and $K_{\alpha 2}$. $K_{\alpha 1}$ has a slightly shorter wavelength and twice the intensity as $K_{\alpha 2}$. The specific wavelengths are characteristic of the target material (Cu, Fe, Mo, Cr). Filtering, by foils or crystal monochrometers, is required to produce monochromatic X-rays needed for diffraction. $K_{\alpha 1}$ and $K_{\alpha 2}$ are sufficiently close in wavelength such that a weighted average of the two is used. Copper is the most common target material for single-crystal diffraction, with Cu K_{α} radiation = 1.5418\AA . These X-rays are collimated and directed onto the sample. As the sample and detector are rotated, the intensity of the reflected X-rays is recorded. When the geometry of the incident X-rays impinging the sample satisfies the Bragg Equation, $2d\sin\theta = n\lambda$, constructive

interference occurs and a peak in intensity occurs. A detector records and processes this X-ray signal and converts the signal to a count rate which is then output to a device such as a printer or computer monitor. The geometry of an X-ray diffractometer is such that the sample rotates in the path of the collimated X-ray beam at an angle θ while the X-ray detector is mounted on an arm to collect the diffracted X-rays and rotates at an angle of 2θ . The instrument used to maintain the angle and rotate the sample is termed a goniometer. In some case multiple detectors are used to records the diffraction patterns. In this case neither the sample nor the detector will move. For typical powder patterns, data is collected at 2θ from $\sim 5^\circ$ to 70° , angles that are preset in the X-ray scan. The d-spacing of each peak is then obtained by solution of the Bragg equation for the appropriate value of λ . Once all d-spacings have been determined, automated search/match routines compare the d 's of the unknown to those of known materials. Because each mineral has a unique set of d-spacings, matching these d-spacings provides an identification of the unknown sample. A systematic procedure is used by ordering the d-spacings in terms of their intensity beginning with the most intense peak. Files of d-spacings for hundreds of thousands of inorganic compounds are available from the International Centre for Diffraction Data as the Powder Diffraction File (PDF). Many other sites contain d-spacings of metals s such as the American Mineralogist Crystal Structure Database. Commonly this information is an integral portion of the software that comes with the instrumentation.

3.5.4 Inert gas fusion technique (Nitrogen Oxygen and Hydrogen)

The inert gas fusion (IGF) principle was developed into an analytical technique introduced in the mid-twentieth century. This method is also referred to as gas fusion analysis (GFA), or carrier gas hot extraction method (CGHE). The principle of operation is based on the fusion of a sample in a high purity graphite crucible at temperatures up to, or in some cases

exceeding, 3000° C in an inert gas such as helium. The typical IGF instrument is computer controlled and consists of an alloy-tipped water-cooled electrode furnace and a measurement unit containing the bulk of the electronics and detectors. A pre-weighed sample [nominal 1-5 g] is placed in a loading chamber located above the graphite crucible in the electrode furnace. After a short gas purge cycle, electric current is passed through the crucible heating it up to 3273K while the carrier gas is flowing over it in order to “out-gas” [remove contaminants] the crucible. Following this out-gas cycle, the crucible temperature is lowered by reducing the current and the sample is transferred to the hot crucible by a sample drop mechanism. The sample melts and any oxygen in the sample reacts with carbon from the crucible to form carbon monoxide (CO), some carbon dioxide (CO₂) may also be released depending on the sample type and crucible temperature. Nitrogen in the sample is released as molecular nitrogen (N₂) while hydrogen elutes as hydrogen gas (H₂). These gasses are swept out of the furnace and on to the detectors by the carrier gas. A cut-away view of a typical electrode furnace is shown in Fig 3.10. Oxygen is typically detected as CO, CO₂, or both using infrared (IR) detectors. CO and CO₂ absorb IR energy at specific wavelengths within the IR spectrum. Nitrogen, as N₂, and hydrogen as H₂, normally are detected using a thermal-conductivity (TC) detector. A TC detector is a universal detector, responding to any gas that has a different thermal conductivity than the carrier gas. Therefore, separation or removal of gases other than the gas being measured and the carrier gas itself, is required before the detector is reached. Dipolar gases such as N₂ and H₂ do not absorb IR energy; therefore, TC detectors are used for nitrogen and hydrogen measurement. The sensitivity of a TC detector is dependent on the thermal conductivity difference between the carrier gas and the analyte gas. Helium is used as a carrier gas for nitrogen measurement because of the large thermal conductivity difference between helium and nitrogen. Helium and H₂ have

similar thermal conductivity; therefore argon (Ar) is typically used as a carrier gas in an instrument designed to measure hydrogen. Since Ar and N₂ have similar thermal conductivity, low levels of nitrogen cannot be accurately determined using Ar as a carrier gas. A TC cell is a very sensitive and generally linear detection device; however it is a universal detector that cannot tell the difference between various gases unless they are separated (or removed) by some means. Gases such as CO, CO₂ and N₂, must be either removed or separated from the H₂ for proper hydrogen measurement.

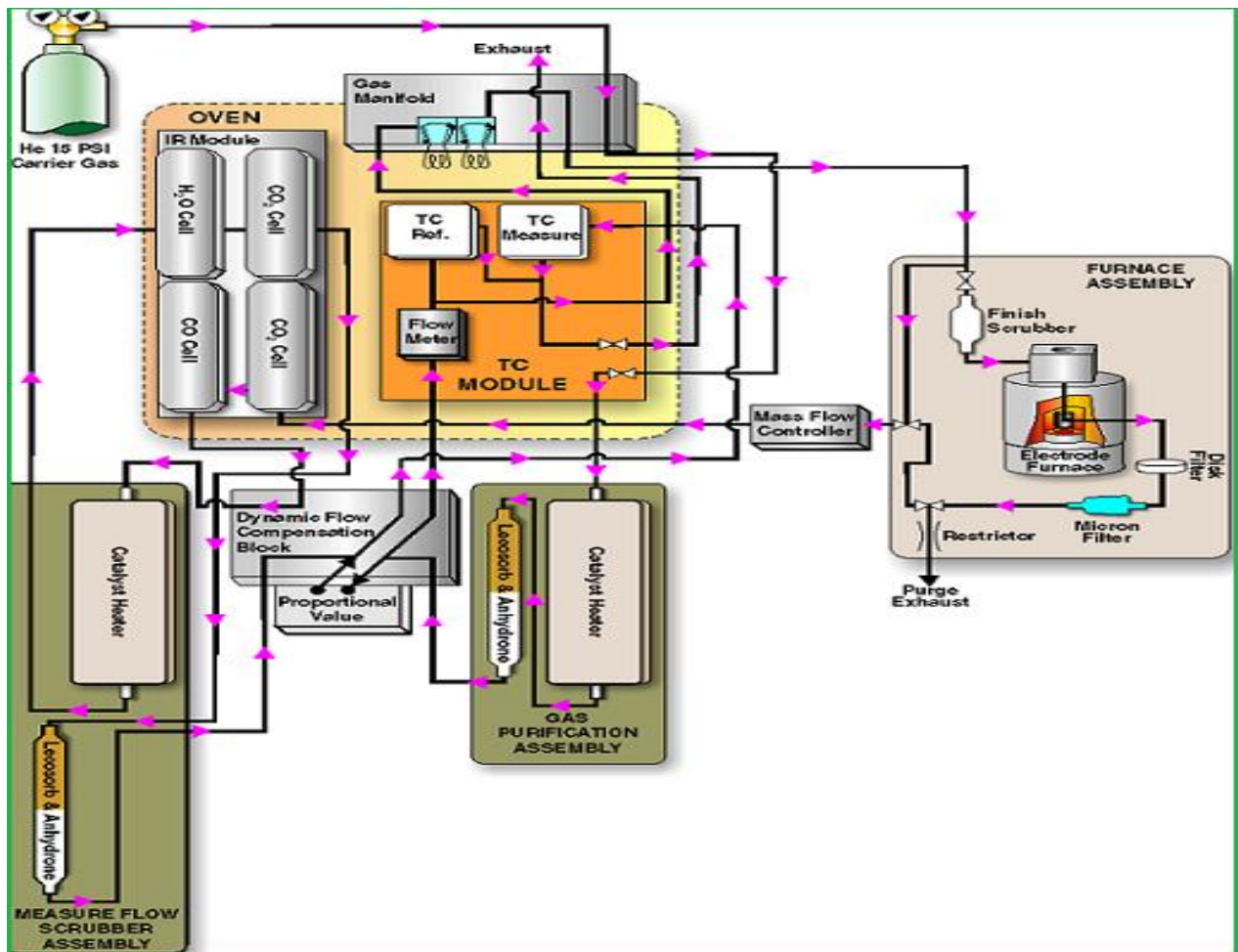


Fig. 3.10: Schematic diagram of inert-gas fusion technique used in the study to determine the non-metallic impurities in the sample [112-113]

In a typical hydrogen determinator using Ar as a carrier gas, the CO released from a sample is converted to CO₂ by passing it over the Schutze reagent (iodine pentoxide on treated silica gel). This conversion takes place at room temperature and does not affect either H₂ or N₂ released from a sample. The CO₂ is subsequently removed using sodium hydroxide (on a clay base). The N₂ cannot be removed; therefore it is separated from the H₂ by passing the gas stream through a long column. The H₂ elutes from the column first and is measured by the TC cell. The N₂ elutes from the column approximately 45 seconds after the hydrogen has been measured.

3.5.5 X-Ray fluorescence (XRF)

When materials are exposed to short-wavelength X-rays or gamma rays, ionization of their component atoms may take place. Ionization consists of the ejection of one or more electrons from the atom, and may occur if the atom is exposed to radiation with energy greater than its ionization potential. X-rays and gamma rays can be energetic enough to expel tightly held electrons from the inner orbitals of the atom. The removal of an electron in this way renders the electronic structure of the atom unstable, and electrons in higher orbitals "fall" into the lower orbital to fill the hole left behind. In falling, energy is released in the form of a photon, the energy of which is equal to the energy difference of the two orbitals involved. Thus, the material emits radiation, which has energy characteristic of the atoms present. The term *fluorescence* is applied to phenomena in which the absorption of radiation of a specific energy results in the re-emission of radiation of a different (generally lower) energy. Each element has electronic orbitals of characteristic energy. Following removal of an inner electron by an energetic photon provided by a primary radiation source, an electron from an outer shell drops into its place. There are a limited number of ways in which this can happen. The main transitions are given names: an L→K transition is traditionally called K_α, an M→K transition is called K_β, an M→L transition is

called $L\alpha$, and so on. Each of these transitions yields a fluorescent photon with a characteristic energy equal to the difference in energy of the initial and final orbital. The wavelength of this fluorescent radiation can be calculated from Planck's Law: $\lambda = hc/E$.

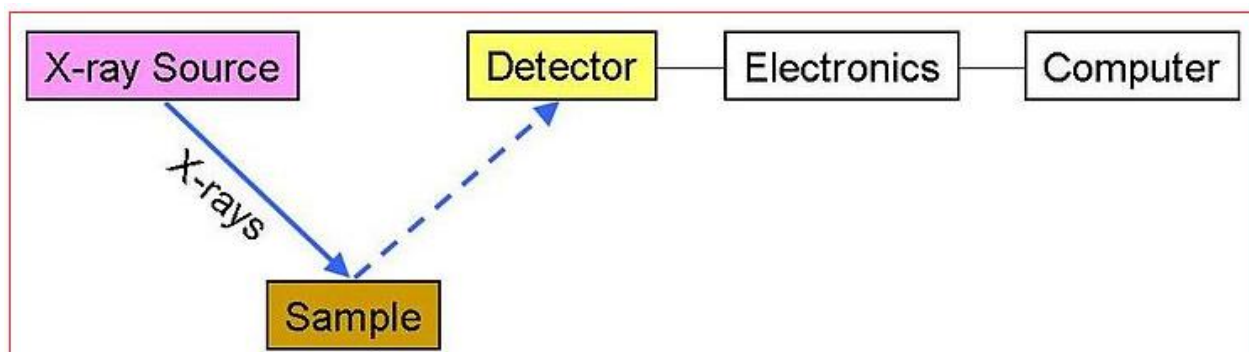


Fig. 3.11: Schematic principle of XRF analysis [113]

The fluorescent radiation can be analysed either by sorting the energies of the photons (energy-dispersive analysis) or by separating the wavelengths of the radiation (wavelength-dispersive analysis). Once sorted, the intensity of each characteristic radiation is directly related to the amount of each element in the material. A Schematic diagram of a XRF unit is shown in the Fig 3.11.

3.5.6 Differential thermal analysis (DTA)

A schematic diagram of DSC unit is shown in the Fig 3.12. It is a thermoanalytical technique in which the difference in the amount of heat required to increase the temperature of a sample and reference is measured as a function of temperature. Both the sample and reference are maintained at nearly the same temperature throughout the experiment. Generally, the temperature program for a DSC analysis is designed such that the sample holder temperature increases linearly as a function of time. The reference sample should have a well-defined heat capacity over the range of temperatures to be scanned. The basic principle underlying this

technique is that when the sample undergoes a physical transformation such as phase transitions, more or less heat will need to flow to it than the reference to maintain both at the same temperature. Whether less or more heat must flow to the sample depends on whether the process occurring in the sample is exothermic or endothermic. For example, as a solid sample melts to a liquid it will require more heat flowing to the sample to increase its temperature at the same rate as the reference. This is due to the absorption of heat by the sample as it undergoes the endothermic phase transition from solid to liquid. Likewise, as the sample undergoes exothermic processes (such as crystallization) less heat is required to raise the sample temperature. By observing the difference in heat flow between the sample and reference, differential scanning calorimeters are able to measure the amount of heat absorbed or released during such transitions. DSC may also be used to observe more subtle phase changes, such as glass transitions. It is widely used in industrial settings as a quality control instrument. An alternative technique, which shares much in common with DSC, is differential thermal analysis (DTA). In this technique it is the heat flow to the sample and reference that remains the same rather than the temperature. When the sample and reference are heated in an identical environment phase changes and other thermal processes occurring in the sample cause a difference in temperature between the sample and reference. The temperature difference is sensed and controlled to information on the thermal events occurring. Both DSC and DTA provide similar information. Many modern commercial DTA are called heat flux DSC.

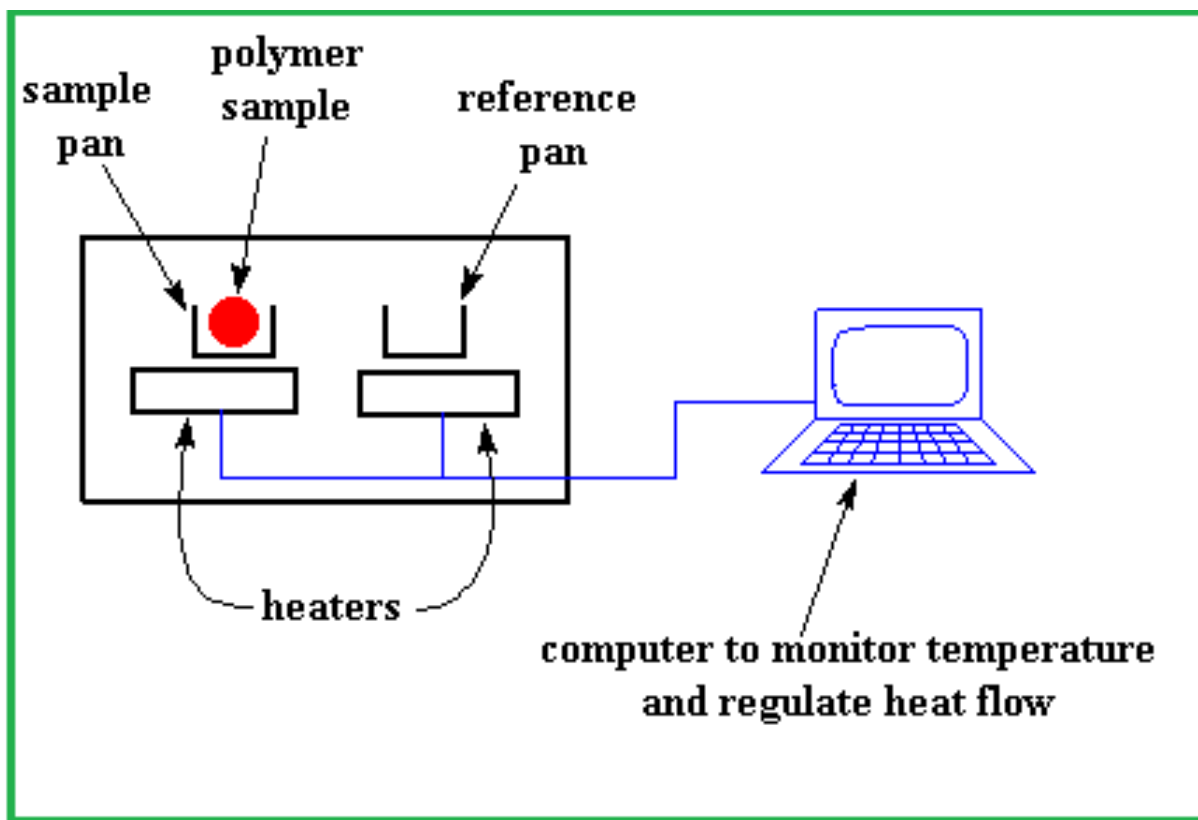


Fig.3.12: Differential thermal analysis unit used to determine the enthalpy of hydrogenation process [112]

3.5.7 Inductively coupled plasma atomic emission spectroscopy (ICP-AES)

ICP-AES also referred as inductively coupled plasma optical emission spectrometry (ICP-AES), is trace analytical technique used for the detection of trace metals in very low concentration in the sample. It is a type of emission spectroscopy that uses the inductively coupled plasma to produce excited atoms and ions that emit electromagnetic radiation at wavelengths characteristic of a particular element. The intensity of this emission is indicative of the concentration of the element within the sample. The ICP-AES is composed of two parts: the ICP and the optical spectrometer. The ICP torch consists of 3 concentric quartz glass tubes. The output or "work" coil of the radio frequency (RF) generator surrounds part of this quartz torch. Argon gas is typically used to create the plasma. When the torch is turned on, an intense

electromagnetic field is created within the coil by the high power radio frequency signal flowing in the coil. This RF signal is created by the RF generator which is, effectively, a high power radio transmitter driving the "work coil" the same way a typical radio transmitter drives a transmitting antenna. The argon gas flowing through the torch is ignited with a Tesla unit that creates a brief discharge arc through the argon flow to initiate the ionization process. Once the plasma is "ignited", the Tesla unit is turned off. The argon gas is ionized in the intense electromagnetic field and flows in a particular rotationally symmetrical pattern towards the magnetic field of the RF coil. Stable high temperature plasma of about 7000 K is then generated as the result of the inelastic collisions created between the neutral argon atoms and the charged particles. A peristaltic pump delivers an aqueous or organic sample into a nebulizer where it is changed into mist and introduced directly inside the plasma flame. The sample immediately collides with the electrons and charged ions in the plasma and is itself broken down into charged ions. The various molecules break up into their respective atoms which then lose electrons and recombine repeatedly in the plasma, giving off radiation at the characteristic wavelengths of the elements involved. In some designs, a shear gas, typically nitrogen or dry compressed air is used to 'cut' the plasma flame at a specific spot. One or two transfer lenses are then used to focus the emitted light on a diffraction grating where it is separated into its component wavelengths in the optical spectrometer. In other designs, the plasma impinges directly upon an optical interface which consists of an orifice from which a constant flow of argon emerges, deflecting the plasma and providing cooling while allowing the emitted light from the plasma to enter the optical chamber. Still other designs use optical fibers to convey some of the light to separate optical chambers. Within the optical chamber(s), after the light is separated into its different wavelengths (colors), the light intensity is measured with a photomultiplier tube or tubes

physically positioned to "view" the specific wavelength(s) for each element line involved, or, in more modern units, (Fig.3.13) the separated colors fall upon an array of semiconductor photo detectors such as charge coupled devices (CCDs). In units using these detector arrays, the intensities of all wavelengths (within the system's range) can be measured simultaneously, allowing the instrument to analyze for every element to which the unit is sensitive all at once. Thus, samples can be analyzed very quickly.

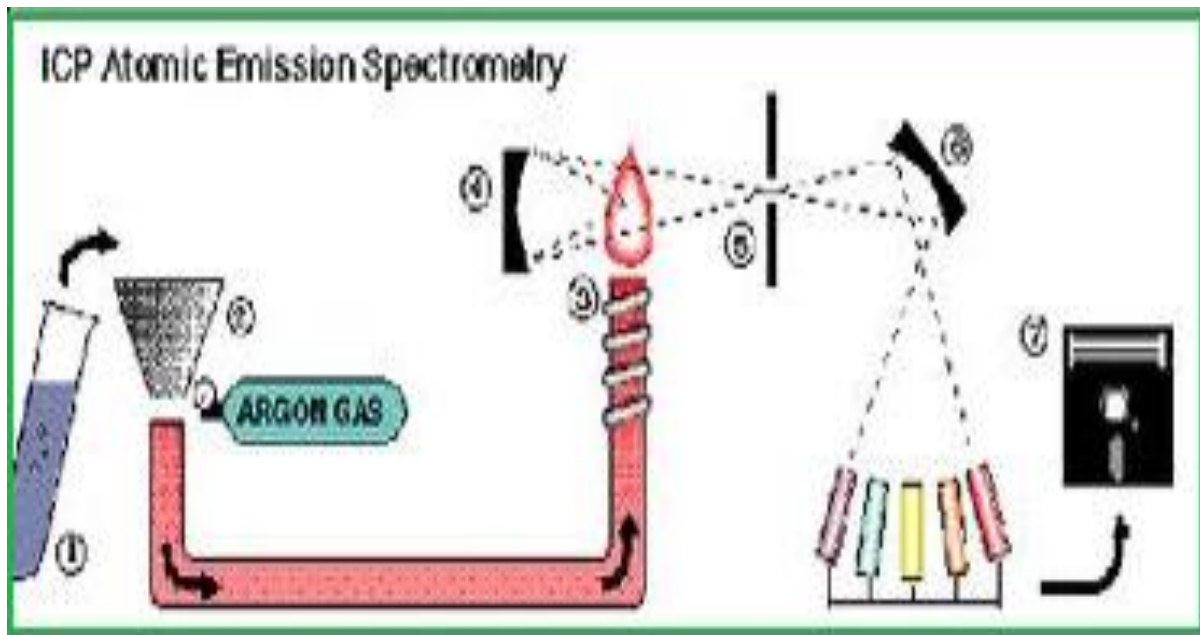


Fig. 3.13: Schematic diagram of Inductively coupled plasma atomic emission spectroscopy (ICP-AES) [113]

3.6 Summary and conclusions

Vanadium metal and V-Al, V-Ti-Cr master alloys were synthesized successfully by reduction and co-reduction of V_2O_5 , Cr_2O_3 and TiO_2 with Aluminum in open bomb reactor. The reduction of V_2O_5 and Cr_2O_3 are highly exothermic and lead to self propagating type of reaction which results in self sustaining reduction of less exothermic TiO_2 by Al. A range of compositions of a

mixture of V_2O_5 , TiO_2 and Cr_2O_3 can be chosen to make the overall reduction with Aluminum sufficiently exothermic for a self- sustaining reaction. The Sieverts apparatus and a modified Sieverts apparatus indigenously fabricated and used to carry-out the investigation for hydrogen absorption and desorption. The methods employed to study the equilibrium hydrogen solubility and the related thermodynamics parameters like enthalpy, entropy and Gibbs free energy has been illustrated. The details of hydrogen absorption kinetics in the metal and alloys and the method applicable to this process have been explained. The details of other instruments used in the present investigation have also been explained.

Chapter... 4

Results and discussion

Contents

4.1 Materials preparation	81-93
4.1.1 Introduction	81
4.1.2 Thermodynamics of aluminothermy reactions.....	81
4.1.3 Vanadium metal and vanadium-aluminum alloys.....	83
4.1.4 Characterization of vanadium-aluminum alloys	86
4.1.5 V-Ti-Cr alloys by aluminothermy process	89
4.1.6 Mechanism of refining process	92
4.2 Vanadium-hydrogen solid solution	94-111
4.2.1 Introduction.....	94
4.2.2 Solution behaviour of hydrogen.....	94
4.2.3 Hydrogen solubility.....	98
4.2.4 Theories on hydrogen solubility.....	103
4.3 Phase stability.....	112-120
4.3.1 Introduction	112
4.3.2 VH_2 (γ) phase.....	112
4.3.3 α and β phase.....	114
4.3.4 Pressure composition isotherm of V-Ti-Cr alloy	119
4.4 Thermodynamics and Kinetics.....	121-151
4.4.1 Introduction.....	121
4.4.2 Enthalpy, Entropy and Gibbs free energy of V-H solution.....	121
4.4.3 Hydrogen absorption kinetics of V-Al and V-Ti-Cr alloys.....	127
4.4.4 Effects of vanadium on the H absorption kinetics of $LaNi_5$	147

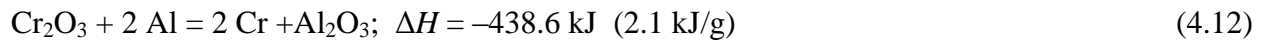
4.1 Materials preparation

4.1.1 Introduction

The aim of the present Ph.D research work is to investigate the effects of aluminum on the hydrogen interaction parameters of vanadium, vanadium based alloys or composite. Therefore, vanadium, vanadium-aluminum, vanadium-titanium-chromium alloys and V-LaNi₅ composite have been prepared in the laboratory by aluminothermy process followed by electron beam refining or by arc melting of pure component. Aldrich make high pure vanadium, and the alloying component aluminum, titanium and chromium have been used for the comparative study. The homogeneity of the alloys thus prepared has been confirmed by chemical analysis of different portions of the sample which was further verified by Vickers-hardness measurement.

4.1.2 Thermodynamics of aluminothermy process

The free energy changes with temperature of the reactions (4.1.1-4.1.3) are shown in the Fig. 4.1.1 and enthalpy of reactions is given below.



The figure indicates the feasibility of the reaction even at low temperature, although heat of reaction is a key parameter to decide the self-sustainability of the reaction. The exothermicity of the reaction, represented as the ratio of the heat of the reaction and the sum of the molecular mass of the charge/products, is calculated and presented along with the equations (4.1.1-4.1.3).

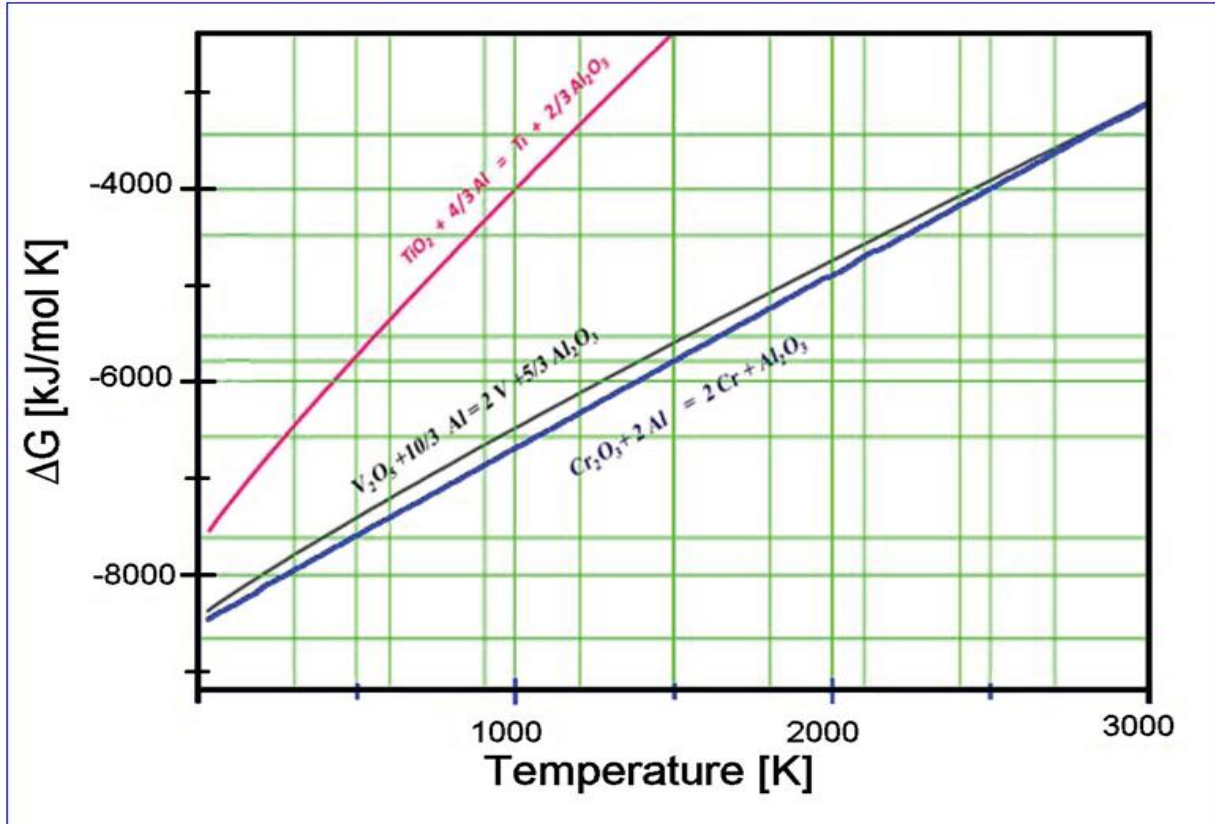


Fig. 4.1.1: Gibbs free energy diagram all the three reactions

The value needed is in the range between 2.2 kJ/g and 4.5 kJ/g for the reaction to develop in a controlled manner, resulting in the melting of both the reduced metal and the slag, and to retain them in the fluid condition long enough for good slag metal separation [114-117]. The heat of aluminothermy reduction of TiO₂ is relatively less and use of heat booster is necessary. The ternary alloy V-Ti-Cr was made by aluminothermy reduction of mixed oxides of V₂O₅, TiO₂ and Cr₂O₃ [115]. The reduction of V₂O₅ and Cr₂O₃ with Al are highly exothermic which provided the shortfall of the heat required for reduction of TiO₂ by aluminum. Alumina, as a slag formed during the thermit reaction, is the highest melting component in the system and its fusion point was lowered by an additive like CaO. The viscosity of the slag was lowered by adding CaF₂. As a result of these factors, improvements in the yield as presented in the Table 4.1.1, [58, 60, 69].

Table 4.1.1: Effects of slag flux and fluidizer on the % yield of V-Al thermit

Charge (Size)	302 g	307g	305g	301g	302g	301g	307g	302g	307g	310g
CaO wt %	-	-	-	-	10	15	20	10	-	-
CaSiO ₃ wt %	-	10	15	20	-	-	-	10	-	-
CaF ₂ wt %	10	-	-	-	-	-	-	10	-	20
% yield	82	83	89	92	80	82	86	89	79	71

As indicated in the Table 4.1.1, CaSiO₃ gives the highest yield, 92%. Besides, in the absence of slag fluidizer only about 20% titanium from titanium oxide ends up in the thermit. Therefore, for loading of titanium the use of slag fluidizers appears necessary.

4.1.3 Vanadium metal and vanadium-aluminum alloys

Vanadium-aluminum thermit prepared by thermit process was analyzed by ICP-AES technique. The quantities of aluminum in the thermit were found to be 8 to 14 wt. %. The non-metallic impurities, oxygen and nitrogen were 900 and 400 ppm respectively. The amount of the aluminum in the thermit has been controlled by using suitable excess amount of aluminum than required by reaction stoichiometric quantity (Eq 4.1.1) in the initial charge. The quantity of aluminum in the initial charge is determined by the requirements of subsequent refining process to be used and determined the amounts of residual aluminum as well as oxygen in the thermit as and in the refined product subsequently. On changing the excess aluminum in the initial charge the aluminum content in the thermit could be varied from 8 to 14 wt. % and after single step electron beam refined alloy the residual aluminum contents were 0.8 to 1.7 wt % whereas the corresponding oxygen contents were from 400 to 200 ppm. However, nitrogen content remained same even after refining process in all the cases. Typically nitrogen content was about 800 ppm

in the thermit prepared in a refractory lined open bomb reactor aluminothermy process and after single step electron beam refining. Mostly, the air entrapped in the reactor supplied this nitrogen. In all the synthesis processes thermit containing more than 8% residual aluminum are aimed by adjusting the aluminum content in the initial charge composition because vanadium thermit containing less than this critical quantity of aluminum cannot be effectively refined with respect to oxygen by pyro-vacuum treatments to yield pure vanadium. However, higher percentage of aluminum in the initial charge yielded V-Al master alloys. The sample products of the vanadium thermit and completely refined product vanadium metal are shown in the Fig 4.1.2.



Fig. 4.1.2: Vanadium-aluminum thermit along with completely refined product vanadium

The as such prepared thermit looks black in color that could be due to surface oxidation. On subsequent refining a silvery white vanadium metal has been obtained as shown in Fig 4.1.2.

The vanadium metals thus prepared was analyzed by XRD. The XRD result presented in Fig 4.1.3 shows single phase vanadium metal.

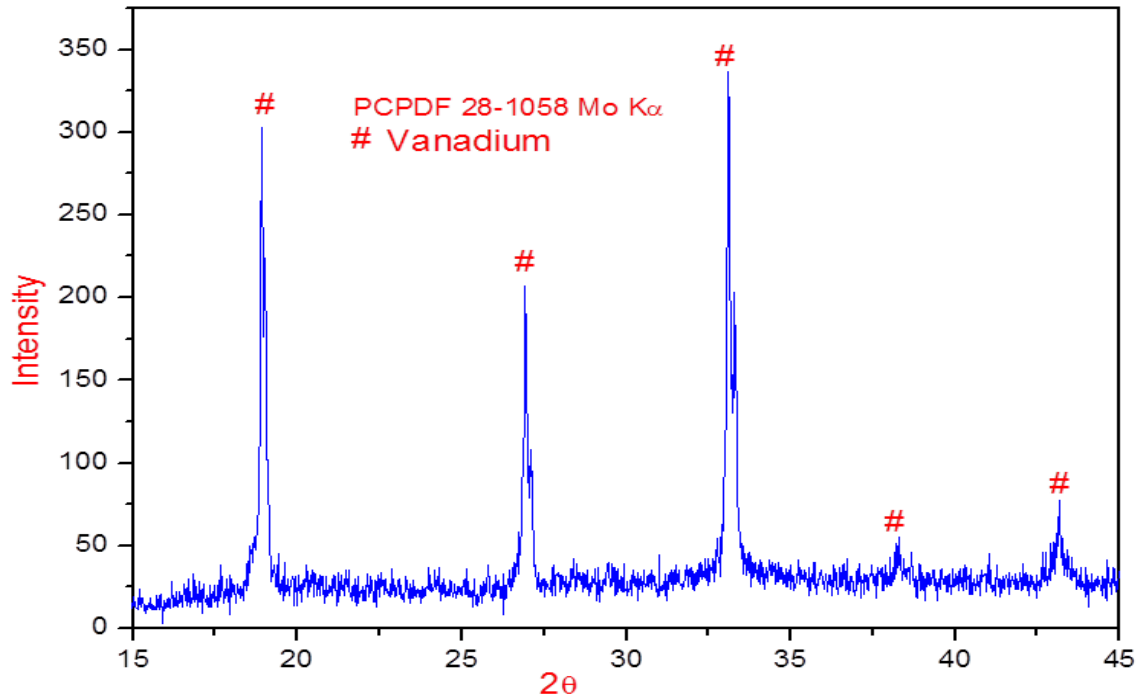


Fig. 4.1.3: X-Ray diffraction analysis of vanadium metals prepared by aluminothermy process and refined by electron beam analysis

The analysis result confirmed the absence of any other phase and indicated that all the impurities (O, N and Al) were well within the solubility limit. An identical phase was observed for the Aldrich make, 99.98 % pure vanadium procured from the market. The optical micrograph of the vanadium was examined using high resolution microscope and presented in the Fig. 4.1.4 (1). The micrograph showed well defined grains. The purity and homogeneity of the metal were analyzed by SEM-EDS technique and the results are presented in Fig 4.1.4 (2). The EDS analysis confirmed that metal prepared by the aluminothermy process is substantially pure and the

aluminum, oxygen and nitrogen were below the detectable limit of the EDS instruments over the entire portion of the sample.

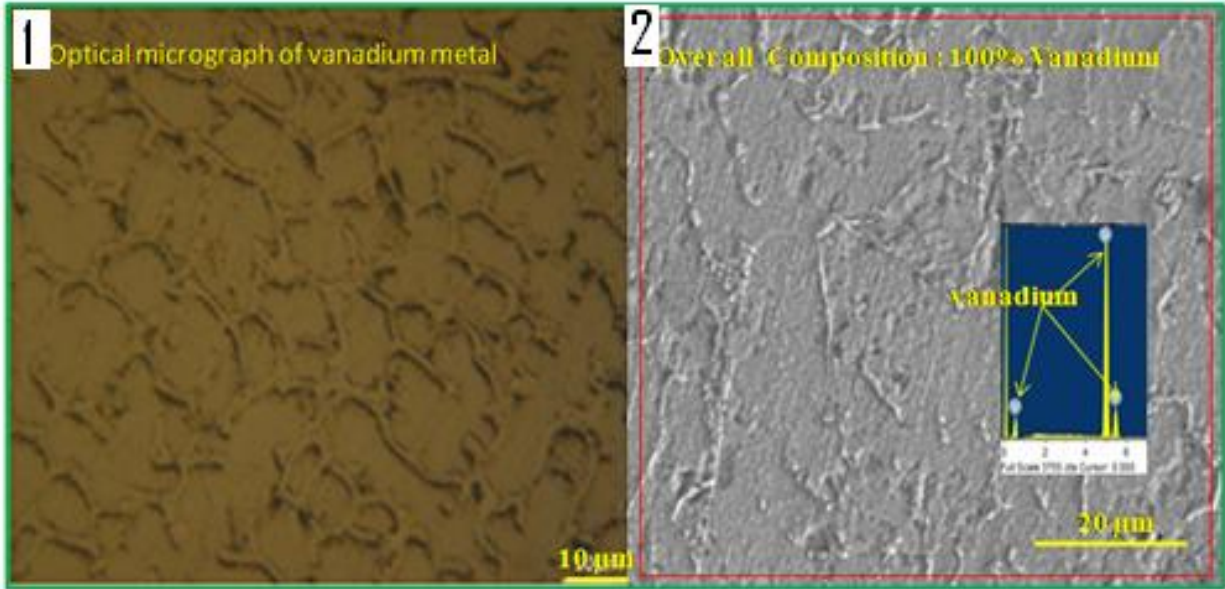


Fig 4.1.4: (1) Optical micrograph and (2) SEM-EDS analysis of the vanadium sample prepared through aluminothermy process

4.1.4 Characterization of vanadium-aluminum alloys

Vanadium-aluminum phase diagram, presented in Fig 4.1.5, indicates that the solubility of aluminum in vanadium mildly depends upon the temperature. The solubility limit of aluminum in vanadium at room temperature is 26 wt. % [112] which increases to 30 wt. % at 924 K. The XRD analysis of a typical V-18wt% aluminum alloy is presented in Fig 4.1.6. The XRD revealed that the aluminum content was within the solubility limit as no intermetallic phases were observed. In the present investigation, all the V-Al alloys contains less than 18 wt % Al therefore, aluminum contents were within the solubility limit.

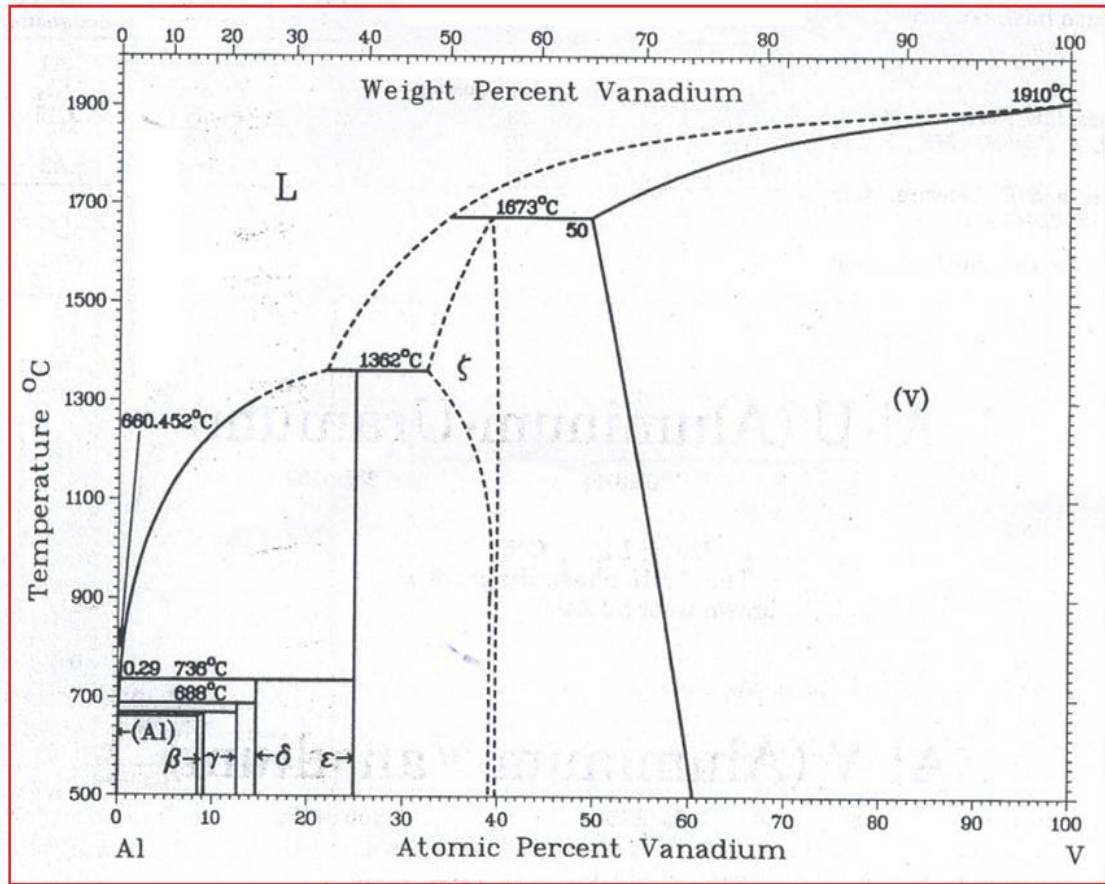


Fig. 4.1.5: Vanadium-aluminum phase diagram [120]

The solid solution behavior of vanadium-aluminum alloys was studied by measuring the lattice constant of vanadium as a function of aluminum and presented in Fig 4.1.7. The lattice constant of the V–Al alloy increases linearly with the increase of Al content and obey Vegard's law. This suggested that the average distance between adjacent interstitial sites, a property that affects the hydrogen solubility in the metal, changed linearly with aluminum content. Hardness of the vanadium was also studied as function of aluminum content.

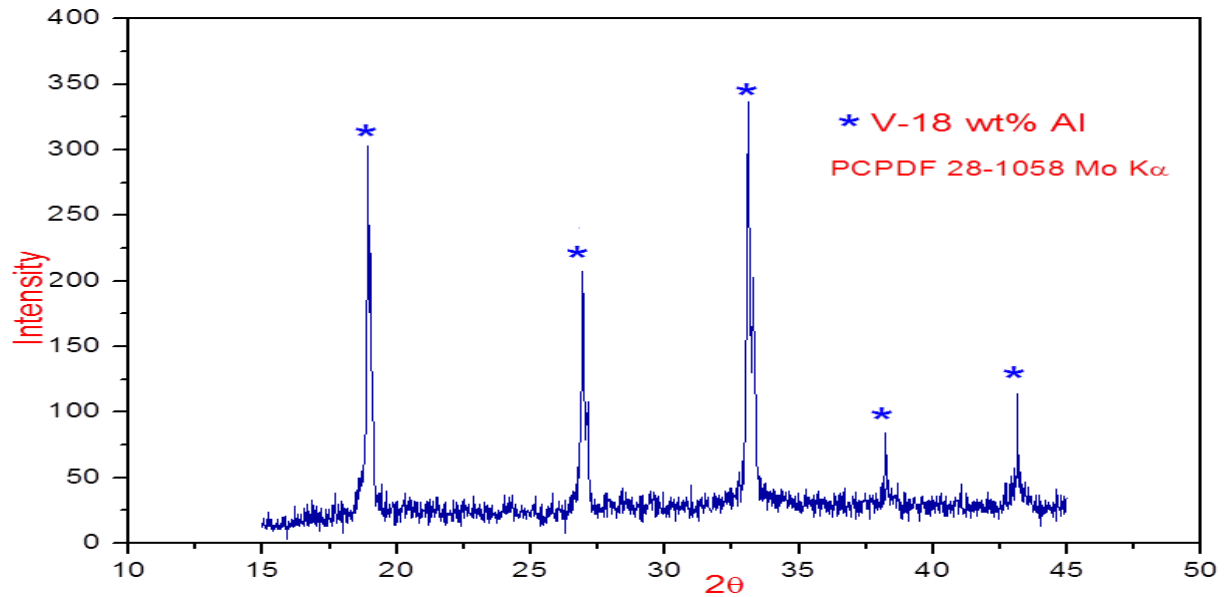


Fig. 4.1.6: X-Ray analysis of the V-18 wt% aluminum: The alloys containing the highest amount of aluminum used in the present study

The result is presented in Fig 4.1.7. The Vickers hardness of the alloys increased linearly with the Al content, suggesting that aluminum hardened the vanadium by a simple solid solution effect. Hardness measurements were also carried out to check the alloys homogeneity by measuring the hardness at 10-12 different locations of the alloy samples. Variation of the hardness of the vanadium-aluminum alloys prepared by aluminothermy process was found to be within $\pm 5\%$ which indicates homogeneity of the sample. However, in case of a vanadium-aluminum alloy prepared by vacuum arc melting using pure components indicate Vickers hardness variation of $\pm 8\%$. Thus it was concluded that the alloys prepared by aluminothermy process gives better homogeneity than the alloy prepared by arc melting in the case of V-Al alloys because of large difference in melting point as well as density of these elements.

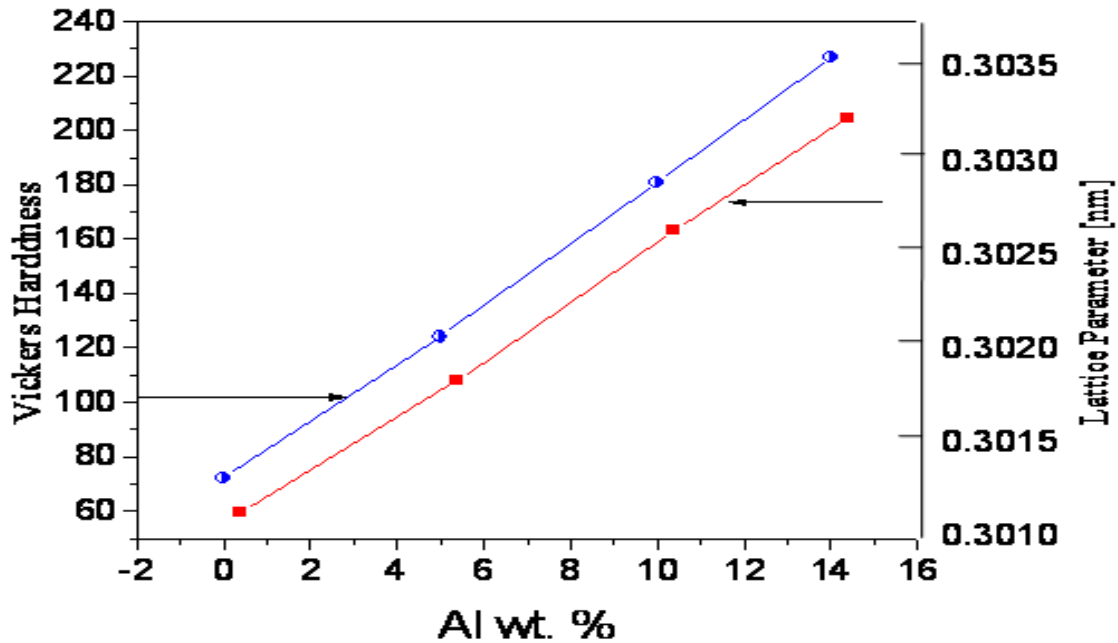


Fig. 4.1.7: Variation of lattice constant and Vickers hardness of V–Al alloys as a function of Al content

4.1.5 V-Ti-Cr alloys by aluminothermy process

Vanadium-titanium-chromium alloys are a proposed structural material for the fusion reactor. These materials are also important for the hydrogen storage point of view. The alloy could be prepared by arc melting of constituent components however; due to cost effectiveness and homogeneity possible by the direct synthesis method, aluminothermy process has been employed in the present investigation. Desired composition of the alloys could not be achieved because of unpredictable loading pattern of titanium. Vanadium-titanium-chromium master alloys were synthesized successfully by co-reduction of V_2O_5 , Cr_2O_3 and TiO_2 with aluminum in open bomb reactor. The reduction of V_2O_5 and Cr_2O_3 are highly exothermic and support the thermal requirements of the less exothermic TiO_2 reduction by aluminum as mentioned earlier and lead to self propagating and self sustaining type of reaction. A range of compositions of

mixture of V_2O_5 , TiO_2 and Cr_2O_3 was chosen to make the overall reduction with aluminum sufficiently exothermic for a self- sustaining reaction. SEM-EDS and chemical analysis confirmed that the co-reduction process lead to V-Ti-Cr-Al-O which was refined to V-Ti-Cr alloy by EB melting and vacuum arc re-melting in sequence. The excess aluminum was removed in metallic as well as sub-oxide forms along with the residual oxygen. Chemical homogeneity has been confirmed by Vickers's hardness measurement, EDS analysis and wet-chemical process. The detailed chemical composition of a typical V4Cr4Ti alloy sample is presented in Tab 4.1.2.

Table 4.1.2: Chemical composition of a typical V-Ti-Cr alloy

Table The chemical composition of V4Cr4Ti alloys.						
V	Ti	Cr	O	N	Al	Fe
Balance	3.979	4.010	0.013	0.101	0.859	0.052

The alloy (V4Cr4Ti) is of silver colour with mild metallic lustre as compared to pure vanadium as presented in Fig 4.1.8 however; Vickers hardness is higher than pure vanadium.



Fig 4.1.8: V-Ti-Cr alloy finger prepared by aluminothermy process, refined by electron beam melting followed by homogenization by vacuum arc melting

The phases of specimen were analyzed by XRD and results are presented in Fig. 4.1.9. In the XRD analysis presence of titanium or chromium in any form was not detected.

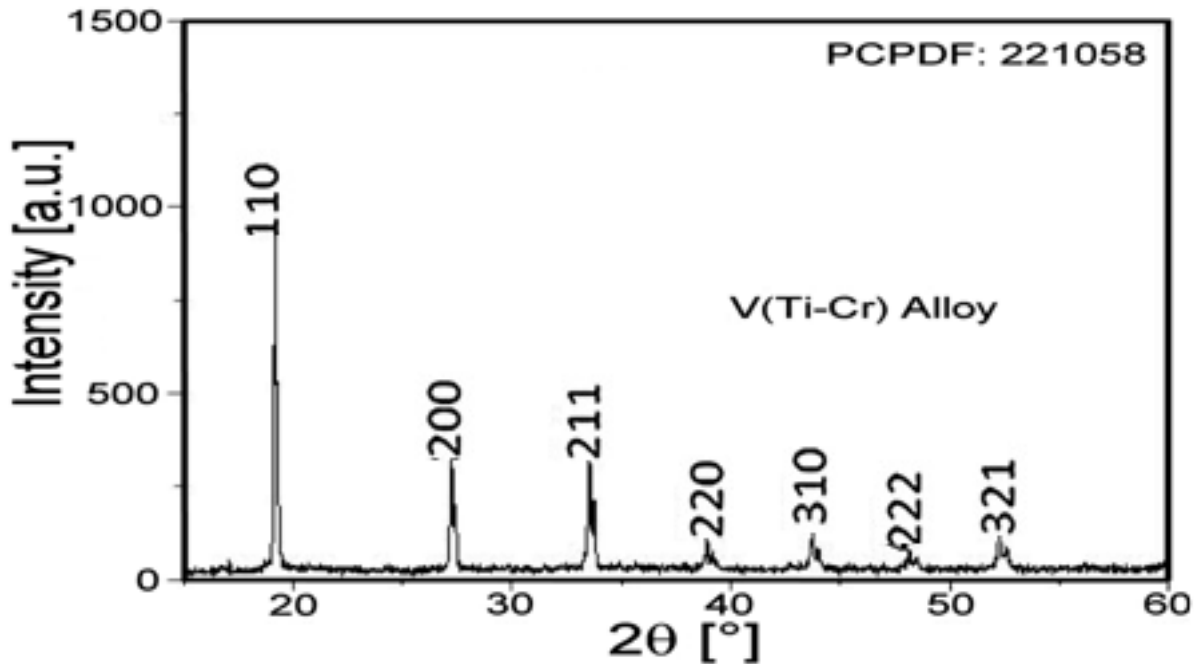


Fig 4.1.9: XRD analysis of V4Cr4Ti alloy, it shows only vanadium peaks

Also a positive shift of 2θ value by 0.1° with respect to vanadium matrix was observed. Essentially, these observations are indication of V-Ti-Cr solid solution formation. The composition of the Ti and Cr in the V-Ti-Cr alloy appears to be within the solid solubility limit according to the V-Ti-Cr ternary phase diagram. The volumetric size of titanium is larger than vanadium which is larger than chromium atom. As the alloy contains higher amount of Cr than Ti, the positive shift of 2θ for 0.1° can be explained with the fact that increase in 2θ value because of chromium is dominant over the decrease in 2θ value because of titanium. Even though oxygen and nitrogen were present in the EB melted V-Cr-Ti solid solution it has not been

detected in XRD. The observation indicates that the oxygen and nitrogen were also below the solid solubility limit. The EB refined V4Ti4Cr alloy thus prepared is shown in Fig 4.1.10.

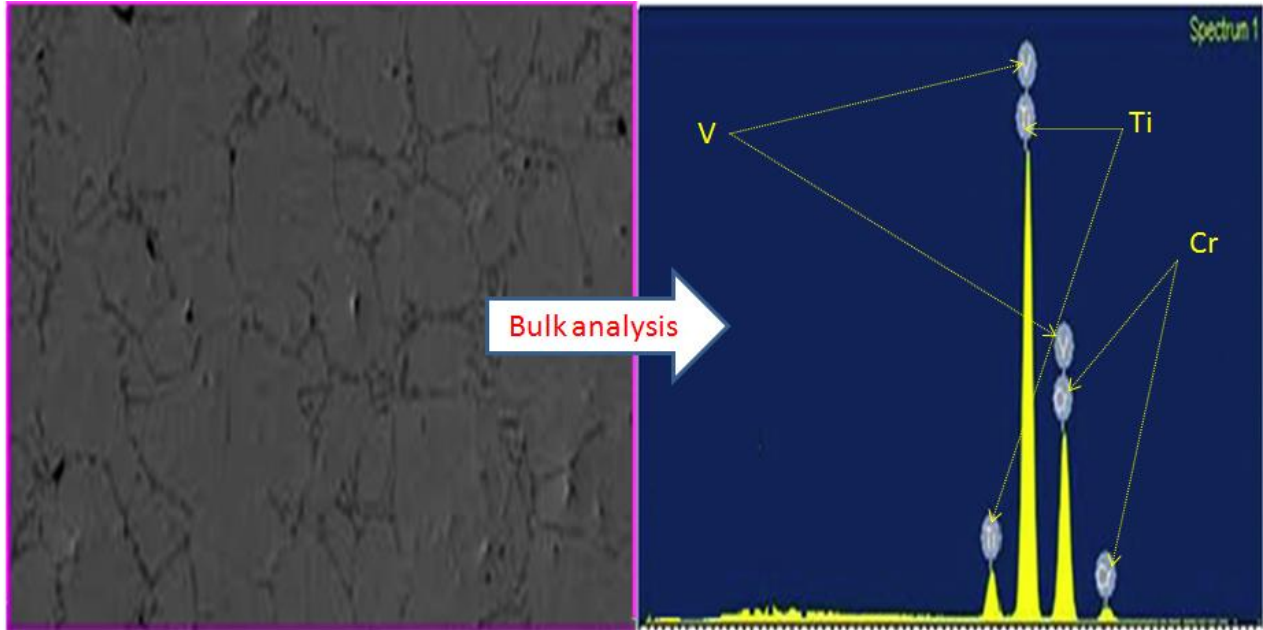


Fig. 4.1.10: SEM-EDS analysis of the samples indicating the phase homogeneity and alloy composition

4.1.6 Mechanism of the refining process

The vapor pressure of pure vanadium at the temperature used for refining (typically 2700K) is 0.02 torr where aluminum 22 torr, chromium 6 Torr and that of titanium 0.1 Torr. However, aluminum is in dilute solutions in vanadium, its actual partial pressure over the vanadium is considerably lower than the value indicated. Taking this into account, the vaporization rate, m_A of an element A (the evaporating species) can be approximated by the following free evaporation equation: (Langmuir equation) [114,115]

$$M_A = 44.32 S_A Y_A X_A P_A^o \sqrt{\frac{M_A}{T}} \text{ g cm}^{-2} \text{ s}^{-1} \quad (4.1.4)$$

Where S_A is the vaporization coefficient, usually taken as equal to 1, P is the vapor pressure of the pure element A in atmospheres, M_A and T are the molecular weight of A in grams and the absolute temperature respectively, Y_A is the activity coefficient of the elements A in the solution and X_A is the mole fraction. Even though P is large, a low value of X_A and possibly of Y_A would seriously limit the vaporization rate. Under these conditions, the thermit was refined by electron beam melting under high vacuum condition to remove excess aluminum and residual oxygen upto a possible extent. The resulting EB melting product was consolidated using vacuum arc melting. The actual refining process is probably complex because sub-oxides of V, Cr, Ti also form and these have significant process at the refining temperature. No systematic investigation has been reported in the literature on this.

4.2 Vanadium-hydrogen solid solution

4.2.1 Introduction

Substitutional impurities can be used to modify the elastic interaction between the hydrogen and parent lattice. In this context, it is essential to investigate the solid solution behavior of vanadium-hydrogen system and then correlate the modified behavior upon alloying. The dissolved hydrogen induces distortions in the vanadium lattice and as a consequence leads to the expansion in the volume of the crystals. This is even true for the hydrogen in vanadium in which the dissolved hydrogen atoms are located in the tetrahedral interstitial sites. The elastic interaction of the dissolved hydrogen atoms with dislocations, impurities and other hydrogen atoms give rise to the overall dilation of the unit cell. However, the local tetragonal symmetry of the defects sites is not transmitted to the long range displacement field, which shows cubic symmetry [25,39,27,84,118]. In the present section, varying amounts of hydrogen were introduced in the samples of vanadium metal. Lattice parameter was determined at different hydrogen concentrations.

4.2.2 Solution behaviour of hydrogen

The lattice parameters of a solid solution may be less than or more than the host matrix depending upon the physico-chemical properties of the solute atom. The solution behavior of vanadium-hydrogen solid solution has been studied by lattice parameter calculations. As indicated in the V-H phase diagram [119], Fig. 4.2.1 the terminal solid solubility of hydrogen in vanadium is around 1200 ppm at room temperature. In the present investigation, the maximum loading of hydrogen was kept below this solid solubility limit. The hydrogen concentration in all the samples was analyzed by inert gas fusion, gravimetric as well as by pressure drop techniques.

All the three techniques showed good agreements in the results. The data shows that the concentrations of hydrogen present in the alloys are within the solid solubility limit.

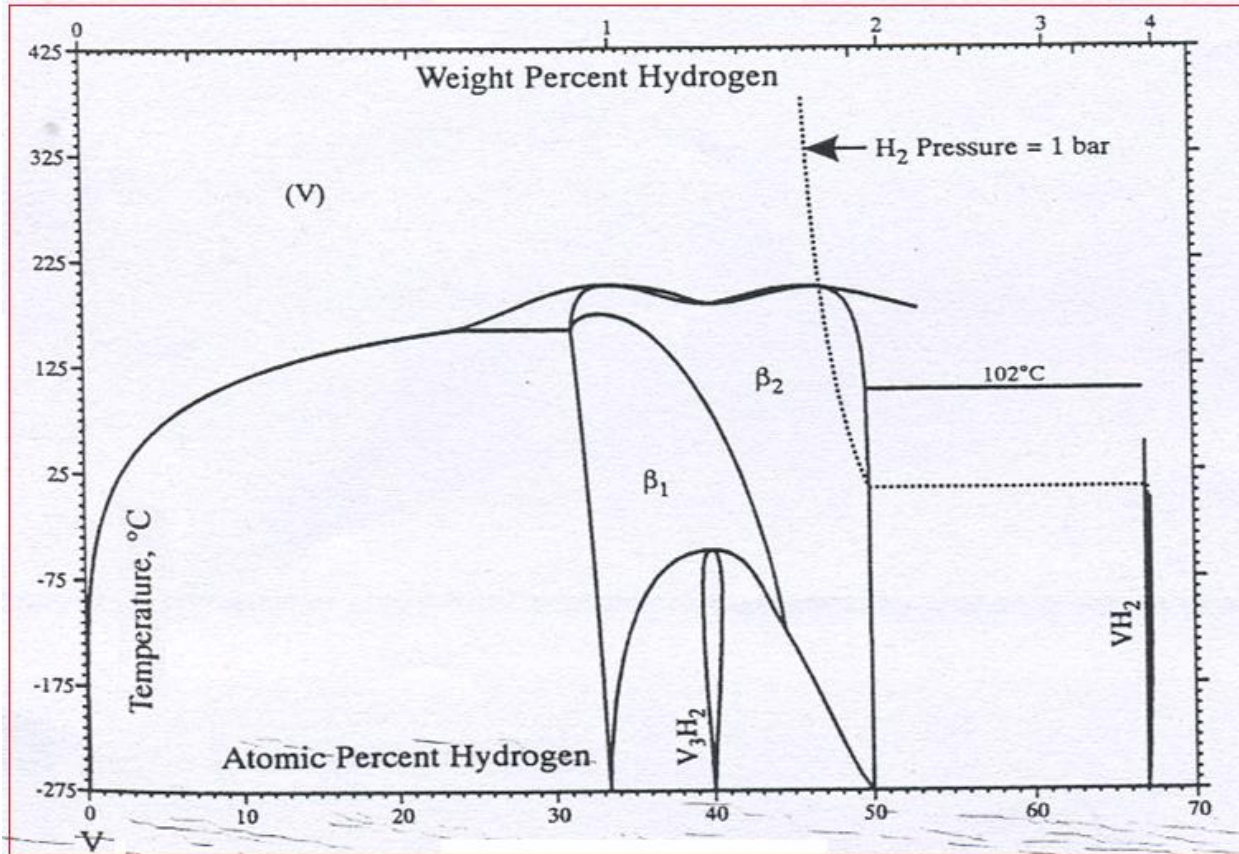


Fig. 4.2.1: Vanadium-hydrogen phases diagram [120]

It was further verified by XRD analysis as no hydride phase is observed in the X-ray diffraction pattern as shown in Fig 4.2.2 (1). Based on the analysis of the XRD data, the distance between the two planes (d) is calculated using Bragg equation, $n\lambda = 2d\sin\theta$. Three high intense peaks for three different θ have been used for the calculation. Using these d values, the lattice parameter a is calculated using the following relation:

$$d_{hkl} = \frac{a}{\sqrt{h^2 + k^2 + l^2}} \quad (4.2.1)$$

The mean value of lattice parameter a is determined. The values of lattice parameter a obtained for different hydrogen concentrations are shown in Fig.4.2.2 (25). The change in lattice parameter is linear with hydrogen concentration.

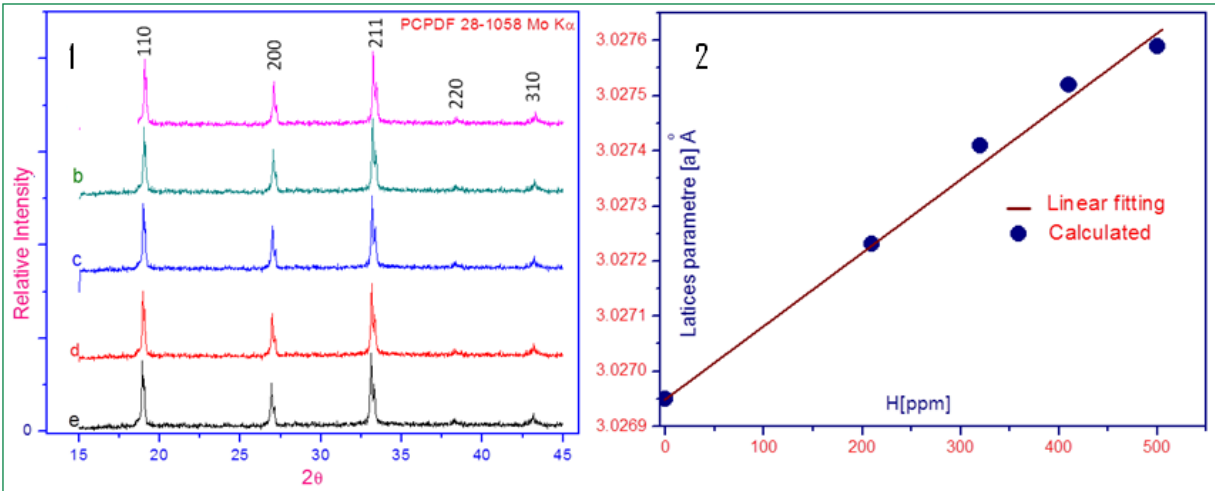


Fig. 4.2.2: (1) XRD pattern of bcc (a) phase vanadium with different amount of soluble hydrogen (a) vanadium (b) vanadium with 240 ppm hydrogen (c) vanadium with 322 ppm hydrogen (d) vanadium with 405 ppm hydrogen (e) vanadium with 457 ppm hydrogen. (2) Variation of lattices parameter with respect to hydrogen concentration

The relative change in lattice parameter has also been calculated and shown in the Fig 4.2.3. The neutron diffraction study shows that hydrogen goes into interstitial tetrahedral sites in the metal lattice. This causes an increase in the volume of the nearest-neighbour shell of atoms because the hydrogen atoms force the nearest-neighbour metal atoms to move away from each other. The relative change in lattice parameter showed a perfect linear relationship with hydrogen concentration. This is a physical phenomenon for the increase of the lattice parameter of the metal upon hydrogen absorption. At equilibrium, uniformly distributed dissolved hydrogen in a metal causes zero hydrostatic stress in the lattice, although each hydrogen atom is individually

under a hydrostatic stress. There is no energy or pressure tending to push the hydrogen atoms together into one interstitial site.

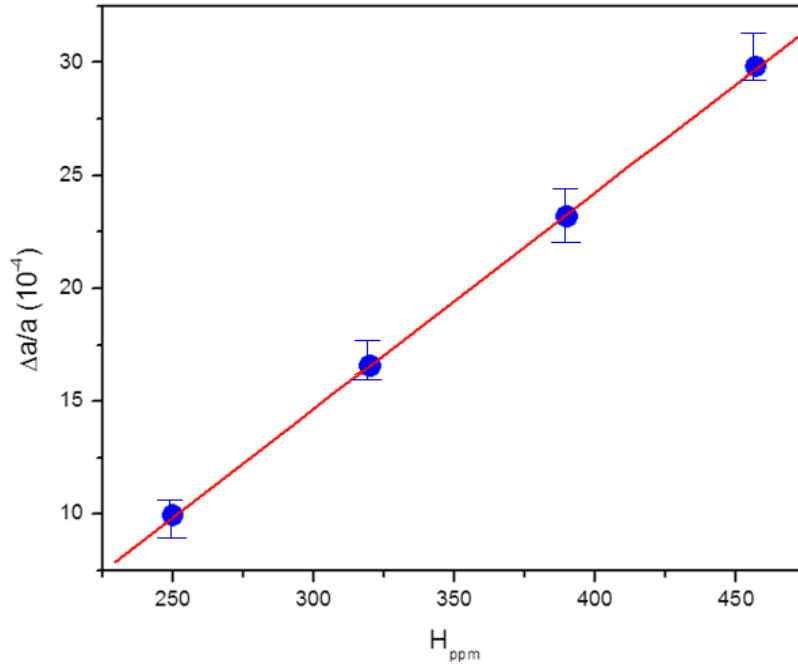


Fig. 4.2.3: Relative change in lattice parameter variation with hydrogen concentration

The above observation could be explained by the density functional theory (DFT) [13]. The theory explained that irrespective of other considerations, the electron density plays important role in determining the lattice parameter. With the introduction of hydrogen in to the metal matrix, the electron density in the valance band increases. As a consequence of increased electrostatic repulsion between electrons, the lattice parameter increases. The results obtained here follow the Vegard's law [86-88] according to which, in solid solutions, lattice parameter is linearly varying with the concentration of solute. Many systems do not follow the Vegard's law because of one or other limitations, but in the present case the results seem to obey the Vegard's law.

4.2.3 Hydrogen solubility

Low temperatures

Hydrogen solubility of pure vanadium and the effect of aluminum on the hydrogen solubility of vanadium have been studied in the low temperature range, 250-450K. A suitable combination of solid carbon-dioxide and ice [111] has been chosen to maintain low temperature of 250 K; within a variation of ± 7 K. The chemical composition of the vanadium metal and vanadium aluminum alloys used in this investigation is shown in Table 4.2.1.

Table 4.2.1: Chemical composition of vanadium metal and vanadium-aluminum alloys

The chemical composition (in wt%) of V and V–Al alloys.

Sample	V	Al	O	N
Pure V	Balance	–	0.001	0.010
V0.78Al	Balance	0.784	0.013	0.022
V1.01Al	Balance	1.014	0.012	0.012
V1.53Al	Balance	1.532	0.020	0.011

The alloys were prepared using aluminothermy followed by electron beam refining-vacuum arc melting in sequence. The aluminum content in all the vanadium–aluminum alloys was within the solubility limit. The alloys homogeneity has been checked by Vickers hardness measurement as well as EDS line scanning. All the samples undergo hydrogen charging process in a Sieverts apparatus. Details of the Sievert’s apparatus have been discussed in the Materials and Methods chapter [chapter 2] of this thesis. The hydrogen content in the samples was measured by pressure drop technique which is further checked by inert gas fusion technique. The solubility of hydrogen (PCT curve) as a function of aluminum content at constant pressure of 760 Torr and at constant temperature of 350K are shown in the Fig. 4.2.4 and 4.2.4 respectively.

The isobaric solubility of hydrogen decreases with the temperature as illustrated in the Fig 4.2.4. The isothermal PCT curve shows increase in hydrogen solubility with pressure, however the solubility does not follows the Sieverts law i.e. $C_H = K_s \sqrt{p}$, where symbols have their usual meanings.

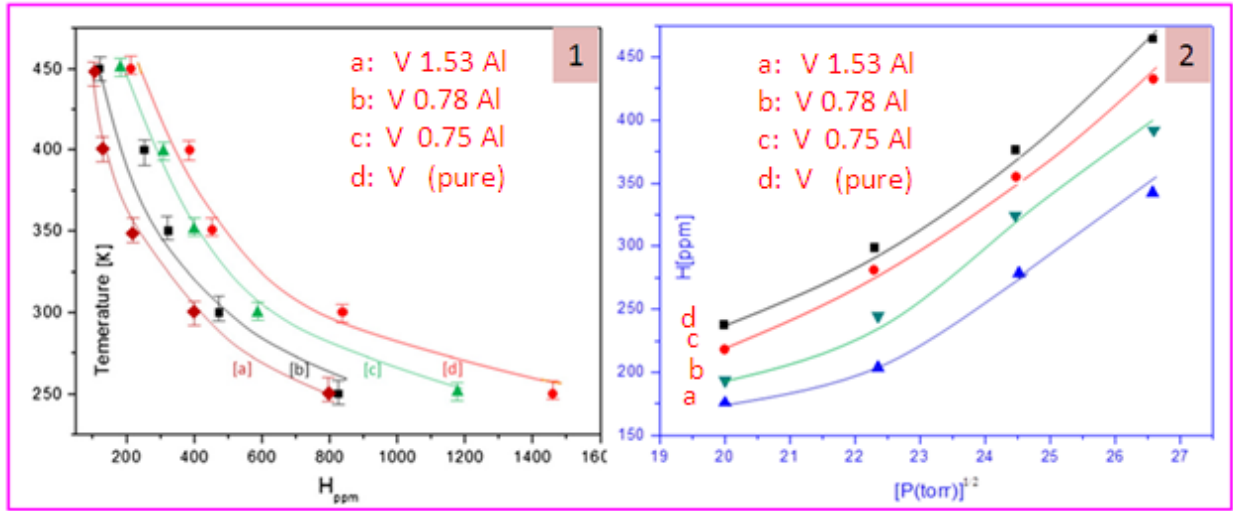


Fig. 4.2.4: Hydrogen solubility curve at (1) constant pressure (760 Torr) (2) Constant temperature (350K) for vanadium and vanadium aluminum alloys

In both the cases, at constant pressure and constant temperature, the hydrogen solubility decreases with aluminum content. It is worth mentioning here that the hydrogen solubility may be related to some other mechanisms and only a comparative solubility for different vanadium-aluminum alloys are presented here at the identical experimental conditions to analyze the effects of aluminum on the solubility.

Partial hydride phase formation (β phase V_2H) was confirmed by the XRD analysis of all the hydrogenated samples at constant temperature as well as constant pressure range

investigated. Thus the hydrogen concentration was corresponding to α [V(H)] + β [V₂H] equilibrium phase. Decreasing hydrogen concentration with temperature could be explained on the basis of decreasing stability of β phase with temperature as indicated by the vanadium-hydrogen phase diagram, Fig 4.2.1. With increasing temperature there is more of the alpha phase which has less hydrogen content than β phase component as shown in the V-H phase diagram (Fig. 4.2.1) and as a result there was a decrease in hydrogen concentration. The Sieverts law follows only within the solid solubility limit of the hydrogen concentration, however in present case the hydrogen concentration was corresponding to two phase α + β region. Therefore, it does not obey the Sieverts law and can't be plotted linearly using Sieverts relation.

High temperature range

Hydrogen solubility of pure vanadium and the effect of aluminum on the hydrogen solubility of vanadium have been studied at higher temperatures. Here the concentration of hydrogen was within the solubility limit and only α phase has been confirmed by XRD analysis. The chemical compositions of the vanadium metal and vanadium aluminum alloys used in this investigation are shown in Table 4.2.1. Phase diagram of vanadium-aluminum system indicates that the aluminum contents in all the vanadium–aluminum alloys were within the solubility limit. The hydrogen concentrations in all the specimens were found to remain within the solubility limit. This has been confirmed by optical micrographic examination as no hydride precipitation was observed.

X-ray diffraction analysis, Fig. 4.2.5 (e)–(h) also shows only alloys phase in the body centred cubic structure.

Table 4.2.1: Composition of the V-Al alloys the present investigation analyzed by chemical analysis

Composition of the specimen used in the present investigation analyzed by chemical analysis.

Alloy	Nomenclature and composition of alloys					
	Composition of analysis (wt%)					
	Al	N	O	Fe	Mn	Mo
V0Al	–	0.019	0.017	0.020	–	–
V5Al	5.005	0.014	0.013	0.003	0.002	0.001
V10Al	10.023	0.013	0.012	0.001	0.001	0.001
V14Al	14.012	0.013	0.013	0.002	0.001	0.001

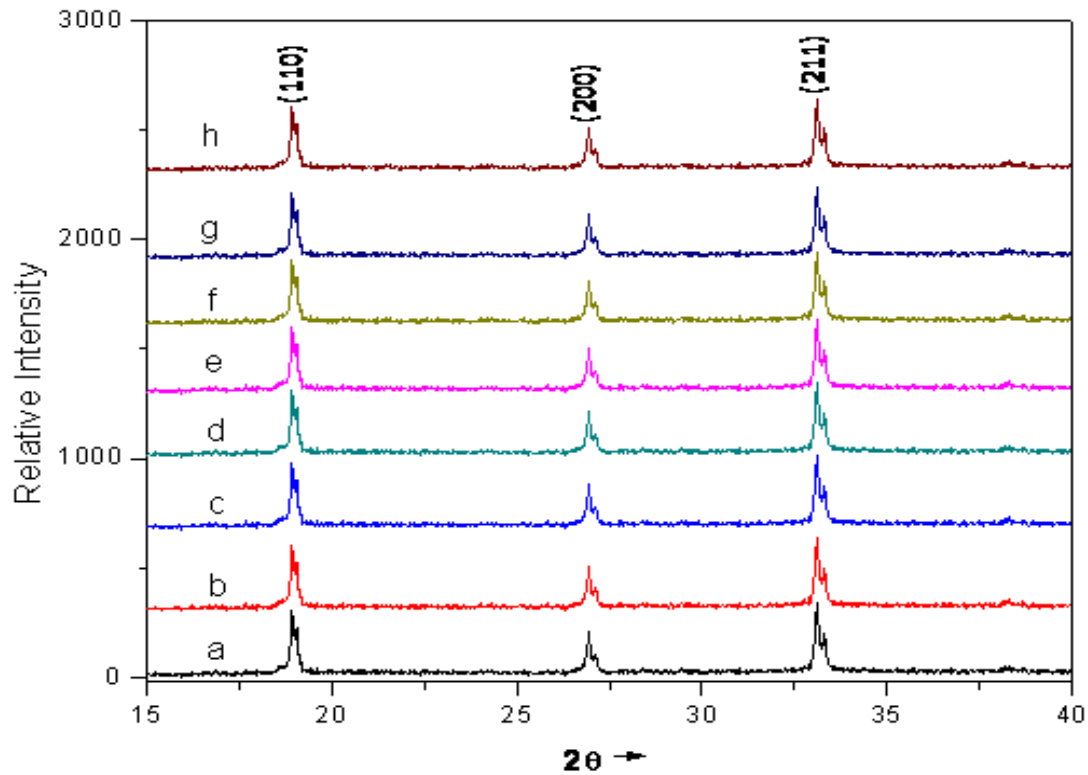


Fig.4.2.5: XRD analysis of (a) V0Al, (b) V5Al, (c) V10Al, (d) V14Al, (e) V0Al+550 ppm H, (f) V5Al+488 ppm H, (g) V10Al+336 ppm H, and (h) V14Al+227 ppm H: PCPDF 28–1058: Mo K α .

Fig. 4.2.6 a shows the solubility of the hydrogen in vanadium and vanadium–aluminum alloys with varying pressures and at a constant temperature of 973K. At this temperature the solubility of hydrogen in the vanadium and vanadium–aluminum alloys follows Sieverts law.

The variation of hydrogen solubility in the same samples at various temperature ranges and at a constant pressure of 250 Torr are shown in Fig.4.2.6 b. The solubility of the hydrogen in the specimen has increased with temperature. An interesting observation was, in either case at constant pressure and constant temperature, hydrogen solubility decreases with the aluminum contents.

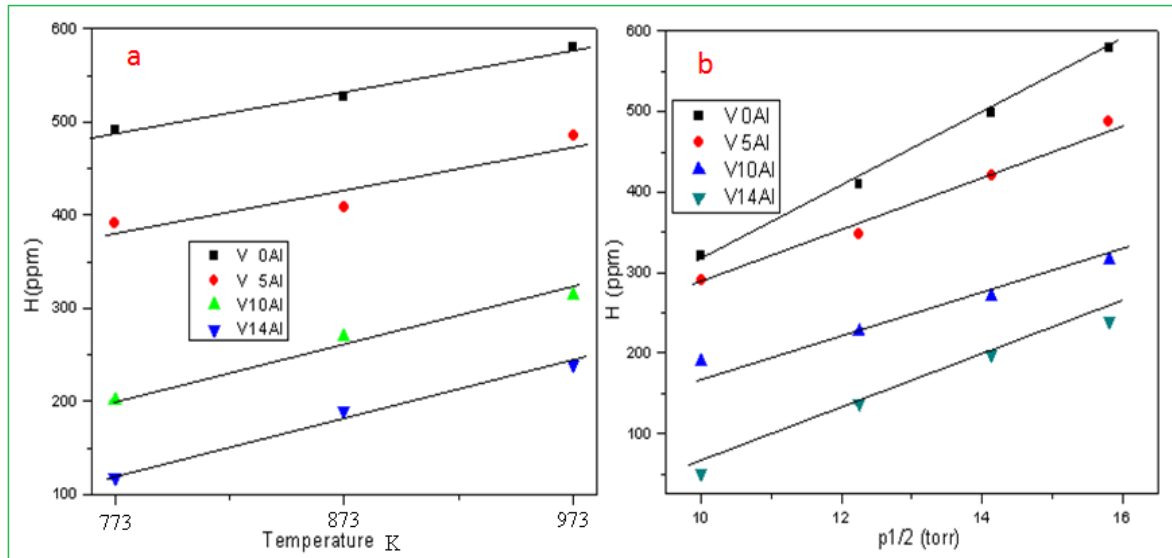


Fig. 4.2.6: (a) Isobaric (250 Torr) hydrogen solubility as function of aluminum at different temperature (b) Isothermal (973K) hydrogen solubility as function of aluminum at different pressure

In the entire temperature 250K-973K and pressure 100-760 Torr range hydrogen solubility decreases with the increase in the aluminum content. In both single phase region [α phase] and two phase region [$\alpha + \beta$ phase] aluminum significantly decreases the solubility.

4.2.4 Theories on hydrogen solubility

Hydrogen solubility: Thermodynamics consideration

At a given temperature, the solubility of hydrogen in a metal increases with the increasing pressure of hydrogen gas as expressed by the Sievert law,

$$C_H = K_s \sqrt{p} \quad (4.2.2)$$

where K_s is a Sieverts constant.

One of the important conditions of this equation is that the hydrogen concentration should be within the solubility limit of the host matrix. The square root dependence follows from the fact that hydrogen molecules dissociate into atoms prior to their incorporation within the host lattices. Another explanation for the square root dependence of hydrogen concentration on hydrogen pressure has been given by Wagner [20,90].

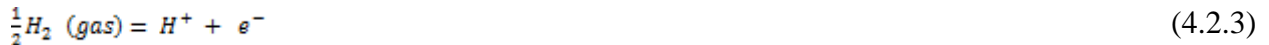
The solubility of any phase is determined by its individual thermodynamic functions as well as by the corresponding functions of the coexisting phase. It is experimentally observed that the presence of hydrogen enhances the stability of bcc phase vis-à-vis close packed hcp and fcc phases. Fukai [119] has proposed that this can be understood by noting that the partial configurational entropy for a given hydrogen concentration is larger in the bcc phase because of the larger number of interstitial sites available. In vanadium-hydrogen and titanium-hydrogen system, the melting point is lowered by the introduction of hydrogen. The reduction in melting point is also associated with the occurrence of distribution coefficient greater than unity between liquid and solid phase. The higher solubility of hydrogen in liquid phase as compared to solid can also be explained by relatively higher configurational entropy of hydrogen in the liquid phase. Vanadium–aluminum system forms substitutional alloy system. Lattice parameters of vanadium show a slight increase on alloying with aluminum [117]. The increase in lattice

parameter upon alloying up to 14 weight percent Al leads to overall volume increase of nearly 1.5 %. Hence, according to Fukai hypothesis, alloying of vanadium with aluminum should enhance the solubility of hydrogen, however; our result shows a decrease in solubility of hydrogen with increase in the aluminum content. In addition, since there is no change in crystal structure of vanadium on alloying with aluminum, the number of interstitial sites per unit cell remains unchanged upon alloying with aluminum. Accordingly, the addition of aluminum will not give rise any change in the configurational entropy of the matrix due to introduction of hydrogen. It is therefore appears that the explanations based on configurational entropy change, a thermodynamic function, are not sufficient to explain the present results.

Hydrogen solubility: Contribution of Fermi energy

Hume Rothery has demonstrated the effect of variation in electronic concentration on the thermodynamic properties [20,90]. For instance, the solubility limit of various elements in Cu corresponds to different atomic percentages but to approximately the same concentration of valence electrons. According to Wagner, the same concept can be used to explain the alloying behavior of hydrogen in metals.

The stoichiometric equation for the dissolution of hydrogen in vanadium could be written as:



and at the equilibrium condition



where G_{H^+} and G_{e^-} are the partial molar free energies of protons and electrons respectively of vanadium. Since the gas phase is ideal and the concentration of proton in the metallic phase is small, Eq 4.2.3 may be written as

$$\frac{1}{2}G_{H_2}^0 + \frac{1}{2}RT \ln P_{H_2} = G_{H^+}^* + RT \ln C + G_{e^-} \quad (4.2.5)$$

Where $G_{H_2}^0$ is the molar free energy of hydrogen gas at unity pressure, C_H is the concentration of hydrogen in vanadium and $G_{H^+}^*$ is the partial molar free energy of protons extrapolated to unity concentration. Solving Eq 4.2.4 for c, we have

$$C_H = \sqrt{P_{H_2}} \exp \left[\frac{\left(\frac{1}{2}G_{H_2}^0 - G_{H^+}^* - G_{e^-} \right)}{RT} \right] \quad (4.2.6)$$

The reduction in hydrogen solubility with the Al content could be explained on the basis of increase in Fermi energy level due to increase in electron to atom (e/a) ratio caused by the addition of aluminum to the vanadium matrix. Aluminum contains three valence electrons and after alloying with vanadium, it will contribute these electrons to the valence band of the matrix. This will increase the number of electrons per atom in the matrix which will lead to increase in the partial molar free energy of electron (G_{e^-}). In these conditions, the Eq. 4.2.5 predicts that the hydrogen solubility will decrease with increase of aluminum content at any given pressure. The Eq. 4.2.1 as well as Eq. 4.2.5 predicts identical dependence of the pressure on the hydrogen solubility. Therefore, the dependence of solubility on the pressure alone can't be used to draw inferences regarding the factors affecting the solubility. At a given temperature and pressure, a consistent decrease of hydrogen solubility with increase of aluminum content was observed experimentally. As discussed, the overriding influence of electronic concentration is controlling the solubility of hydrogen in vanadium matrix.

The explanation regarding the dissolution behavior of hydrogen in vanadium-aluminum solid solution hinges on the assumption that the addition of aluminum to the vanadium metals raises its Fermi energy level. The support for this observation comes from the alloying and chemical behavior of vanadium towards aluminum. Vanadium forms an intermetallic compound

V_3Al_2 [120] where it behaves as a divalent metal. In addition, this compound coexists with vanadium rich V-Al single phase alloy which occurs as a terminal phase in V-Al phase diagram. The observation shows that Fermi energy level in V-Al solid solution alloys and V_3Al_2 intermetallic are identical. It appears that even in single phase solid solution alloys, vanadium exhibits divalency. These observations are further supported by Pauling's scale of electronegativity of pure metals. The electronegativity values ascribed to vanadium and aluminum are 1.63 and 1.61, respectively. As a result, there will be no significant tendency for transfer of electrons between the solvent and solute atoms in the matrix. Hence, the valence electrons contributed by aluminum will go to the conduction band of vanadium leading to the increase in electron to atom ratio of the alloy matrix. The increase of electron to atom ratio will raise the Fermi level and decrease the solubility of hydrogen with increase of Al content as predicted by Eq (4.2.5).

The resistivity for pure vanadium and vanadium aluminum alloys have been measured at room temperature using standard techniques. In general, alloy addition decreases the resistivity, however; in present case resistivity of vanadium aluminum alloys decreases with aluminum content as illustrated in Fig 4.2.7. Thus there is a clear indication of increased Fermi energy level of vanadium-aluminum alloys as compared to pure vanadium. The electrical resistivity of a matrix indirectly depends upon the electronic concentration in the Fermi energy level. More number of electrons in the Fermi energy level decreases the electrical resistivity. Therefore, in present case it appears that aluminum increased the Fermi energy level by contributing its electron to the valance band of host matrix vanadium and as a consequence electrical resistivity decreased. However, higher concentration of aluminum (more than 5 wt %) gives random value of electrical resistivity that could be due to formation Al_2O_3 at the alloys surface. The available

data on several other systems indicate the electronic consideration, which is eventually related to Fermi energy level, govern the solubility behaviour of hydrogen. Hydrogen storage capacity of intermetallic compound LaNi_5 is enhanced on the addition of excess nickel [23,121-122]. Addition of Ni decreases the electron to atom ratio indicate the decrease in the Fermi energy level of the system, eventually the hydrogen storage capacity increases. Lead lithium eutectic ($\text{Pb}_{83}\text{Li}_{17}$), is proposed to be used as the coolant, neutron multiplier and secondary tritium breeder in the test blanket modules of ITER. The hydrogen solubility in this alloy decreases with addition of excess lead [123]. The hydrogen solubility decreases because of the increase in electron to atom ratio contributed by lead which eventually may increase the Fermi energy level.

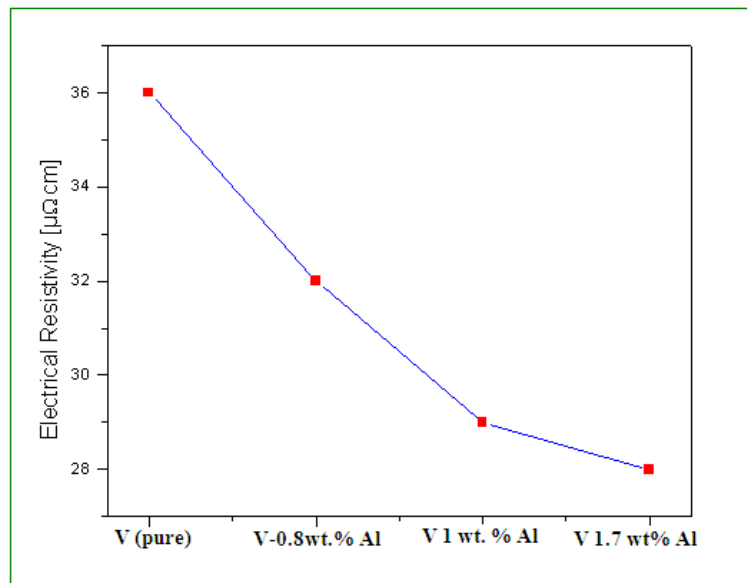


Fig. 4.2.7: Electrical resistivity of vanadium and vanadium-aluminum alloys at room temperature

Hydrogen solubility study carried out by Zhang et al. [106] on V-Mo alloys indicates the decrease in hydrogen solubility with the concentration of molybdenum. Molybdenum contributes

more electrons to the Fermi energy level of the host matrix vanadium and hence the observed solubility could be explained on the basis of the proposed e/a ratio and Fermi energy theory. A very similar explanation based on the electronegativity of the alloying elements on the hydrogen solubility is given by Wang et.al [58] and Nakajima et.al [98] for V-Ti-Cr alloys. They pointed out that the electromigration and solubility of hydrogen in vanadium alloys is not fully explained by a simple two step trapping model. The change of the electronic structure by alloying should be considered to account for the hydrogen solubility.

Hydrogen solubility: Chemical behavior of alloying element

The solubility results could also be explained on the basis of chemical behavior of aluminum with hydrogen. The solubility of hydrogen in solid Al is very less, which is less than 1 ppm at about 1000 torr hydrogen pressure [106] and increases but always remains small with the melting of aluminum..

Al-H phase diagram [1] Fig 4.2.8, contains a eutectic type reaction near the melting point of aluminum and a lowering of melting point of 2K has been reported. The temperature dependent hydrogen solubility equations have been reported as shown by equation 4.2.6 and 4.2.7.

$$\frac{H}{Al} = 2.164 \times 10^{-6} - (1.105 \times 10^{-8})T + (1.444 \times 10^{-10})T^2 \quad (4.2.7)$$

for the solid solution phase (< 660°C)

$$\frac{H}{Al} = 1.570 \times 10^{-4} - (5. \times 10^{-7})T + (4.340 \times 10^{-10})T^2 \quad (4.2.8)$$

for liquid phase (>660°C)

The solubility of hydrogen in different phase regions is shown in the phase diagram Fig. [4.2.8] Interestingly, no hydride phase of aluminum is possible at ambient pressure, however; at very high pressure (>10000 torr) AlH_3 will be forming.

The solubility of the hydrogen of vanadium could be due to increase in the aluminum content which prevents the hydrogen ingress. The presence of aluminum reduced the hydrogen solubility due to this reason. Zhang et.al [106] proposed that on the account of chemical inertness towards each other, Al atoms in the V-lattices will repel hydrogen and block their incorporation in the lattices in their local neighborhood. This hypothesis appears logical however; more experimental data are needed to verify this concept. The data on the alloying behaviors of hydrogen in vanadium after addition of titanium and zirconium may be useful in this context. The explanation based on the formation of adherent Al_2O_3 on the specimen surface, which can act as a strong activation barrier for the hydrogen ingress into the vanadium matrix and consequently reduction in hydrogen solubility, is reported earlier [28]. In the present investigation, hydrogen charging apparatus was flushed with argon gas followed by evacuation. Evacuated apparatus was filled with argon and then specimen was placed inside the apparatus under the cover of argon gas. Whole apparatus was again evacuated and then hydrogen gas was filled. The specimen was exposed to high temperature only in the hydrogen atmosphere. These conditions don't favor the formation of Al_2O_3 film on the specimen surface. It appears, therefore, the decrease in solubility upon addition of aluminum probably reflects the inherent characteristics of V-Al alloys brought about by the presence of solute aluminum atoms. Waisman et al. [124] studied the diffusion of hydrogen in Ti-Al alloys. The study revealed that the free energy of hydrogen in a Ti matrix increases with Al contents due to increase in activity of

hydrogen and hence solubility decreases. This may be true for V-Al alloys also but no direct evidence is available in the existing literature.

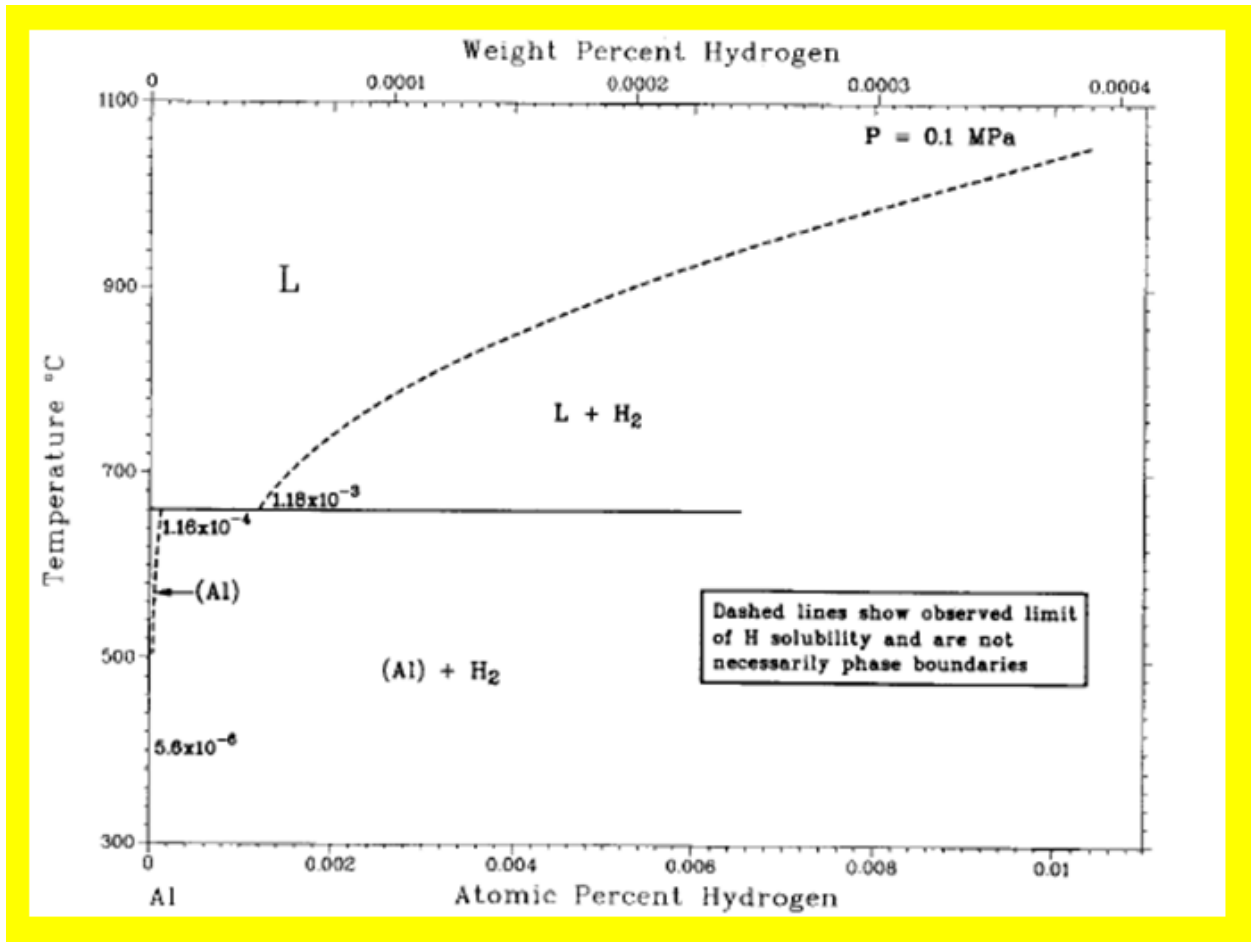


Fig 4.2.8: Aluminum –hydrogen phase diagram

Hydrogen solubility: mechanical effect of alloying element

Another explanation is based on the mechanical effects of which were advanced by Volkl and Alefeld [14]. They pointed out that as the distance between interstitial sites of host matrix increases with solute content, the activation barrier for hydrogen solubility rises and results in decrease of hydrogen solubility. The influence of the electronic structure and the lattice constant on hydrogen absorption in bulk for the various alloys had been studied by Density – Function

theory (DFT) [11]. The study revealed that the calculated absorption energy of hydrogen shows greater dependency on electronic structure vis-a-vis the lattice constant. Though the theory given by Volkl et al. [14] is covering hydrogen solubility data in many systems but explanation based on electronic structure appears more logical and explains hydrogen solubility behaviour in various alloys and compounds. The solubility of hydrogen in a metallic matrix can be explained either on thermodynamic or electronic considerations.

4.3 Phase stability

4.3.1 Introduction

Stability of the phases formed during the hydrogenation of potential hydrogen storage materials is an important parameter on which the recovery of absorbed hydrogen by subsequent desorption depends. The mechanism of hydrogen absorption in vanadium proceeds with the formation of vanadium-hydrogen solid solution, $V(\alpha)$, phase which on further hydrogenation precipitated as β hydride phase. Furthermore, first order phase transition from β_1 phase (V_2H) to β_2 phase (VH) progressed on further hydrogenation. Finally, the γ phase (VH_2) is formed when it is fully hydrogenated. The hydride phase stability is influenced by the presence of the one or more alloying components. Vanadium and most of its alloys are generally produced via aluminothermy reduction of appropriate mixture of oxides. This production process is highly cost effective. However, the product can retain several atom percent of aluminum depending upon the conditions of purification. The present discussion is on the phase stability of vanadium hydride and the effects of aluminum on the phase stability.

4.3.2 VH_2 (γ) phase

The VH_2 phase of vanadium is the highest hydrogen content phase of vanadium as shown in the V-H phase diagram Fig [4.2.1]. The hydrogen absorption capacity is 4wt % in the form of VH_2 phase. However; only 2wt% hydrogen could be desorbed at ambient temperature and pressure because VH phase is stable even at high temperatures [14]. The decomposition pressure and temperature of VH_2 phase substantially depends upon the alloying elements. The effects of aluminum on the partial decomposition of VH_2 phase have been studied. PCT curves are measured at 330K for pure vanadium, vanadium 0.81 wt % aluminum and vanadium 1.78 wt %

aluminum alloys. A relatively large hysteresis is observed in each PCT curve. The PCT curves measured in the course of hydrogen desorption are shown in Fig. 4.13 a-c.

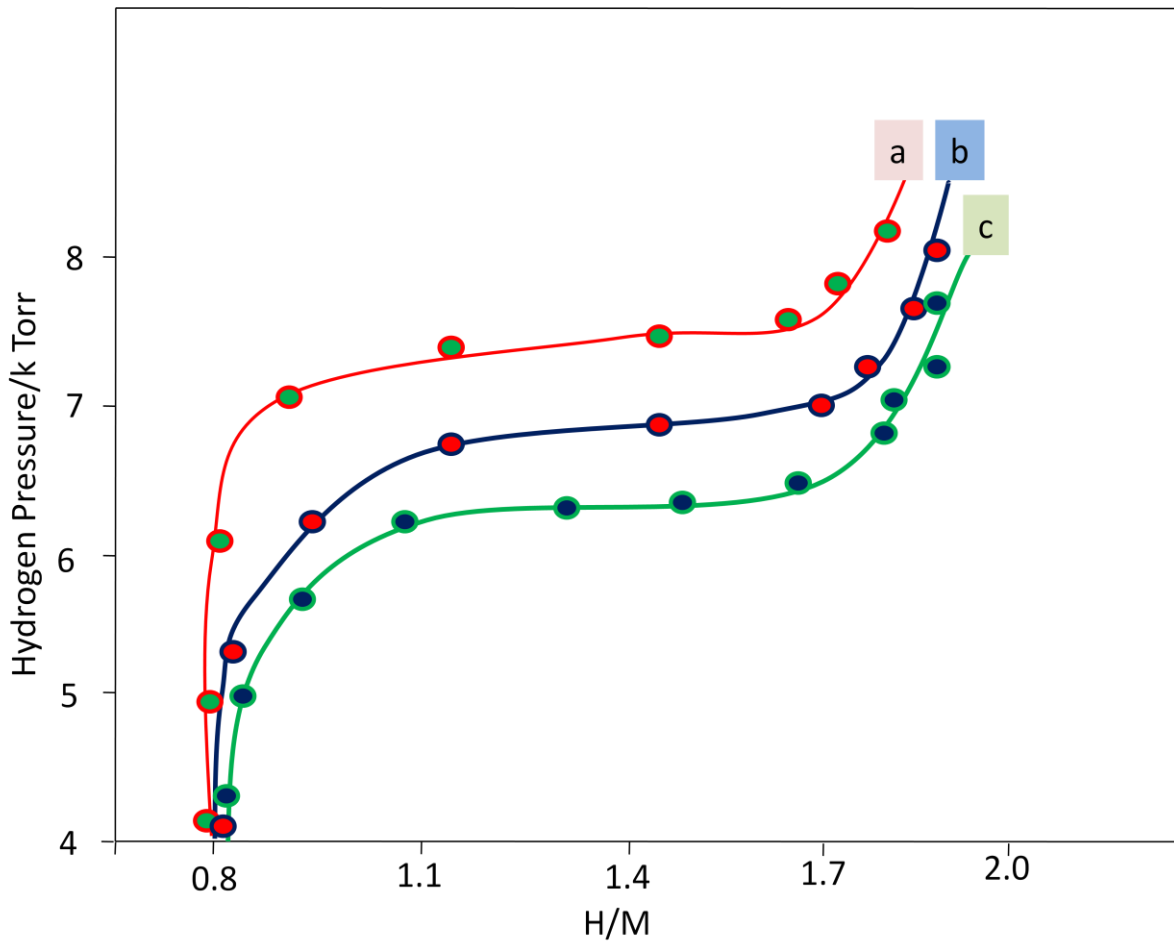


Fig. 4.3.1: γ phase stability of (a) Vanadium 1.532 wt% aluminum Al (b) Vanadium 0.784 wt% aluminum (c) High pure vanadium

As shown in Fig 4.3.1, a plateau is seen in all the three samples. The value of the pressure at the centre of each plateau is referred to as the plateau pressure. As evident from this figure, the stability of the γ phase is strongly dependent on the aluminum content. The plateau pressure changes in a systematic manner with aluminum contents. The observation is according to the facts that the plateau pressure may be high in those elements which possess the small atomic

radius or the high electronegativity compared to the host matrix. The aluminum being slightly more electronegative than the host matrix vanadium on Pauling's scale of electronegativity, it may lead to increase in the plateau pressure. According to the least squares analysis [28], the correlation coefficient is about 0.45 between the plateau pressure and the atomic radius and about 0.66 between the plateau pressure and the electronegativity.

4.3.3 α and β phase

The effect of aluminum β phase stability of vanadium–hydrogen system have been investigated employing thermo gravimetric (TG), differential thermal analysis (DTA) and X-ray diffraction techniques. To check the effects of aluminum on the hydrogen desorption from β phase of vanadium, TG and DTA experiments were performed on V_2H samples. The hydrides (β phase) of pure vanadium and V–Al alloys were prepared under identical conditions. Identical β phases (V_2H and $(V,Al)_2H$) were confirmed by XRD analysis presented in Fig. 4.3.2.

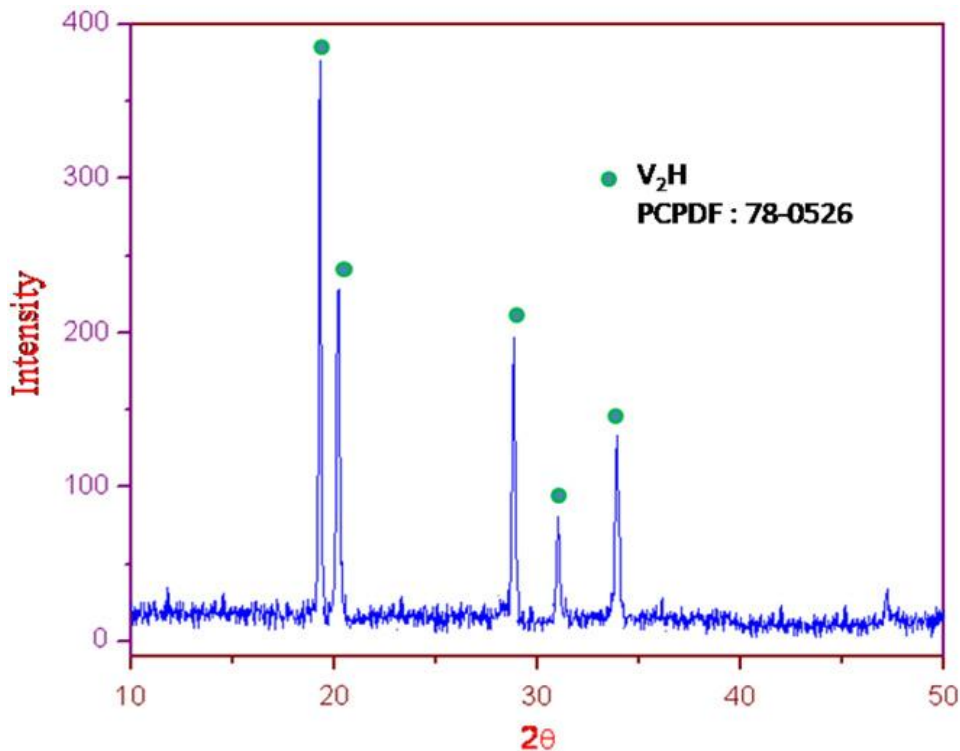


Fig. 4.3.2: X-ray diffraction patterns of as such prepared V_2H

Slight peaks shift was observed in $(V,Al)_2H$ as compared to V_2H . This observation is according to solid solution of V–Al alloys. Hydride of pure vanadium (β phase) sample was decomposed by heating it at the rate of 2 K min^{-1} in M/s Setaram make thermogravimetric analyzer unit (TG-DTA). The slow heating rate was kept to accommodate the kinetics interference in the decomposition behaviour. The TG-DTA combined curves are shown in Fig. 4.3.3(a).

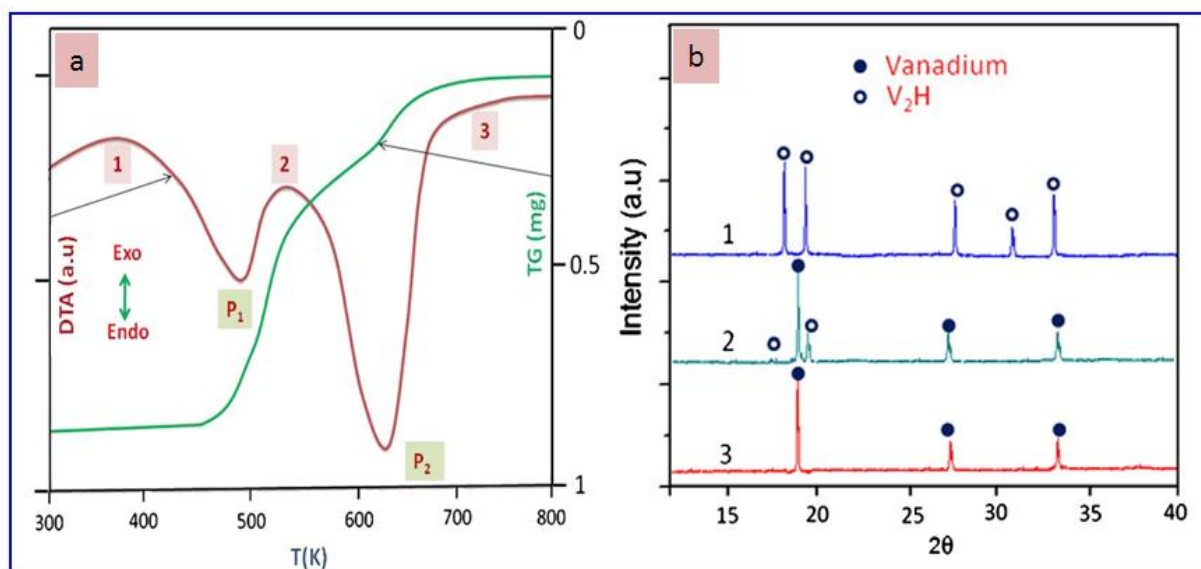


Fig. 4.3.3: (a) TG-DTA study of decomposition pattern of β phase of pure vanadium hydride (b) X-ray diffraction patterns of decomposition pattern of β phase of pure vanadium hydride

Two step weight loss events were observed on the TG analysis. Corresponding endothermic peaks were present at the same temperature on the DTA curve. The combined curve of TG-DTA clearly indicates that the gas desorption phenomena occurred in two steps. The first desorption step started at $\sim 487\text{ K}$ (Peak P_1) while the other desorption step was at $\sim 596\text{ K}$ (Peak P_2) temperature. To check the phenomena at these temperatures, XRD analysis was performed

for the samples quenched at point 1, 2 and 3: before peak P_1 between peak P_1 and P_2 and after P_2 respectively as shown in Fig. 4.3.3(b).

The XRD pattern shown in figure indicates the presence of single low temperature β phase (V_2H) for the sample quenched before the first peak P_1 . Body centred cubic (bcc) vanadium along with low temperature phase β (V_2H) appeared in the sample quenched between peaks P_1 and P_2 . However, considerable peak shift was observed in bcc vanadium phase that could be due to soluble hydrogen and this was further confirmed by lattice parameter determination and chemical analysis. The sample quenched after P_2 indicates bcc vanadium without any considerably peak shift. Furthermore, chemical analysis of the sample indicates negligible hydrogen concentration. The observation revealed that vanadium released the entire content of hydrogen beyond P_2 . In conclusion, low temperature peak P_1 appears due to the transformation of the β phase to the bcc (α) phase containing hydrogen, high temperature peak P_2 originates from the transformation of this bcc (α) phase to the hydrogen-free bcc vanadium, since hydrogen is released readily from vanadium at temperatures as high as 730 K. The effects of aluminum on the decomposition behaviour of β hydride phase were studied using DTA. Low temperature hydride phase β [$(V,Al)_2H$] of vanadium aluminum alloys were decomposed at identical condition as discussed above and decomposition DTA patterns are shown in Fig.4.3.4. To compare the results, DTA of pure vanadium hydride has been incorporated in the same figure. The two endothermic peaks P_1 and P_2 were clearly observed during the decomposition of the first two aluminum containing β phase, $(V,Al)_2H$ samples: vanadium 0.784% aluminum and vanadium 1.014 wt% aluminum. The peak P_1 was diminished substantially for the sample containing 1.532 wt% of aluminum. In the DTA analysis it was also observed that the shape and the position of the two endothermic peaks P_1 and P_2 changed significantly with aluminum

content. For example, P_1 peaks became broader with aluminum content and then substantially diminished for the vanadium aluminum alloys with aluminum concentration higher than 1.5%. The DTA analysis indicates that the peak P_2 which was 596 K for α phase of pure vanadium shifted to 585, 574 and 561 K for α phase of V0.78Al, V1.01Al and V1.53Al, respectively.

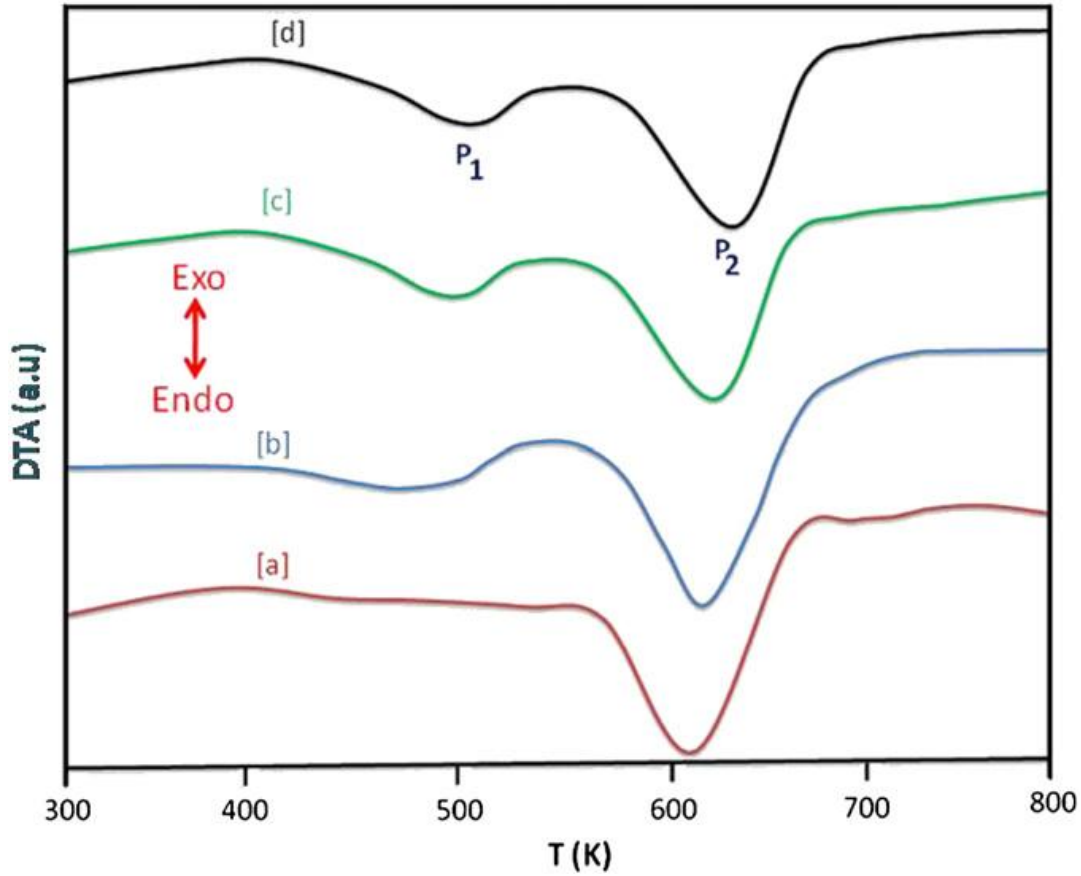


Fig. 4.3.4: DTA study on effects of aluminum on decomposition pattern of $(V,Al)_2H$ (a) V1.532 wt% Al, (b) V1.014 wt% Al, (c) V0.784 wt% Al and (d) pure V

Possible reasons for these observations could be (a) the change in the desorption kinetics, (b) modification of desorption mechanism, (c) stability of β phase at higher temperature, and (d) instability of α phase due to aluminum addition. As already reported from the laboratory, [125-126] the hydrogen absorption activation energy increases with aluminum concentration and

consequently, reversible desorption reaction could shift to lower temperature. But in the present case, interference of kinetics could be overlooked as heating rate was too slow. Thus modification and stability of α and β phase could be the other possible reason. An indirect support of modification of desorption mechanism and stability of α (Peak P₂) was given by Waisman et al. [124]. They pointed out that the presence of aluminum in titanium increased the activity of hydrogen and as a consequence desorption temperature is lowered. This might be true for the vanadium aluminum system also. As the activity of hydrogen increases due to the presence of aluminum, desorption becomes less endothermic and it requires more time and less temperature for the desorption reaction; consequently modification in P₁ peak and temperature shift in P₂ peaks were observed. However, no direct evidence is available in the literature for the activity correlation of hydrogen in the V–Al system. Another explanation could be based on Fermi energy level complemented with DFT theory [13]. As reported earlier, [117] aluminum contributes its electron to the Fermi energy level of vanadium which destabilizes the hydrogen–metal bonding and as a consequence alpha phase with dissolved hydrogen destabilizes which leads to decomposition at a lower temperature. Furthermore, Matumura et al. [41] noted that aluminum significantly modifies the chemical interaction between hydrogen and vanadium atoms in the hydride. The ionic interaction due the electron transfer between hydrogen and alloying elements associated with the measured dissociation temperature. The mechanism of electron transfer of the solute atom, aluminum, to the host matrix vanadium, and their correlation with the β phase stability could be helpful to understand the observed DTA events which require a theoretical assessment.

4.3.4 Pressure composition isotherm of V-Ti-Cr alloy (PCT)

Pressure composition curve at 330K has been generated for V₄Cr₄Ti and given Fig 4.3.5. The PCT as illustrated in the figure is for a typical hydrogen absorbing bcc alloy. However, the alloy shows two plateau pressures, first plateau pressure at 775 torr and second at 795 torr hydrogen pressure. The slope in the plateau region and the pressure difference between the two plateaus is undesirable for the application of metal hydride as a hydrogen storage material because it could slow down the hydrogen absorption kinetics. The figure also indicates the maximum hydrogen capacity as 1.8 weight % hydrogen, which is even lesser than the metallic vanadium which is reported as 4 weight % of hydrogen.

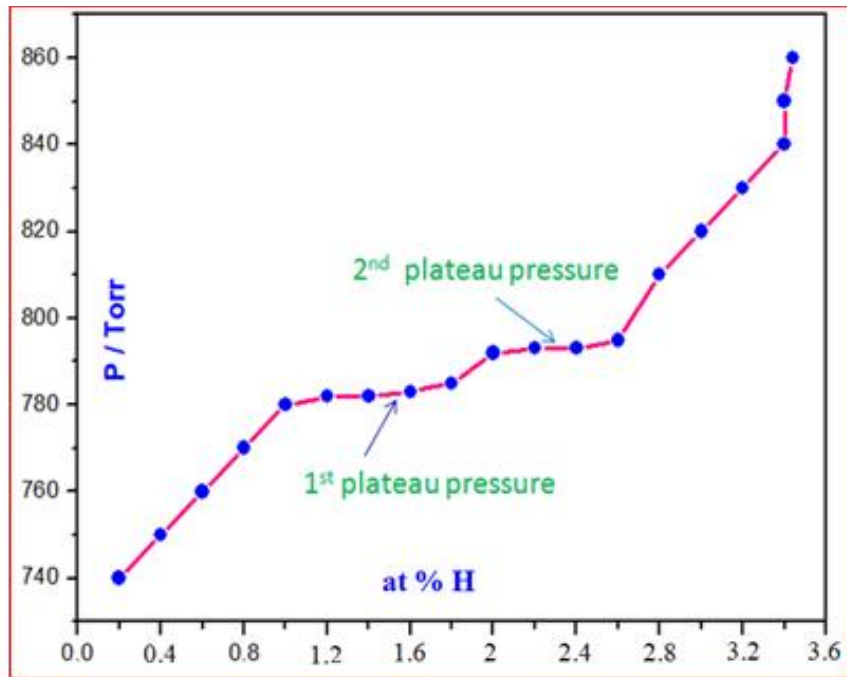


Fig. 4.3.5: PCT curve of the V₄Cr₄Ti alloy prepared by aluminothermy process at 330K. Kinetics of these alloys has been studied to investigate the effects of split PCT

In general trend, the alloying elements with less affinity for hydrogen could be able to split the plateau region and reduce the overall hydrogen absorption capacity. The aluminum in the present case is inert towards hydrogen and hence the PCT curve of the alloy has two plateau pressure and lesser hydrogen absorption capacity.

4.4 Thermodynamics and Kinetics of V(Al)-H System

4.4.1 Introduction

Thermodynamic parameters decide the feasibility of a process however the kinetic parameters decide the conditions to be set for the execution, scaling-up and commercialization of the process. Enthalpy, entropy and Gibbs free energy are the few thermodynamic parameters which have been discussed in this chapter for the V(Al)-H system [20,83,90]. Subsequently, the kinetic parameters of the V-Al-H system also have been elucidated. In this connection the reaction kinetics, models of reaction mechanism and the related activation energy [18,49,43,93] of hydrogen absorption process in V(Al)-H system has been discussed. All these parameters have been discussed with reference to aluminum.

4.4.2 Enthalpy, entropy and Gibbs free energy of V-H solution

Thermodynamic parameters are important factor to be considered for vanadium-hydrogen solid solution and the effects of aluminum on these parameters. The standard enthalpy and entropy of vanadium- hydrogen solid solution has been investigated as a function of aluminum content by using the equation (4.4.1) [89, 91]

$$\ln K_s = -\frac{\overline{\Delta H_H^0}}{RT} + \frac{\overline{\Delta S_H^0}}{R} \quad (4.4.1)$$

Where K_s is a Sieverts constant, ΔH^0 and ΔS^0 are the standard enthalpy and entropy of vanadium hydrogen solid solution respectively.

The K_s values were calculated using Sievert's law for the hydrogen in V-Al alloys at various temperatures and at one atmosphere hydrogen pressure using the equation (4.4.2)

$$\frac{H}{M} = K_s \sqrt{P} \quad (4.4.2)$$

Where, P is pressure in Pascal

The variation of K_s with temperature for vanadium and vanadium-aluminum alloys has been presented in Fig. 4.4.1. The Sieverts constant decreases with increasing temperature as well as with increasing aluminum content.

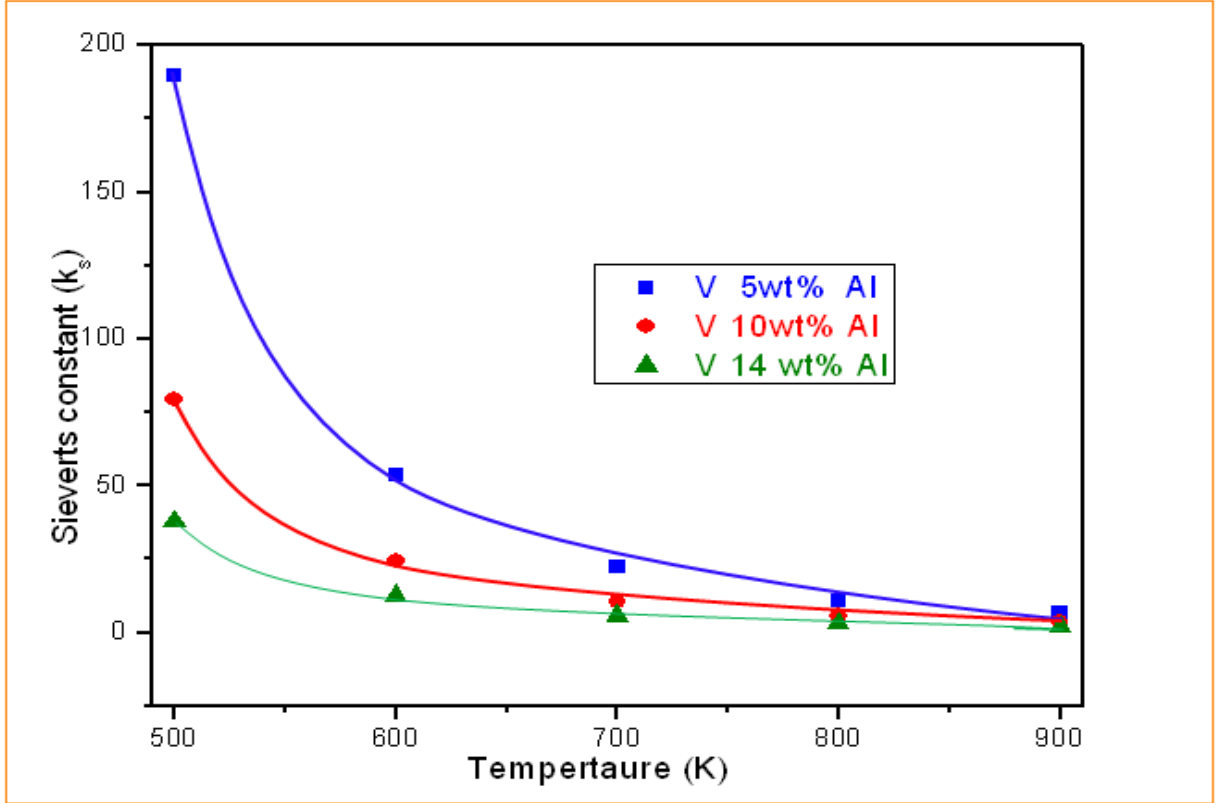


Fig 4.4.1: Variation of Sieverts constant with temperature and aluminum concentration

The Sievert's constant (K_s) is related with change in enthalpy ($\overline{\Delta H_H^0}$) and change in entropy ($-\overline{\Delta S_H^0}$) of the solution for hydrogen [19,130,131] by the following relation,

$$K_s = \frac{H/M}{\sqrt{P}} = \exp\left(-\frac{\overline{\Delta H_H^0}}{RT}\right) \exp\left(\frac{\overline{\Delta S_H^0}}{R}\right) \quad (4.4.3)$$

Logarithmic form of the equation could be expressed as shown below,

$$K_s = \ln \frac{H/M}{\sqrt{P}} = 0.22\left(-\frac{\overline{\Delta H_H^0}}{T} + \overline{\Delta S_H^0}\right) \quad (4.4.4)$$

The Sieverts constant, $\ln K_s$ has been plotted against inverse of temperature in Kelvin and presented in Fig 4.4.2. The slopes and intercepts of linearly fitted $\ln K_s$ versus $1/T$ (K) plots yielded the value of $(-\frac{\overline{\Delta H_H^0}}{R})$ and $(\frac{\overline{\Delta S_H^0}}{R})$ respectively. Thus enthalpy and entropy of V(Al)-H solid solution has been determined and presented in Table 4.4.1.

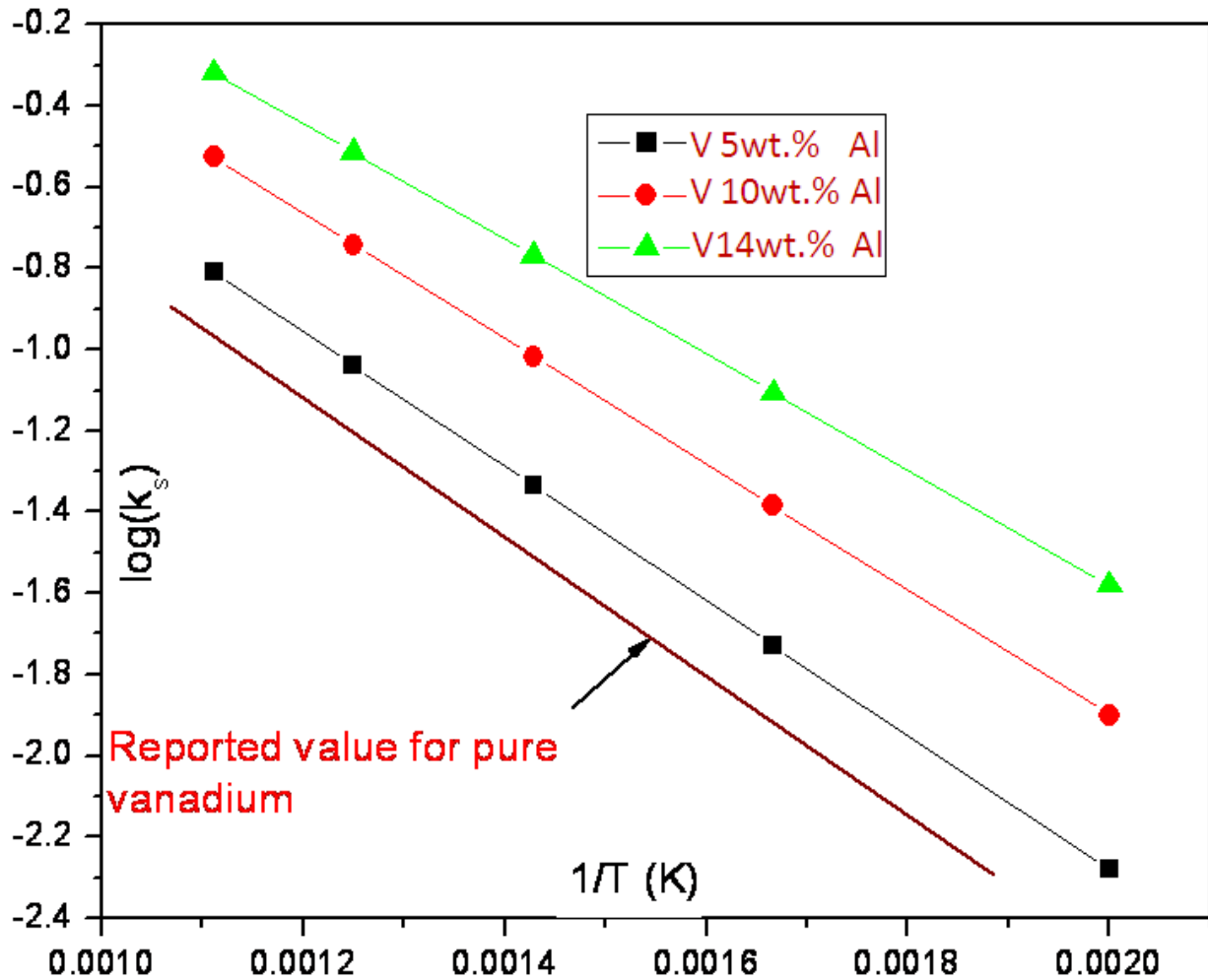


Fig.4.4.2: $\log(K_s)$ versus $1/T$ plot for entropy and enthalpy calculation

Table 4.4.1: Standard enthalpies and entropies of solution of hydrogen in vanadium- aluminum alloys

Alloys	$\Delta H_H^o \frac{kJ}{mol H}$	$\Delta S_H^o \frac{J}{K mol H}$
V 5wt% Al	-31.7 ± 1.4	-19.7 ± 3.2
V10wt%Al	-29.6 ± 1.4	-22.8 ± 3.2
V 14wt% Al	-27.2 ± 1.4	-24.1 ± 3.2

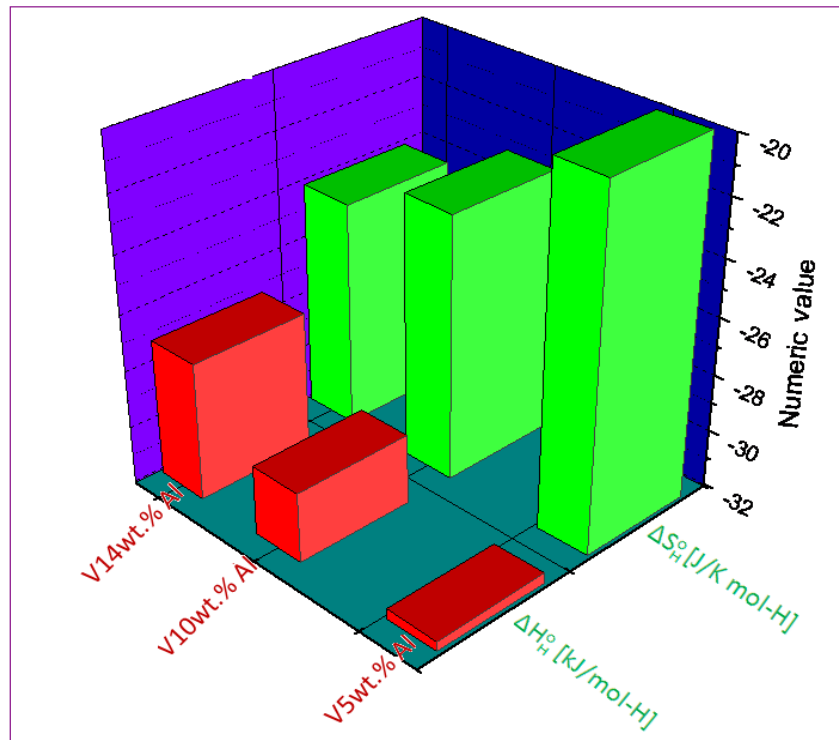


Fig. 4.4.3: Variation of standard enthalpy and entropy with aluminum content

The variation in enthalpy and entropy for the solution of hydrogen in the vanadium as a function of aluminum were calculated and reported in table 4.4.1 as well as illustrated in Fig. 4.4.3. Furthermore, enthalpies were separately measured for vanadium-hydrogen solid solution using differential thermal analysis (DTA) technique by dehydrogenation of the V(α) phase. The results obtained by these two techniques are in good agreement. The analysis revealed that the standard enthalpy was increased (became less negative) and standard entropy was decreased (became more negative) with increase of aluminum content. Using these data standard Gibbs free energy has been calculated and presented in Fig 4.4.4.

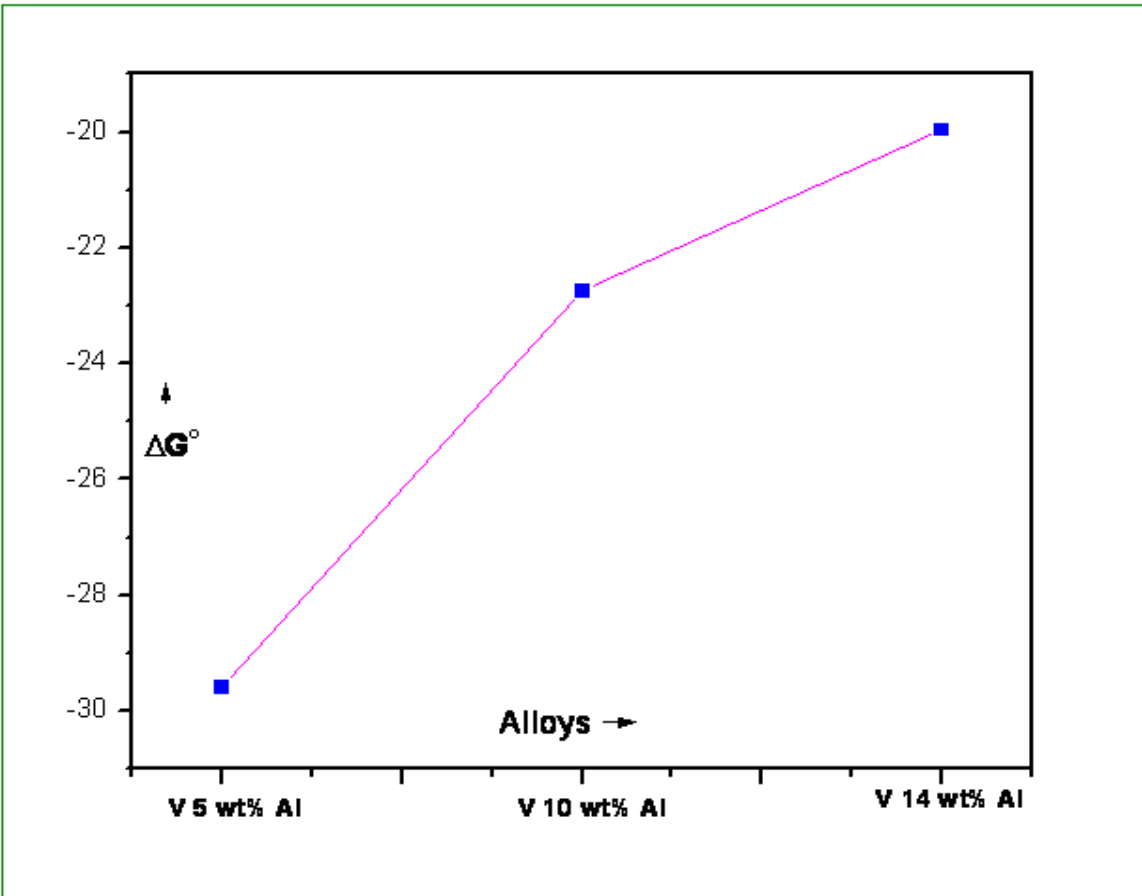


Fig. 4.4.4: Variation of Gibbs free energy of hydrogen solid solution as function of aluminum content

The results indicated that the hydrogen absorption processes are feasible thermodynamically in the present temperature range. The Gibbs free energy of V(Al)-H solid solution increases with the aluminum content. The variation of Gibbs free energy could be explained by various theories. The alloying elements which increase the lattice parameter are able to increase the activity of hydrogen and as a consequence Gibbs free energy is increased (became less negative) [126,116]. Another reason could be increase in the Fermi energy level of vanadium by aluminum as discussed earlier [117,128]. Increased Fermi energy level decreases the solubility which is indirectly related to the Gibbs free energy. Waisman et al. [124] studied the diffusion kinetics of hydrogen in Ti-Al alloys. The study revealed that the Gibbs free energy of hydrogen in Ti matrix increases with Al content. This may also be true for V-Al alloys but no confirmatory information is available in the literature. The influence of the electronic structure and the lattice constant on hydrogen absorption in bulk for the various alloys of palladium had been studied by density – function theory (DFT) [13]. The calculations revealed that the activity of hydrogen in metals matrix showed greater dependency on electronic structure vis-a-vis the lattice constant. On chemisorptions, atomic hydrogen is converted into H^+ and e^- . The electron thus produced affects the Fermi energy level of the host matrix. As reported earlier, aluminum enhanced the Fermi energy level in vanadium matrix [129]. Higher Fermi energy level interacts feebly with the electron resulting in the suppression of dissociation of hydrogen into H^+ and e^- . Therefore the increased Fermi energy level due to dissolved solute aluminum atoms slowed down the absorption kinetics. The electronic effect seems to significantly contribute in the Gibbs free energy.

4.4.3 Hydrogen absorption kinetics of V-Al and V-Ti-Cr alloys

Hydrogen absorption kinetics is an important parameter which is very much useful to the development of hydrogen storage/permeable materials for the practical applications. Several steps are involved in hydrogen gas- material interaction as illustrated schematically in the Fig. 4.4.5. [126-131]. In all of these interaction steps, diffusion of hydrogen and nucleation & growth of hydride phase plays an integral role to control the kinetics.

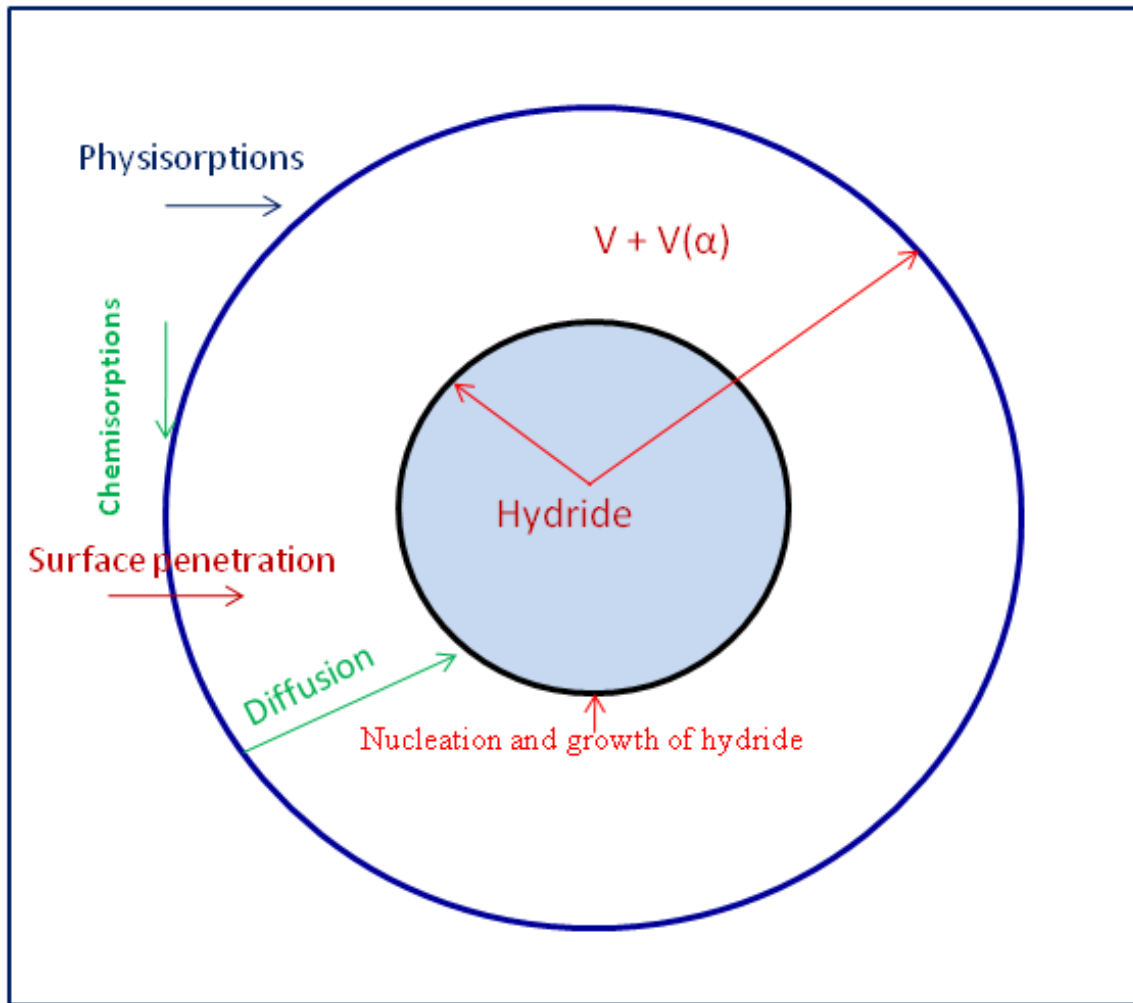


Fig. 4.4.5: Steps involved in hydrogen absorption process

Out of these two, diffusion process is extremely important in the development of hydrogen storage and permeable membrane material. At lower temperatures, kinetics of merely diffusion

process is difficult to elucidate because nucleation & growth of hydride phase occurs simultaneously and mechanism becomes very complex. In the case of vanadium-hydrogen system the nucleation & growth kinetics does not hold beyond 600 K temperature because vanadium hydrides are not stable beyond this temperature. Therefore, kinetics of diffusion process could be evaluated at temperature higher than 600 K, however below 600 K kinetics of nucleation and growth and diffusion could be determined simultaneously. As investigated by many researchers gas absorption of three-dimensional solid sample is controlled by the mechanism of three-dimensional diffusion. This is also valid for the hydrogen absorption in three-dimensional samples of vanadium and its alloys. Table 4.4.2 indicates the possible three-dimensional diffusion mechanism function involved in the gas absorption by solid and used to derive the suitable mechanism function in the present study.

Table 4.4.2: Three dimensional diffusion mechanism involved in the gas solid reaction which is used in the present study to select the suitable mechanism function

Name of Function	Type of Mechanism	Form of Function	
		F(α)	G(α)
Jander equation	3-D diffusion	$1.5 (1-\alpha)^{2/3} [1-(1-\alpha)^{1/3}]^{-1}$	$[1-(1-\alpha)^{1/3}]^2$
Anti Jander Equation	3-D diffusion decelerator	$1.5 (1-\alpha)^{2/3} [(1-\alpha)^{1/3} - 1]^{-1}$	$[(1-\alpha)^{1/3} - 1]^2$
Ginstling-Brounstein Eq	3-D diffusion	$1.5[(1-\alpha)^{-1/3} - 1]^{-1}$	$1-2/3\alpha-(1-\alpha)^{2/3}$
Zhuralev-Lesokin T Eq	3-D diffusion	$1.5 (1-\alpha)^{4/3} [(1-\alpha)^{-1/3} - 1]^{-1}$	$[(1-\alpha)^{-1/3} - 1]^2$
Avrami –Erofeev Eq	3-D random nucleation	$3(1-\alpha)[- \ln(1-\alpha)]^{2/3}$	$[- \ln(1-\alpha)]^{1/2}$

Activation energy calculation

Arrhenius equation in logarithmic form is as follows:

$$\ln\left(\frac{\Delta\alpha}{\Delta t}\right) = \ln A + \ln t - \frac{E_a}{RT} \quad (4.4.5)$$

Which may be converted into the equation

$$\ln k(T) = \ln A - \frac{E_a}{RT} \quad (4.4.6)$$

Because rate constant, $k(T) = \frac{\Delta\alpha}{\Delta t}$ (4.4.7)

Where, A is the pre-exponential factor, R is the molar gas constant [J/(mol K) or eV/(atom K)], T is hydrogenation temperature in Kelvin and E_a is the apparent activation energy of the reaction (J/mol or eV/atom) and t is time. The apparent activation energy E_a of the hydrogen absorption was obtained from the slope of linearly fitted $\ln k(T)$ versus $\frac{1}{T}$ curve.

V-thermit

The hydrogen absorption kinetics of as prepared V-Al thermit has been investigated using thermogravimetry technique at constant pressure. The chemical composition of the thermit used in the investigation is shown in the Table 4.4.3.

Table 4.4.3: Chemical composition of the crude thermit

Table 1 The chemical composition of V–Al alloys (wt%)

Alloy	Al	O	N	Fe
V17A1	17.098	0.021	0.043	0.054

The isothermal thermogravimetric curve obtained for this sample at all the four temperatures, 327°C, 377°C, 427°C and 477°C, are shown in the Fig. 4.4.6. The mass of the sample increases linearly with time and gains mass stability at equilibrium. The mass gain at 327°C was recorded higher than that of other higher temperature that could be attributed to the

larger sample mass. The reacted fractions α - t kinetic curve derived from the mass gain data and plotted in Fig. 4.4.7.

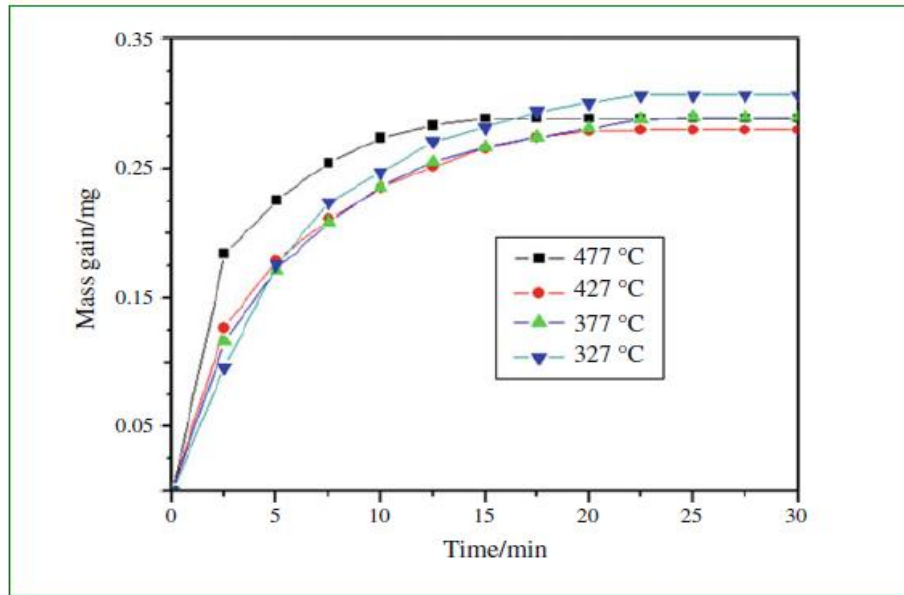


Fig 4.4.6: Thermogravimetric curve for hydrogen absorption in V-Al alloys

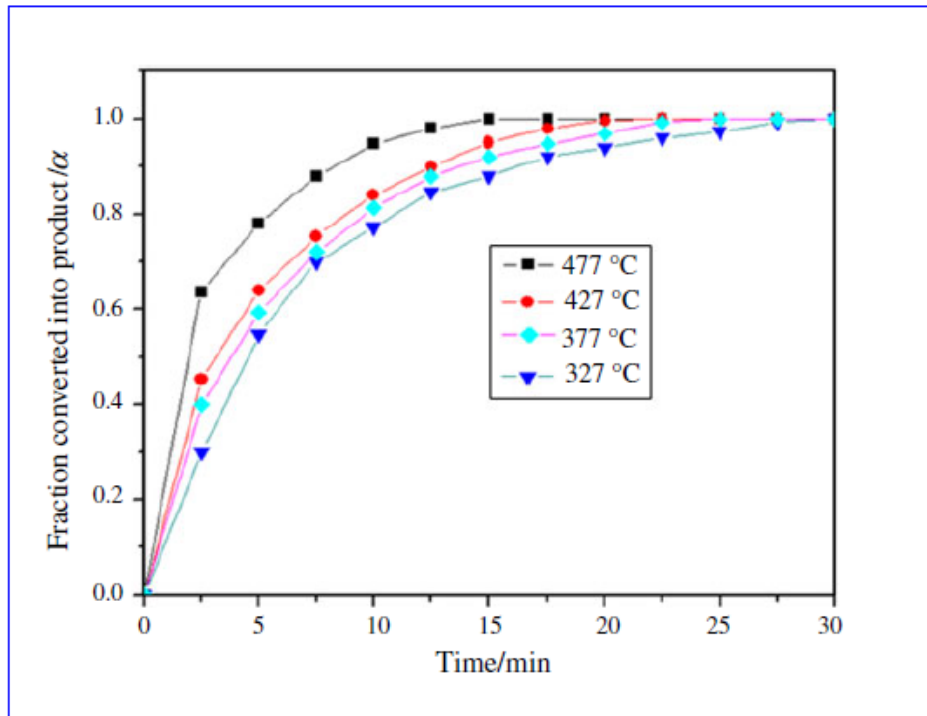


Fig. 4.4.7: α - t kinetics curve for the hydrogen absorption in V-Al alloys

The experimental α - t data were linearly fitted to various three-dimensional rate equations listed in the Table 4.4.2. The fitting equation with largest co-relation coefficient and smallest standard deviation is considered as the best indicative of actual reaction mechanism to describe the hydrogen absorption process. Three-dimension diffusion process known as Ginstling-Brounstein equation and represented as $[1 - 0.6\alpha - (1 - \alpha)^{0.6}]$ has been found to be the appropriate mechanism function. The best linearly fitted equation of hydrogen absorption process at temperature 327°C-477°C is shown in the Fig. 4.4.8.

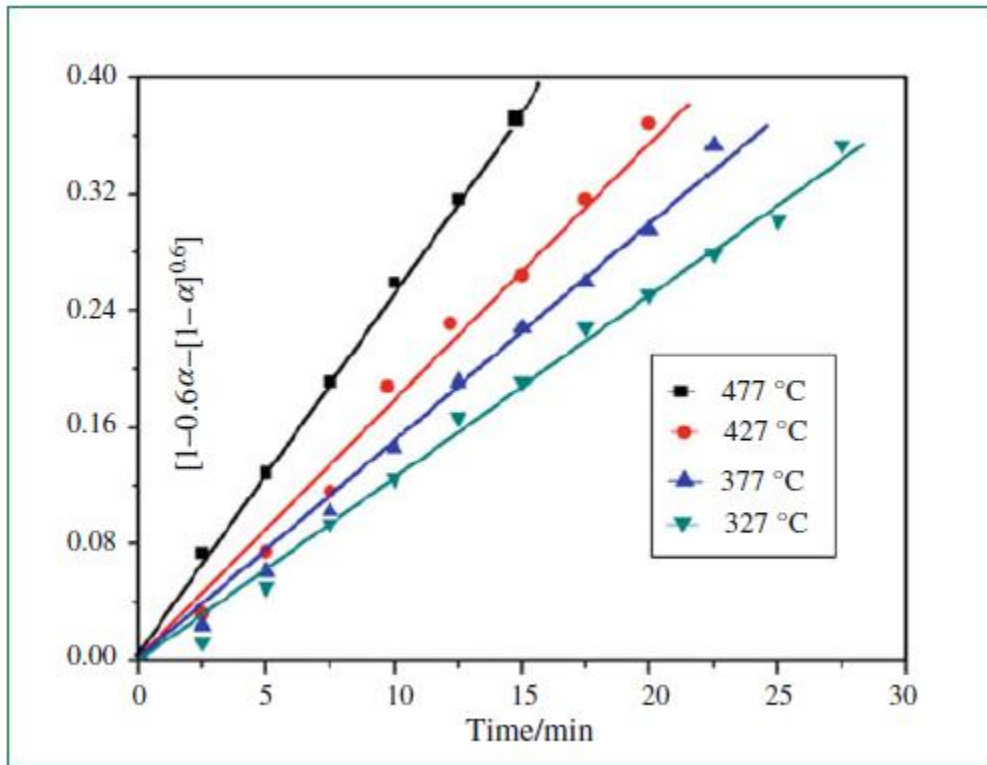


Fig. 4.4.8: Reaction mechanism function curve for hydrogen absorption in V-Al alloys

The slopes of the linearly fitted curve gave the rate constants at these four temperatures. Using rate constant the Arrhenius plot is constructed using equation 4.4.6 and presented in the Fig. 4.4.9. The fitting correlation coefficient was 0.95. Using Arrhenius equation, apparent

activation energy was calculated and it was found to be 16.77kJ/mole hydrogen [128]. The activation energy calculated appears to be higher as compared to pure vanadium reported earlier (4kJ/mole hydrogen) [132]. To remove the experimental uncertainty and to investigate that the increased activation energy indeed due to presence of aluminum, activation energy of a series of vanadium aluminum alloys were investigated using constant temperature and variable pressure methods.

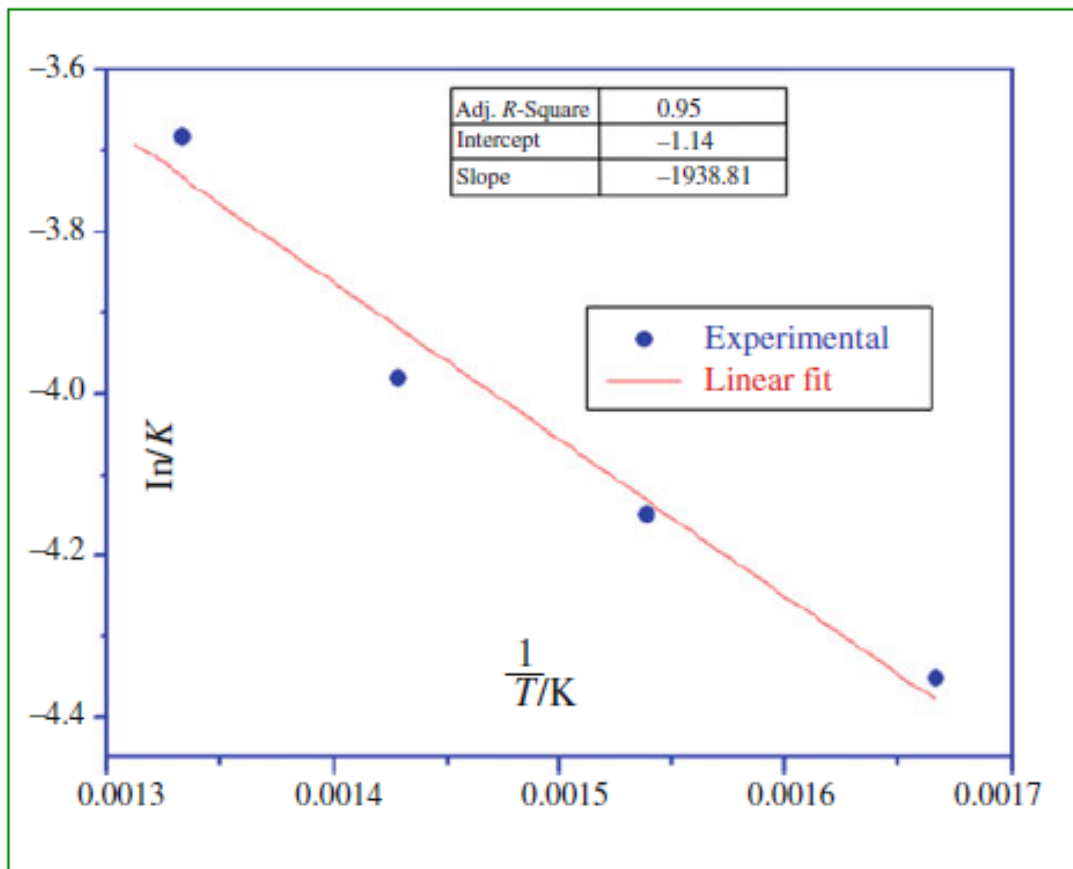


Fig 4.4.9: Arrhenius plot for Activation energy calculation

V-Al alloys

The activation energy of hydrogen absorption in as such prepared V-Al alloys has been investigated and it was found that the hydrogen absorption activation energy in the crude thermit

is many times (17kJ/mol) higher than the reported values for pure vanadium (~4kJ/mole). The roles of aluminum in the increased activation energy have been investigated. The chemical composition of the V-Al alloys used in this investigation is presented in Tab 4.4.4 Constant temperature and variable pressure method was employed [126]. Isothermal instantaneous pressure drop plots of all the three alloys are shown in the Fig. 4.4.10 a-c. The pressure continuously decreased with time and finally reached the equilibrium value. Hydrogen absorption is an exothermic reaction, hence time required to attend the equilibrium will be shorter with increasing temperature.

Table 4.4.4: Chemical composition of V-Al alloys used in the present investigation

Alloy	Al	N	O	Fe	Mn	Mo
V 5wt% Al	5.005	0.014	0.013	0.003	0.002	0.001
V10wt%Al	10.023	0.013	0.012	0.001	0.001	0.001
V 14wt% Al	14.012	0.013	0.013	0.002	0.001	0.001

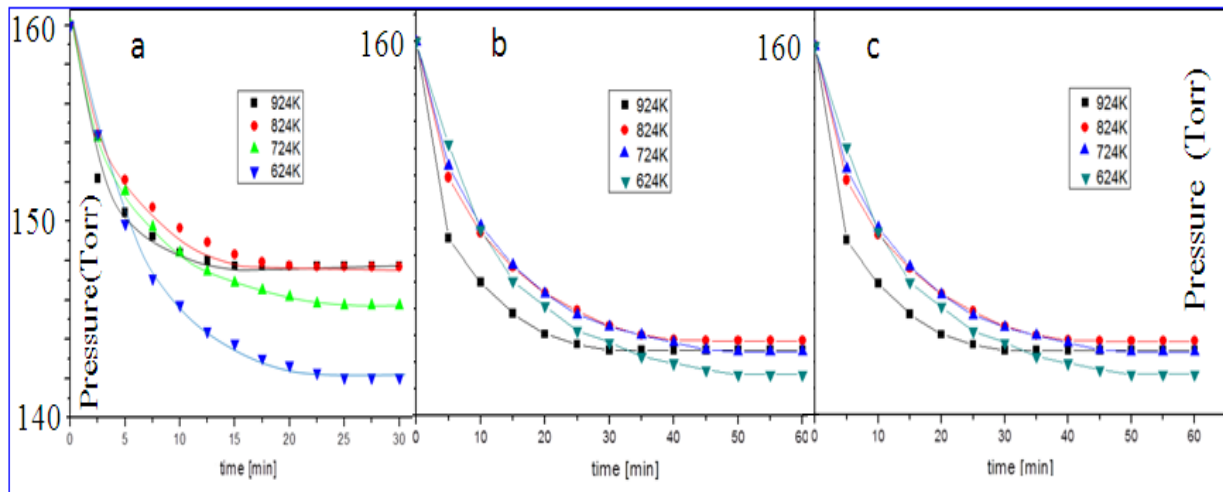


Fig.4.4.10: Isothermal instantaneous pressure curves of (a) V5wt%Al (b) V10wt%Al(c) V14wt%Al alloys

The instantaneous reacted fractions α for all the three samples at four different temperatures has been calculated using equation 4.4.8 and are presented in Fig. 4.4.11 a-c.

$$\alpha = \frac{p_0 - p_t}{p_0 - p_{eq}} \quad (4.4.8)$$

The curve is derived from the isothermal instantaneous pressure data and it shows the literal nature of hydrogen absorption process. For a given temperature, reacted fraction α varies with time and reaches its maximum value, which is '1' by definition. The kinetic curve derived by using reacted fraction α and substituting these values in different possible reaction mechanism functions listed in the literature.

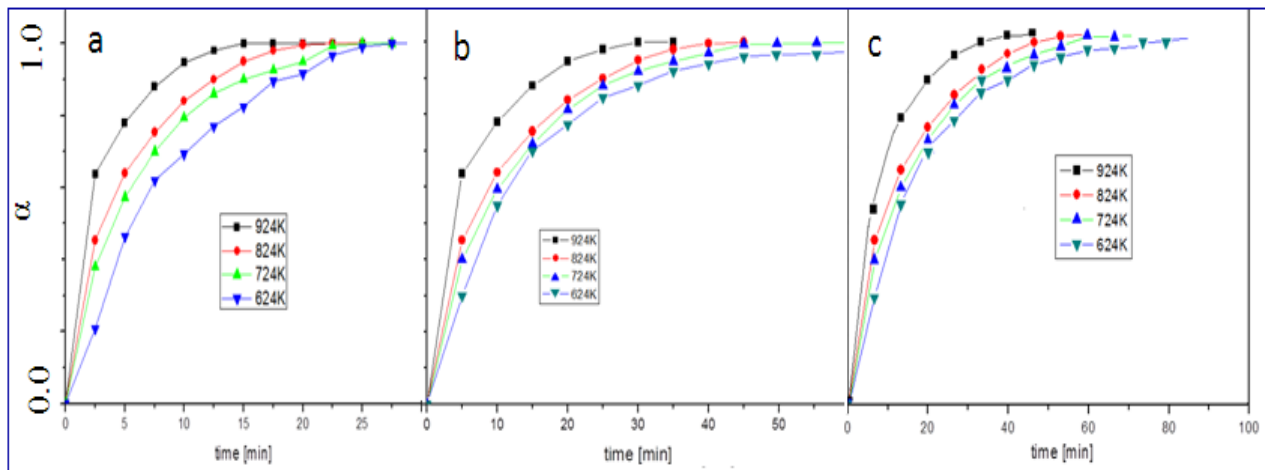


Fig. 4.4.11: Reacted fraction α - t curves of hydrogen absorption at different temperatures in (a) V5wt%Al (b) V10wt%Al (c) V14wt%Al alloys

The linear fitting equation with largest correlation coefficient and smallest standard deviation was considered as the best kinetics reaction mechanism to describe the hydrogen absorption. The result indicates that the three-dimensional diffusion is responsible for the hydrogen absorption in each setting temperature. The best linear fitting equations of hydrogen absorption process at the temperatures investigated were shown in Fig. 4.4.12 a-c.

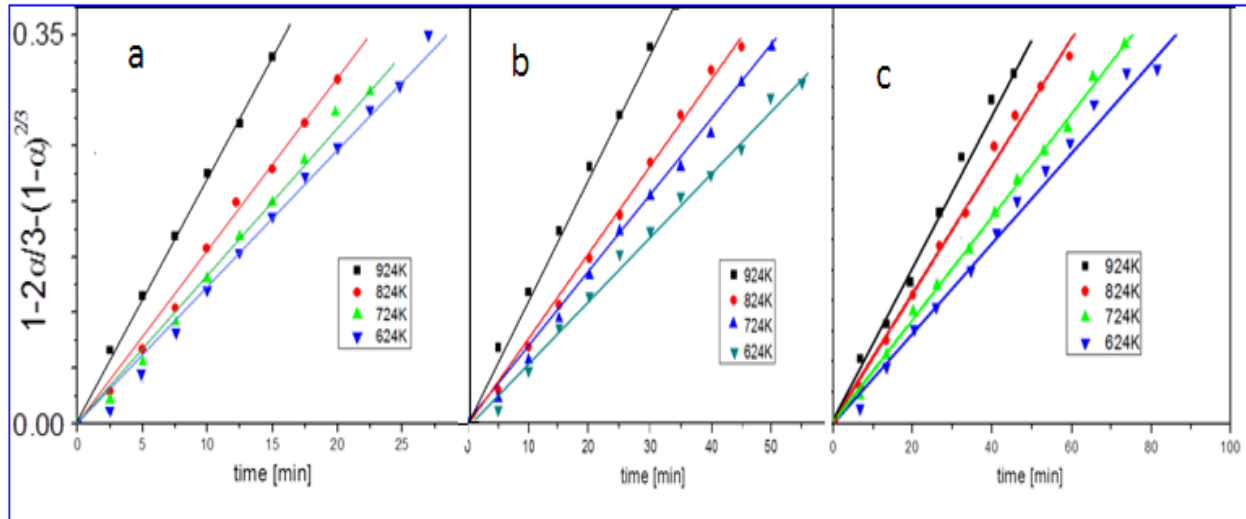


Fig. 4.4.12: Mechanism function of hydrogen absorption in (a) V5wt%Al (b) V10wt%Al (c) V14wt%Al alloys

The figure illustrates that the pressure decreased with increasing time and finally reached equilibrium. With varying temperature, the equilibration time become shorter, that could be attributed to exothermicity of hydrogen absorption reaction. The rate constants $k(T)$ were obtained from the slope of isothermal hydrogen absorption kinetics data [$g(\alpha)$ versus time]. Slope of $\ln k(T)$ versus inverse of temperature in Kelvin will give the value of $-E_a/R$ which is eventually converted into the activation energy E_a . As the same reaction mechanism controls the reaction at all the four temperatures hence, the combined Arrhenius plots for all the alloys are shown in Fig.4.4.13 a. The fitted correlation coefficients in all the cases were greater than 0.9899, indicating that the selected mechanism function was appropriate to describe the absorption process. The variation of activation energies as a function of aluminum are shown in Fig.4.4.13 [83]. The plot illustrates that the activation energy increases with increase of aluminum content. The kinetics parameters, mechanism of absorption and apparent activation energy for hydrogen absorption of the alloys at four different temperatures are listed in Table 4.4.5.

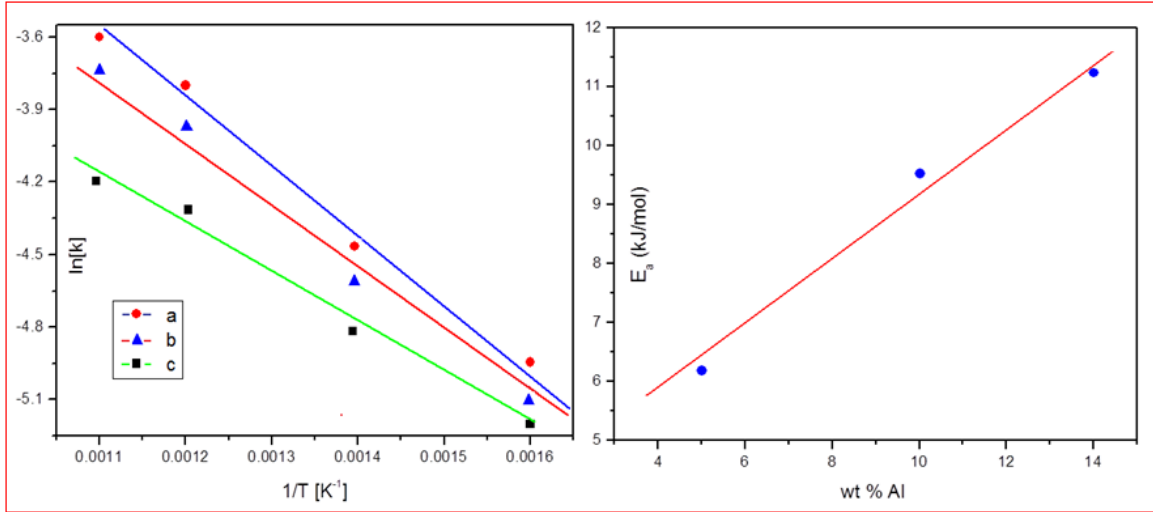


Fig. 4.4.13: (1) Arrhenius plot of hydrogen absorption reaction rate in (a) V14wt%Al (b) V10wt%Al (c) V5 wt %Al alloys (2) Variation of activation energy with aluminum contents

Table 4.4.5: Temperature dependent kinetic parameters, mechanism equation and apparent activation energies in V-Al alloys

Alloy	Best fitting equation	E_a (kJ/mol)	Temperature Range [K]
V 5wt% Al	$1-2\alpha/3 - (1-\alpha)^{2/3}$	7.54	624-924
V10wt%Al	$1-2\alpha/3 - (1-\alpha)^{2/3}$	9.51	624-924
V 14wt% Al	$1-2\alpha/3 - (1-\alpha)^{2/3}$	11.23	624-924

The increase in activation energy with aluminum content could be explained by various theories. Various alloy systems with aluminum as one of the component, prevent gas absorption including hydrogen [133,94,105,106]. The alloys surfaced were covered by adherent layer of Al_2O_3 , which acts as a strong barrier for the gas absorption kinetics. However, this explanation is not valid in the present investigation as the experiments were done under the control of argon gas and whenever necessary oxide layer was removed from the specimen surface. Another

explanation is based on chemical behavior of aluminum. Aluminum shows chemical inertness towards the various metals including vanadium [92,95-96]. Presence of aluminum in the host matrix will repel hydrogen and block their incorporation in the lattices in their local neighborhood. With increasing aluminum content, repulsive force for the hydrogen incorporation increased and as a result the activation energy increased. The present results could be explained on the basis of the theory given by Volkl and Alefeld [14]. These authors reported that as the distance between interstitial sites of host matrix increased (with solute content, aluminum in present case) the activation barrier for hydrogen solubility rose, resulting in decrease of hydrogen absorption kinetics due to increase in activation energy. A study on the diffusion of hydrogen in Ti-Al alloys [124] revealed that the free energy of hydrogen absorption in a Ti matrix increased with aluminum content due to increase in activity of hydrogen and hence the process became less feasible. This may also be true for V-Al alloys but no direct evidence is available in the existing literature. The influence of the electronic structure and the lattice constants on hydrogen absorption in bulk for the various alloys of palladium had been studied by density – function calculation (DFT) [13]. The density function theory (DFT) consideration revealed that the calculated activation energy for absorption of hydrogen showed greater dependency on electronic structure vis a vis the lattice constant. Hence, the electronic effect seems to be more important in the controlling the overall kinetics in the matrix. The presence of Aluminum in vanadium metal increased the Fermi energy level by contributing its valance electron to the Fermi energy level of the host matrix [117]. The increased Fermi energy level creates strong activation barrier for hydrogen adsorption and as consequence absorption kinetic decreased. The same Fermi level energy consideration complements the DFT theory and probably explains the present kinetics result. It is worth mentioning here that the kinetic evaluation in this part was

corresponding to the diffusion process. The solubility limit of hydrogen in the vanadium-aluminum alloys is not known. However, all the three alloy samples examined at 624 K contained 1,200 ppm hydrogen. The X-ray diffraction (XRD) analyses of these hydrogenated samples are given in Fig. 4.4.14 a-c.

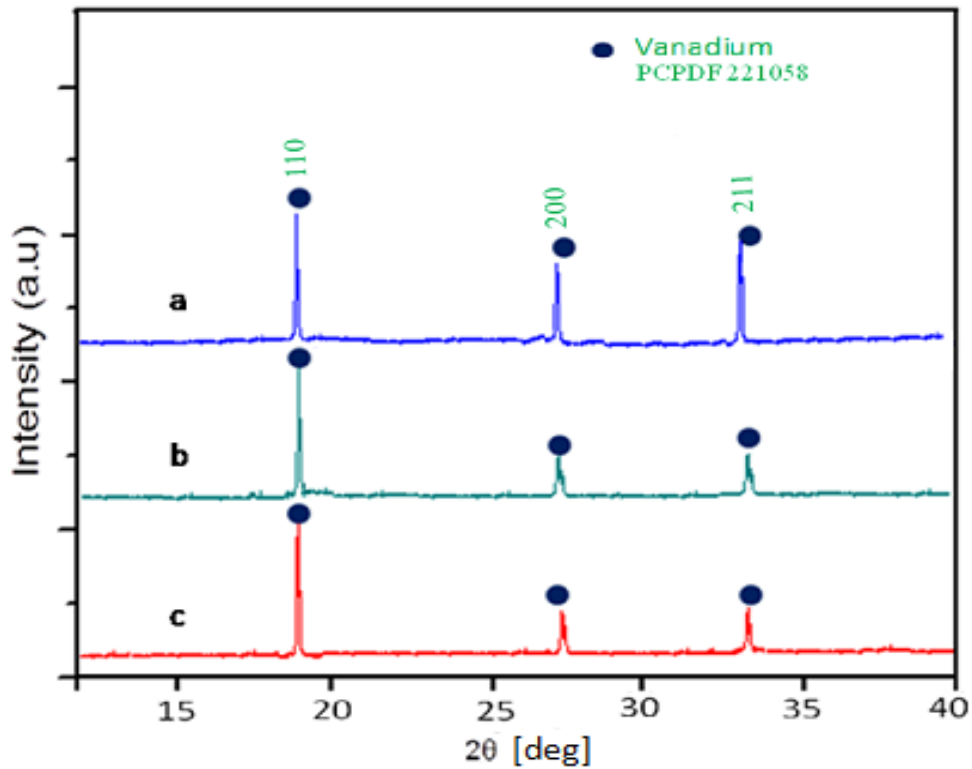


Fig. 4.4.14: XRD analyses of (a) V14wt%Al (b) V10wt%Al and (c) V5wt%Al after hydrogenation

The absence of hydride phase in the XRD analysis confirmed that the hydrogen was within the solubility limit. Furthermore, equal peak shift in the hydrogenated samples indicates that, after hydrogenation (V,Al) α phase have been formed. Shifting of peak, of the hydrogenated samples with respect to original samples could be attributed to the dissolution of the hydrogen in vanadium.

V-Ti-Cr alloy

The effect of aluminum on the hydrogen interaction of the potential hydrogen storage alloys, V-Ti-Cr [16,125,66,68,99,107,110] has been investigated. The alloy was synthesized by aluminothermic co-reduction of the oxide mixture. The alloy thus obtained was refined by electron beam melting and homogenized by vacuum arc melting. In general, a homogeneous master alloy is obtained by aluminothermy followed by electron beam melting. However, homogeneity of the final alloy has been confirmed by the line scanning of the sample using energy disperse spectroscopy (EDS) technique. The residual aluminum and oxygen & nitrogen have been analyzed by wet chemical methods and by inert gas fusion technique, respectively. The results are given in Table 4.4.6. The refined alloy ingot was sliced into pieces and later hot rolled to the final thickness. The hot rolled samples were annealed to stress relieve. Approximately 200-300 mg sizes sample were used for the kinetic studies. Thermogravimetric technique at constant pressure has been employed. The sample weight gain, due to hydrogen absorption, as a function of temperature during the continuous heating has been shown in the Fig. 4.4.15 a.

Table 4.4.6: Chemical composition of V4Ti4Cr alloy

V	Ti	Cr	O	N	Al	Fe
Balance	3.979	4.010	0.013	0.101	0.859	0.052

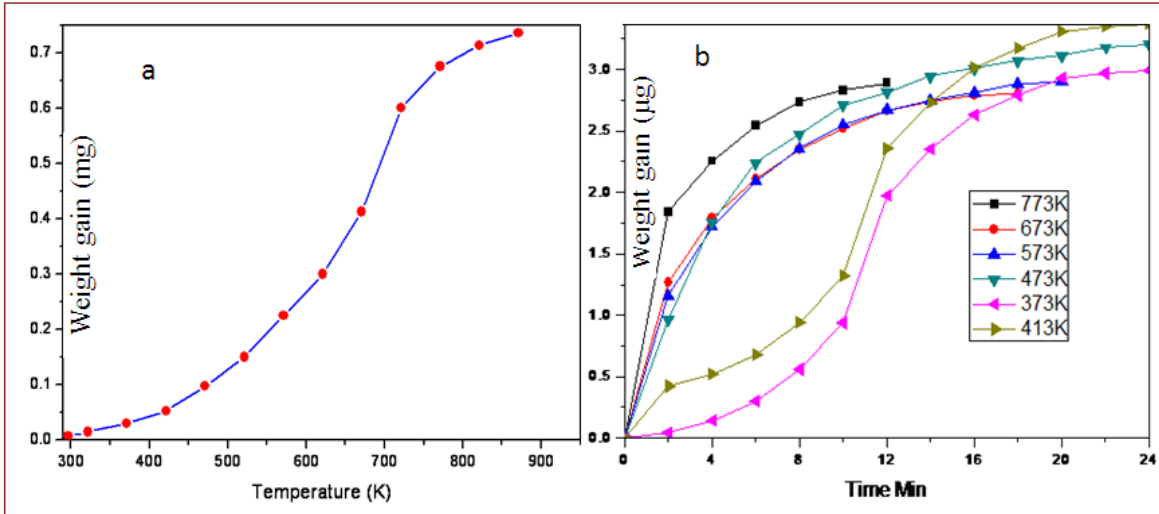


Fig. 4.4.15: Weight gain curve due to hydrogenation of V4Cr4Ti alloy during the continuously heating process (b) Isothermal weight gain curve during hydrogenation of V4Cr4Ti alloys at different temperatures

Significant weight gain was observed between 327-873 K. The observation has been confirmed by DTG. Hydrogen absorption and desorption are two parallel processes. Initially, the absorption rate was high but with increasing temperature, desorption rate was increased and after certain temperature, latter was dominating over the former process. In the present case, once the temperature increased above 800 K, the sample weight gain was found to be considerably less, indicating that the hydrogen desorption rate starts dominating. It is intricate to comment on the initial hydrogen absorption temperature in the present investigation, as the alloy was prepared by aluminothermy process, and no information is available in the literature regarding kinetics of such samples. However, compared to existing literature data for similar alloys prepared by other synthesis routes, the starting temperature of hydrogen absorption appears to be high. Based on the continuous heating result, the isothermal hydrogenation temperatures for the alloy were kept in between 373 K and 773 K, a range of temperature where kinetics was reasonably good. An isothermal weight gain verses time curve is shown in the Fig 4.4.15 b. The figure shows that the

sample weight increased with time and finally reached a steady state. With increasing temperature, the equilibration time became shorter. The reacted fractions ‘ α ’ calculated as a function of time at different temperatures, using equation 4.4.9 is presented in Fig. 4.4.16 a.

$$\alpha = \frac{\omega_t - \omega_o}{\omega_{eq} - \omega_o} \quad (4.4.9)$$

Where ω_o is the initial weight; ω_t and ω_{eq} are the weight at time t and final equilibrium, respectively. The data for $d\alpha/dt$ were calculated by dividing instantaneous rate of weight change by $\omega_{eq} - \omega_o$.

For a given time, α varies with temperature, for example after 12 min, the reacted fraction α is upto 1 at 773 K, however, it could be only reach to 0.59 at 373 K. The relative rate of weight change with time which is defined as ‘ $d\alpha/dt$ ’ at different isothermal temperatures is shown in the Fig. 4.22 b. The curve is similar to derivative thermal gravimetry (DTG) which indicates the instantaneous isothermal rate of weight change with respect to time and equilibrium weight gain. This curve is critically important to understand the reaction mechanism of hydrogen absorption process. Every abrupt change in this curve could be corresponding to a new reaction process. Increase of initial rate of weight change with temperature was observed from Fig. 4.4.16.b. It is clear from the figure that at the temperature 373 K, relative rate of weight changes is substantially less and remains almost constant up to 4 min and then increases with time and reaches to its maximum value within 10 min and then continuously decreases and becomes zero at equilibrium.

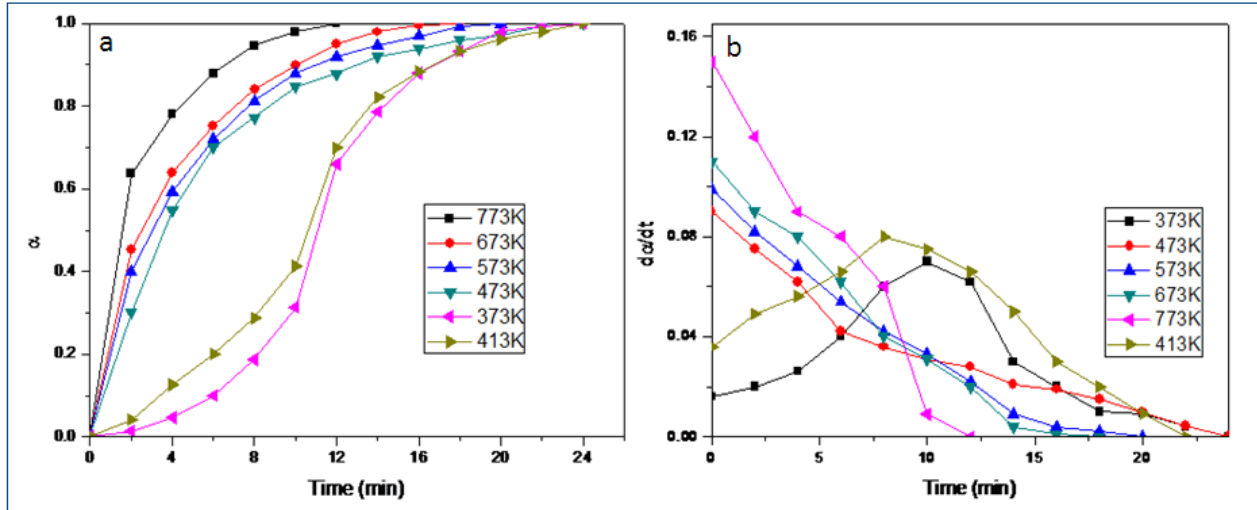


Fig. 4.4.16: (a) Reacted fraction curves of hydrogen absorption in V4Cr4Ti alloys at different temperatures (b) Hydrogen absorption rate curve with respect to time and temperature of V4Cr4Ti alloy at different temperatures

This observation was further supported by isothermal weight gain curve shown in Fig. 4.4.15 a. Essentially, at this temperature the hydrogen absorption process was composed of three stages; at the beginning the reaction rate was slow and almost constant indicating that there was an incubation stage. Incubation stage was due to the low surface activity and slow nucleation rate at low temperature, which hinders the hydrogen absorption process. The length of incubation period was related to hydrogen absorption activity and surface conditions of the samples. The first hydrogen absorption period (4-10 min) was the activation stage, during which the hydrogen absorption rate increased with time. Further, as time increased beyond 10 min, the reaction rate decreased to the minimum level and the sample approached to mass stability. This was the second hydrogen absorption period. The decrease of the reaction rate was attributed to the reduction of driving force, which was reflected in longer hydrogen absorption time. At temperature 413 K, the reaction rate continuously increased and reached its maximum value in around 8 min. With further increase in time, the reaction rate decreased to zero at steady state.

The curve indicates the absence of incubation stage at this temperature, though first and second hydrogen absorption stage appeared. The disappearance of incubation period could be due to the higher nucleation rate at higher temperature. Eventually, the duration of first absorption stage also became shorter compared to 373 K temperature. At the other four investigated temperatures (473 K, 573 K, 673 K and 773 K), reaction rate decreased continuously and became zero at steady state. Results at these temperatures indicate the absence of incubation as well as first absorption stage. Second absorption stage appeared similar to that of the temperature 373 K and 413 K, however duration to attain the equilibrium decreased with temperature. These observations revealed that the mechanism of hydrogen absorption varied with temperature.

Reacted fractions were linearly fitted to various rate equation listed in the literature with respect to time at different stages. The fitting equations with largest correlation coefficient and smallest standard deviation were considered as the best fit to describe the hydrogen absorption process. At the temperature 373 K, the increasing part of the reactions ((0)-(10) min), the reacted fraction data α , could not be linearly fitted in a single mechanism function. The first part data, 0-4 min, were linearly fitted into nucleation and growth process which was eventually related to incubation process, the reacted fraction data of 4-10 min, were linearly fitted into one dimensional diffusion process (power law). At the latter stage of reaction, 10 min to final equilibrium, data were linearly fitted to a mechanism function of three-dimensional diffusion process. The whole mechanism function curves are illustrated in Fig. 4.4.17 a- c. One minute interval data were used for the curve of 0-4 min duration. For other curves, data at the interval of 2 min were used to keep the figures clear. At 413 K, reacted fraction data α during 0-8 min, were linearly fitted into mechanism of one-dimensional diffusion processes (power law) which gave the best correlation coefficient. At the latter stage of the reaction, 8 min to final equilibrium,

reacted fraction data α were linearly fitted into a mechanism function of three-dimensional diffusion processes. The whole mechanism functions curves at this temperature are presented in Fig. 4.4.18 a-b.

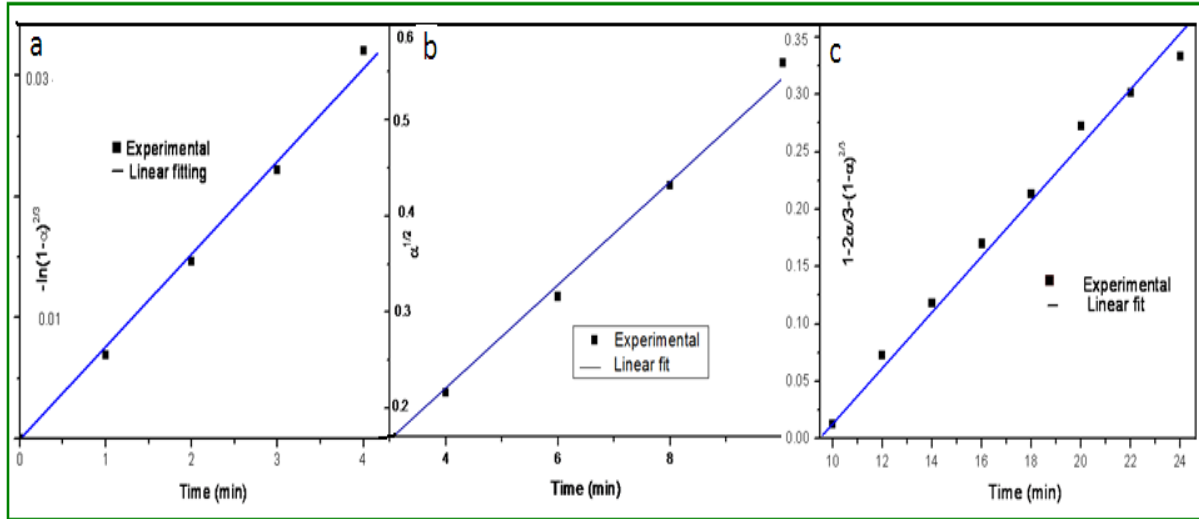


Fig. 4.4.17: Relation of reaction function with time in different hydrogen absorption reaction stages of V4Cr4Ti at 373 K (a) Incubation period (b) first hydrogen absorption period (c) second hydrogen absorption period

The reacted fraction data α , at other four temperatures from 473 K to 773 K, were linearly fitted into a single mechanism function of three-dimensional diffusion processes. Combined curve at all the six temperatures which is followed by same three-dimension diffusion are presented in Fig. 4.4.20 a. The rate constants at different temperatures were extracted from hydrogen absorption curves, the apparent activation energy E_a of the hydrogen absorption was obtained from the slope of $\ln[k]$ versus $1/T$ curve.

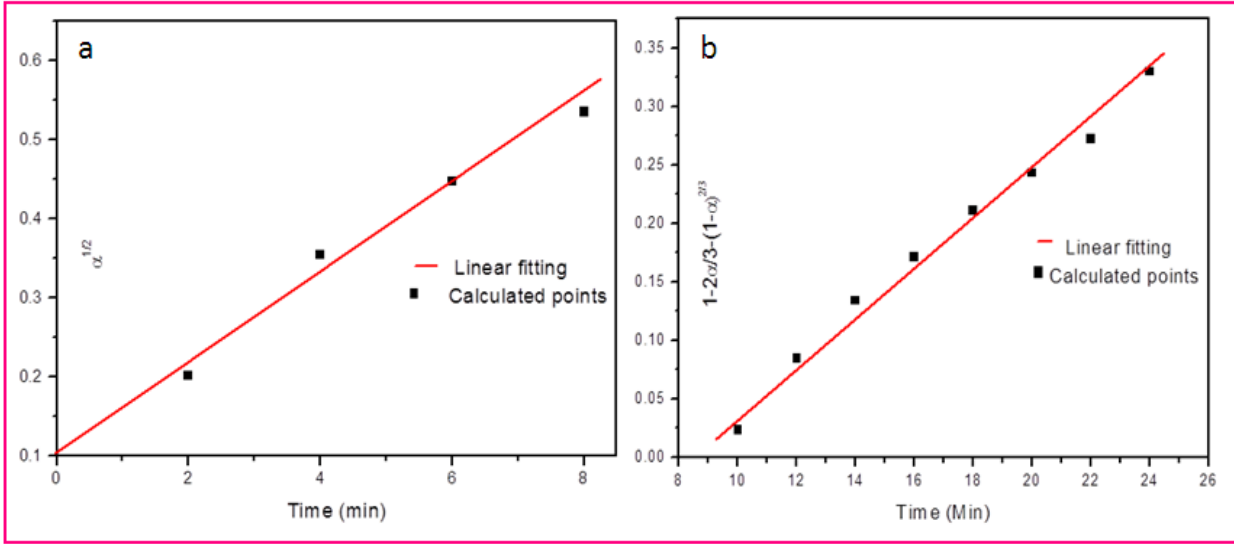


Fig. 4.4.18: Relation of reaction mechanism function with time in different hydrogen absorption reaction stages of V_4Cr_4Ti at 413 K (a) First hydrogen absorption (b) Second hydrogen absorption period

Since the hydrogen absorption process in the alloy was controlled by the same reaction mechanism in the temperature range of 473-773 K, and latter part at temperatures 373 K (10 min to final equilibrium) and 413 K (8 min to final equilibrium).

The Arrhenius plot is constructed in Fig.4.4.19 b. The fitting correlation coefficient is 0.9846, indicating that the method is feasible. The kinetic parameters and the mechanism equations for hydrogen absorption in the alloy at different temperatures are listed in Table 4.4.7. The observations have indicated that the rate of the three-dimensional diffusion processes was common and the slowest in each setting temperatures.

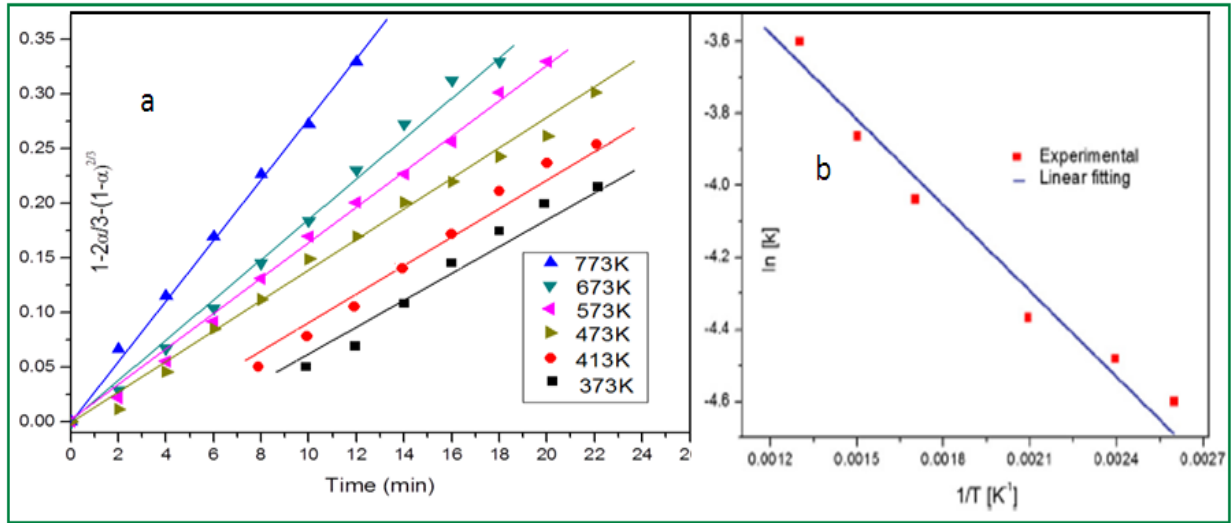


Fig. 4.4.19: (a) Relation of common mechanism functions with time for hydrogen absorption in V4Cr4Ti between 373 K and 773 K (b) Arrhenius plot of hydrogen absorption reaction rate in V4Cr4Ti alloy

Table 4.4.7: Temperature depended kinetic parameters, and mechanism equations of V4Cr4Ti alloy

Table 2 – Temperature depended kinetics parameters, and mechanism equations of V4Cr4Ti alloy.				
Temp (K)	Reaction stage	Best fitting equation	Rate constant (min ⁻¹)	Correlation constant
373	I	$(-\ln(1-\alpha))^{2/3}$ [$0 \leq \alpha \leq 0.09$]	0.06012	0.99911
	II	$\alpha^{1/2}$ [$0.09 \leq \alpha \leq 0.31$]	0.05498	0.99631
	III	$1 - 2\alpha/3 - (1-\alpha)^{2/3}$ [$0.31 \leq \alpha \leq 1$]	0.01139	0.98998
413	II	$\alpha^{1/2}$ [$0 \leq \alpha \leq 0.24$]	0.06578	0.99839
	III	$1 - 2\alpha/3 - (1-\alpha)^{2/3}$ [$0.24 \leq \alpha \leq 1$]	0.01231	0.98895
473	III	$1 - 2\alpha/3 - (1-\alpha)^{2/3}$ [$0 \leq \alpha \leq 1$]	0.01388	0.99729
573	III	$1 - 2\alpha/3 - (1-\alpha)^{2/3}$ [$0 \leq \alpha \leq 1$]	0.01694	0.99891
673	III	$1 - 2\alpha/3 - (1-\alpha)^{2/3}$ [$0 \leq \alpha \leq 1$]	0.01947	0.99854
773	III	$1 - 2\alpha/3 - (1-\alpha)^{2/3}$ [$0 \leq \alpha \leq 1$]	0.02719	0.99931

Thus it was reasonable to summarize that the three-dimensional diffusion process as the rate limiting step of the hydrogen absorption process. Slopes of three-dimensional diffusion

process curves at all investigated temperatures were used to calculate the activation energy. The calculated activation energy E_a was 6.1 kJ/mol.

4.4.4 Effects of vanadium on the hydrogen absorption kinetics of LaNi₅

Technical applications that rely on hydrogen absorption in intermetallic compounds which are under investigation presently include hydrogen purification, heat pumping and energy storage. Lanthanum penta-nickel (LaNi₅) is a widely accepted material for hydrogen storage because of its excellent absorption-desorption kinetics and it has been investigated extensively. Two serious drawbacks to the practical use of LaNi₅ are crumbling/pulverization during hydrogen charging which eventually degrade the mechanical strength of materials and thermal stability of hydride which leads to reduced usable hydrogen storage capacity. These two problems could possibly be solved and circumvented by using composite materials. It is known from literature that vanadium [39] is used to prevent the pulverization in many cases. Also thermal stability of the alloy could be decreased by using vanadium as an alloying component. The hydrogen absorption process in the pure LaNi₅ is controlled by diffusion process [33]. However, in case of composite materials the process is controlled by surface reaction [34]. Usually the kinetics of surface reaction is relatively faster. Therefore, to design new hydrogen storage alloys with fast desorption rate of hydrogen, it is very important to study the diffusion behavior of LaNi₅ composite materials. In present investigation kinetics and pulverization behaviors of V + 80 wt% LaNi₅ composite has been investigated. LaNi₅ intermetallic was prepared using in house made lanthanum of 3N purity as well as using Ni metal which was of 4N purity. Both the components were taken in a stoichiometric ratio and are melted under argon gas atmosphere. The melting was repeated to ensure homogeneity of the sample. Lanthanum penta-nickel (LaNi₅) compound thus prepared was ball milled. Aldrich make Analytical grade

vanadium powder was mixed with LaNi_5 chunk in the ratio of 20:80 wt% and then it was ball milled using tungsten carbide balls in argon atmosphere for four hours. Powder thus obtained was cleaned using acetone. The product was analyzed by XRD/SEM.

The scanning electron micrograph of the product (composite) composites has been shown in Fig. 4.4.20 (a).

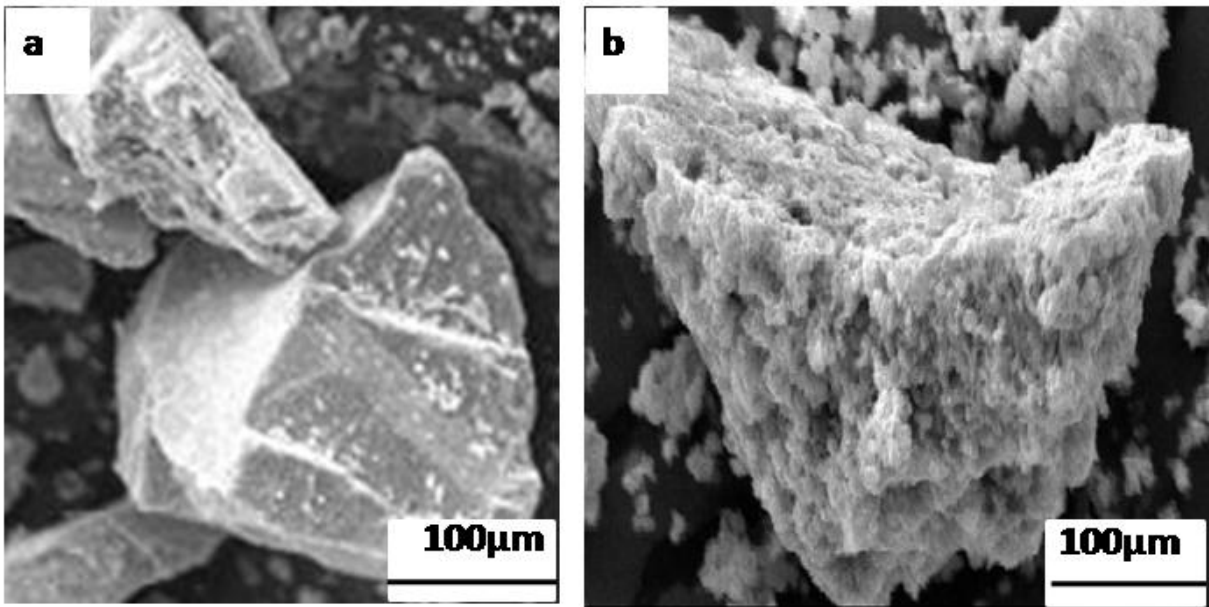


Fig.4.4.20: SEM Microstructure of (a) as prepared composite (b) After 20 hydriding-dehydriding cycle

It has been found that all the crystals were of the same size that could be due to perfect crystallinity of the composite. The XRD analysis of the composite has been shown in the Fig. 4.4.21 The XRD analysis showed two phases corresponding to LaNi_5 as well as vanadium. However, slight peaks in the LaNi_5 shift indicate the solubility of vanadium in LaNi_5 . The mass gain data with time for the powdered LaNi_5 , Vanadium and the composites have been shown in Fig. 4.4.22. The mass gain data for all the three samples had shown the usual parabolic variation

with time which is a clear indication that the three-dimensional diffusion process controlling the hydrogen absorption process. The equilibrium time for all the samples is given in Fig. 4.4..23.

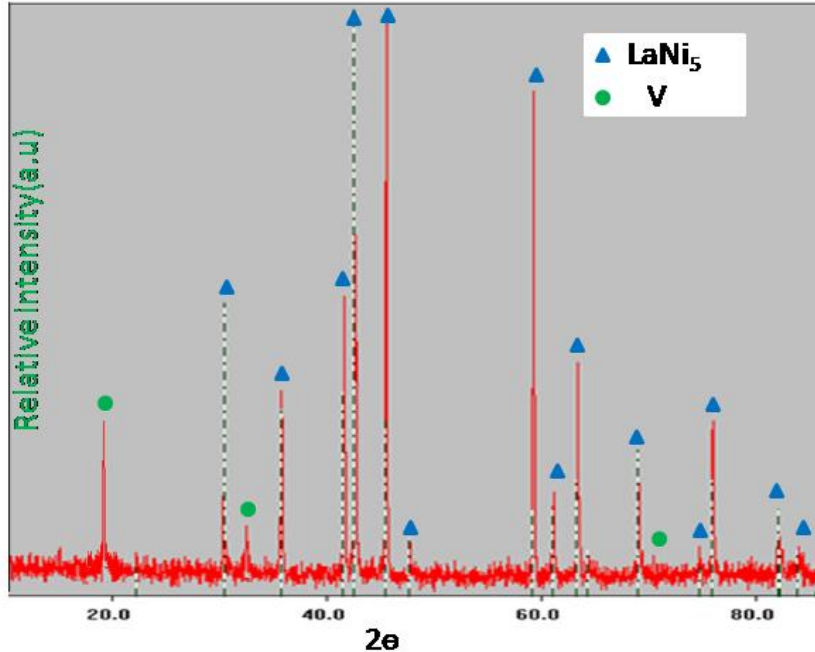


Fig 4.4.21: Phase analysis of composite using X-Ray analysis technique

On comparison of hydrogen absorption kinetics of LaNi₅, vanadium and composite it was found that on addition of vanadium to the LaNi₅ the kinetics became relatively fast. The SEM micrograph of composites after 20 hydriding-dehydriding cycles is shown in Fig. 4.4.20 (b). It was found that even after 20 cycles of hydrogen charging-desorption the morphology of composite remains intact however, the surface modification has been observed. The enhanced absorption kinetics of the composite could be explained on the basis of decreased Fermi level of composite. Electrical conductivity of LaNi₅, vanadium and composite has been measured at liquid nitrogen temperature and it was found that conductivity is least for V–LaNi₅ composite. The electrical conductivity is directly connected with the Fermi energy level [126].

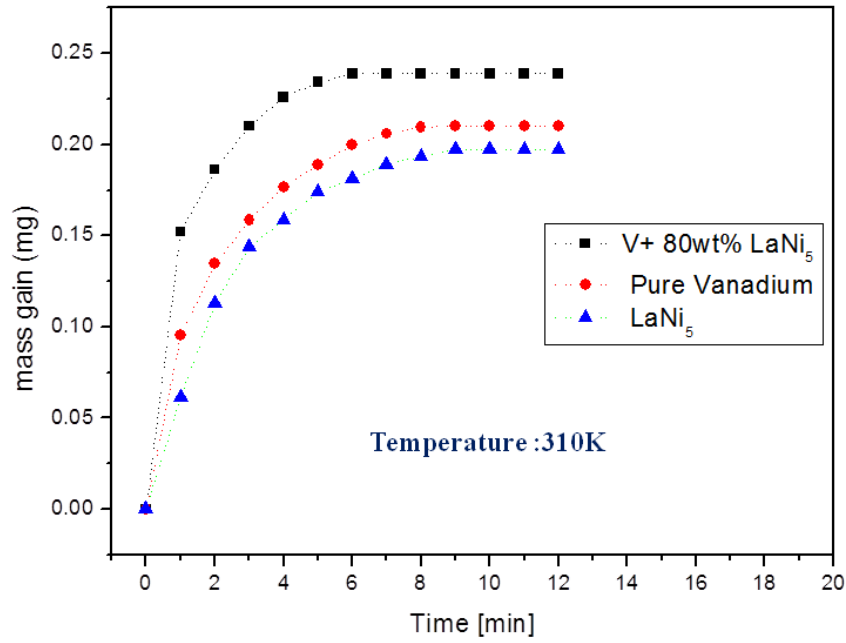


Fig. 4.4.22: Isothermal hydrogen absorption kinetic curve

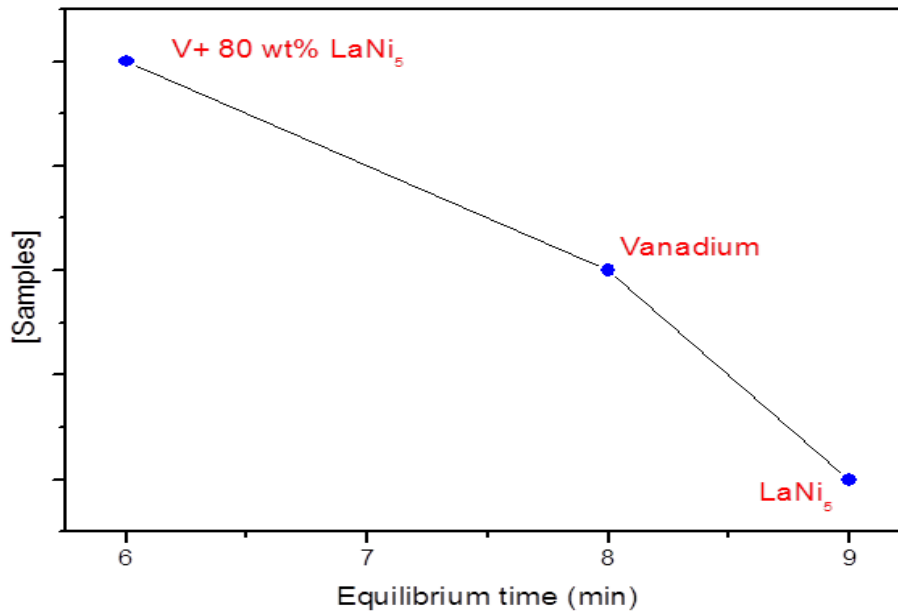


Fig. 4.4.23: Relative hydrogen absorption equilibrium time

As a conclusion, the Fermi level of LaNi_5 is apparently lowered by vanadium. On chemisorption, atomic hydrogen is converted into H^+ and e^- [124]. The electron thus produced interacted with the Fermi energy level of the host matrix. As explained, the Fermi energy level of LaNi_5 is lowered upon vanadium addition and a decreased Fermi energy level favors faster hydrogen absorption. The electronic effect seems to be significantly control the overall kinetics in the matrix. The present results could also be explained on the basis of the theory given by Volkl and Alefeld [14]. These authors reported that as the distance between interstitial sites of the host matrix increases, the activation barrier for hydrogen solubility decreases, resulting in the increase of hydrogen absorption kinetics due to decrease in activation energy. It has been recognized that the V-LaNi_5 composite is effective in increasing the lattices constant. The influence of the electronic structure and the lattice constant on hydrogen absorption in bulk for the various alloys of palladium had been studied by density – functional theory (DFT) [13,133]. The calculations revealed that the calculated absorption activation energy of hydrogen showed greater dependency on electronic structure vis-a-vis the lattice constant. Hence, the electronic effect may be responsible for better the control of the overall kinetics of hydrogen absorption in the matrix. The decreased Fermi energy level creates weak activation barrier for hydrogen adsorption and as a consequence absorption kinetics increased. The same Fermi energy level consideration along with DFT theory supports the results obtained in the present investigation.

Chapter... 5

Summary and conclusions

Contents

5.1 Summary and conclusions	154
5.2 Future scope of the work.....	155

5.1 Summary and conclusions

Aluminothermic reduction process is a potential route to produce vanadium and its master alloys with titanium, chromium and aluminum. The post reduction refining process could considerably reduce the aluminum and oxygen contents in the alloy. Vanadium-aluminum solid solution follows the Vegards law and hardness of the vanadium-aluminum alloys followed the simple solid solution effect. In general, titanium oxide reduction by aluminum require heat booster because the heat of reaction is not sufficient to sustain the reaction for completion. However, along with chromium and vanadium titanium could be loaded in vanadium matrix through aluminothermy process because of overall exothermicity. The increase in lattice parameter upon aluminum addition should increase the hydrogen solubility as per the existing theory. However, the solubility of hydrogen in single phase as well as co-existing two phase region is significantly reduced by the presence of aluminum. The enthalpy, entropy and Gibbs free energy of the vanadium-hydrogen solution were obtained using Sieverts constant measurements. The enthalpy data obtained was further verified using DTA technique. It was observed that both, enthalpy as well as entropy of the hydrogen solution in vanadium is increased by the presence of aluminum as a consequence desorption from the solid solutions required less temperature. Substantial modification in the β phase decomposition was observed with increase in aluminum content. It was assumed that kinetics could be one of the reasons and hence activation energy was calculated in a series of vanadium-aluminum alloys. The results indicate that the activation energy of hydrogen absorption increases with the increase in aluminum content. The decrease in hydrogen solubility with aluminum content has also been explained on the basis of Fermi energy level. It was found that Fermi energy of vanadium increases with the increase in aluminum content and therefore, increased Fermi energy level hinders the hydrogen

solubility as well as kinetics. The hydrogen absorption kinetics parameters have also been investigated for V-4Cr-4Ti synthesized by aluminothermy process. This alloy is a potential hydrogen storage material. The activation energy of hydrogen absorption in V-4Cr-4Ti was higher than the reported value in which these alloys were prepared through vacuum arc melting of high pure components. The hydrogen absorption mechanism in vanadium and its alloys with Al, Cr-Ti changes with temperature. At lower temperatures nucleation and growth, one-dimensional diffusion and three-dimensional diffusion control the overall process however, at higher temperatures three-dimensional diffusion controls the reaction. Activation energy of hydrogen absorption by vanadium linearly varied with aluminum concentration and all the alloys followed a mechanism of three-dimensional diffusion process. PCT curve of V and V-Al alloy has been found similar to that of a typical bcc. However, the equilibrium plateau pressure was higher for V-Al compared to vanadium. PCT curve of V-4Cr-4Ti alloy shows two plateau pressures which is due to the presence of aluminum and also substantial reduction in hydrogen capacity has been observed compared to the reported value. Vanadium enhanced the absorption kinetics of the V-LaNi₅ composites. The mechanical properties of LaNi₅ related to hydrogen absorption could be improved by making composites with vanadium.

5.2 Future scope of the work

From the data analysis of V-H hydrogen system and the effects of aluminum on the various parameters of hydrogen interaction with aluminum it appears that the Fermi energy of the host matrix controlling the hydrogen absorption, kinetics and thermodynamic properties. These phenomena have been explained on the basis of the Fermi energy level using theoretical considerations. However, the theory could be validated experimentally also. One of the techniques to evaluate the change in the Fermi energy level is by measuring the electrical

conductivity at low temperature as a function of alloy composition. The experimental validation of the Fermi energy theory could be very much useful to design and develop a material model which could illustrate/produce the behaviors of these materials towards hydrogen. Another technique to measure the Fermi energy level is by measuring the band gap. The band gap could be measured by diffuse reflectance spectra [96]. According to Kubelka-Munk relationship;

$$f(R_{\infty}) = \frac{(1-R_{\infty})^2}{2R_{\infty}} = \frac{\alpha}{s}, \quad (5.1.1)$$

Where, R_{∞} is the absolute reflectance of the alloy, s is a scattering coefficient, and α is the absorption coefficient.

Knowing the value of absorption coefficient, band gap could be calculated as:

$$\alpha = \frac{(h\nu - E_g)^2}{h\nu}, \quad (5.1.2)$$

Where, E_g is the energy of the forbidden gap, h is Planck's constant, ν is optical frequency.

Another work that could be added in the future work is to investigate the hydrogen permeability of vanadium as function of aluminum content.

Chapter... 6

Bibliography

Bibliography

- [1] http://en.wikipedia.org/wiki/Hydrogen_vehicle/hydrogen_interaction/absorption_kinetics.
- [2] G Marban, T V Solis. Towards the hydrogen economy. *Int J Hydrogen Energy* 2007; 32: 1625-37.
- [3] L Zhou, Progress and problems in hydrogen storage methods. *Renew Sustain Energy Rev* 2005; 9:395–408.
- [4] A Zuttel. Materials for hydrogen storage. *Mater Today* 2003; 24–33.
- [5] Sanjay Kumar and N Krishnamurthy. Corrosion of Fe9Cr1Mo steel in stagnant liquid lead-lithium eutectic. *Fusion Engineering and Design*. 2012; 87: 509–14.
- [6] T Ozaki, Y Zhang, M Komaki, C Nishimura. Hydrogen permeation characteristics of V-Ni-Al alloys. *Int J Hydrogen Energy* 2003; 28: 1229-35.
- [7] B Sakintuna, F Lamari-Darkrim, M Hirscher. Metal hydride materials for solid hydrogen storage: A review. *Int J Hydrogen Energy* 2007; 32:1121-40.
- [8] W E Kofstad Wallace and L J Hyvonen. Vapor Pressure Studies of the Vanadium-Hydrogen System and Thermodynamics of Formation of Vanadium-Hydrogen Solid Solution. *J Chem Phys* 1959; 81: 5019-22.
- [9] X Song, P Pei, P Zhang and G Chen. Effects vanadium on hydrogen storage property in Ti-V-Cr alloys. *Rare Metals* 2006; 25: 374-8.
- [10] H C Lin, K M Lin, K C Wu, H H Hsiung, H K Tsai. Cyclic hydrogen absorption-desorption characteristics of TiCrV and Ti_{0.8}Cr_{1.2}V alloys. *Int J Hydrogen Energy* 2007; 32: 4966-72.
- [11] M V Lototsky, V A Yartys, I Y Zavaliy. Vanadium-based BCC alloys: phase-structural characteristics and hydrogen sorption properties. *J Alloys Comps* 2005; 404-406:421-6.
- [12] A Kagawa, E Ono, T Kusakabe and Y Sakamoto. Absorption of hydrogen by vanadium-rich V-Ti based alloys. *Journal of the Less-Common Metals* 1991, 172-174 :64-70.
- [13] Ke X, Kramer J G, O M Løvvik. The influence of electronic structure on hydrogen absorption in palladium alloys. *J Phys: Condens Matter* 2004; 16 :6267-77.
- [14] J Volkl and G Alefeld, *Hydrogen in metal I*, Berlin: Springer-Verlag 1978; 333.
- [15] H Arashima, F Takahashi, T Ebisawa, H Itoh, T. Kabutomori, Correlation between hydrogen absorption properties and homogeneity of Ti–Cr–V alloys, *J Alloys Comps*, 356–357 (2003) 405-8.

- [16] D J Pine and R M Cotts, Diffusion and electrotransport of hydrogen and deuterium in vanadium-chromium alloys, *Physical Review B*, 28 (2) (1983) 641-7.
- [17] H M Moshe, Bloch J. Evaluation of the kinetics and mechanism of hydriding reactions. *Prog. Solid St Chem*. 1985; 16: 163-194.
- [18] H J Grabke and Horz G. Kinetics and Mechanism of gas-metal interaction: *Ann Rev Mater Sci* 1977; 7: 155-78.
- [19] D T Peterson, Nelson S O. Isopiestic Solubility of Hydrogen in Vanadium Alloys at low Temperatures. *Meta Trans A* 1985; 16A: 367-74.
- [20] V Ewald, Edward R K. Thermodynamic properties in the System Vanadium-Hydrogen, Niobium –Hydrogen and Tantalum-Hydrogen. *J Phy Chem* 1969; 73(3):683-92.
- [21] U S Department of Energy. Essential features of hydrogen storage materials, Website: (<http://www.doe.gov>).
- [22] L Schlapbach, A Zuttel. Hydrogen-storage materials for mobile applications. *Nature* 2001; 414:353-8.
- [23] D Lu, Li W, Hu S, Xiao F, Tang R. Uniform nanocrystalline AB₅-type hydrogen storage alloy: preparation and properties as negative materials of Ni/MH battery. *Int J Hydrogen Energy* 2006; 31(6):678–82.
- [24] D Elena. An overview of advance materials for hydrogen storage. *J Mat Proc Tech* 2005; 162-163: 169-77.
- [25] T Tanaka, Keita M, Azofeifa DE. Theory of hydrogen absorption in metal hydrides. *Physical Review B* 1981; 24 (4): 1771-76.
- [26] T Schober. Vanadium, Niobium and Tantalum-Hydrogen, *Solid State Phenomena Vols*. 1996; 49-50: 357-422.
- [27] R Wiswall. Hydrogen in metals II. *Top Appl Phys* 1978; 29:201-42.
- [28] H Yukawa, Yamashita D, Ito S, Morinaga M, Yamaguchi S. Compositional dependence of hydriding properties of vanadium alloys at low hydrogen pressure: *J Alloys Comps* 2003; 356-357 : 45-49
- [29] X P Song, P Pei, P L Zhang, G L Chen. The influence of alloy elements on the hydrogen storage properties in vanadium-based solid solution alloys, *Journal of Alloys and Compounds* 2008; 455 :392-397.
- [30] J F Lynch, J J Reilly and F Millot. The absorption of hydrogen by binary vanadium-chromium alloys. *J Phys Chem Solids* 1978; 39: 883-890.

- [31] J J Reilly, R H Wiswall. The higher Hydride of vanadium and Niobium. *Inorganic Chemistry* 1970; 9(7):1678-1683.
- [32] N N Gerard and S Ono, L Schlapbach (editor), *Hydrogen in Intermetallic Compounds H*, Springer, Berlin, 1992, Chapter 4.
- [33] R Dus, E Nowicka, Z Wolfram. Surface phenomena in the process of vanadium hydride formation. *J Alloys Compds* 1997; 253-254: 496-499.
- [34] Y P Zheng, T Y Zhang. Effects of absorption and desorption on hydrogen permeation –II Experimental Measurement of Activation Energies. *Acta Mater* 1998: 46 (14); 5035-43.
- [35] T Troev, A Markovski, Petrova M , Peneva S, Yoshiie T. Positron lifetime calculations of defects in vanadium containing hydrogen. *Nuclear instruments and Methods in Physics Research B* 2006; 248: 297-304.
- [36] D G Westlake, S T Ockers and Gray W R. Electrical Resistivity of V-H Alloys. *Metallurgical Transactions* 1970;1:1361-66
- [37] A N Golubkov, A A Yukhimchuk. Synthesis of the dihydride phase of vanadium. *J Alloys and Compds* 2005: 404-406: 35-7.
- [38] R R Arons, H G Bohn and Lutgemeier H. Comparison of the V-H and V-D phase diagrams by means of NMR. *J Phys Chem Solids* 1974; 35: 207-214.
- [39] J R Richard and Thomas R P, Gibbes J. X-ray Diffraction Studies of the Effects of Trace of Hydrogen in Vanadium. *J Phys Chem* 1964, 68 :2197-2203
- [40] C-Y Seo, J-H Kim, P S Lee, J-Y Lee, Hydrogen storage properties of vanadium-based BCC solid solution metal hydrides, *Journal of Alloys and Compounds*, 348 (2003) 252-7.
- [41] T Matumura, H Yukawa, M Morinaga, Alloying effect on the electronic structure of VH_2 and V_2H , *Journal of Alloys and Compounds* 1999; 284 :82-88.
- [42] H Yukawa, M Takagi, A Teshima, M Morinaga, Alloying effect on stability of vanadium hydrides, *Journal of Alloys and Compds* 2002; 330-332 : 105-9.
- [43] M Martin, C Gommel, C Borkhart, E Fromm. Absorption and desorption kinetics of hydrogen storage alloys. *J Alloys Compd.* 1996; 238: 193–201.
- [44] A J Maeland, G G Libowitz, J F Lynch and G Rak. Hydride formation rates of BCC. group V metals, *Journal of the Less-Common Metals*, 104 (1984) 133-9.
- [45] Pauling L, location of hydrogen in tetragonal and monoclinic structure. *J Sol. St Chem* 1989; 79 ; 63-4
- [46] T Schober, Vanadium-Deuterium: Calorimetry and phase diagram. *Scripta Met* 1978; 12:549-54.

- [47] Yu X B, Yang Z X, Feng S L, Wu Z, Xu N X. Influence of Fe addition on hydrogen storage characteristics of Ti–V-based alloy. *Int J Hydrogen Energy* 2006; 31(9):1176–81.
- [48] H Homma, H Saitoh, T Misawa. et al, Effect of laves phase on hydrogen behavior in V-Zr-Ti-Ni hydrogen absorption alloys, *Materials Transaction* 2002; 43(5) : 110-6.
- [49] Q Guo, H Hou, X Ren, Hydrogen absorption kinetics of porous Ti6Al4V. *J Alloys Compds.* 486 (1-2) (2009) 754-8.
- [50] D C, Michael, Janice K L Darlene K S, Mirna R. Hydrogen uptake characteristics of mechanically alloyed Ti-V-Ni. *J Alloys and Compds* 2006; 417: 159-63.
- [51] S Basak, K Shashikala, S K Kulshreshtha. Hydrogen absorption characteristics of Zr substituted Ti_{0.85}VFe_{0.16} alloy. *Int J Hydrogen Energy* 2008; 33: 350-5.
- [52] T Dou, Wu Z, Mao J, Xu N. Application of commercial ferrovandium to reduce cost of Ti-V-based bcc phase hydrogen storage alloys. *Materials Science and engineering A* 2008: 476; 34-8.
- [53] Ono S, Nomura K and Ikeda Y , Synthesis and purification of vanadium metal. *J Less-Common Met* 1980; 72:159-64
- [54] K Nomura, E Akiba. H₂ Absorbing–desorbing characterization of the Ti–V–Fe alloy system. *J Alloys Compds* 1995;231:513–7.
- [55] Lynch J F, Maeland A J and Libowitz G G. Mechanism of metal-hydrogen interaction. *J Phys Chem N F* 1985; 145 : 51-7.
- [56] M Khrussanova, E Zhecheva, R Stoyanova and P Peshev, Hydrogen absorption by Nickel-containing vanadium-titanium alloys, *Mat Res Bull* 1993; 28:377-384.
- [57] H Miao, Wei Guo Wang, Mechanisms of improving the cyclic stability of V-Ti-based hydrogen storage electrode alloys, *Journal of Alloys and Compounds* 2010; 508:592-598.
- [58] H B Wang, Q Wang, C Dong, L Yuan, F Xu, L X Sun. Composition design for Laves phase-related BCC-V solid solution alloys with large hydrogen storage capacities. *J Phys: Conference series* 2008; 98 012018: 1-8.
- [59] T Kabutomori, H Takeda, Y Wakisaka, K Ohnishi, Hydrogen absorption properties of Ti□Cr□A (A ≡ V, Mo or other transition metal) B.C.C. solid solution alloys, *Journal of Alloys and Compounds* 1995; 231:528-532.
- [60] D S Santos dos, M Bououdina, D Fruchart. Structural and hydrogenation properties of an 80 wt% TiCr_{1.1}V_{0.9}–20 wt% LaNi₅ composite material. *Int J Hydrogen Energy* 2003;28: 1237–41.
- [61] M Okada, T Kuriwa, T Tamura, H Takamura, A Kamegawa. Ti–V–Cr B.C.C. alloys with high protium content. *J Alloys Compds* 2002; 330–332:511–6.

- [62] T Matsunaga, M Kon, K Washio, Shinozawa, M Ishikiriya. TiCrVMo alloys with high dissociation pressure for high-pressure MH tank. *Int J Hydrogen Energy* 2009; 34: 1458-62.
- [63] XP Liu F Cuevas, L J Jiang, M Latroche, Z N Li, S M Wang. Improvement of the hydrogen storage properties of Ti-Cr-V-Fe BCC alloy by Ce addition. *J Alloys Comps* 2009; 476; 403-7.
- [64] M Giovanni. Some physical aspects of hydrogen behaviour in the H-Storage bcc alloys $Ti_{35}V_xCr_{65-x}, Ti_{40}V_x Mn_{50-x}Cr_{10}$ and $Ti_xCr_{97.5-x} Mo_{2.5}$. *Int J Hydrogen Energy* 2008; 34: 7116-21.
- [65] B K Singh, G Shim, S W Cho. Effects of mechanical milling on hydrogen storage properties of $Ti_{0.32}Cr_{0.43}V_{0.25}$ alloy. *Int J Hydrogen Energy* 2007; 32: 4961-65.
- [66] Kulsartov T V, Shestakov V P Tazhibaeva IL Kenzhin E A. Hydrogen permeation through vanadium alloy V-4Cr-4Ti 'in situ' of reactor irradiation. *J Nuclear Materials* 2000; 283-287; 872-5.
- [67] Yu XB, Wu Z, Xia BJ, Xu NX. Enhancement of hydrogen storage capacity of Ti-V-Cr-Mn BCC phase alloys. *J Alloys Comps* 2004; 372:272-7.
- [68] Y Q Hu, C Yan, H F Zhang, L Ye, ZQ Hu. Preparation and hydrogenation characteristics of Mg-30wt% $Ti_{37.5}V_{25}Cr_{37.5}$ composite. *J Alloys Comps* 2004; 375: 265-9.
- [69] T Kuriwa, A Kamegawa, M Okada, T Maruyama, Development of V-rich V-Ti-Cr and V-Ti-Cr-Al Alloys with High Hydrogen Desorption Pressure for High Pressure MH Tank, 18th World Hydrogen Energy Conference 2010 - WHEC 2010 Proceedings of the WHEC, May 16-21, 2010, Essen, (2010) 151-158.
- [70] E Akiba, H Iba. Hydrogen absorption by Laves phase related BCC solid solution, *Intermetallic* 1998;6; 461-70.
- [71] G G Libowitz and A Maeland , hydrogen solubility in titanium alloys, *Material Science Forum* 1998, 30, 177-81
- [72] M Tsukahara, , K Mishima, A Somura and T Sakai Reversible room-temperature absorption of large quantities of hydrogen by intermetallic J alloys *Comps* 1995; 236 :151-5
- [73] H Iba and E Akiba. Metallic hydrides III: Body-centered-cubic solid-solution alloys *J alloys Comps* 1995; 7231 : 513-8.
- [74] P Torres, K Aoyogi, T Suda, Watanabe, S Ohnuki. Hydride formation and fracture of vanadium alloys. *J Nuclr Mater* 2002: 307-311; 625-9.

- [75] M Tsukahara, K Takahashi, Mishima T, Isomura A, Sakai T. V-based solid solution alloys with Laves phase network: hydrogen absorption properties and microstructure. *J Alloys Comps* 1996; 236: 151-5.
- [76] K Asano, S Hayashi, Y Nakamura, E Akiba. Effect of substitutional Mo on diffusion and site occupation of hydrogen in the BCT monohydride phase of V-H system studied by ^1H NMR. *J Alloys Comps* 2010; 507: 399-404.
- [77] S W Cho, C S Han, C N Park and E Akiba, Hydrogen in metals. *J Alloy Compd* 1999; 3: 288 -294
- [78] T Tamura, T Kazumi, A Kamegawa, Takamura H, Okada M. Vanadium based hydrogen permeation materials. *J Alloy Comps* 2003; 3: 356-7.
- [79] F R Boer de and D G Pettifor Cohesion in metals and transition metals alloys Amsterdam: North Holland publication 1989; p 167-71.
- [80] D B Miracle and W S Sanders 2003 *philos. Metals-Hydrogen system*. *Mah* 83:2409-22.
- [81] T Kuriiwa, T Tamura, T Amemiya, T Fuda, A. Kamegawa, H. Takamura, M. Okada, New V-based alloys with high protium absorption and desorption capacity, *Journal of Alloys and Compounds*, 293–295 (1999) 433-436
- [82] J F Lynch, G G Libowitz and A J Maeland, Hysteresis in the Nb-V-H system. *J Less Common Metals* 1984; 103 : 117-22.
- [83] W E Kofstad Wallace and LJ Hyvonen. Vapor Pressure Studies of the Vanadium-Hydrogen System and Thermodynamics of Formation of Vanadium-Hydrogen Solid Solution. *J Chem Phys* 1959: 81: 5019-22.
- [84] D Richter, R Hempelmann and R C Bowman, Jr., in L. Schlapbach (ed.), *Hydrogen in intermetallic Compounds H*, Springer, Berlin, Chapter 3.
- [85] A Mageri, N Stump, H Wipf and G Alfeld. Interstitial Position of hydrogen in metals from entropy of solution. *J Phys Chem Solids* 1977: 38; 683-6.
- [86] A J Maeland. Investigation of the Vanadium –Hydrogen System by X-Ray Diffraction Techniques. *Journal of physical Chemistry* 1964. 68(8) 2197-200
- [87] S W Stafford, B M Rex. Statistical Mechanical Models for Intersititials Solids Solution of hydrogen in Nb, V and Ta. *Acta Metallurgica* 1974: 22; 1147-51
- [88] J Bethin, D O Welch and M A Picks. Phase equilibrium in the Niobium-Vanadium-Hydrogen System. *J Phys Chem Solids* 1990; 51(3): 259-71.
- [89] O J Kleppa, P Dantzer, M E Meinichak. High Temperature thermodynamics of the solid solutions of the hydrogen in bcc vanadium –niobium and tantalum. *J Chemical Physics* 1974: 61(10) 4048.

- [90] C Wagner. Thermodynamics of alloys. Addison-Wesley Press: 1952 : 43-50
- [91] J C Langeberg and B M Rex, Thermodynamics of bcc solid solutions of hydrogen in niobium vanadium and tantalum. *Acta Metallurgica* 1973; 21: 897-901.
- [92] M Tsukahara, K Takahashi, T Mishima, A Isomura, T Sakai. Vanadium –based solid solution alloys with three-dimensional network structure for high capacity metal hydride electrodes. *J of Alloys Compds* 1997; 253-254: 583-6.
- [93] Eremina and Khodosov E V Thermokinetics of hydrogen generation from metal hydrogen compounds based on transition metals of group V (V Nb and Ta). *Atomnaya Energiya* 1978; 44 (4): 365-6.
- [94] M Khrussanova, P Peshev, B Barriet, S Petrova. Hydrogen absorption by alloys of vanadium and some 3d –transition metals. *Mat. Res. Bull* 1992: 27; 611-6.
- [95] K-H Muller, H Paulus, G Kiss: The influence of the surface effects on the hydrogen absorption investigated on the V-H model system. *Applied Surface Science* 2001: 179; 292-300.
- [96] M Amano, M Komaki, C Nishimura. Hydrogen permeation characteristics of palladium-plated V- Ni alloy membranes. *J Less Comm Met* 1991; 172-174:727-31.
- [97] M Koiwa, O Yoshinari, Twist effect of V-H, Nb-H and Ta-H alloys associated with the precipitation of hydrides, *Acta Metallurgica* 1983: 31(12); 2073-81
- [98] Nakajima H, Yoshioka M and Koiwa M, Electromigration of hydrogen in vanadium and its alloys, *Acta Metallurgica* 1987; 35, 11:2731-6.
- [99] B M Rex, M Yoshihara. The diffusion of hydrogen in bcc V-Ti solid solutions. *J Phys Chem Solids* 1987: 48(7); 661-665.
- [100] D T Peterson and B J Schlader, Solubility and Diffusion of hydrogen in Vanadium-Oxygen alloys, *Metallurgical Transactions A* 1988 19A : 67-72.
- [101] M Beutl, J Lesnik, Lundgren, C Konvicka, P Varga, K D Rendulic. Interaction of H₂, CO, and O₂ with vanadium (111) surface . *Surface Science* 2000: 447; 245-58.
- [102] B Tepper, B Richter, A C Dupuis, H Kuhlenbeck, C Hucho, P Schibe, M A B Yarmo, Freund H J. Absorption of molecular and atomic hydrogen on vacuum-cleaved V₂O₅ (001). *Surface Science* 2002; 496: 64-72.
- [103] S Yamanaka, Y Fujita, M Uno. Influence of interstitials oxygen on hydrogen solubility in metals. *J Alloys and Compds* 1999: 293-295: 42-51.
- [104] A I Shirley, Hall C K. Trapping of hydrogen by metallic substitutional Impurities in niobium vanadium and tantalum. *Acta metal* 1984: 32 (1): 49-56.

- [105] V C Srivastava, S Gupta, K N Rai, J Kumar. Hydrogen Absorption in vanadium pentoxide. *Mat Res Bull* 1988; 23; 341-348.
- [106] Y. Zhang, T. Ozaki, M. Komaki, C. Nishimura, hydrogen permeation characteristics of vanadium-aluminium alloys, *Scripta Materialia* 2002, 47: 601-6.
- [107] Nishimura C, Komaki M, Amano M. Hydrogen permeation characteristics of vanadium-molybdenum alloys. *Tran Mater Res. Soc. Jpn* 1994; 18B: 1273-76.
- [108] T Tomoyasu, K Mamadou and E A Daniel. Theory of hydrogen absorption in metal hydride. *Physical Review B* 1981; 24(4):1771-75
- [109] L Zhou, Progress and problems in hydrogen storage methods, *Renew Sustain Energy Rev* 2005; 9:395-408.
- [110] Z Dehouche, J Goyette, T K Bose, R Schulz. Moisture effect on hydrogen storage properties of nanostructured MgH_2-V-Ti composite. *Int J Hydrogen Energy* 2003;28(9):983-8.
- [111] L Zhou, Y Zhou, Y Sun. Studies on the mechanism and capacity of hydrogen uptake by physisorption-based materials. *Int J Hydrogen Energy* 2006; 31(2):259-64.
- [112] www.wikipedia.co.in/XRF/XRD/ICP-AES/DSC/aluminothermy
- [113] [www.image.google.co.in/inert gas fusion technique/thermit analysis](http://www.image.google.co.in/inert%20gas%20fusion%20technique/thermit%20analysis)
- [114] N. Krishnamurthy, Sanjay Kumar, A. Awasthi. Preparation of binary alloys of refractory metals by co-reduction: Group V Metals alloy. Vol.1 RM30/1-RM30/10, 17th Plansee Seminar Proceeding, Plansee Group, Austria2009; 1-10.
- [115] Sanjay Kumar and N Krishnamurthy. Synthesis of V-Ti-Cr alloys by aluminothermy co-reduction of its oxide. *Int J of Proc and Appl of Ceram* 2011; 5(4): 181-6.
- [116] Sanjay Kumar and N. Krishnamurthy. Development of vanadium based hydrogen storage materials: a review. *Progress in Materials Science* 2012; Under preparation.
- [117] Sanjay Kumar, M Taxak, N Krishnamurthy, A K Suri and GP Tiwari. Terminal solid solubility of hydrogen in V-Al solid solution. *Int J Refra Met and Hard Mater* 2012; 31: 76-81.
- [118] M Taxak, Sanjay Kumar, N. Krishnamurthy, A.K Suri. Change in lattice parameter of tantalum due to dissolved hydrogen. *Int J Proc Appl Cer* 2012 ; 6(2): 73-76
- [119] Y Fukai. *The metal-hydrogen system*. Berlin Heidelberg: Springer-Verlag; 2005.
- [120] JF Smith, DE Peterson. *Bull Alloy Phase Diagrams* 1982;3(1):55-60.

- [121] M Kondo, K Asano, Y Iijima. Effect of nickel addition and microstructure on absorption and desorption behavior of hydrogen in LaNi₅. *J Alloys Compds* 2005;393: 269–73
- [122] M Taxak, S Kumar. Hydrogen absorption in ball milled powdered LaNi₅ intermetallic. In: Kalsi PC, Pai RV, Pai MR, Bharadwaj S, Venugopal V, editors. *Proceedings of the 17th national symposium on thermal analysis*; 2010. p. 263–4. Krukshetra, India.
- [123] S Kumar, M Taxak, N Krishnamurthy, A K Suri. Interaction of hydrogen with Pb₈₃Li₁₇eutectic alloy. 2nd international symposium on advance nuclear materials ANM Mumbai, India; 2011. p. 205.
- [124] J L Waisman, G Sine, L B Robinson. Diffusion of hydrogen in titanium alloys due to composition, temperature and stress gradients. *Metall Trans* 1973:291–302
- [125] Sanjay Kumar, M. Taxak, N Krishnamurthy. Hydrogen absorption kinetics of V₄Cr₄Ti alloy prepared by aluminothermy process. *Int J Hydrogen Energy* 2012; 37(4): 3283-91
- [126] Sanjay Kumar and N Krishnamurthy, Variation of activation energy of hydrogen absorption of vanadium as a function of aluminum. *Int J Hydrogen Energy*, 2012;37(18) :13429-36
- [127] Sanjay Kumar and N Krishnamurthy, Effects of aluminum on solubility and β phase stability of vanadium-hydrogen system. *Int J Refra Met and Hard Mater* 2012;35: 191-195
- [128] Sanjay Kumar, M Taxak and N Krishnamurthy, Hydrogen absorption kinetics of V-Al alloy. *J Thermal Analysis and Calorimetry* 2012; In Press, DOI: 10.1007/s10973-012-2558-1
- [129] Sanjay Kumar, Manju Taxak and N Krishnamurthy, Synthesis and hydrogen absorption kinetics of V₄Cr₄Ti alloy. *J Thermal Analysis and Calorimetry* 2012; DOI: 10.1007/s10973-012-2643-5
- [130] *Interaction of metals and Gases, vol.1, Thermodynamics and Phase Relations* by J.D.Fast, Macmillan Press Ltd., London and Basingstoke, Philips, 1965, p. 123-126.
- [131] H.M. Lee. The solubility of hydrogen in transition metals, *Metallurgical Transactions A*, 7A, 1976, 431- 433.
- [132] R.A Oriani, In ICCF4, Fourth International Conference on Cold Fusion 1993. Lahaina, Maui: Electric Power Research Institute 3412 Hillview Ave. Palo Alto, CA 94304.
- [133] Sanjay Kumar and N. Krishnamurthy. Development of vanadium based hydrogen storage materials: a review. *Progress in Materials Science* 2012; Under preparation.
-